1-1-2013

Iridium-Ruthenium/Osmium-Gold Cluster Complexes: Unique Structures and Properties

QIANG ZHANG
University of South Carolina

IRIDIUM-RUTHENIUM/OSMIUM-GOLD CLUSTER COMPLEXES: UNIQUE STRUCTURES AND PROPERTIES

by

Qiang Zhang

Bachelor of Science
Jilin University, 2008

Submitted in Partial Fulfillment of the Requirements

For the Degree of Doctor of Philosophy in

Chemistry

College of Arts and Sciences

University of South Carolina

2013

Accepted by:

Richard D. Adams, Major Professor

Daniel L. Reger, Committee Member

Linda S. Shimizu, Committee Member

Krishna C. Mandal, Committee Member

Lacy Ford, Vice Provost and Dean of Graduate Studies

ACKNOWLEDGEMENTS

An accomplished disciple owes his accomplishment to his great teacher. My accomplishments in graduate study would not have been possible if it weren't for the passion and faith of my advisor Professor Richard Adams has for chemistry. It is him who told me what chemistry is; it is him who told me what research is; and it is him who taught me how to do research and how to do it well. His expertise and experience in this field has help me went through the difficulties that I had faced and made me more capable of solving problems. I would like to thank him devoutly for his precise guidance, helpful assistance and kind support through the past four and half years and, hopefully, also in the future.

I would like to express my heartfelt gratitude to the members of my research committee; Professors Daniel Reger, Linda Shimizu and Krishna Mandal for their kindly advises and time that have been taken for all of my comprehensive exams and dissertation defense. I would also like to thank Professor Vitaly Rassolov and Dr. Xinzheng Yang for their help with some of the DFT calculations. Also, I would like to thank the people in the Chemistry office and the Chemistry stock room, especially Jennifer Merkel for her kindly help. I would like to thank Dr. Mark Smith for some of the crystal structure solutions and for helping me to learn more about crystallography, I would also like to thank Dr. Perry Pellechia for his help with variable temperature NMR experiments and numerous ^{31}P NMR measurements. I also would like to thank Dr. Mike Walla and Dr. William Cotham for their help with the MS measurements.

I would like to thank members of the Adams' group, Professor Minglai Fu, Dr. William Pearl, Eszter Trufan, Dr. Mingwei Chen, Dr. Yuwei Kan, Gaya Elpitiya, Onn Wong, Joseph Kiprotich, Jonathan Tedder and Fang Fang for being the best lab partners. I would also like to express my special thanks to Gaya Elpitiya and Prasanna Malinda Witharana for the wonderful Sri Lankan food and the great time that we spent together.

I would like to express my deepest gratitude to my family. My parents Xuehua Na and Xiliang Zhang, my sisters Bo Zhang, Yan Zhang and Peng Wu, it wouldn't have been possible for me to study in the US without their support. It wouldn't have been possible for me to work for Professor Adams if it weren't for the love of my lovely wife Yuwei Kan. You are the reason I am here in the US, you are the reason I am here at USC, you are the reason I am here in chemistry department and you are the reason I am here for this Ph.D. degree. I thank you very very much for being a perfect partner and supportive in the past 3162 days, for the most precious gifts in the world our son Jason and our daughter Kaylee. Thank you for everything you did for this family. I love you so so so so so much, I was born for you and I will always be here for you.

I would also like to thank my son Jason Zhang for showing his happy face every day which makes me feel so pleasant and powerful. I am grateful to my parents in law for their help with everything. Also, I would like to thank my future daughter Kaylee Zhang, she brings so much happy to me, to this family. I would also like to thank all my friends for the fun times we have spent in the past four years.

Last but not the least I would like to thank the National Science Foundation for the financial support through my graduate study.

ABSTRACT

Chapter Two

The first Ir-Ru cluster complex was synthesized was the electron–rich, anionic, planar cluster complex [PPN][$IrRu_6(CO)_{23}$], **2.5**, (PPN=Bis(triphenylphophoranylidene)-ammonium) which obtained from the reaction of [PPN][$IrRu_3(CO)_{13}$] with one equivalent ruthenium carbonyl ($Ru_3(CO)_{12}$) at 66 ^oC (THF reflux) for 12h. Compound **2.5** could also be synthesized by using the mono-Iridium compound [PPN][$Ir(CO)_4$] reacts with two equivalent of ruthenium carbonyl. In compound **2.5,** all seven metal atoms lie in a plane (max deviation = 0.043(1) Å) with the iridium atom in the center circumscribed by a hexagonal ring of six ruthenium atoms. The anion **2.5** contains 104 valence electrons while both the EAN rule and the PSEP theory predict a total of 102 electrons for this structure. Complex **2.5** is highly colored and exhibits two broad absorptions in the visible region of the spectrum. Even more interestingly, anion **2.5** exhibits a rare luminescence in the 350 nm region when excited with 235 or 275 nm radiations. Computational analyses have been performed to explain its metal–metal bonding and electronic properties.

Anion **2.5** reacts with [Ph_3PAu][NO_3] to yield the uncharged planar complex $Ru_5Ir(CO)_{20}AuPPh_3$, **2.6** in low yield (3%) by metal atom substitution. The structure of **2.6** is same to that of **2.5** except one of the Ru atoms replaced by a gold atom. All of the metal atoms in **2.6** lie virtually in the same plane. The Au atom exhibits the greatest deviation from the best least-squares plane, 0.140Å. The Ir-Ru and Ru-Ru distances are similar to those in **2.5**. Complex **2.6** contains only 102 valence electrons, which agreed

with the EAN rule and the PSEP theory. Interestingly, compound **2.6** also exhibits a significant absorption in the visible region of the spectrum: two overlapping absorptions at 494 nm (ε = 14082 $cm^{-1}\cdot M^{-1}$), 520 nm (ε =16858 $cm^{-1}\cdot M^{-1}$) and one broad absorption at 649 nm (ε =3198 $cm^{-1}\cdot M^{-1}$). DFT calculations have also been performed to explain its metal–metal bonding and electronic properties.

Chapter Three

Four new compounds were obtained from the reaction of $HIrRu_3(CO)_{13}$ with PBu^t_3 (tri-*tert*-butylphosphine) in CH_2Cl_2 at reflux temperature. They have been identified as $IrRu_3(CO)_{12}P(t\text{-}Bu)_3(\mu\text{-}H)$, **3.1**, (15%), $Ir_2Ru_3(CO)_{15}P(t\text{-}Bu)_3$, **3.2**, (2.6% based on Ruthenium), $IrRu_2(CO)_9[P(t\text{-}Bu)_3](\mu\text{-}H)$, **3.3**, (29%) and $IrRu_3(CO)_{10}[P(t\text{-}Bu)_3]_2(\mu_3\text{-}\eta^2\text{-}CO)(\mu\text{-}H)$, **3.4**, (19%). When compound **3.1** was treated with excess of PBu^t_3, compounds **3.3** and **3.4** were obtained in 18.3% and 36.8% yields respectively. When compound 3.4 was allowed to react with excess $Ru(CO)_5$, which was generated by irradiation of $Ru_3(CO)_{12}$ in a hexane solvent, a new compound $IrRu_4(CO)_{12}(\mu_4\text{-}CO)[P(t\text{-}Bu)_3]_2(\mu_3\text{-}H)$, **3.5**, was obtained in 66% yield. When compound **3.5** was treated with CO in a refluxed hexane solution, a new compound $IrRu_4(CO)_{14}P(t\text{-}Bu)_3(\mu_4\text{-}\eta^2\text{-}CO)(\mu\text{-}H)$, **3.6**, was obtained in 18% yield. Compound **3.6** can further react with CO at 10 atm 70 ℃ to produce compound **3.3** in 36% yield.

Compound **3.1** is brown in color and simply a $P(t\text{-}Bu)_3$ substitution derivative of its parent $IrRu_3(CO)_{13}(\mu_3\text{-}H)$. Compound **3.1** contains a closed tetrahedral cluster of four metal atoms, one of Ir and three of Ru. There is one hydrido ligand in **3.1** that bridges the Ir(1) – Ru(1) bond. The phosphine ligand is coordinated to the iridium atom, Ir(1) – P(1) = 2.4825(15) Å. The cluster contains a total of 60 valence electrons and is thus,

electronically saturated, i.e. all metal atoms formally have 18 electron configurations. Compound **3.2** contains five metal atoms, two of Ir and three of Ru. The metal atoms are arranged in the form of a spiked-tetrahedron. The tetrahedral group contains the two iridium atoms and two of the ruthenium atoms. The fourth Ru atom, Ru(1), is the "spike" that is bonded only to the iridium atom. There is one $P(t\text{-}Bu)_3$ ligand in **3.2**, and it is coordinated to Ru(1). There is an η^2-quadruply bridging carbonyl ligand which is coordinated to three metal atoms Ir(1), Ru(2) and Ru(3) by its carbon atom. The oxygen atom is coordinated only to Ru(1). Compound **3.2** contains a total of 76 valence electrons which is precisely the number expected for a spiked-tetrahedral cluster of five metal atoms. Compound **3.3** contains only three metal atoms, one of Ir and two Ru. They are arranged in a triangle. There is one hydrido ligand that bridges the Ir(1) – Ru(1) bond. The phosphine ligand is coordinated to the iridium atom. There are eight terminally coordinated carbonyl ligands and there is one CO, C(1) – O(1), ligand that bridges the Ir(1) – Ru(1) bond. Overall, compound **3.3** contains a total of 46 valence electrons and it is thus electron deficient by the amount of two electrons. DFT molecular orbital calculations were performed by using the PBEsol functional in the ADF program library. Compound **3.4** contains four metal atoms, one of Ir and three of Ru. They are arranged in the form of a butterfly tetrahedron. There are two $P(t\text{-}Bu)_3$ ligands, one on Ir(1) and the other on Ru(1) and these two metal atoms occupy the less crowded "wing-tip" positions of the butterfly tetrahedron. The metal – metal bond distances are fairly normal. The long length of Ru(1) – Ru(3) can be attributed to the presence of a hydrido ligand that bridges that bond. The most interesting ligand in **3.4** is a η^2-triply-bridging CO ligand, C(2) – O(2). The carbon atom is bonded to three of the metal atoms. The oxygen atom is bonded

to Ru(1) and as a result, the CO bond distance is long compared that of the terminally coordinated CO ligands.

In order to understand the nature of the coordination of the triply-bridging CO ligand better, a geometry-optimized DFT molecular orbital analysis of compound **3.4** was performed. Compound **3.5** contains five metal atoms, one of Ir and four of Ru. The metal atoms are arranged in the form of an iridium-capped butterfly tetrahedron of four ruthenium atoms. There are two $P(t\text{-}Bu)_3$ ligands, one on the iridium atom Ir(1) and the other on Ru(2). The hydrido ligand was found to be a triply-bridging ligand across the Ir(1) - Ru(1) - Ru(3) triangle. Compound **3.5** contains a η^2-quadruply-bridging CO ligand, C(1) – O(1). The carbon atom is bonded to all four ruthenium atoms. The oxygen atom is bonded only to Ru(2). As found in **3.4**, the CO bond distance is also long. In order to understand the nature of the coordination of the interesting CO ligand, a geometry-optimized DFT molecular orbital analysis of compound **3.5** was also performed. Compound **3.6** also contains five metal atoms, one of Ir and four of Ru. The cluster is very similar to that of **3.2** having the metal atoms are arranged in the form of a spiked-tetrahedron. The iridium atom is contained in the tetrahedral portion of the cluster. Ru(1) is the "spike" that is bonded only to the iridium atom. There is only one $P(t\text{-}Bu)_3$ ligand in **3.6**, and it is coordinated to the ruthenium atom labeled Ru(1). There is one hydrido ligand H(1) that bridges the Ru(2) – Ru(3) bond. An η^2-quadruply bridging carbonyl ligand, C(1) – O(1) is coordinated to three metal atoms Ir(1), Ru(2) and Ru(4) by its carbon atom. The oxygen atom is coordinated only to Ru(1), which is very similar to that found in **3.2**. Like **3.2**, compound **3.6** contains a total of 76 valence electrons

which is precisely the number expected for a spiked-tetrahedral cluster of five metal atoms. DFT molecular orbital analysis of compound **3.6** was also performed.

Chapter Four

Three new Ir-Ru-Au trimetallic cluster complexes: $IrRu_3(CO)_{13}AuPPh_3$, **4.1**, $HIrRu_3(CO)_{12}(AuPPh_3)_2$, **4.2,** and $IrRu_3(CO)_{12}(AuPPh_3)_3$, **4.3** were obtained in low yields from the reaction of $HIrRu_3(CO)_{13}$ with $[(AuPPh_3)_3O][BF_4]$. Compounds **4.1** and **4.3** were subsequently obtained in much better yields (82%) and (84%) from the reactions of $[AuPPh_3][NO_3]$ and $[(AuPPh_3)_3O][BF_4]$ with $[PPN][IrRu_3(CO)_{13}]$ respectively. The Compounds **4.1** contains an $Au(PPh_3)$ group that bridging a Ru_3 triangular face of the tetrahedral $IrRu_3$ cluster. Compound **4.1** could be viewed as an $Au(PPh_3)$ capped tetrahedral $IrRu_3$ structure which has 60 valence electrons. The metal cluster in **4.2** can be described as an $Au(PPh_3)$ capped trigonal-bipyramidal $AuIrRu_3$ cluster, but this $AuIrRu_3$ cluster is not the same as that in **4.1**. The Au atom in $AuIrRu_3$ cluster in **4.2** caps an $IrRu_2$ triangle not the Ru_3 triangle as in **4.1** and the $Au(PPh_3)$ cap on that bridges one of the Au-Ir-Ru triangles. There is a hydride that bridges one of the Ru-Ru bonds. If we see the $Au(PPh_3)$ group as a ligand which donates one electron to the cluster, compound **4.2** will have 60 valence electrons which obey both the EAN rule and the PSEP theory. Compound **4.2** exhibits only one phosphorus resonance in its ^{31}P NMR spectrum at room temperature, but it shows two resonances as expected at -80 ^{o}C. This temperature dependence can be explained by a dynamical exchange process that leads to an interchange of the environments of the two inequivalent $Au(PPh_3)$ groups in **4.2** on the NMR timescale at room temperature. A possible mechanism was proposed to explain this

dynamical exchange process. Compound **4.3** contains three $Au(PPh_3)$ groups combined with the $IrRu_3$ cluster of the original reagents $HIrRu_3(CO)_{13}$ or anion $[IrRu_3(CO)_{13}]^-$. The metal cluster in **4.3** can be described in different ways. It could be described as an $IrRu_3$ tetrahedron with three bridging $Au(PPh_3)$ groups. Alternatively, the cluster could be described as a seven atom pentagonal bipyramidal Au_3IrRu_3 cluster with an additional bond between the apical atoms. If one considers compound **4.3** as a $IrRu_3$ tetrahedron with three one electron $Au(PPh_3)$ donors, then the cluster contains a total of 60 electrons and the Ir and each of the Ru atoms will formally have 18 electron configurations. The ^{31}P NMR spectrum of **4.3** exhibits only one phosphorus resonance at room temperature, but shows two resonances in a 2/1 ratio resonances as expected at -80 ^oC. As the temperature is raised, the two resonances broaden and coalesce in a process indicative of a dynamical averaging. The broadened spectra were simulated in order to obtain exchange rates and activation parameters for the exchange process. A dynamical exchange process that leads to an interchange of the two types $Au(PPh_3)$ groups on the NMR timescale at room temperature seems to be the most likely. A variety of mechanisms can be envisioned, but all must involve the cleavage of at least one of the Au-Au bonds.

Chapter Five

The reaction of $Os_3(CO)_{10}(NCMe)_2$, **5.1** with $C_6H_5Au(PPh_3)$ has yielded the complex $Os_3(CO)_{10}(\mu,\eta^1\text{-}C_6H_5)(\mu\text{-}AuPPh_3)$, **5.2**, which contains an bridging η^1-phenyl ligand and an $Au(PPh_3)$ group that bridges the same unsaturated Os−Os bond in the 46-electron cluster complex. When it was heated to reflux in an octane solution (125 ℃), compound **5.2** was decarbonylated and converted to the complex $Os_3(CO)_9(\mu_3\text{-}C_6H_4)(\mu\text{-}$

$AuPPh_3$)(μ-H), **5.3**, which contains a triply bridging benzyne ligand by a CH cleavage on the bridging phenyl ring. The reaction of **5.1** with (1-$C_{10}H_7$)Au(PPh_3) (1-$C_{10}H_7$ = 1-naphthyl) or (2-$C_{10}H_7$)Au(PPh_3) (2-$C_{10}H_7$ = 2-naphthyl) yielded the complex $Os_3(CO)_{10}$(μ-2-$C_{10}H_7$)(μ-$AuPPh_3$), **5.4**, which exists as two isomeric forms in the solid state. A 1,2-hydrogen shift in the naphthyl ligand occurred in the formation of **5.4**. The green isomer **5.4a** is structurally similar to **5.2** and contains a bridging η^1-2-naphthyl ligand and a bridging Au(PPh_3) group and is electronically unsaturated overall. The pink isomer **5.4b** contains a bridging η^2-2- naphthyl ligand and a bridging Au(PPh_3) group and is electronically saturated. The pink isomer is found in hexane solution and was converted to the complex $Os_3(CO)_9$(μ_3-$C_{10}H_6$)(μ-$AuPPh_3$)(μ-H), **5.5** when heated to reflux in octane (125 ℃) for 30 min. Compound **5.5** is the first naphthyne compound that has ever been made which contains a triply bridging 1,2-naphthyne ligand. The reaction of **5.1** with (1-$C_{16}H_9$)Au(PPh_3) (1-$C_{16}H_9$ = 1-pyrenyl) yielded the complex $Os_3(CO)_{10}$(μ-2-$C_{16}H_9$)(μ-$AuPPh_3$), **5.6**, which also exists as two isomeric forms. A 1,2-hydrogen shift and 2,4-hydrogen shift in the pyrenyl ligand occurred in the formation of **5.6.** The green isomer **5.6** is structurally similar to **5.2** and contains a bridging η^1-2-pyrenyl ligand and a bridging Au(PPh_3) group and is electronically unsaturated overall. The brown isomer **5.7** contains a bridging η^1-4-pyrenyl ligand and a bridging Au(PPh_3) group and is also electronically unsaturated. When heated to reflux in an octane solution (125 ℃), both compound **5.6** and **5.7** were decarbonylated and converted to the corresponding pyryne complex $Os_3(CO)_9$(μ_3-1,2-$C_{16}H_8$)(μ-$AuPPh_3$)(μ-H), **5.8** and $Os_3(CO)_9$(μ_3-4,5-$C_{16}H_8$)(μ-$AuPPh_3$)(μ-H), **5.9** which contain triply bridging pyryne ligands by a CH cleavage on the bridging pyrenyl ring. To further understand the bonding between the phenyl group and

the metal cluster, DFT (Density Functional Theory) calculation on compound **5.2** was conducted, the fragment analysis revealed the bonding of the phenyl to the unsaturated Os-Os bond not only consist with σ-bond, but π donation from the phenyl ligand to the cluster was involved as well.

Chapter Six

Variable temperature NMR studies of the compound $Os_3(CO)_{10}(\mu\text{-}\eta^1\text{-}C_6H_5)(\mu\text{-}AuPPh_3)$, **6.1** (**5.2)** have revealed the first example of hindered rotation of the bridging phenyl ligand about the metal-metal bond. The activation parameters for the process:$\Delta H^{\ddagger}$ = 72.34 KJ/mol, $\Delta S^{\ddagger}$= -2.65 J/K•mol were determined. A density functional theory analysis has provided a mechanism that involves a partial shift of the ligand out of the bridging position with the formation of an agostic interaction of one of the *ortho*-positioned CH bonds of the phenyl ring at the neighboring metal atom. Compound **6.2** (5.**6)** was also found to behave similarly. Surprisingly, the calculated activation parameters for compound **6.2**: $\Delta H^{\ddagger}$ = 70.93(61) kJ/mol and $\Delta S^{\ddagger}$= = −6.98(1.83) J/(K•mol) which are very similar to those for compound **6.1**.

TABLE OF CONTENTS

Acknowledgements……..ii

Abstract……...iv

List of Tables……xiv

List of Figures……...xvi

List of Schemes……..xx

Chapter One: Introduction ……..1

References……..37

Chapter Two: Two Dimensional Bimetallic Carbonyl Cluster Complexes with New Properties and Reactivities……..44

References……..74

Chapter Three: Structures and Bonding of η^2-bridging CO Ligands and Their Influence on the Structures and Rearrangements of Higher Nuclearity Metal Carbonyl Cluster Complexes……..76

References……119

Chapter Four: Iridium-Ruthenium-Gold Cluster Complexes: Structures and Skeletal Rearrangements……...……122

References……146

Chapter Five: Structures and Transformations of Bridging Aryl Ligands in Triosmium Carbonyl Cluster Complexes……...148

References……197

Chapter Six: Rotational Behavior of Bridging Aryl Ligands in Unsaturated Metal Carbonyl Cluster Complexes ……199

References……217

Cumulative References……219

LIST OF TABLES

Table 2.1 Crystallographic Data for Compounds **2.5** and **2.6**.....69

Table 2.2 Calculated TDDFT Electronic Transtions for $Ru_6Ir(CO)_{23}^-$, **2.5**.....70

Table 2.3 Summary of TDDFT calculated singlet excited-states of $Ru_5Ir(CO)_{20}AuPPh_3$ **2.6**, with stronger oscillator strength.....71

Table 2.4 Selected intramolecular angles and bond distances for compound **2.5**.....72

Table 2.5 Selected intramolecular angles and bond distances for compound **2.6**.....73

Table 3.1 Crystallographic Data for Compounds **3.1** – **3.6**.....107

Table 3.2 Selected intramolecular angles and bond distances for compound **3.1**.....109

Table 3.3 Selected intramolecular angles and bond distances for compound **3.2**.....110

Table 3.4 Selected intramolecular angles and bond distances for compound **3.3**.....111

Table 3.5 Selected intramolecular angles and bond distances for compound **3.4**.....112

Table 3.6 Selected intramolecular angles and bond distances for compound **3.5**.....113

Table 3.7 Selected intramolecular angles and bond distances for compound **3.6**.....114

Table 3.8 Geometry optimized coodinates of **3.3** 115

Table 3.9 Geometry optimized coodinates of **3.4** 116

Table 3.10 Geometry optimized coodinates of **3.5** 117

Table 3.11 Geometry optimized coodinates of **3.6** 118

Table 4.1 Crystallographic Data for Compounds **4.1** – **4.3**.....142

Table 4.2 Selected intramolecular angles and bond distances for compound **4.1**.....143

Table 4.3 Selected intramolecular angles and bond distances for compound **4.2**.....144

Table 4.4 Selected intramolecular angles and bond distances for compound **4.3**.....145

Table 5.1 Crystallographic Data for Compounds **5.2**– **5.9**.....185

Table 5.2 Selected intramolecular angles and bond distances for compound **5.2**.....188

Table 5.3 Selected intramolecular angles and bond distances for compound **5.3**.....189

Table 5.4 Selected intramolecular angles and bond distances for compound **5.4a**.....190

Table 5.5 Selected intramolecular angles and bond distances for compound **5.4b** 191

Table 5.6 Selected intramolecular angles and bond distances for compound **5.5**.....192

Table 5.7 Selected intramolecular angles and bond distances for compound **5.6**.....193

Table 5.8 Selected intramolecular angles and bond distances for compound **5.7**.....194

Table 5.9 Selected intramolecular angles and bond distances for compound **5.8**.....195

Table 5.10 Selected intramolecular angles and bond distances for compound **5.9**.....196

Table 6.1 XYZ coordinates of C 214

Table 6.2 XYZ coordinates of D.....215

Table 6.3 XYZ coordinates of TS2 216

LIST OF FIGURES

Figure 1.1 Variable-temperature ^{1}H NMR spectra for (μ-H)$_2$Os$_3$(CO)$_{10}$(GePh$_3$)$_2$ in CD_2Cl_2 solvent recorded in the high-field region of the spectrum.....25

Figure 1.2 Bar chart summarizing the relative performances and selectivities of the Ru_5Pt and $Ru_{10}Pt_2$ catalysts when compared to other bimetallic nanocatalysts for the hydrogenation of benzoic acid. 34

Figure 1.3 Bar chart comparing the activity and selectivity of the Ru_5PtSn catalyst with those of other bi- and trimetallic catalysts for the hydrogenation of DMT 36

Figure 2.1 An ORTEP diagram of cluster anion $[Ru_6Ir(CO)_{23}]^-$, **2.5**, showing 40% thermal probability.....55

Figure 2.2 UV-vis absorption spectrum of **2.5** in CH_2Cl_2 solvent.....56

Figure 2.3 Excitation and emission spectra for **2.5** in CH_2Cl_2 solvent.....57

Figure 2.4 The infrared spectrum of the purple intermediate 58

Figure 2.5 Selected molecular orbitals that show the two lowest unoccupied orbitals and some important metal–metal bonding orbitals for $Ru_6Ir(CO)_{23}^-$, **2.5**.....59

Figure 2.6 Selected molecular orbitals of the low energy metal –metal bonding orbitals for **$Ru_6Ir(CO)_{23}^-$**, **2.5** 60

Figure 2.7 Simulated TDDFT UV-vis absorption spectrum for anion **2.5** 61

Figure 2.8 An ORTEP diagram of **2.6** showing 40% thermal probability. Hydrogen atoms have been omitted for clarity.....62

Figure 2.9 Selected Molecular Orbital Diagrams Show Metal-Metal Interactions In Compound $Ru_5Ir(CO)_{20}AuPPh_3$, **2.6** 63

Figure 2.10 Selected Low energy Molecular Orbital Diagrams Show Gold-Iridium Interactions In $Ru_5Ir(CO)_{20}AuPPh_3$, **2.6**.....64

Figure 2.11 UV-vis absorption spectrum of **2.6** in CH_2Cl_2 solvent.....65

Figure 2.12 Simulated TDDFT UV-vis absorption spectrum for $Ru_5Ir(CO)_{20}AuPPh_3$, **2.6**.....66

Figure 3.1 An ORTEP diagram of the molecular structure of $IrRu_3(CO)_{12}P(t\text{-}Bu)_3$ (μ-H), **3.1** showing 30% thermal ellipsoid probability.....93

Figure 3.2 An ORTEP diagram of the molecular structure of $Ir_2Ru_3(CO)_{15}P(t\text{-}Bu)_3$ (μ-H), **3.2** showing 30% thermal ellipsoid probability.....94

Figure 3.3 An ORTEP diagram of molecular structure of $IrRu_2(CO)_9P(t\text{-}Bu)_3(\mu\text{-}H)$, **3.3** showing 30% thermal ellipsoid probability.....95

Figure 3.4 ADF MO diagrams of the LUMO, (left) and HOMO, (right) for compound **3.3**. A large component of the LUMO in golden color lies in the proximity of the vacant coordination site on the iridium atom, violet = Ir, green = Ru; Isovalue = 0.03.....96

Figure 3.5 An ORTEP diagram of molecular structure of $IrRu_3(CO)_{10}(\mu_3\text{-}CO)\text{-}[P(t\text{-}Bu)_3]_2(\mu\text{-}H)$, **3.4**, showing 30% thermal ellipsoid probability.....97

Figure 3.6 Selected ADF MO diagrams for compound **3.4** showing the bonding of the bridging CO ligand to the metal atoms, violet = Ir, green = Ru; Isovalue = 0.03.....98

Figure 3.7 An ORTEP diagram of molecular structure of $IrRu_4(CO)_{12}[P(t\text{-}Bu)_3]_2(\mu_4\text{-}\eta^2\text{-}CO)(\mu_3\text{-}H)$, **3.5**, showing 30% thermal ellipsoid probability.....99

Figure 3.8 Selected ADF MO diagrams with energies for compound **3.5** showing the bonding of the quadruply bridging CO ligand to the metal atoms of the cluster, violet = Ir, green = Ru; Isovalue = 0.03.....100

Figure 3.9 An ORTEP diagram of molecular structure of $IrRu_4(CO)_{14}P(t\text{-}Bu)_3(\mu_4\text{-}\eta^2\text{-}CO)(\mu\text{-}H)$, **3.6**, showing 30% thermal ellipsoid probability.....101

Figure 3.10 ADF MO diagrams with energies for compound **3.6** showing the bonding of the quadruply bridging CO ligand to the metal atoms of the cluster, violet = Ir, green = Ru; Isovalue = 0.03.....102

Figure 4.1 An ORTEP diagram of the molecular structure of $IrRu_3(CO)_{13}AuPPh_3$, **4.1** showing 20% thermal ellipsoid probability.....132

Figure 4.2 An ORTEP diagram of the molecular structure of $HIrRu_3(CO)_{12}(AuPPh_3)_2$,

4.2 showing 20% thermal ellipsoid probability 133

Figure 4.3 An ORTEP diagram of the molecular structure of $IrRu_3(CO)_{12}(AuPPh_3)_3$, **4.3** showing 20% thermal ellipsoid probability 134

Figure 4.4 ^{31}P {H} NMR spectra for compound **4.2** in CD_2Cl_2 solvent at room temperature 135

Figure 4.5 ^{31}P {H} NMR spectra for compound **4.3** in CD_2Cl_2 solvent at various temperatures.....136

Figure 4.6 Simulated NMR ^{31}P {H} NMR spectra for compound **4.3** at various temperatures 137

Figure 5.1 An ORTEP diagram of the molecular structure of $Os_3(CO)_{10}(\mu\text{-}C_6H_5)(\mu\text{-}AuPPh_3)$, **5.2** showing 30% thermal ellipsoid probability 166

Figure 5.2 The LUMO, HOMO, HOMO-3, HOMO-5, HOMO-6, HOMO-14 and HOMO-18 with calculated energies show the bonding of the η^1-bridging phenyl ligand to the osmium atoms in **5.2**.....167

Figure 5.3 Energy level diagram of the molecular orbitals with calculated energies from fragment analysis shows the origin of the MOs in Figure 5.2 for compound **5.2**.....168

Figure 5.4 An ORTEP diagram of the molecular structure of $Os_3(CO)_9(\mu_3\text{-}C_6H_4)(\mu_3\text{-}AuPPh_3)(\mu\text{-}H)$, **5.3** showing 30% thermal ellipsoid probability 169

Figure 5.5 An ORTEP diagram of the molecular structure of $Os_3(CO)_{10}(\mu\text{-}2\text{-}Np)(\mu\text{-}AuPPh_3)$, **5.4a** obtained from the green crystals showing 30% thermal ellipsoid probability 170

Figure 5.6 An ORTEP diagram of the molecular structure of $Os_3(CO)_{10}(\mu_3\text{-}\eta^2\text{-}2\text{-}Np)(\mu\text{-}AuPPh_3)$, **5.4b** showing 30% thermal ellipsoid probability 171

Figure 5.7 An ORTEP diagram of the molecular structure of $Os_3(CO)_9(\mu_3\text{-}C_{10}H_6)(\mu\text{-}AuPPh_3)(\mu\text{-}H)$, **5.5** showing 30% thermal ellipsoid probability 172

Figure 5.8 Calculated energy profile shows the decarbonylation and CH activation in the transformation from naphthyl to naphthyne.....173

Figure 5.9 The computed intermediate of the naphthyne formation shows the agostic interaction between the ortho-CH bond in the Naphthyl group to the third osmium atom (left). The HOMO-13 of this intermediate shows the bonding of the hydrogen atom to the osmium (right) 174

Figure 5.10 The computed transition state of the naphthyne formation shows the cleavage of the C-H bond (left). The HOMO of this transition state shows hydrogen-osmium bonding (right).....175

Figure 5.11 An ORTEP diagram of the molecular structure of $Os_3(CO)_{10}(AuPPh_3)$ (2-Pyryl), **5.6** showing 30% thermal ellipsoid probability 176

Figure 5.12 An ORTEP diagram of molecular structure of $Os_3(CO)_{10}(AuPPh_3)$ (4-Pyryl), **5.7,** showing 30% thermal ellipsoid probability 177

Figure 5.13 An ORTEP diagram of molecular structure of $Os_3(CO)_{10}(AuPPh_3)$ (μ-1,2-Pyryne)(μ-H), **5.8**, showing 30% thermal ellipsoid probability 178

Figure 5.14 An ORTEP diagram of molecular structure of $Os_3(CO)_{10}(AuPPh_3)$(μ-4,5-Pyryne)(μ-H), **5.9**, showing 30% thermal ellipsoid probability 179

Figure 5.15 UV-Vis absorption spectra of compound **5.2** in CH_2Cl_2.....180

Figure 5.16 UV-vis absorption spectra for compounds **5.4b** in CH_2Cl_2.....181

Figure 5.17 UV-vis absorption spectra for compounds **5.7** in CH_2Cl_2.....182

Figure 6.1 Variable temperature ^1H NMR spectra of **6.1** in the phenyl region of the spectrum recorded in d_8-toluene.....205

Figure 6.2 The HOMO-27 of the intermediate **C** 206

Figure 6.3 The energy profile shows energies for the two intermediates and three transition states in the pathway of phenyl rotation.....207

Figure 6.4 Variable temperature ^1H NMR spectra of **6.2** in the aromatic region of the spectrum recorded in d_8-toluene.....20

LIST OF SCHEMES

Scheme 1.1 The bonding between a terminal carbonyl ligand and metal atom 18

Scheme 1.2 Bonding modes of η^1-carbonyl ligand on various metal centers 19

Scheme 1.3 Bonding modes of η^2-carbonyl ligand in different metal clusters 20

Scheme 1.4 The rotation of benzene ring in compound (μ-H)(RuC_5Me_5)$_3$(μ_3-η^6-C_6H_6).....21

Scheme 1.5 Some of the bonding modes of the phenyl group on metal centers.....22

Scheme 1.6 The bonding of η^1-phenyl ligand to metal atoms.....23

Scheme 1.7 Some of the bonding modes of the benzyne ligand to metal center(s).....24

Scheme 1.8 A proposed mechanism for hydrogen averaging mechanism for the compound (μ-H)$_2$$Os_3(CO)_{10}(GePh_3)_2$ 26

Scheme 1.9 The migration of Pt-P groups in Ru-Pt cluster complexes 27

Scheme 1.10 The transformation of a carbonyl ligand about a trimetallic cluster.....28

Scheme 1.11 A proposed mechanism for a model Fisher-Tropsch process.....29

Scheme 1.12 A proposed mechanism for the activation of C-H and C-S bonds in the cluster complex (μ-H)$Os_3(CO)_9[C(H)NR_2]$(μ-SPh).....30

Scheme 1.13 A proposed mechanism for the catalytic hydrogenation of PhC_2H by the octahedral cluster complex $Ru_5(CO)_{15}$(μ_6-C)$PtPBu^t_3$.....31

Scheme 1.14 A proposed mechanism for the catalytic hydrogenation of PhC_2Ph by the layer-segregated cluster complex (μ_3-H)(μ-H)$Pt_3Ru_6(CO)_{20}$(μ_3-PhC_2Ph).....32

Scheme 1.15 The products from the hydrogenation of Benzoic acid and the industrial use of Cyclohexanecarboxylic acid to produce Nylon 6.....23

Scheme 1.16 The products from the hydrogenation of Dimethyl terephthalate.....35

Scheme 2.1 Some reported 2-D cluster complexes 67

Scheme 2.2 Transformation of **2.5** to **2.6** 68

Scheme 3.1 Bonding modes of η^2-carbonyl ligand in different metal clusters 103

Scheme 3.2 The formation of μ-η^2-phenyl ligand in Ir-Ru cluster complex.....104

Scheme 3.3 The transformation of compound **3.5** to **3.6** under CO atmosphere 105

Scheme 3.4 The reaction of $HIrRu_3(CO)_{13}$ with PBu^t_3 and the transformation of carbonyl ligand through Ir-Ru cluster complexes.....106

Scheme 4.1 $IrRu_3(AuPPh_3)_n$ complexes obtained from reaction of $IrRu_3$ complexes with Au cations.....138

Scheme 4.2 Proposed mechanism for the dynamic averaging of $(AuPPh_3)$ groups in **4.2** 139

Scheme 4.3 The $IrRu_3Au_3$ structure compared with the normal M_4Au_3 140

Scheme 4.4 Proposed mechanism for the dynamic averaging of $(AuPPh_3)$ groups in **4.3** 141

Scheme 5.1 The computed mechanism for the formation of Naphthyne compound **5.5** via ortho-C-H activation on the naphthyl ligand of **5.4b** 183

Scheme 5.2 The reaction of $Os_3(CO)_{10}(NCMe)_2$ with $ArylAuPPh_3$ and the transformations of $ArylOs_3(CO)_{10}AuPPh_3$ to $Aryne(\mu\text{-}H)Os_3(CO)_9AuPPh_3$.....184

Scheme 6.1 η1-bridging phenyl ligand.....209

Scheme 6.2 The proposed mechanism for the phenyl rotation where the phenyl rotates along a C_2 axis.....210

Scheme 6.3 The proposed mechanism for the phenyl rotation where the shifting of the phenyl from bridging position to terminal position is involved.....211

Scheme 6.4 The computed mechanism for the phenyl rotation 212

Scheme 6.5 The pyrenyl rotation in compound **6.2**.....213

CHAPTER 1

INTRODUCTION

About 50 years ago, F. A. Cotton provided the definition of cluster in inorganic chemistry, "A group of three or more metal atoms linked together at least in part by metal-metal bonding".[1] Nowadays, the term "clusters" would be considered as complexes which contain metal atoms that are directly or substantially interacting. One of the earliest fields of study was the area of transition metal carbonyl cluster chemistry. $Fe_3(CO)_{12}$ has been considered to be one of the earliest, if not the very earliest, metal carbonyl cluster complex, which has been known for more than a century,[2] however, the crystal structure of it was only revealed about 60 years later by Dahl.[3] Some other metal carbonyl cluster complexes such as $Ru_3(CO)_{12}$, $Os_3(CO)_{12}$[4] and $Co_4(CO)_{12}$[5] have been known for more than 70 years. Transition metal carbonyl cluster complexes are intriguing compounds for many reasons including the divertive metal-ligand bonding interactions, the dynamic ligand exchange and skeletal rearrangement, and, of course, catalysis.

1.1 Carbonyl ligands in Metal Carbonyl Cluster Complexes

Carbonyl is an adequate ligand in metal cluster complexes. The bonding between metal and terminal carbonyl ligand is dominated by σ-donation from the lone pair electrons on the carbon atom, 5σ bonding orbital, of CO and significant electron donation from the filled metal *d*-orbitals to the empty $2\pi^*$ orbitals of CO, namely π back bonding. The third bonding interaction is contributed by the electron donation from the π bonding

orbitals of CO to the empty *d*-orbitals of the metal, which is a very rare phenomenon (Scheme 1.1).[6] The π back bonding helps stabilize the electron-rich low-valent metal centers. The most common bonding mode between carbonyl and metal is in a fashion of terminal coordination, where one carbonyl ligand, by the σ donation or through π back bonding on the carbon atom, interacts with only one metal. There are also numbers of metal cluster complexes contain η^1-bridging carbonyl ligands, doubly μ_2-bridging mode and triply μ_3-bridging mode. The quadruply μ_4-bridging mode, however, is very rare (Scheme 1.2).[7] The η^2-bridging carbonyl ligand, where the oxygen atom in the CO has been involved in bonding, binds to metals in more bonding forms compare to the η^1 coordinated ones. Generally, the η^2-bridging carbonyl serves as a four electron donor, **A**,[8] **C**,[9] **E**[10] and **F**[11] in Scheme 1.3, but in some unusual cases, it could be a six electron donor as well, mode **B**[12] and **G**[13]. In the ordinary way, the η^2-bridging carbonyl could further be classified into two sub-groups based on the electron origin from the CO; 1) electron donation from the π bonding orbitals of CO to the empty *d*-orbitals on metals, **B**, **D**, **E** and **G**, 2) binding metals by the use of the lone pair electrons on the oxygen atom of the CO, **A**, **C** and **F**.

The most important technique for characterizing metal carbonyl compounds is infrared spectroscopy, which is a sensitive probe for distinguishing the bonding modes of carbonyl ligands. The C-O stretching frequency is a finger print for the coordinated carbonyl ligand; the energies of the ν_{CO} band largely correlate with the strength of the carbon-oxygen bond, and, obviously, are inversely correlated with the amount of the π back bonding. The strength of the π back bonding, for terminally coordinated carbonyl ligands, depends on the π basicity of a metal center which is, to a large degree, influenced

by the charge of the metal. For example, the carbon-oxygen stretching frequency occurs at 2030 cm^{-1} for the neutral $Fe(CO)_5$; for the anion $[Fe(CO)_4]^{2-}$, which has more electrons on the iron center the π back bonding is increased and therefore, the carbon-oxygen vibrational energy is decreased, which leading to a low energy band at 1815 cm^{-1}. On the other hand, a high energy band at 2215 cm^{-1} for the carbon-oxygen stretch has been observed for the cation $[Fe(CO)_6]^{2+}$.[14]

Apart from the π basicity for a given metal, the carbon-oxygen bond stretching frequency can also be greatly affected by the various bonding modes, which have been discussed above. More metals will, beyond a shadow of doubt, donate more electrons to the $2\pi^*$ orbitals of the CO, thus more extensively weaken the carbon-oxygen bond and lower the infrared frequency for carbon-oxygen stretching vibration. The typically denoted $\nu_{CO,}$ occurs at 2143 cm^{-1} for the free molecule CO (CO gas). For neutral metal carbonyl cluster complexes, the ν_{CO} occurs in the region 2120-1850 cm^{-1} for terminally coordinated CO, 1850-1720 cm^{-1} for doubly-bridged CO and 1730-1500 cm^{-1} for triply- and quadruply-bridged carbonyl ligands.[7]

1.2 Metal Cluster Complexes Containing Aromatic Ligands

As the field of metal carbonyl cluster chemistry continues to expand, many other new classes of clusters have joined the group. Among which, the metal clusters that contain aromatic ligands have drawn a great attention for the interesting metal-ligand bonding interactions and the potential of such system that serves as a model helping researchers to study the transformation of small molecules on the metal surfaces,

therefore gain deeper insight to catalysis. Generally, aromatic ligands in metal cluster complexes can be classified into three categories: 1) Arene, 2) Aryl and 3) Aryne.

1.21 Metal cluster complexes containing Arene Ligands

In Arenes, there are no unpaired electrons and the Arene bonds to metal centers only through its π orbitals. The simplest Arene ligand is benzene. Johnson and Lewis reported the first facial-benzene metal cluster complex, $Os_3(CO)_9(\mu_3\text{-}\eta^6\text{-}C_6H_6)$, where the benzene ring serves as a six electron donor and it is only π bonded to the triangular Os_3 cluster. This compound contains 48 valence electrons indicating that it is saturated, that is, each of the metal atoms achieves an 18 electron configuration.[15] The ruthenium analogue, $Ru_3(CO)_9(\mu_3\text{-}\eta^6\text{-}C_6H_6)$,[16] was synthesized and reported by the same group. Another novel facial-benzene cluster compound, $(\mu\text{-H})(RuC_5Me_5)_3(\mu_3\text{-}\eta^6\text{-}C_6H_6)$,[17] has been found to be able to transfer the benzene from the $(\mu_3\text{-}\eta^2\text{:}\eta^2\text{:}\eta^2\text{-}C_6H_6)$ bridging mode to $(\mu_3\text{-}\eta^3\text{:}\eta^3\text{-}C_6H_6)$ bridging mode (Scheme 1.4), upon oxidation by ferricinium salt, to result the 46 electron unsaturated cation.

1.22 Metal cluster complexes containing Aryl ligands

Aryl refers to any functional group derived from a 6-membered aromatic ring that has one unpaired electron available for bonding. The simplest Aryl ligand is phenyl, C_6H_5. The bonding of phenyl ring to metal center(s) (Scheme 1.5) can be much more diverse than that of benzene. The terminal phenyl ligand (type **A**) is σ-bonded to the metal center using the one unpaired electron (Scheme 1.6).[18] There are two η^1-bridging modes, the symmetrical (type **B**) and asymmetrical (type **C**) bridging phenyls. In the symmetrical η^1-

bridging mode, the phenyl ring binds to two metals by using that unpaired electron to form a three-center two-electron σ-bond. Even the phenyl serves as a one electron donor, it has been recognized that this bonding mode also involves the electron donation from one of the filled π orbitals of the phenyl to empty *d*-orbitals no the two metal atoms (Scheme 1.6).[19] For the asymmetrical η^1-bridging phenyl, the phenyl is mainly σ-bonded to one of the metal atoms and, to a certain extent, bonded with another metal through a π-interaction. Interestingly, this asymmetrical η^1-bridging phenyl serves as a one electron donor in the compound $Ir_4(CO)_{11}(\mu\text{-}\eta^1\text{-Ph})[\mu_3\text{-Cu(NCMe)}]$,[20] but, in another case, it has been claimed to be a three electron donor in the compound $Os_3(CO)_8(\mu_3\text{-Se})_2(\mu\text{-}\eta^1\text{-Ph})(\mu\text{-PhCO})$.[21] The bonding between a phenyl group and metal atoms could also involve interactions of metal centers with two carbon atoms in the ring. In this situation, the bonding mode can be described as $(\mu\text{-}\eta^2\text{-Ph})$ which serves as a three electron donor (type **D**). The first tri-nuclear metal cluster complex, $Ru_3(CO)_7(\mu\text{-}\eta^2\text{-Ph})(\mu\text{-PPh}_2)(PPh_3)(\mu_3\text{-S})$, where the $(\mu\text{-}\eta^2\text{-Ph})$ was formed by the fragmentation of PPh_3, was reported by Süss-Fink in 1996.[22] Some higher nuclearity Iridium-Ruthenium cluster complexes containing $\mu\text{-}\eta^2$-Ph and the reactivity of these cluster complexes have been reported by Adams and co-workers.[23] The metal cluster complexes containing $(\mu\text{-}\eta^1\text{:}\eta^6\text{-Ph})$ (type **E)**, $M_3(\mu\text{-}\eta^1\text{:}\eta^6\text{-Ph})\text{-}(\mu\text{-X})(CO)_8$, where the phenyl ring is a seven electron donor, have been reported by Rosenberg and co-workers in 1996.[24] To my knowledge, there was only one compound, $Os_4Ru(\mu\text{-H})_3(CO)_{12}(\mu_3\text{-}\eta^1\text{:}\eta^6\text{-Ph})P(OMe)_3$, which contains a very rare $\mu_3\text{-}\eta^1\text{:}\eta^6$-Ph (type **F**), that has been reported by Raithby and Lewis in 1997.[25] It has been recently reported by Adams and co-workers that a cluster dimer, $[Ir_4(CO)_{11}]_2(\mu_4\text{-Ag})(\mu\text{-Ag})(\mu_3\text{-}\eta^1\text{:}\eta^3\text{-Ph})(\mu\text{-Ph})$, contains a unique $\mu_3\text{-}\eta^1\text{:}\eta^3$-Ph ligand.[20]

1.23 Metal cluster complexes containing the Aryne ligands

Aryne could be considered as functional group that derived from an aromatic ring that has two unpaired electrons available for bonding. It binds to metal(s) through two σ-bonds. The simplest Aryne group is benzyne, C_6H_4. The bonding mode of benzyne group to metal(s) is more complicated than that of phenyl. (Scheme 1.7) Benzyne can terminally bind to one metal center through two σ-bonds and serves as a two electron donor (type **A**).[26] Benzyne can also σ-bond to two metals, cal it di-σ-bonded, where it donates one electron to each of the two metal centers (type **B**).[27] When benzyne is bonded to three metal atoms, the circumstances can be very different. In one mode, the benzyne serves as a two electron donor, one of the unpaired electrons from benzyne is σ-bonded to one metal to form a two-center two electron bond; another unpaired electron, however, is bonded to the other two metals to form a three center two electron σ-bond (type **C**).[27(a)] The benzyne ligand can also be a four electron donor, both of the unpaired electrons are σ-bonded to two metals (donate one electron to each metal) and the π bond between those two carbon atoms donating two more electrons to the third metal (type **D**) [28] which can be seen as an extension of type B. The benzyne ligand in the Osmium cluster complex, (μ-H)$_2$Os$_3$(CO)$_9$(μ_3-η^2-C_6H_4), shows the above bonding mode; this complex can be obtained by either the reaction of $Os_3(CO)_{10}(NCMe)_2$ with benzene,[29] or the photolysis of $Os_3(CO)_9(\mu_3\text{-}\eta^6\text{-}C_6H_6)$ under 290 nm UV-light irradiation in toluene solvent.[30] The benzyne group has also been found to serve as a six-electron donor in $Ru_4(CO)_{11}(\mu_4$-PPh)(μ_4-η^4-C_6H_4)[31] (type **E**) and a eight-electron donor in $Ru_5(CO)_{13}(\mu_4$-PPh)(μ_5-η^6-C_6H_4) (type **H**).[32] The bonding type **F** and **G** where the Aryne serves as a four electron donor

were found in the compounds $Ru_4(CO)_{10}(\mu\text{-}CO)[\mu_4\text{-}As(C_{10}H_7)](\mu_4\text{-}C_{10}H_6)$,[33] and $Ru_4(\mu_4\text{-}\eta^2\text{-}C_{14}H_8)(CO)_{12}$,[34] respectively.

1.3 Dynamic Behavior in Metal Cluster Complexes

Even though the bonding interactions between metals and carbonyls are very strong, in metal cluster complexes, the carbonyl ligands can easily migrate from one metal to another. The discovery of $Fe_3(CO)_{12}$ not only inspired the enthusiasm of inorganic chemists, but a debating topic on the mechanism of its fluxional behavior was aroused as well. The molecular geometry of $Fe_3(CO)_{12}$ in the crystalline state has revealed, although the structure is disordered (Star of David) in all the cases, there are ten terminal coordinated CO ligands and two doubly bridging CO ligands, on the same Fe-Fe bond, bonded to the Fe_3 triangle. Interestingly, only one kind of carbonyl ligand has been observed in the ^{13}C NMR spectra at room temperature. It has been pointed out by Cotton that the $Fe_3(CO)_{12}$ undergoes rapid CO scrambling in solution, the ^{13}C NMR spectrum shows only a single resonance at -150 ^oC,[35] indicating that the activation energy for this averaging process is very low, < 5 kcal/mol. In order to explain and understand this fascinating fluxionality, numerous mechanisms have been proposed, among which, there were five main stream mechanisms that have drawn more attention as they have shown, to some degree, agreement with the experimental measurements: 1) The Cotton merry-go-round mechanism.[35] 2) The concerted bridge-opening bridge-closing mechanism.[36] 3) The C_2 libration mechanism.[37] 4) The C_3 rotation mechanism.[38] 5) The rotation of either the Fe_3 triangle or the carbonyl icosahedron about a S_{10} axis of the icosahedron through a bridging ligand and an axial ligand on the unbridged iron.[39] Mann[40] has concluded that

the concerted bridge-opening bridge-closing mechanism accounts for the lowest energy dynamic process, which is the same as the mechanism of S_{10} rotation about the axis. This mechanism was strongly supported by the ^{13}C NMR evidence. In contrast, the solid state structures of the other two congeners, $Ru_3(CO)_{12}$ and $Os_3(CO)_{12}$, agree with the IR and ^{13}C NMR spectra in solution which indicated no detectable bridging carbonyl ligands in these two cluster complexes. Nevertheless, the ^{13}C NMR spectra of $Ru_3(CO)_{12}$ also exhibits a single peak which indicates a rapid interchange between the axial and equatorial carbonyl ligands. It has been reported by Aime and coworkers that the activation energy for this inter-site exchange is, considerably low, approximately 20 $kJ \cdot mol^{-1}$.[41] Similarly, the activation energy for the axial-equatorial CO exchange for $Os_3(CO)_{12}$ is considerably higher, approximately 70 $kJ \cdot mol^{-1}$.[42]

There are, not only the carbonyl, but also some other ligands that have been reported to show dynamic exchange behaviors in solution as well. It has been proved that hydrogen, called hydride ligand in metal cluster complexes, migrates easily in metal clusters between different metal-metal bonds.[43] In some cases, the exchange can be very complicated. It has recently been reported that the compound $(\mu\text{-}H)_2Os_3(CO)_{10}(GePh_3)_2$, exhibits only one single resonance for the two inequivalent hydride ligands at room temperature. The variable temperature ^1H NMR measurement has revealed that not only are the two hydride resonances of the isomer found in the solid state are averaged, but there is also a second isomer present in solution at low temperatures which also exhibits two separate hydride resonances (Figure 1.1). The most likely mechanism involves the interchange between three possible isomers as described in Scheme 1.8.[44] Another proposed mechanism involves the polytopal ligand rearrangement,[45] which can't explain

the averaging of the two hydrides in one giving isomer without combination with hydride exchange. By using ^{1}H NMR spin saturation transfer technique, Shapley and co-workers have also reported a very intriguing reversible proton exchange between ring and metal sites in $H_2Os_3(CO)_9(\mu_3\text{-}\eta^2\text{-Aryne})$ compounds.[46] Several larger ligands, for example $GeMe_2$,[47] PMe_2Ph[48] and AsMePh[49] have also been reported to dynamically migrate between the metal atoms in metal cluster complexes. More interestingly, couples of phosphine ligated metal groups have been found to be dynamically averaging as well, particularly Pt-PBu^t_3 group and $AuPPh_3$ group. Adams and co-workers have discovered several attractive metal cluster complexes which contain one or more Pt-PBu^t_3 group(s) and the variable temperature ^{31}P NMR studies have revealed the intriguing dynamic behavior of these Pt-PBu^t_3 groups (Scheme 1.9).[50] Salter and co-workers have investigated the dynamic exchange of phosphine ligated gold groups in some early mixed cluster complexes.[51]

1.4 Metal Cluster Complexes in Catalysis

In addition to the colorful bonding and dynamic activities of metal cluster complexes, the use of metal cluster compounds in catalysis is, beyond a doubt, a more important area of research. Three aspects of metal clusters in catalysis have attracted increasing attention. 1) Metal clusters as models for heterogeneous catalysis; 2) Metal clusters in homogeneous catalysis; 3) Metal clusters in heterogeneous catalysis.

1.41 Metal Clusters as Models for Heterogeneous Catalysis

In a given heterogeneous catalytic process, Infrared spectroscopy, GC or GC-MS are usually used as probes to characterize the product contents. This is what the chemical engineers would mainly focus on. Chemists, more likely, would put their efforts on the mechanism of this process, attempt to gain some deep insight to the surface chemistry to help with designing new catalysts to improve the selectivity, stability of the catalysts and enhance the yield of desired products. In reality, it is almost impossible to capture all of the species on the catalyst surface. Current spectroscopy is not sensitive enough to provide accurate structural information of reaction intermediates. This gives metal cluster complexes a great opportunity to serve as models for the transformations of small molecules on catalyst surfaces, for example, the transformation of carbonyl ligand from a terminally coordinated mode to triply-bridged mode in metal cluster compounds (Scheme 1.10). This has been referred to as the structural cluster-surface analogy. [52]

As an example, the mechanism of the Fisher-Tropsch process has been successfully explained by the transformation of CO to methane in the tri-nuclear osmium cluster compound, $Os_3(CO)_{12}$.[53] Interestingly, deuterated methane can be observed only when deuterium-labeled potassium salt K[BD(O-*i*-Pr)$_3$] was used. In order to gain deeper insight of the Fisher-Tropsch process, a reasonable mechanism was proposed as follows: (Scheme 1.11) The reaction of $Os_3(CO)_{12}$ with K[BD(O-*i*-Pr)$_3$] in the first step has yielded a cluster anion, $[Os_3(CO)_{11}(CDO)]^-$, **1**, which contains an aldehyde group formed through the hydrogen anion insertion to the carbonyl triple bond. The addition of phosphoric acid (H_3PO_4) to this cluster anion has been proposed to yield a neutral intermediate, $Os_3(CO)_{11}$(=CDOH), **2**, which then reacts with **1**, to yield, $[Os_3(CO)_{11}(CD_2OH)]^-$, **3**, which is also an anion and contains a λ^3-D_2-methanol group,

accompanied by the elimination of $Os_3(CO)_{12}$. This λ^3-methanol group will further react with acid, to eliminate one equivalent of water, to yield a neutral compound, $Os_3(CO)_{11}CD_2$,[54] which contains a deuterated methylene group. Upon heating at 70-80 °C under D_2 or H_2 atmosphere, the methylene containing compound decomposed to $Os_3(CO)_{12}$ with the formation of CD_4 or CD_2H_2 respectively.[55]

The trinuclear osmium carbonyl cluster complexes have been considered as ideal candidates for studying of structural cluster-surface analogy. Adams et al. have reported a series of transformations of carbene ligands and activation of C-H and C-S bonds in thiolato-tri-osmium cluster carbonyl complexes.[56] As a representational example, (Scheme 1.12) the compound (μ-H)$Os_3(CO)_9$[C(H)NR_2](μ-SPh), **1**, lost one carbonyl ligand on the un-bridged osmium atom upon irradiation, can be transformed to compound (μ-H)$_2Os_3(CO)_8$[C(H)NR_2](μ_3-SC_6H_4), **2**, and compound (μ-H)$_2Os_3(CO)_8$[μ-C=NR_2](μ-SPh), **3**, through intermediate **A**. Compound **3** can also obtained by heating compound **2** in hexane solution. Heating of compound **3** in octane solution at 125 °C afforded compound (μ-H)$_2Os_3(CO)_8$[C(Ph)NR_2](μ_3-S), **4**, via two possible intermediates **B** and **C** which were not structurally characterized.[56(a)]

The size of metal cluster complexes compared to the bulk material might also be an important consideration for the structural cluster-surface analogy. However, many large metal cluster compounds with considerable sizes have been reported, especially for some osmium,[57] rhodium,[58] platinum[59] and palladium clusters. The highly condensed palladium clusters Pd_{69}[60] and Pd_{145}[61], whose diameters are on the scale of nanometers, have close-packed frameworks and can be described as ccp (cubic close-packed) stacking layers, which is comparable with bulk materials.

1.42 Metal Carbonyl Clusters in Homogeneous Catalysis

Although, the industrial process usually uses heterogeneous catalysts for chemical production and transformations, the true reaction pathways that take place on the local surface of a solid catalyst remain obscure. This is mainly due to the lack of tools for the study of surface chemistry. On the other hand, polynuclear transition-metal carbonyl derivatives are normally soluble in common organic solvents, as they are molecular coordination compounds. As we discussed above, the carbonyl ligands in metal carbonyl cluster complexes can be easily monitored by infrared spectroscopy. Therefore, the use of metal carbonyl clusters in homogeneous catalysis is essential for investigating catalytic mechanisms and the capture and isolation of reaction intermediates.

Considerable numbers of homogeneous catalysts involving metal carbonyl cluster complexes have been reported, including the Fisher-Tropsch process that was discussed above. Among these, the hydrogenation of alkynes has been one of the more thoroughly studied reactions, since alkynes are optimal compounds for use as model substrates for hydrogenation reactions. The direct hydrogenation products are alkenes, thus, the hydrogenation of alkynes can help researchers to study not only the activity of the catalyst, but its selectivity towards the hydrogenation of triple bonds compared with double bonds.[62]

Triruthenium dodecacarbonyl has been found to be a good alkyne hydrogenation catalyst by Valle and co-workers 30 years ago.[63] More ruthenium carbonyl cluster derivatives have been investigated during the past 20 years by researchers. Heteronuclear carbonyl cluster complexes may exhibit synergistic effects between the different metal

atoms. Adams et al. have reported a remarkable ruthenium-platinum cluster compound, $Ru_5(CO)_{15}(\mu_6\text{-}C)PtPBu^t_3$, **1**, in addition to its skeletal rearrangement that have been discussed above, compound **1** has been found to be capable of activating both hydrogen and PhC_2H separately and in combination. As shown in Scheme 1.13, when compound **1** reacts with hydrogen at 97 ℃, it loses a CO and forms the compound $(\mu\text{-}H)_2Ru_5(CO)_{14}(\mu_6\text{-}C)Pt(PBu^t_3)$, **2**. Alternatively, when compound **1** reacts with phenyl acetylene at 40 ℃, it loses two CO ligands and $Ru_5(CO)_{13}(\mu_5\text{-}C)(\mu_3\text{-}PhC_2H)Pt(PBu^t_3)$, **3,** was obtained. Compound **3** was able to further react with hydrogen to form the compound $(\mu\text{-}H)_2Ru_5(CO)_{12}(\mu_5\text{-}C)(\mu_3\text{-}PhC_2H)Pt(PBu^t_3)$, **4**. When compound **4** was treated with CO at room temperature, compound **1** reformed and released one equivalent of styrene. More importantly, they also found that when compound **4** was allowed to react with hydrogen and an excess of PhC_2H in solution, the catalytic formation of styrene was confirmed with 21(2) turnovers/h. By contrast, when the homonuclear cluster $Ru_6(CO)_{17}(\mu_6\text{-}C)$ was treated with hydrogen and PhC_2H under similar conditions, no evidence on the production of styrene was observed.[64]

In another case, Adams and co-workers reported a layer-segregated platinum-ruthenium cluster complex, $(\mu_3\text{-}H)(\mu\text{-}H)Pt_3Ru_6(CO)_{20}(\mu_3\text{-}PhC_2Ph)$, which is capable of selectively hydrogenating diphenylacetylene to produce (Z)-stilbene at a turn over frequency of 47 h^{-1}. As shown in scheme 1.14, the dissociation of one CO ligand from the above compound has generated an unsaturated species, $(\mu_3\text{-}H)(\mu\text{-}H)Pt_3Ru_6(CO)_{19}(\mu_3\text{-}PhC_2Ph)$, **A**, which believed to be catalytic active. The intermediate **A** picks up one equivalent of hydrogen in solution to produce the saturated intermediate, $(\mu_3\text{-}H)_3(\mu\text{-}H)Pt_3Ru_6(CO)_{19}(\mu_3\text{-}PhC_2Ph)$, **B**. When **B** is treated with one equivalent of PhC_2Ph,

intermediate **C**, (μ_3-H)(μ-H)$_2$Pt$_3$Ru$_6$(CO)$_{19}$(μ-PhCCHPh)(PhC$_2$Ph), was formed. They have proposed that the transformation from **B** to **C** is the rate determine step, for the difficulty of adding diphenylacetylene to the already saturated **B** and the simultaneous transfer of one of the hydride ligand to the PhC$_2$Ph group to form a 1,2-diphenylvinyl ligand to reduce the over-saturation. The transfer of second hydride ligand to the 1,2-diphenylvinyl ligand will yield another intermediate, (μ-H)$_2$Pt$_3$Ru$_6$(CO)$_{19}$(μ-stilbene)(μ_3-PhC$_2$Ph), **D**, which loses one equivalent of (Z)-stilbene to complete the catalytic cycle. Detailed evidences for the mechanism and kinetic studies can be found in the reference and the references there in.[65]

1.43 Metal Carbonyl Clusters in Heterogeneous Catalysis

Industry uses heterogeneous catalysts, particularly those containing platinum, for a large majority of its chemical transformations.[66] It has been shown by Sinfelt and co-workers[67] that the bimetallic catalysts, Pt-Re, Pt-Ir and Pt-Sn supported on Al_2O_3 possess superior catalytic activities for petroleum reforming compared to that of monometallic catalysts. These discoveries emphasized the importance of synergism between two different metal species, so called bimetallic effect, and inspired the research interest in bimetallic catalysis systems. The generation of bimetallic nanoparticle catalysts from bimetallic cluster complex precursors has attracted increasing attention based on the following reasons: 1) metal cluster complexes are normally soluble in common organic solvents, the incipient wetness impregnation technique can be used for the preparation of the heterogeneous catalysts; 2) the structure and contents of the metal cluster complexes can be predesigned, so the resulting nanoparticles will have a well-defined integrity and

stoichiometry, 3) the strong metal-metal interactions in the cluster complex precursors allow for the formation of stoichiometrically-precise bi- and multi-metallic nanoparticles on the surface of the support.[68]

As a classic example, Thomas et al.[69] have reported series of single-site, solvent-free catalytic hydrogenation processes by bimetallic nanoparticles which were prepared from bimetallic cluster complexes. Different nanocatalysts, Ru_5Pt_1, $Ru_{10}Pt_2$, Pd_6Ru_6, Ru_6Sn and Cu_4Ru_{12} were prepared from the corresponding metal clusters, by loading the clusters into mesoporous silica supports, such as MCM 41, by making a slurry in some common organic solvents (such as diethyl ether, methylene chloride and acetone), followed by activation of the encapsulated clusters upon heating at ~200 ℃ in vacuo. The hydrogenation of benzoic acid by using above nanocatalysts was tested. Theoretically, three products should be obtained from the hydrogenation of benzoic acid, 1,3-cyclohexa-diene-1-carboxylic acid, cyclohexene-1-carboxylic acid and cyclohexane-carboxylic acid (Scheme 1.15). The completely hydrogenated product cyclohexane-carboxylic acid is desired because it has been used industrially to produce Caprolactam which is a precursor to synthesize Nylon 6 via ROP (Ring Opening Polymerization). The results of this catalytic hydrogenation are shown in a column chart (Figure 1.2), the Ru_5Pt nanocatalyst is superior compared to those Ru-Pd, Ru-Sn and Ru-Cu catalysts for both conversion and selectivity. Interestingly, when larger metal cluster complexes were used as the catalyst precursor, $Ru_{10}Pt_2$ has the same Ru:Pt ratio as Ru_5Pt, an increase in reagent conversion was observed. Remarkably, the catalyst generated from $Ru_{10}Pt_2$ shows almost 100% selectivity for the desired product at almost double the TOF (Turnover Frequency) compared to that generated from the Ru_5Pt cluster.[69]

Hydrogenation of dimethyl terephthalate (DMT) has attracted more attention, because the complete hydrogenation product 1,4-cyclohexanedimethanol (CHDM) is a desired feedstock in industry to produce polyesters. The industrial production of CHDM involves two steps, where a Pd catalyst is used in the first step to produce Dimethyl hexahydro-terephthalate (DMHT); and copper–chromite catalyst is used in the second step to hydrogenate DMHT to produce CHDM accompanied by some by-products (Scheme 1.16). Adams and co-workers have recently reported some interesting nanocatalysts that are capable of hydrogenating DMT to form CHDM in one step. The catalysts were prepared similar to those mentioned above from bimetallic cluster compounds Ru_6Sn and Ru_5Pt, and two new tri-metallic cluster complexes Ru_5PtGe and Ru_5PtSn. As shown in Figure 1.3, some of the catalysts like Ru_6Sn and Ru_5Pt have been shown to possess high activities for the hydrogenation of unsaturated hydrocarbons, for example 1,5-cyclooctadiene and benzene, but were found to be less active or lack of selectivity in the hydrogenation of DMT. On the other hand, the tri-metallic catalyst Ru_5PtSn shows very high conversion and selectivity in the production of CHDM from DMT.[70]

1.5 Summary

Transition metal carbonyl cluster complexes are very important not only in helping researchers to gain deep insight of the mechanisms for small molecule transformation pathways, but also they serve as homogeneous and nanocatalysts precursors for variety of catalytic processes as well. The synthesis of transition metal carbonyl complexes is relatively easy and allows for a variety of modifications, i.e. the

change in structure geometry or control of the stoichiometry can be readily achieved. Furthermore, the dynamics and skeletal fluxionality will help facilitate the understanding of some aspects of the surface chemistry at the atomic level. In this thesis, synthesis and characterization of series of iridium-ruthenium carbonyl cluster complexes with bridging carbonyl ligands, and some intriguing osmium-gold cluster complexes with bridging aryl ligands will be discussed along with some computational molecular orbital analyses that were performed in order to understand the bonding of the ligands to the metal atoms.

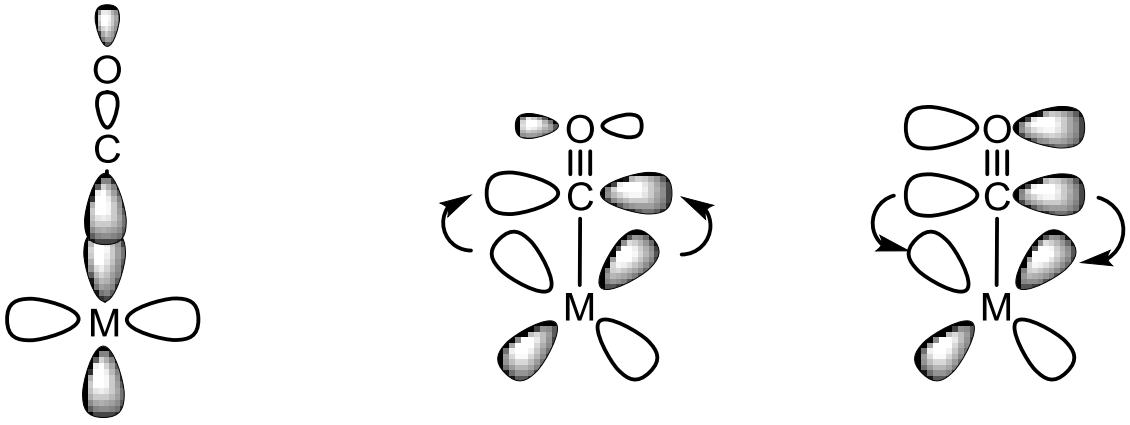

Scheme 1.1. The bonding between a terminal carbonyl ligand and metal atom.

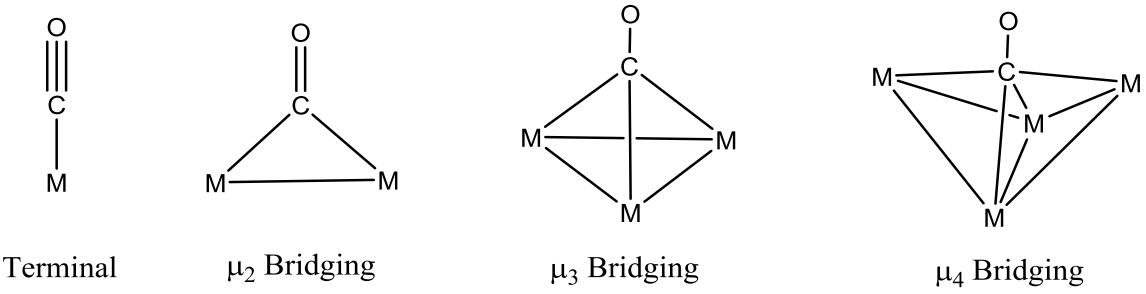

Terminal μ_2 Bridging μ_3 Bridging μ_4 Bridging

Scheme 1.2. Bonding modes of η^1-carbonyl ligand on various metal centers.

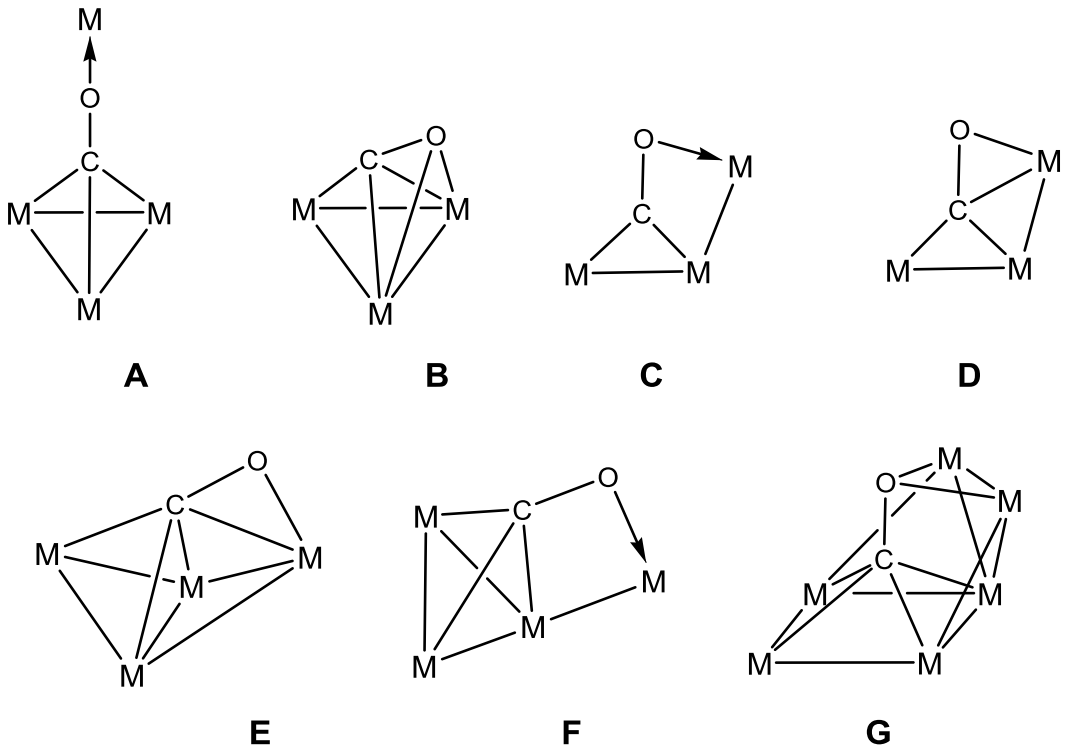

Scheme 1.3. Bonding modes of η^2-carbonyl ligand in different metal clusters.

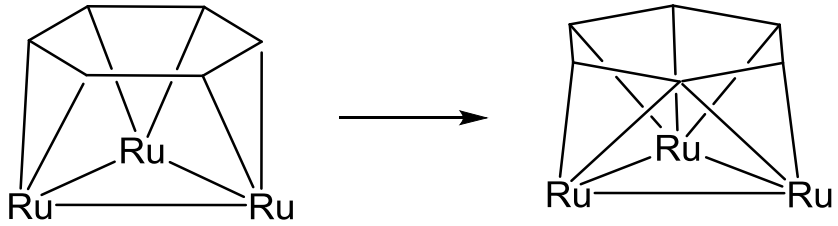

Scheme 1.4. The rotation of benzene ring in compound (μ-H)(RuC_5Me_5)$_3$(μ_3-η^6-C_6H_6).

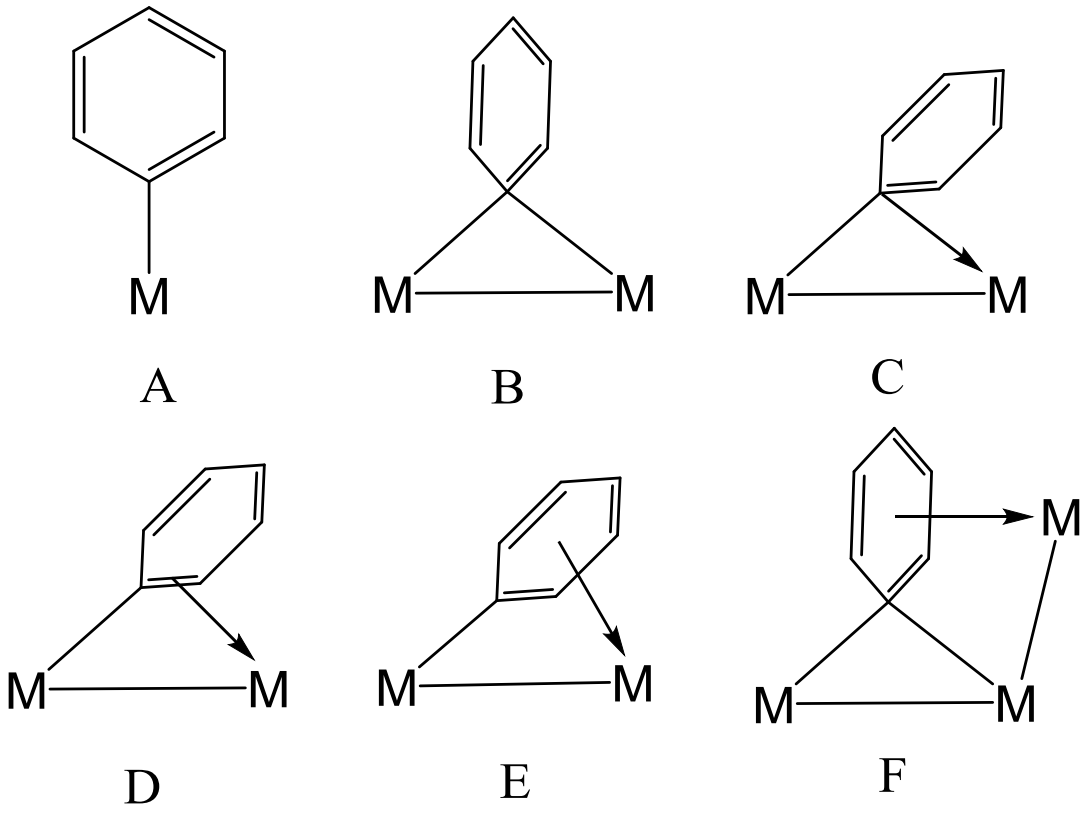

Scheme 1.5. Some of the bonding modes of the phenyl group on metal centers.

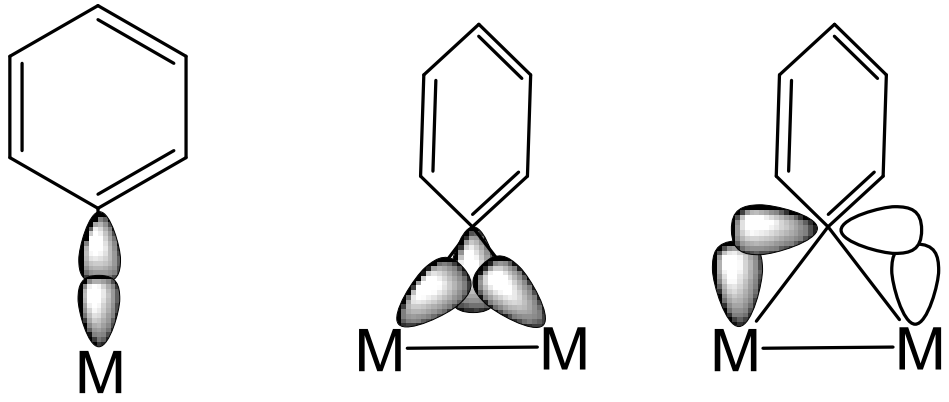

Scheme 1.6. The bonding of η^1-phenyl ligand to metal atoms.

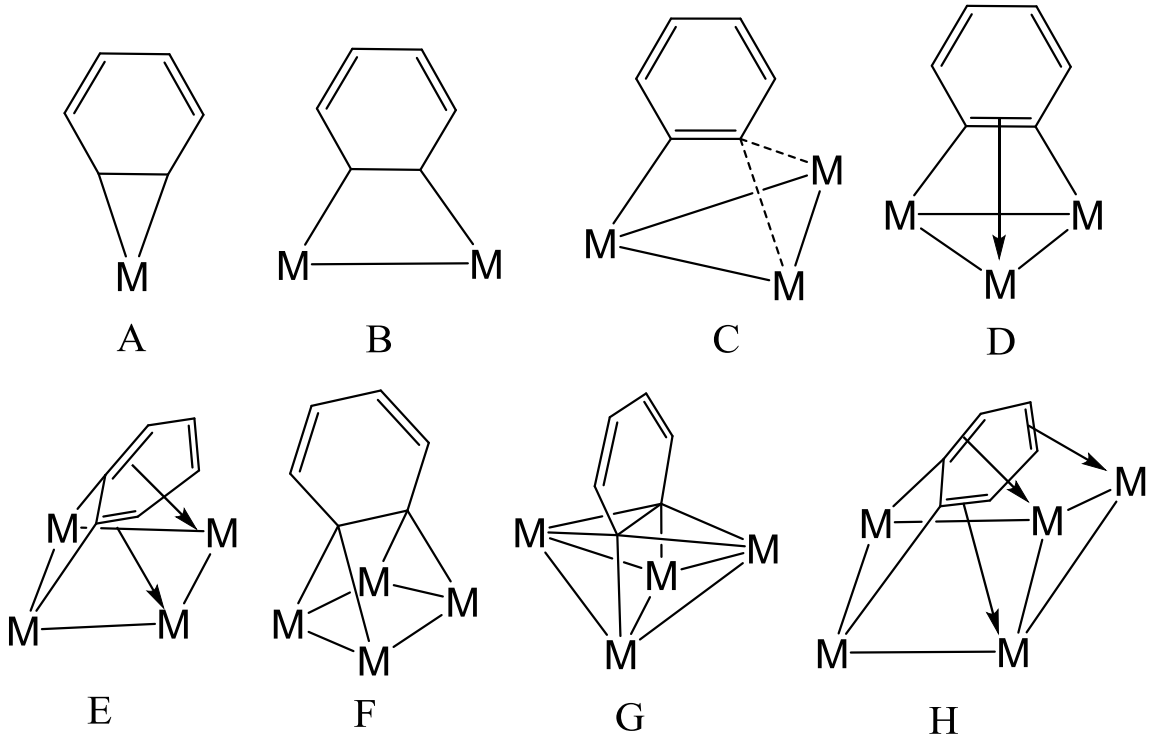

Scheme 1.7. Some of the bonding modes of the benzyne ligand to metal center(s).

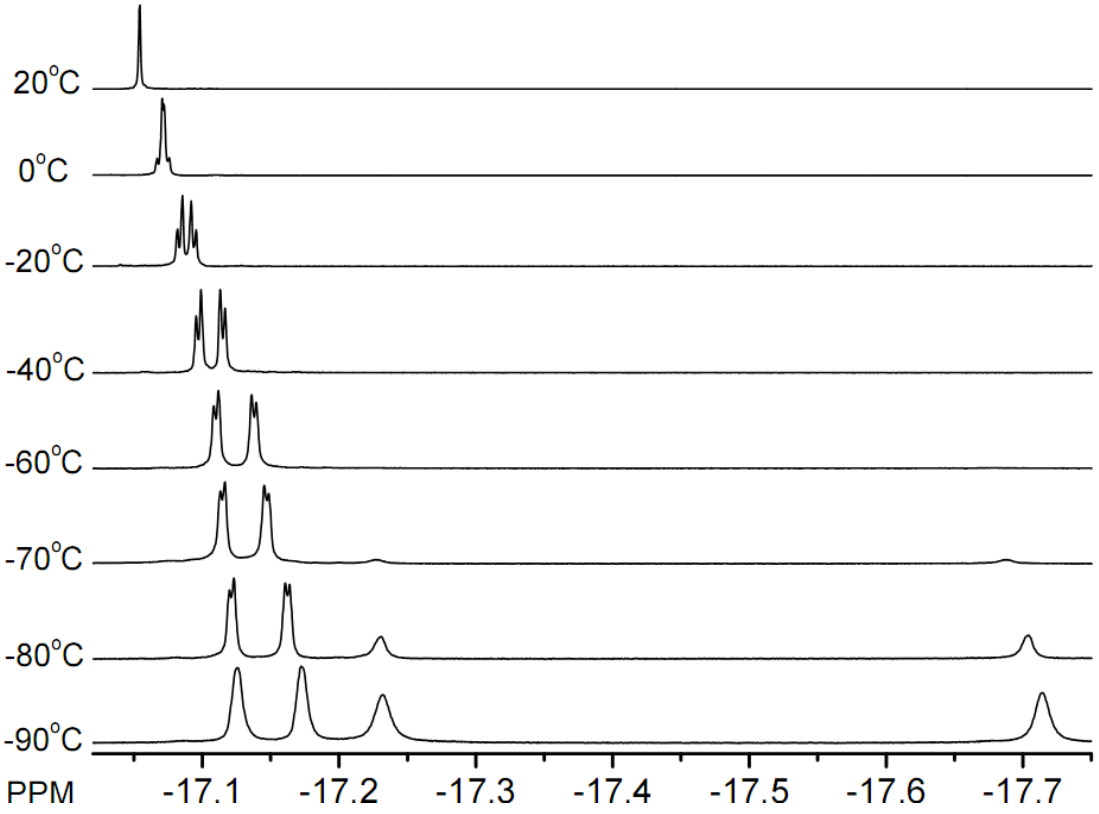

Figure 1.1. Variable-temperature ^{1}H NMR spectra for $(\mu\text{-H})_2Os_3(CO)_{10}(GePh_3)_2$ in CD_2Cl_2 solvent recorded in the high-field region of the spectrum.

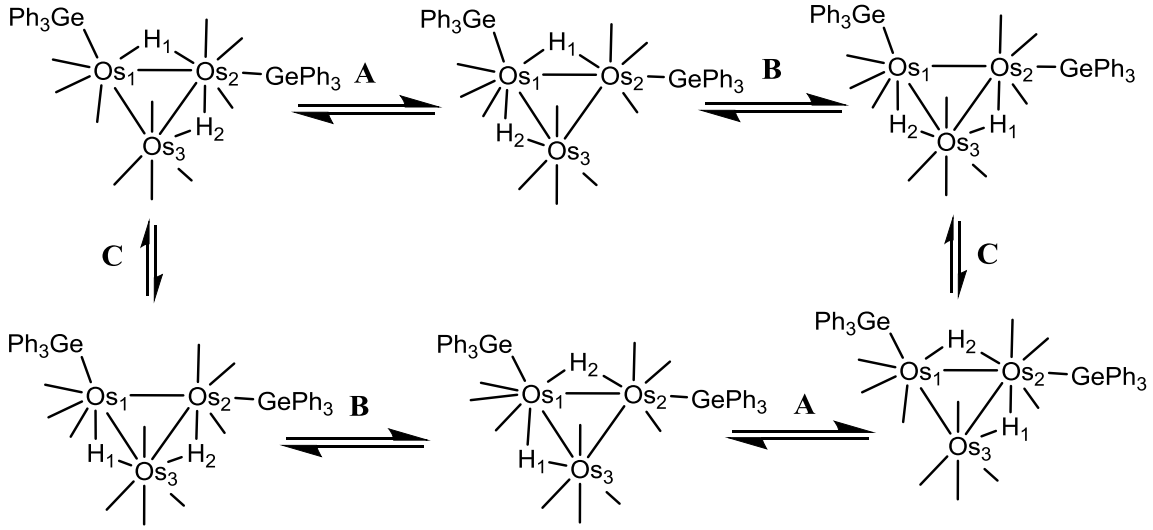

Scheme 1.8. A proposed mechanism for hydrogen averaging mechanism for the compound (μ-H)$_2$Os$_3$(CO)$_{10}$(GePh$_3$)$_2$.

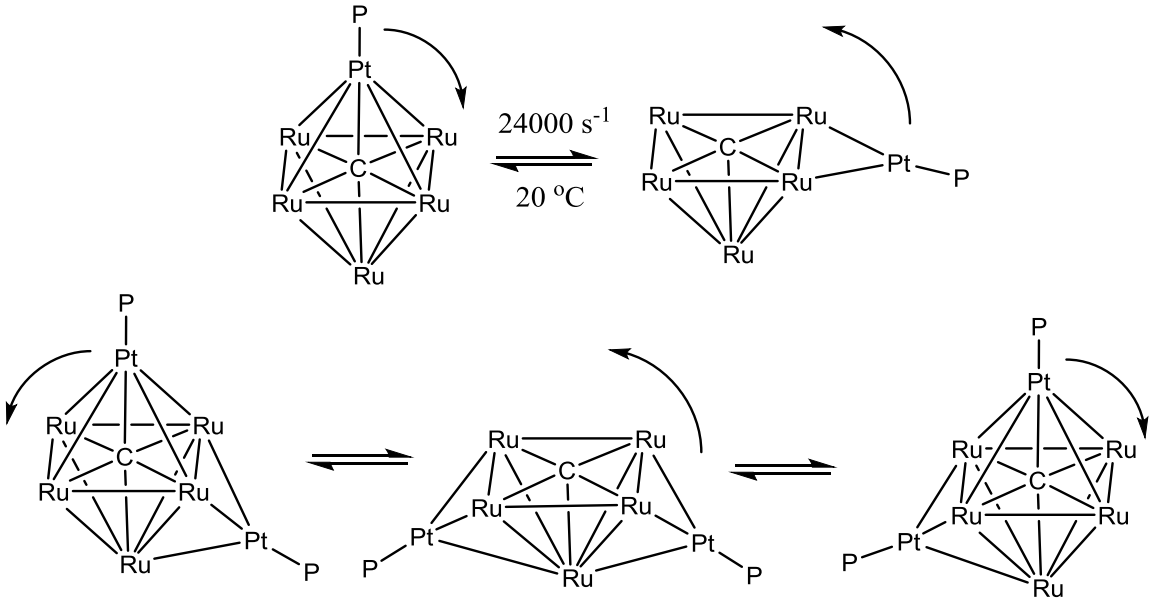

Scheme 1.9. The migration of Pt-P groups in Ru-Pt cluster complexes.

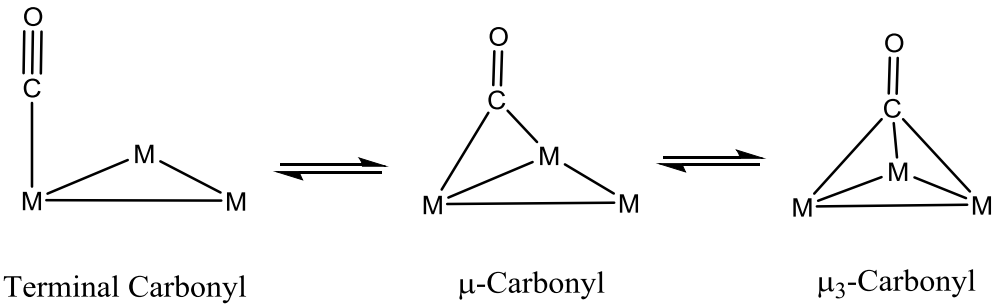

Scheme 1.10. The transformation of a carbonyl ligand about a trimetallic cluster.

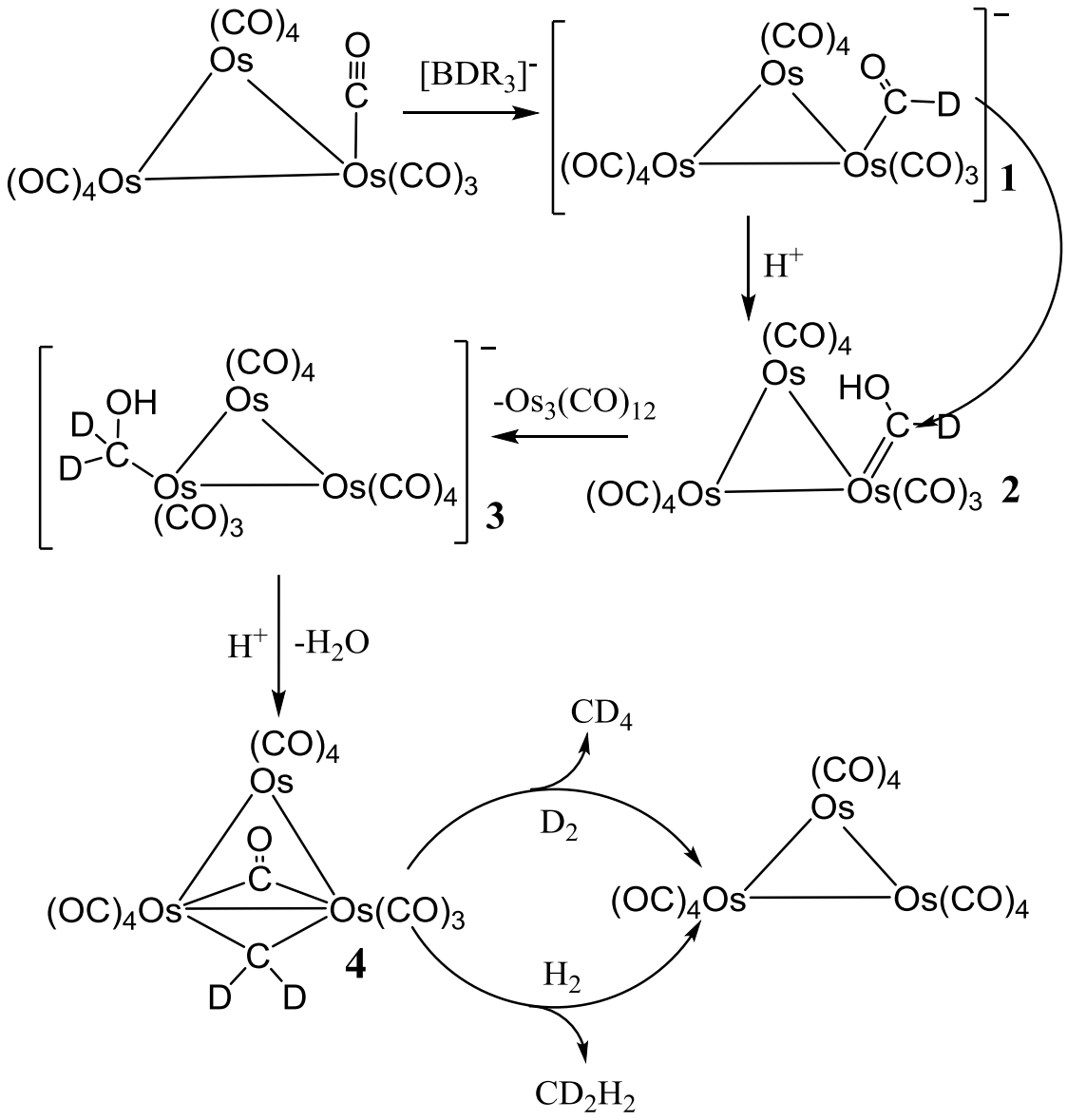

Scheme 1.11. A proposed mechanism for a model Fisher-Tropsch process.

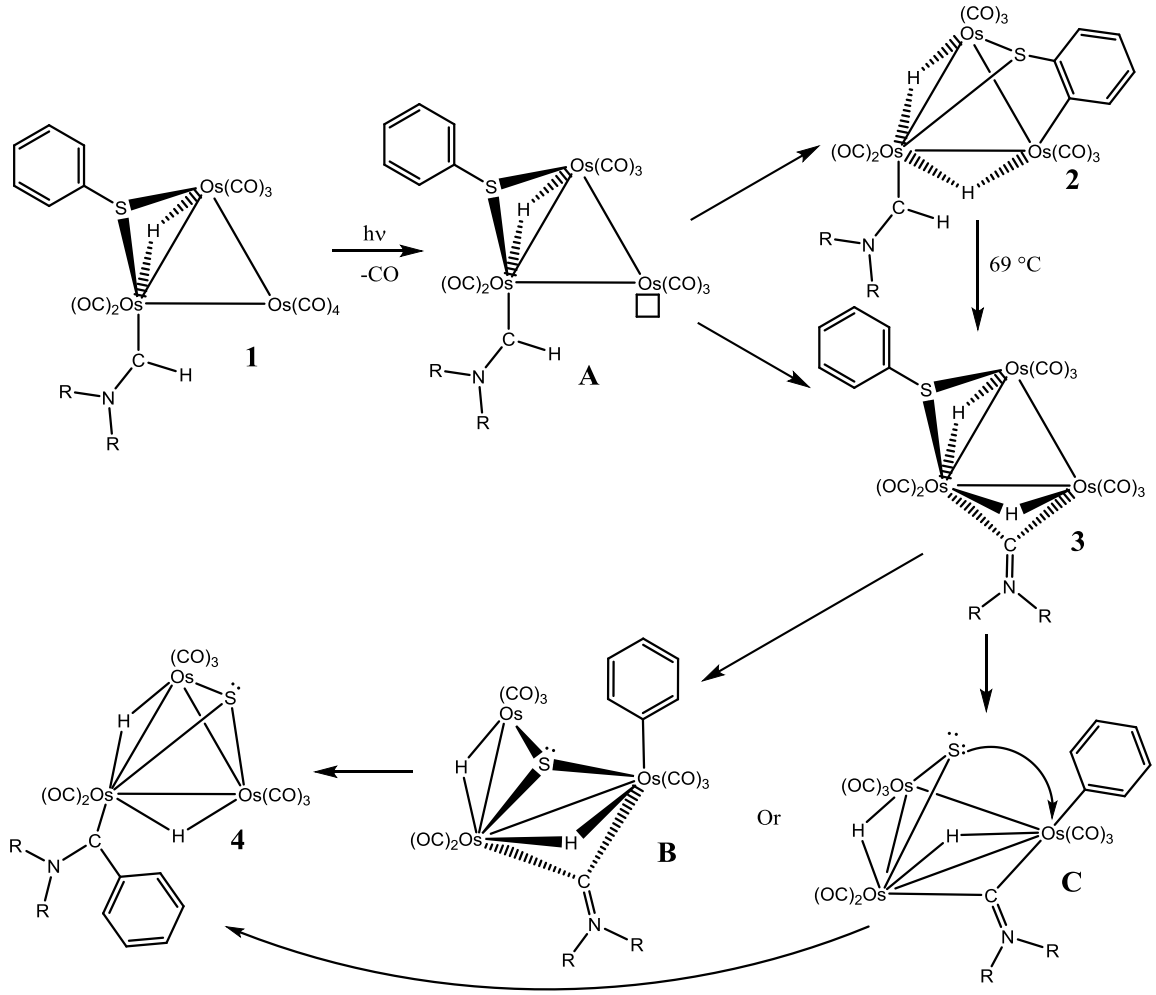

Scheme 1.12. A proposed mechanism for the activation of C-H and C-S bonds in the cluster complex (μ-H)$Os_3(CO)_9$[C(H)NR_2](μ-SPh).

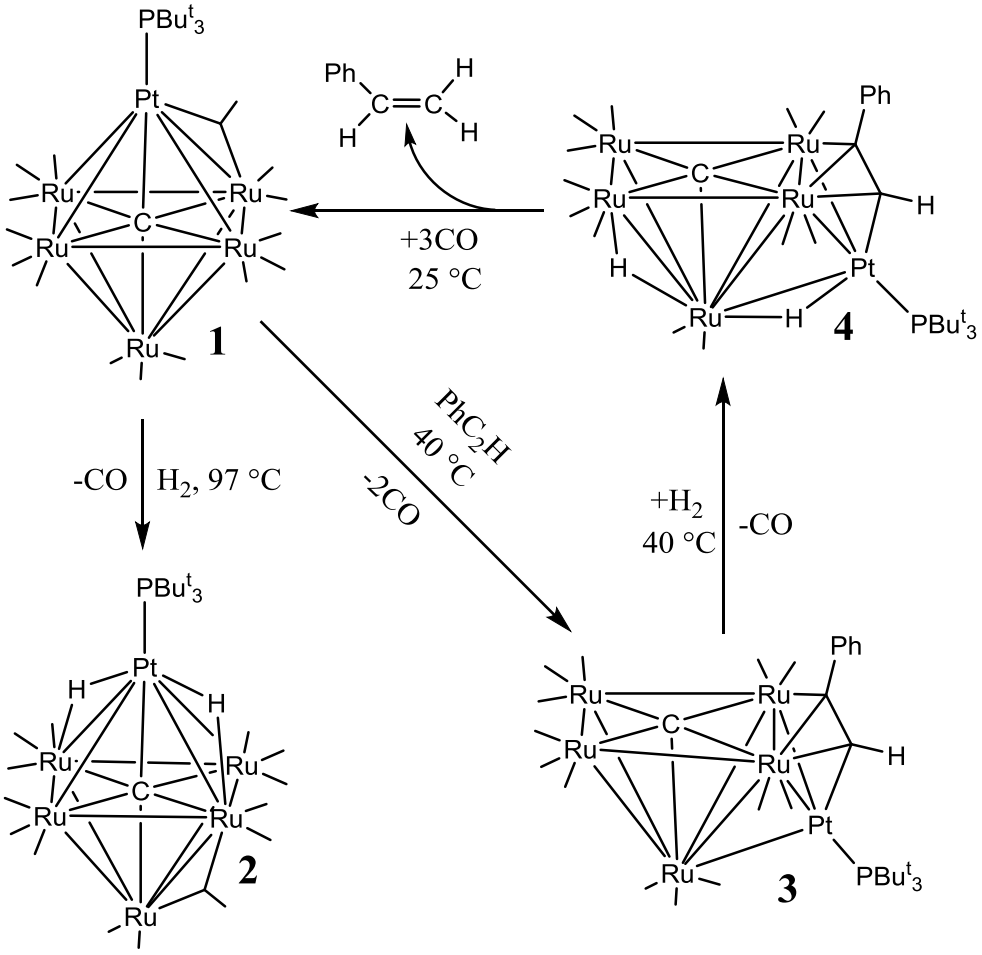

Scheme 1.13. A proposed mechanism for the catalytic hydrogenation of PhC_2H by the octahedral cluster complex $Ru_5(CO)_{15}(\mu_6\text{-}C)PtPBu^t_3$.

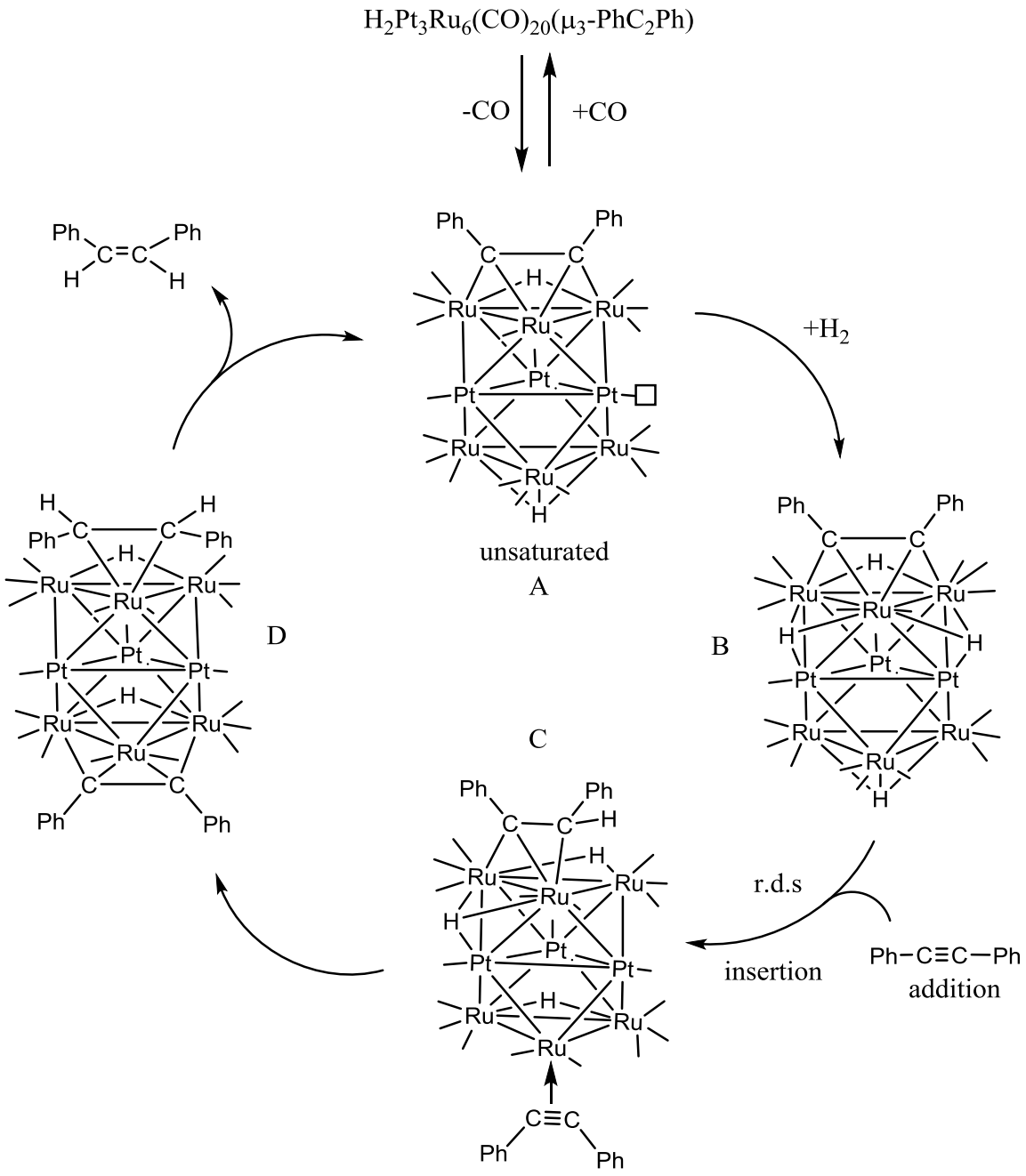

Scheme 1.14. A proposed mechanism for the catalytic hydrogenation of PhC_2Ph by the layer-segregated cluster complex (μ_3-H)(μ-H)$Pt_3Ru_6(CO)_{20}$(μ_3-PhC_2Ph).

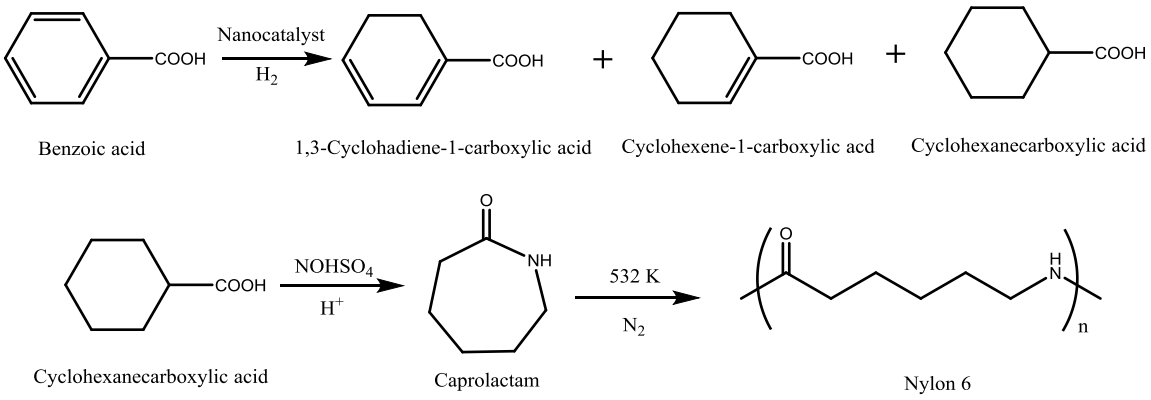

Scheme 1.15. The products from the hydrogenation of Benzoic acid and the industrial use of Cyclohexanecarboxylic acid to produce Nylon 6.

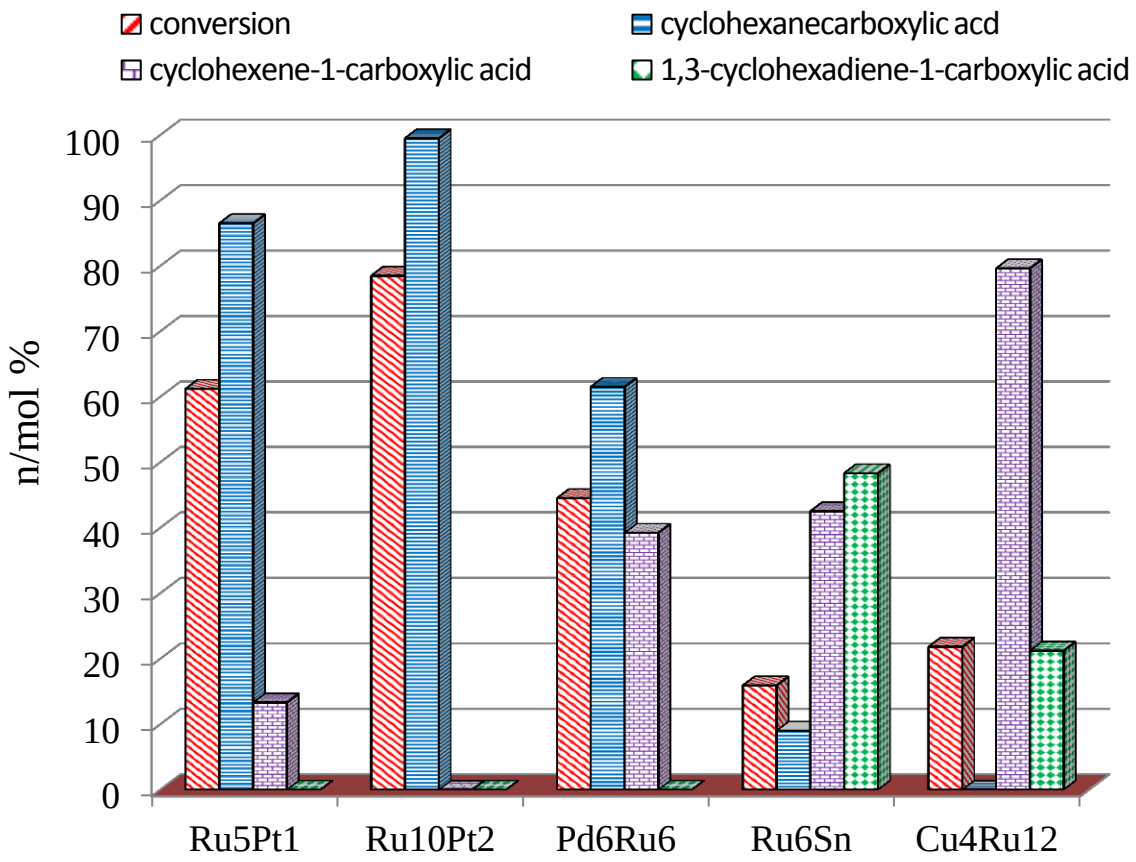

Figure 1.2. Bar chart summarizing the relative performances and selectivities of the Ru_5Pt and $Ru_{10}Pt_2$ catalysts when compared to other bimetallic nanocatalysts for the hydrogenation of benzoic acid.

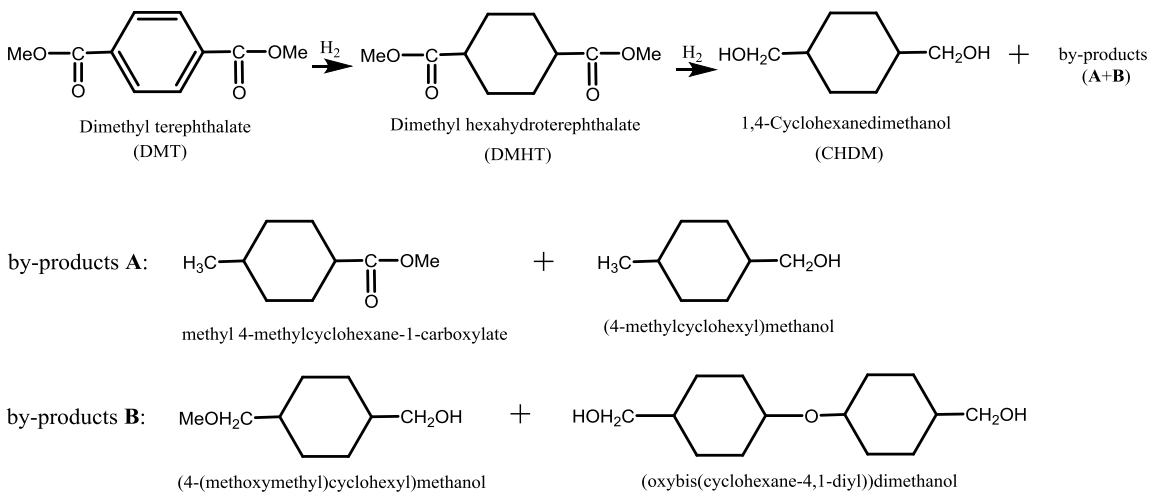

Scheme 1.16. The products from the hydrogenation of Dimethyl terephthalate.

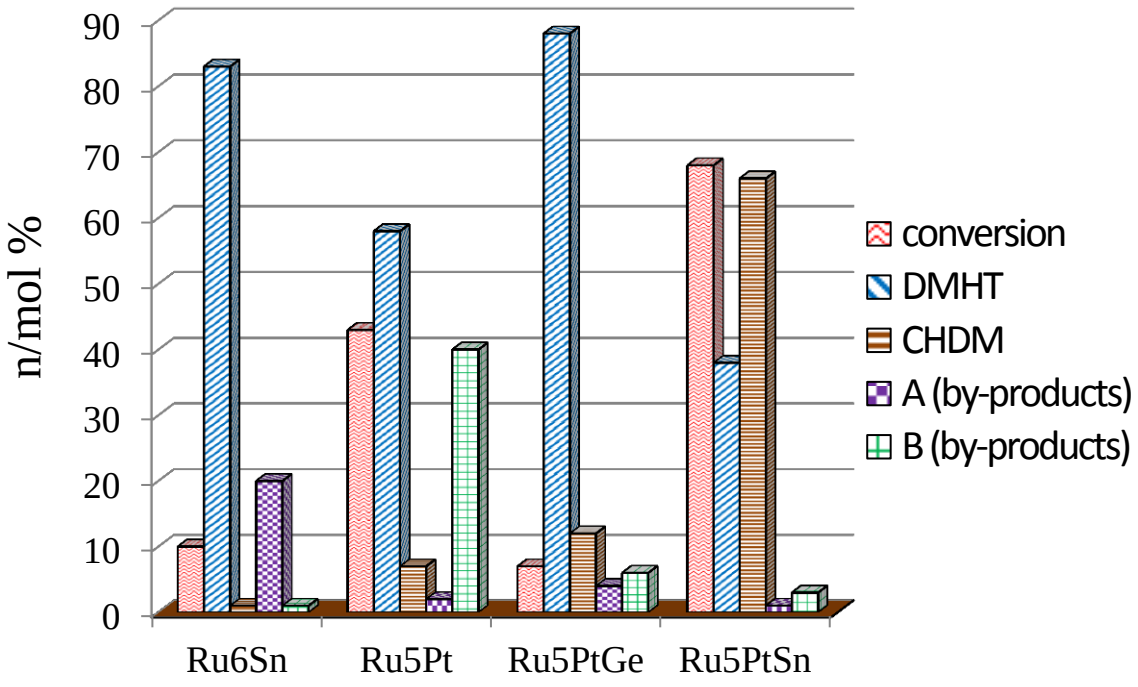

Figure 1.3. Bar chart comparing the activity and selectivity of the Ru_5PtSn catalyst with those of other bi- and trimetallic catalysts for the hydrogenation of DMT.

REFERENCES

1. F. A. Cotton, *Acc. Chem. Res.* **1969**, *2*, 240 − 247.

2. (a) Dewar, J.; Jones, H. O. *Proc. Roy. Soc.* (London), **1905**, *A76*, 558 – 577; (b) Dewar, J.; Jones, H. O. *Proc. Roy. Soc.* (London), **1907**, *A79*, 66 − 80.

3. (a) Wei, C. H.; Dahl, L. F. *J. Am. Chem. Soc.* **1966**, *88*, 1821 − 1822. (b) Wei, C. H.; Dahl, L. F. *J. Am. Chem. Soc.* **1969**, *91*, 1351 − 1361.

4. Corey, E. R.; Dahl, L. F. *J. Am. Chem. Soc.* **1961**, 83, 2203 − 2204.

5. Chini, P.; Albano, V.; Martinengo, S. *J. Organomet. Chem.* **1969**, *16*, 471 − 477.

6. Cotton, F. A.; Wilkinson, G.; Murillo, C. A.; Bochmann, M. *Advanced Inorganic Chemistry*, six ed., Wiley, New York, **1999**.

7. (a) Li, P.; Curtis, M. D. *J. Am. Chem. Soc.* **1989**, *111*, 8279 − 8280. (b) Adams, R. D.; Captain, B.; Pellechia, P. J.; Smith, J. L. Jr. *Inorg. Chem.* **2004**, *43*, 2695 − 2702.

8. (a) Niibayashi, S.; Mitsui, K.; Matsubara, K.; Nagashima, H. *Organometallics* **2003**, *22*, 4885 − 4892. (b) Stutte, B.; Batzel, V.; Boese, R.; Schmid, G. *Chem. Ber.* **1978**, *111*, 1603 − 1618. (c) Schmid, G.; Stutte, B.; Boese, R. *Chem. Ber.* **1978**, *111*, 1239 − 1245. (d) Gambarotta, S.; Stella, S.; Floriani, C.; Chiesi-Villa, A.; Guastini, C. *Angew. Chem., int. Ed.* **1986**, *25*, 254 − 255. (e) Fachinetti, G.; Fochi, G.; Funaioli, T.; Zanazzi, P. F. *Angew. Chem., int. Ed.* **1987**, *26*, 680 − 681.

9. (a) Field, J. S.; Haines, R. J.; Jay, J. A. *J. Organomet. Chem.* **1989**, *377*, C35 − C39. (b) Adams, R. D.; Li, Z.; Lii, J.-C.; Wu, W. *Organometallics* **1992**, *11*,4001 − 4009.

10. (a) Adams, R. D.; Babin, J. E.; Tasi, M. *Inorg. Chem.* **1988**, *27*, 2618 − 2625. (b) Cabeza, J. A.; del Rio, I.; Miguel, D.; Pérez-Carreno, E.; Sánchez-Vega, M. G. *Dalton Trans.* **2008**, 1937 − 1942. (c) Yun, C.; Su, C. J.; Tseng, W. C.; Peng, S. M.; Lee, G. H. *J. Cluster Sci.* **1997**, *8*, 507 − 519. (d) Yun, C.; Su, C. J.; Peng, S. M.; Lee, G. H. *J. Am. Chem. Soc.* **1997**, *119*, 11114 − 11115. (e) Su, P. C.; Chi, Y.; Su, C. J.; Peng, S. M.; Lee, G. H. *Organometallics* **1997**, *16*, 1870 − 1874. (f) Adams, R. D.; Alexander, M. S.; Arafa, I.; Wu, W. *Inorg. Chem.* **1991**, *30*, 4717 − 4723. (g) Gibson, C. P.; Dahl, L. F. *Organometallics* **1988**, *7*, 535 − 543. (h) Chi, Y.; Chuang, S. H.; Liu, L. K.; Wen, Y. S. *Organometallics* **1991**, *10*, 2485 − 2492. (i) Notaras, E. G. A.; Lucas, N. T.; Humphrey, M. G. *J. Organomet. Chem.* **2001**, *631*, 139 − 142. (j) Nahar, S.; Davies, J. E.; Shields, G. P.; Raithby, P. R. *J. Cluster Sci.* **2010**, *21*, 379 − 396. (k) Femoni, C.; Iapalucci, M.C.; Longoni, G.; Zacchini, S. *Dalton Trans.* **2011**, *40*, 8685 − 8694. (l) Horwitz, C. P., Holt, E. M.; Brock, C. P.; Shriver, D. F. *J. Am. Chem. Soc.* **1985**, *107*, 8136 − 8146. (m) Bailey, P. J.; Duer, M. J.; Johnson, B. F. G.; Lewis, J.;

Conole, G.; McPartlin, M.; Powell, H. R.; Anson, C. E. *J. Organomet. Chem.***1990**, *383*, 441 − 461.

11. (a) Brun, P.; Dawkins, G. M.; Green, M.; Miles, A. D.; Orpen, A. G.; Stone, F. G. A. *Chem. Commun.***1982**, 926 − 927. (b) Johnson, B. F. G.; Lewis, J.; McPartlin, M.; Pearsall, M. -A.; Sironi, A. *Chem. Commun.* **1984**, 1089 − 1090. (c) Leung, K. S. -Y. *Inorg. Chem. Commun.* **1999**, *2*, 498 − 502. (d) Leung, K. S. -Y.; Wong, W. T. *J. Chem. Soc., Dalton Trans.* **1997**, 4357 − 4360. (e) Chisholm, M. H.; Folting, K.; Hampden-Smith, M. J.; Hammond, C. E. *J. Am. Chem. Soc.* **1989**, *111*, 7283 − 7285.

12. (a) Herrmann, W. A.; Ziegler, M. L.; Windenhammer, K.; Biersack, H. *Angew. Chem., int. Ed. Engl.*, **1979**, *18*, 960 − 962. (b) Herrmann, W. A.; Biersack, H.; Ziegler, M. L.; Windenhammer, K.; Siegel, R.; Rehder, D. *J. Am. Chem. Soc.* **1981**, *103*, 1692 − 1699.

13. (a) Bailey, P. J.; Johnson, B. F. G.; Lewis, J. *Inorg. Chim. Acta* **1994**, *227*, 197 − 200. (b) Martin, C. M.; Dyson, P. J.; Ingham, S. L.; Johnson; B. F. G.; Blake, A. J. *J. Chem. Soc., Dalton Trans.* **1995**, 2741 − 2748. (c) Anson, C. E.; Bailey, P. J.; Conole, G.; Johnson, B. F. G.; Lewis, J.; McPartlin, M.; Powell, H. R. *J. Chem. Soc., Chem. Commun.*, **1989**, 442 − 444. (d) Shriver, D. F.; Sailor, M. J. *Acc. Chem. Res.* **1988**, *21*, 374 − 379.

14. Bernhardt, E.; Bley, B.; Wartchow, R.; Willner, H.; Bill, E.; Kuhn, P.; Sham, I. H. T.; Bodenbinder, M.; Bröchler, R.; Aubke, F. *J. Am. Chem. Soc.* **1999**, *121*, 7188 − 7200.

15. (a)Johnson, B. F. G. *J. Organornet. Chem.* **1994**, *475*, 31 − 43. (b) Gallop, M. A.; Gomez-Sal, M. P.; Housecroft, C. E.; Johnson, B. F. G.; Lewis, J.; Owen, S. M.; Raithby, P. R.; Wright, A. H. *J. Am. Chem. Soc.*, **1992**, *114* , 2502 − 2509.

16. (a)Johnson, B. F. J.; Lewis, J.; Martinelli, M.; Wright, A. H.; Braga, D.; Grepioni, F. *J. Chem. Soc., Chem. Commun.*, 1990, 364 − 366. (b) Edwards, A. J.; Gallop, M. A.; Johnson, B. F. G.; Köhler, J. U.; Lewis, J.; Raithby, P. R. *Angew. Chem. Int. Ed. Eng.* 1994, *33*, 1093 − 1094. (c) Edwards, A. J.; Leadbeater, N. E.; Lewis, J; Raithby, P. R. *J. Chem. Soc., Dalton Trans.*1995, 3785 − 3787.

17. Inagaki, A.; Takaya, Y.; Takemori, T.; Suzaki, H. *J. Am. Chem. Soc.* **1997**, *119*, 625 − 626.

18. Taylor, N. J.; Chieh, P. C.; Carty, A. J. *J. Chem. Soc., Chem. Commun.*, **1975**, 448 − 449.

19. (a)Cotton, F. A.; Millar, M. *J. Am. Chem. Soc.*, **1977**, *99*, 7886 − 7891. (b) Cotton, F. A.; Lewis, G. E.; Mott, G. N. *Inorg. Chem.*, **1983**, *22*, 560 − 561.

20. Adams, R. D.; Chen, M.; Elpitiya, G.; Yang, X.; Zhang, Q. *Organometallics*, **2013**, *32*, 2416 − 2426.

21. Arce, A. J.; Arrojo, P.; Deeming, A. J.; De Sanctis, Y. *J. Chem. Soc., Chem. Commun.*, **1991**,1491 − 1492.

22. Hoferkamp, L. A.; Rheinwald, G.; Stoeckli-Evans, H.; Süss-Fink, G. *Organometallics*, **1996**, *15*, 704 − 712.

23. Adams, R. D.; Kan, Y.; Zhang, Q. Organometallics, **2011**, *30*, 328 − 333.

24. Kabir, S. E.; Rosenberg, E.; Stetson, J.; Yin, M. *Organometallics*, **1996**, *15*, 4473 − 4479.

25. Al-Mandhary Muna, R. A.; Lewis, J.; Raithby, P. R. *J. Organomet. Chem.* **1997**, *530*, 247 − 250.

26. (a) McLain, S. J.; Schrock, R. R.; Sharp, P. R.; Churchill, M. R.; Youngs, M. J. *J. Am. Chem. Soc.* **1979**, *101*, 263 − 265.(b) Buchwald, S. L.; Watson, B. T.; Huffman, J. C.; *J. Am. Chem. Soc.*, **1986**, *108*, 7411 − 7413. (c) Arnold, J.; Wilkinson, G.; Hussain, B.; Hursthouse, M. B. *Organometallics*, **1989**, *8*, 415 − 420. (d) Bennett, M. A.; Drage, J. S.; Griffiths, K. D.; Roberts, N. K.; Robertson, G. B.; Wickramasinghe, W. A. *Angew. Chem. Int. Ed. Eng.*, **1988**, *27*, 941 − 942.

27. (a) Tinga, M. A. G. M.; Akkerman, O. S.; Bickelhaupt, F.; Horn, E.; Spek, A. L. *J. Am. Chem. Soc.*, **1991**, *113*, 3604 − 3605. (b) Dam, M. A.; Nijbacker, T.; de Pater, B. C.; de Kanter, F. J. J.; Akkerman, O. S.; Bickelhaupt, F.;Smeets, W. J. J.; Spek, A. L. *Organometallics*, **1991**, *16*, 511 − 512. (c) McGhee, W. D.; Foo, T.; Hollander, F. G.; Bergman, R. G. *J. Am. Chem. Soc.*, **1988**, *110*, 8543 − 8545. (e) Adams, R. D.; Pearl, W. C. Jr. *Inorg. Chem.*, **2010**, *49*, 7170 − 7175.

28. (a) Deeming, A. J.; Underhill, M. *J. Chem. Soc. Dalton Trans.*, **1974**, 1415 − 1419. (b) Gainsford, G. J.; Guss, J. M.; Ircland, P. R.; Mason, R.; Bradford, C. W.; Nyholm, R. S. *J. Organomet. Chem.* **1972**, *40*, C70 − C72.

29. Goudsmit, R. J.; Johnson, B. F. J.; Lewis, J.; Raithby, P. R.; Rosales, M. J. *J. Chem. Soc., Dalton Trans.*, **1983**, 2257 − 2261.

30. (a) Gallop, M. A.; Johnson, B. F. G.; Lewis, J.; McCamley, A.; Perutz, R. N. *J. Chem. Soc., Chem. Commun.*, **1988**, 1071 − 1073. (b) Johnson, B. F. G.; Nairn, J. G. M.; Brown, D. B.; Lewis, J.; Gallop, M.; Parker, D. G. *Chem. Eur. J.*, **1995**, *1*, 252 − 260.

31. (a) Bruce, M. I.; Humphrey, P. A.; Snow, M. R.; Tiekink, E. R. T.; Cullen, W. R. *Organometallics*, **1990**, *9*, 2910 − 2919. (b) Zheng, T.; Cullen, W. R.; Rettig, S. J. *Organometallics*, **1994**, *13*, 3594 − 3604.

32. (a) Knox, S. A. R.; Lloyd, B. R.; Orpen, A. G.; Vifias, I. M.; Weber, M. *J. Chem. Soc. Chem. Commum.***1987**, 1498 − 1500. (b) Knox, S. A. R.; Lloyd, B. R.; Morton, D. A. V.; Nicholls, S. M.; Orpen, A. G.; Viñas, J. M.; Weber, M.; Willaims, G. K. *J. Organomet. Chem.***1990**, *394*, 385 − 415.

33. Cullen, W. R.; Rettig, S. J.; Zheng, T. C. *Organometallics* **1995**, *14*, 1466 − 1470.

34. Deeming, A. J.; Speel, D. M. *Organometallics* **1997**, *16*, 289 − 291.

35. Cotton, F. A. *Inorg. Chem.***1966**, *5*, 1083 − 1085.

36. Adams, H.; Bailey, N. A.; Bentley, G. W.; Mann, B. E. *J. Chem. Soc., Dalton Trans.* **1989**, 1831 − 1844.

37. Johnson, B. F. G.; Bott, A. *J. Chem. Soc., Dalton Trans.* **1990**, 2437 − 2444.

38. (a) Dorn, H. C.; Hanson, B. E.; Motell, E. *Inorg. Chim. Acta*, **1981**, *54*, L71 – L73; (b) Hanson, B. E.; Lisic, E. C.; Petty, J. T.; Iannaconne, G. A. *Inorg. Chem.* **1986**, *25*, 4062 − 4064; (c)Gleeson, G. W.; Vaughan, R. W. *J. Chem. Phys.***1983**, *78*, 5384 − 5392.

39. Lentz, D.;Marschall, R. *Organometallics* **1991**, *10*, 1487 − 1496.

40. Mann, B. E. *J. Chem. Soc., Dalton Trans*. **1997**, 1457 − 1471.

41. Aime, S.; Dastrù, W.; Gobetto, R.; Krause, J.; Milone, L. *Organometallics* **1996**, *14*, 4435 − 4438.

42. Forstebr, A.; Johnson, I. G.; Lewis, J.; Matheson, T. R.; Robinson, B. H.; Jackson, W. *J. Chem. Soc. Chem. Commun.*, **1974**, 1042 − 1044.

43. (a) Hyder, M. I.; Begum, N.; Sikder, M. D. H.; Hossain, G. M. G.; Hogarth, G.; Kabir, S. E.; Richard, C. J. *J. Organomet. Chem.*, **2009**, *694*, 304 − 308. (b) Musaev, D. G.; Nowroozi-Isfahani, T.; Morokuna, K. *Organometallics*, **2006**, *25*, 203 − 213.

44. Adams, R. D.; Kan, Y.; Zhang, Q. *Organometallics* **2012**, *31*, 8639 − 8646.

45. Adams, R. D.; Chen, M.; Elpitiya, G.; Zhang, Q. *Organometallics* **2012**, *31*, 7264 − 7271.

46. Kneuper, H.-J.; Shapley, J. R. *Organometallics* **1987**, *6*, 2455 − 2456.

47. Adams, R. D.; Cotton, F. A. *J. Am. Chem. Soc.* **1970**, *92*, 5003 − 5004.

48. (a) Adams, R. D.; Captain, B.; Fu, W.; Pellechia, P. J. *Inorg. Chem.* **2003**, *42*, 3111 − 3118. (b) Adams, R. D.; Captain, B.; Fu, W.; Pellechia, P. J. *Chem. Commun.*, **2000**, 937 − 938.

49. Adams, R. D.; Cotton, F. A.; Cullen, W. R.; Hunter, D. L. *Inorg. Chem.* **1975**, *1*4, 1395 − 1399.

50. (a) Adams, R. D.; Captain, B.; Fu, W.; Pellechia, P. J.; Smith, M. D. *Inorg. Chem.*, **2003**, *42*, 2094 − 2101. (b) Adams, R. D.; Captain, B.; Pellechia, P. J.; Smith, J. L. Jr. *Inorg. Chem.*, **2004**, *43*, 2695 − 2702. (c) Adams, R. D.; Captain, B.; Fu, W.; Pellechia, P. J.; Smith, M. D. *Angew. Chem. Int. Ed.* **2002**, *41*, 1951 − 1953.

51. (a) Brown, S. D. S.; Salter, I. D. *J. Chem. Soc. Dalton Trans.* **1988**, 1795 − 1801. (b) Collins, C. A.; Salter, I. D., Šik, V.; Williams, S. A.; Adatia, T. *J. Chem. Soc., Dalton Trans.*, **1998**, 1107 − 1114. (c) Salter, I. D.; Šik, V.; Williams, S. A.; Adatia, T. *J. Chem. Soc., Dalton Trans.*, **1996**, 643 − 652. (d) Brown, S. D. S.; Salter, I. D. *J. Chem. Soc. Dalton Trans.* **1989**, 1227 − 1236.

52. (a) Muetterties, E. L.; Rhodin, T. N.; Band, E.; Brucker, C. F.; Retzer, W. R. *Chem. Rev.* **1979**, *79*, 91 − 137. (b) Muetterties, E. L. *Bull. Soc. Chim. Belg.* **1976**, *85*, 451 − 470. (c) Muetterties, E. L. *Bull Soc. Chim. Belg.* **1975**, *84*, 959 − 968.

53. Brady, R. C. III; Pettit, R. *J. Am. Chem. Soc.* **1981**, *103*, 1287 − 1289.

54. Churchill, M. R.; Wasserman, H. J. *Inorg. Chem.* **1982**, *21*, 825 − 827.

55. Steinmetz, G. R.; Geoffroy, G. L. *J. Am. Chem. Soc.* **1981**, *103*, 1278 − 1279.

56. (a) Adams, R. D.; Babin, J. E.; Kim, H.-S. *J. Am. Chem. Soc.* **1987**, *109*, 1414 − 1424. (b) Adams, R. D.; Babin, J. E. *Organometallics* **1987**, *6*, 2236 − 2241. (c) Adams, R. D.; Babin, J. E. *Organometallics* **1988**, *7*, 963 − 969. (d) Adams, R. D.; Babin, J. E. *Organometallics* **1988**, *7*, 2300 − 2306. (e) Adams, R. D.; Babin, J. E.; Kim, H.-S.; Tanner, J. T.; Wofe, T. A. *J. Am. Chem. Soc.* **1990**, *112*, 3426 − 3435. (f) Adams, R. D.; Chen, G.; Tanner, J. T.; Yin, J. *Organometallics* **1990**, *9*, 1523 − 1529. (g) Adams, R. D.; Chen, G.; Tanner, J. T. *Organometallics* **1990**, *9*, 1530 − 1538. (h) Adams, R. D.; Pompeo, M. P.; Tanner, J. T. *Organometallics* **1991**, *10*, 1068 − 1078. (i) Adams, R. D.; Chen, G. *Organometallics* **1991**, *10*, 3020 − 3027. (j) Adams, R. D.; Chen, G. *Organometallics* **1991**, *10*, 3028 − 3035. (k) Adams, R. D.; Chen, G. *Organometallics* **1992**, *11*, 837 − 845. (l) Adams, R. D.; Babin, J. E.; Kim, H.-S. *Inorg. Chem.* **1986**, *25*, 4319 − 4320. (m) Adams, R. D.; Babin, J. E. *J. Am. Chem. Soc.* **1987**, *109*, 6872 − 6873. (n) Adams, R. D.; Babin, J. E. *Organometallics* **1987**, *6*,

1364 − 1365. (o) Adams, R. D.; Tanner, J. T. *Organometallics* **1988**, *7*, 2241 − 2243. (p) Adams, R. D.; Chen, G.; Tanner, J. T.; Yin, J. *Organometallics* **1989**, *8*, 2493 − 2495. (q) Adams, R. D.; Chen, G. *Organometallics* **1990**, *9*, 2882 − 2883.

57. Amoroso, A. J.; Gade, L. H.; Johnson, B. F. G.; Lewis, J.; Raithby, P. R.; Wong, W. T. *Angew. Chem. Int. Ed. Engl.* **1985**, *24*, 697 − 698.

58. Fumagalli, A.; Martinengo, S.; Bernasconi, G.; Ciani, G.; Proserpio, D. M.; Sironi, A. *J. Am. Chem. Soc.* **1997**, *119*, 1450 − 1451.

59. (a) Chini, P. *J. Organomet. Chem.* **1980**, *200*, 37 − 61; (b) Ceriotti, A.; Masciocchi, N.; Macchi, P.; Longoni, G. *Angew. Chem. Int. Ed.* **1999**, *38*, 3941 − 3944, (c) Roth, J . D.; Lewis, G. J.; Safford, L. K.; Jiang, X.; Dahl, L. F.; Weaver, M. J. *J. Am. Chem. Soc.* **1992**, *114*, 6159 − 6169.

60. Mednikov, E. G.; Ivanov, S. A.; Slovokhotova, I. V.; Dahl, L. F. *Angew. Chem. Int. Ed.* **2005**, *44*, 6848 − 6854.

61. Tran, N. T.; Powell, D. R.; Dahl, L. F. *Angew. Chem. Int. Ed.* **2000**, *39*, 4121 − 4125.

62. Braunstein, P.; Oro, L. A.; Raithby, P. R. *Metal Clusters in Chemistry*, Wiley, New York, **1999**.

63. Michelin-Lausarot, P.; Vaglio, G. A.; Valle, M. *J. Organomet. Chem.* **1984**, *275*, 233 − 237.

64. Adams, R. D.; Captain, B.; Zhu, L. *J. Am. Chem. Soc.* **2004**, *126*, 3042 − 3043.

65. Adams, R. D.; Barnard, T. S.; Li, Z.; Wu, W.; Yamamoto, J. H. *J. Am. Chem. Soc.* **1994**, *116*, 9103 − 9113.

66. (a) Xiao, J.; Puddephatt, R. J. *Coord. Chem. Rev.* **1995**, *143*, 457 − 500. (b) Dees, M. J.; Ponec, V. *J. Catal.* **1989**, *115*, 347 − 355. (c) Rice, R. W.; Lu, K. *J. Catal.* **1982**, *77*, 104 − 117. (d) Rasser, J. C.; Beindorff, W. H.; Scholten, J. F. *J. Catal.* **1979**, *59*, 211 − 222.

67. (a) Sinfelt, J. H. *Bimetallic Catalysts: Discoveries, Concepts, and Applications*; Wiley, New York, **1983**. (b) Sinfelt, J. H. *Adv. Chem. Eng.* **1964**, *5*, 37 − 74. (c) Sinfelt, J. H. *Sci. Am.* **1985**, *253*, 90 − 98. (d) Sinfelt, J. H.; Via, G. H. *J. Catal.* **1979**, *56*, 1 − 11.

68. (a) Johnson, B. F. G. *Coord. Chem. Rev.* **1999**, *192*, 1269 − 1285. (b) Hills, C. W.; Nashner, M. S.; Frenkel, A. I.; Shapely, J. R.; Nuzzo, R. G. *Langmuir*, **1999**, *15*, 690 − 700.

69. Thomas, J. M.; Johnson, B. F. G.; Raja, R.; Sankar, G. Midgley, P. *Acc. Chem. Res.* **2003**, *36*, 20 − 30.

70. Hungria, A. G.; Raja, R.; Adams, R. D.; Captain, B.; Thomas, J. M.; Midgley, P. A.; Golovko, V.; Johnson, B. F. G. *Angew. Chem. Int. Ed.* **2006**, *45*, 4782 − 4785.

CHAPTER 2

Two Dimensional Bimetallic Carbonyl Cluster Complexes with New Properties and Reactivities

Introduction

Two–dimensional (2–D) bimetallic carbonyl cluster complexes having six or more metal atoms are interesting simply because there are so very few of them.[1,2,3,4] The majority of the planar 2–D cluster complexes contain significant numbers of metal atoms from the copper subgroup having closed (d10) subshells, e.g. **2.1** and **2.2**: $[Au_6Ag(\mu–2,4,6–C_6H_2R_3)_6]^+$, **2.1**, R = $CHMe_2$; $[Cu_5Fe_4(CO)_{16}]^{3–}$, **2.2**, and $Ru_3(CO)_9(\mu–SnPh_2)_3$, **2.3**, etc., see Scheme 2.1, CO ligands are represented only as lines from the metal atoms.2[–4]

In recent studies, our group has been synthesizing bimetallic carbonyl cluster complexes for use as precursors to new selective heterogeneous nanocluster hydrogenation catalysts.[5,6,7] It has been shown that the planar cluster complex **2.3** can be chemisorbed and imaged intact on a monolayer of SiO_2.[8] 2–D clusters are of interest in catalysis because all of the metal atoms lie on the surface. 2–D metal clusters have also been found to exhibit interesting magnetic properties.[9] 2–D molecular clusters may also exhibit interesting physical and reactivity properties that depend on their sizes and shapes. For example, it has been shown that one can add a series of $Pt(P–t–Bu_3)$ groups to the Ru–Sn bonds of complex **2.3** to form an extended 2–D structure.2 The addition of each platinum grouping progressively modifies the absorption of light by the Ru_3Sn_3 cluster. We have now prepared a new 2D transition metal carbonyl cluster that may form

the basis for a series of new complexes that also exhibits interesting optical and reactivity properties that may be traced to its structure and bonding.

Experimental

General Data.

Reagent grade solvents were dried by the standard procedures and were freshly distilled prior to use. Infrared spectra were recorded on a Thermo Nicolet Avatar 360 FT-IR spectrophotometer. Absorption and fluorescence measurements using an Agilent 8453 UV–Visible spectrophotometer and a Varian Cary Eclipse spectrometer, respectively, were performed in CH_2Cl_2 solutions. Mass spectrometric (MS) measurements performed either by direct-exposure probe using electron impact ionization (EI) or electrospray techniques (ES) were made on a VG 70S instrument. $Ir_4(CO)_{12}$, $Ru_3(CO)_{12}$ and $ClAuPPh_3$ were obtained from STREM and were used without further purification. $[PPN][Ir(CO)_4]$[10] and $[PPh_3Au][NO_3]$[11] were prepared according to the literatures. Product separations were performed by TLC in air on Analtech 0.25 and 0.5 mm silica gel 60 Å F_{254} glass plates.

Synthesis of $[PPN][Ru_6Ir(CO)_{23}]$, 2.5

A 230.0 mg amount of $Ru_3(CO)_{12}$ (0.360 mmol) was dissolved in 30 mL THF solvent in a 100 mL three-neck flask. A 100 mg amount of $[PPN][Ir(CO)_4]$ (0.180 mmol) was added, the reaction continued at 66^{o}C for 12 h. The solvent was removed *in vacuo* and the products were isolated by column using pure hexane first to separate unreacted

ruthenium carbonyl, and then pure methylene chloride was used to elute the product to yield 195.8 mg purple [PPN][$Ru_6Ir(CO)_{23}$], **2.5** (91% yield).

Spectral data for **2.5**: IR ν_{CO} (cm^{-1} in CH_2Cl_2): 2060 (vs), 2031 (vs), 1986 (m), 1789 (m). UV-vis (in CH_2Cl_2): 529 nm (ε=15640 $cm^{-1}\cdot M^{-1}$); 674 nm, (ε= 8180 $cm^{-1}\cdot M^{-1}$), see Figure 2.1. Negative ion ES/MS *m*/*z*, 1443, HM^-; 1415, HM^--CO; 1387, HM^--2CO; 1359, HM^--3CO; 1331, HM^--4CO; 1303, HM-5CO.

Synthesis of $Ru_5Ir(CO)_{20}AuPPh_3$, 2.6.

A 30 mg (0.015 mmol) amount of **2.5** was dissolved in a 30 mL methylene chloride solvent in a 100 mL three-neck flask. 8.0 mg (0.015 mmol) [PPh_3Au][NO_3] was added to above solution. The reaction was running at room temperature for 30 min, and the solvent was removed by vacuo. The residue was dissolved in small amount of methylene chloride and isolated by TLC using 1:2 methylene chloride: hexane to give 0.71 mg pink-purple **2.6** (2.8%). 15.2 mg compound **2.5** was recovered from the TLC plate.

Spectral data for **2.6**. IR ν_{CO} (cm^{-1} in CH_2Cl_2): 2116 (w), 2072 (vs), 2040 (vs), 2011 (m), 2000 (w), 1790 (w). ^{31}P NMR(CD_2Cl_2): δ=10.34 (PPh_3). Anal. Calcd for $Ru_5IrAuPO_{20}C_{41}H_{22}$: C, 29.31; H, 1.62; Found: C, 30.87; H, 2.18. Uv-vis (in CH_2Cl_2): 494 nm (ε=14082 $cm^{-1}\cdot M^{-1}$), 520 nm (ε=16858 $cm^{-1}\cdot M^{-1}$) and 649 nm, (ε=3198 $cm^{-1}\cdot M^{-1}$), see Figure 2.2.

Crystallographic Analyses:

Black single crystals of **2.5** suitable for x-ray diffraction analyses were obtained by slow evaporation of solvent from a pure benzene solvent at 4 ℃. Black single crystals of **2.6** suitable for x-ray diffraction analyses were obtained by slow evaporation from a hexane/methylene chloride solvent mixture at -25 ℃. Each data crystal was glued onto the end of a thin glass fiber. X-ray intensity data were measured by using a Bruker SMART APEX CCD-based diffractometer by using Mo Kα radiation (λ = 0.71073 Å). The raw data frames were integrated with the SAINT+ program by using a narrow-frame integration algorithm.[12] Corrections for Lorentz and polarization effects were also applied with SAINT+. An empirical absorption correction based on the multiple measurement of equivalent reflections was applied by using the program SADABS. All structures were solved by a combination of direct methods/Patterson methods and difference Fourier syntheses, and refined by full-matrix least-squares on F^2, by using the SHELXTL software package.[13] All non-hydrogen atoms were refined with anisotropic displacement parameters. Hydrogen atoms were placed in geometrically idealized positions and included as standard riding atoms during the least-squares refinements. Crystal data, data collection parameters, and results of the analyses are listed in Table 2.1. Compounds **2.5** and **2.6** both crystallized in the triclinic crystal system. The space group P $\bar{1}$ was assumed and confirmed by the successful solution and refinement for each of the structures.

Computational Details

All density functional theory (DFT) calculations were performed using the Gaussian 03 suite of *ab initio* programs[14] at the hybrid meta-GGA level of Boese-Martin

kinetics (BMK) functional[15] with all-electron 6-31G(d) basis set for C and O atoms and Stuttgart quasi-relativistic effect core potential basis set for Ru (ECP28MWB) and Ir (ECP60MWB) atoms.[16] We believe such basis sets (1057 basis functions) used in our study are sufficient for accurate DFT calculations. The geometric structure of $[Ru_6Ir(CO)_{23}]^-$, **2.5** was optimized as gas-phase with point symmetric group of D_{3h}. In time-dependent DFT (TDDFT) calculation, 20 singlet excited states were calculated at optimized structures by using the BMK functional and the same basis sets mentioned above. The effect of solvent was taken into account in TDDFT calculation using integral equation formalism polarizable continuum model (IEFPCM) for CH_2Cl_2 (ε = 8.93). The transitions to triplet and higher order multiplet excited states from the ground state are forbidden because the ground states of the species in this study are singlets. Even if some of these forbidden transitions gain intensity by spin-orbit splitting, their intensities in absorption spectrum should still be very weak relative to the transitions to the singlet excited states. Therefore, the detailed effects of spin-orbit coupling do not need to be considered in the calculations for the simulation of the absorption spectrum.

Results and Discussion

The reaction of $[PPN][Ir(CO)_4]$ with $Ru_3(CO)_{12}$ in equimolar amounts has been reported to yield the anionic tetranuclear cluster complex $[IrRu_3(CO)_{13}]^-$, **2.4**, which has been shown to have a tetrahedral shape.[17] Interestingly, however, when $[PPN][Ir(CO)_4]$ was allowed to react with two equivalents of $Ru_3(CO)_{12}$, the new monoanionic cluster complex $[IrRu_6(CO)_{23}]^-$, **2.5**, was formed and was isolated as its PPN salt in 91% yield (Note: Anion **2.5** can also be obtained from **2.4** by reaction with one additional equivalent

of $Ru_3(CO)_{12}$). An ORTEP diagram of the molecular structure of anion **2.5** is shown in Figure 2.1. All seven metal atoms lie in a plane (max deviation = 0.043(1) Å) with the iridium atom in the center circumscribed by a hexagonal ring of six ruthenium atoms. The six Ir–Ru distances range from 2.8585(8) Å to 2.9045(8) Å and are significantly longer than those found in **2.4**, (ave 2.75 Å).[17] The Ru–Ru distances are all similar, range 2.8712(11) Å – 2.9068(10) Å, despite the fact that three of the Ru–Ru bonds contain a bridging CO ligand and the other three do not. Each Ru atom contains three terminal CO ligands; one that lies in the $IrRu_6$ plane and two lie perpendicular to it on opposite sides. The iridium atom contains only two CO ligands that lie on opposite sides and perpendicular to the $IrRu_6$ plane.

The metal–metal bonding of planar metal clusters frequently violates the traditional electron counting rules and such is the case with **2.5**. The anion **2.5** contains 104 valence electrons while both the EAN rule and the PSEP theory predict a total of 102 electrons for this structure.[1a,18] In order to understand the metal–metal bonding in **2.5** a series of geometry-optimized DFT molecular orbital calculations were performed.[19] The key molecular orbitals of **2.5** are shown in Figure 2.5 and 2.6. The in plane σ–bonding between the Ir and Ru atoms is nicely represented by the orbitals: HOMO–5, HOMO–6, HOMO–7, HOMO–8, HOMO–14, HOMO–15, HOMO–16, HOMO–23, HOMO–24, and the HOMO–26. The out of plane π–bonding between the Ir and Ru atoms is nicely represented by the orbitals: HOMO–1, HOMO–2, HOMO–27 and HOMO–28. The HOMO contains no interactions with the Ir atom and is Ru–Ru antibonding. Although there are significant bonding interactions between the ruthenium atoms and the bridging CO ligands, the HOMO contributes very little to the stabilization of the metal cluster.

However, because this orbital is filled the complex contains two more electrons than expected by the conventional bonding theories.

Computed Molecular Orbitals are shown in Figure 2.5 and 2.6. Different density functional may lead slightly different distribution of molecular oribtals. As shown in the figures for the molecular orbitals obtained from the BMK functional, the LUMO and LUMO+1 of $Ru_6Ir(CO)_{23}^-$ are degenerate E' orbitals and derived mainly from the d_{xy} and d_{x2-y2} orbitals of Ir and Ru. The HOMO has a'_2 symmetry and shows the interaction between two $Ru(CO)_3$ fragments and their bridging CO. There is no atomic orbital component of Ir in the HOMO of $Ru_6Ir(CO)_{23}^-$. HOMO−1 and HOMO−2 are degenerate e' orbitals and show strong interactions between Ir and Ru through the mixing of d orbitals. HOMO−5 and HOMO−6, as well as HOMO−7 and HOMO−8, are also degenerate e' orbitals that show the interaction between $Ru_2(CO)_7$ fragments and their interaction with Ir.

Complex **2.5** is highly colored and exhibits two broad absorptions in the visible region of the spectrum, see Figure 2.2. The absorptions were simulated by TDDFT computations.[19] The dominant absorption at 529 nm (ε =15640 cm^{-1}·M^{-1}) arises from an allowed transition from the A_1' HOMO–3 to the degenerate E′ LUMO/LUMO+1 pair (λ_{calcd}= 525 nm, oscillator strength = 0.3172). This transition may contain an element of metal to metal charge transfer from the Ru_6 ring to the central Ir atom, because the HOMO–3 orbital contains no contributions from the Ir atom and the E' excited state does contain Ir contributions. The broad absorption at 674 nm, (ε = 8180 cm^{-1}·M^{-1}) arises from a transition from the degenerate E′ HOMO–1/HOMO–2 to the E′ LUMO/LUMO+1 pair (λ_{calcd} = 705 nm, oscillator strength = 0.02).

TDDFT calculated singlet excited state energies of $Ru_6Ir(CO)_{23}^-$ are listed in Table 2.2. HOMO and LUMO are orbitals 218 and 219. It can be seen that the degenerate excited state 7 and 8 at 525 nm which have the greatest oscillator strength, match well with the observed strong absorption peak at 530 nm, see Figure 2.7. The degenerate excited states 3, 4 and 5 are at 705 nm with much smaller oscillator strength, correspond to the observed weaker absorption peak at 675 nm. Other calculated weak transitions may not be able to be observed experimentally because the small oscillator strength is too small. The observed very high absorption peak at 230 nm is not calculated due to limitations of the computational facility.

Even more interestingly, anion **2.5** exhibits a rare luminescence in the 350 nm regions when excited with 235 nm or 275 nm radiation, see Figure 2.3. Luminescence in metal carbonyl cluster complexes is very rare. In most cases, luminescence by metal carbonyl cluster complexes is created by attaching a luminophore as a ligand or a tag.[20] The luminescence in **2.5** may be related to its unusual 2D structure and the existence of delocalized virtual π–orbitals. Calculations to identify the relevant transitions are currently in progress. The related nonplanar anion **2.4** exhibits no luminescence.

In an attempt to obtain an uncharged derivative of **2.5**, the anion was treated with $[PPh_3Au][NO_3]$ in CH_2Cl_2 solvent. From this reaction solution, the pink/purple compound $Ru_5Ir(CO)_{20}AuPPh_3$, **2.6** was isolated. The yield of **2.6** is low (3%) and there is an intermediate that has not yet been fully characterized. This purple intermediate exhibits CO absorption in the IR spectrum in CH_2Cl_2 (cm^{-1}) at 2119(w), 2086(s), 2071(m), 2042(vs), 2030(w,sh), 2010(w), 1976(w), 2995(w,br), 1789(w,br), the IR spectrum is shown in Figure 2.4. This compound slowly decomposes to regenerate **2.5**

and small amounts of **2.6**. Compound **2.6** was characterized structurally by a single crystal X–ray diffraction analysis and an ORTEP diagram of the molecular structure of **2.6** is shown in Figure 2.8. All of the metal atoms lie virtually in the same plane. The Au atom exhibits the greatest deviation from the best least-squares plane, 0.140(1) Å. The Ir–Ru and Ru–Ru distances are similar to those in **2.5**. The Au–M distances are significantly shorter, Ir(1)–Au(1) = 2.6580(12) Å, Ru(1)–Au(1) = 2.7480(17) Å, Ru(5)–Au(1) = 2.7403(17) Å.

Complex **2.6** contains only 102 valence electrons, and the HOMO and HOMO–1, see Figure 2.9, show significant in plane σ– and π–bonding between the Ir and Au atoms that could help to explain the shortness of the Ir–Au bonds. Some frontier molecular orbital diagrams of $Ru_5Ir(CO)_{20}AuPPh_3$ are shown in Figure 2.9. The LUMO and LUMO+1 of $Ru_5Ir(CO)_{20}AuPPh_3$ have almost equal contributions from the metal atoms. The HOMO, HOMO−1 and HOMO−2 show strong interactions between Au, Ru and Ir atoms with similar contributions from the *d* orbitals of metal atoms and the *p* orbitals of two bridging CO groups. HOMO−4 and HOMO−5 are primarily formed from the *d* orbitals of Ru and Ir without many contributions from Au. The bonding interactions between the $Ru_5Ir(CO)_{20}$ and $AuPPh_3$ fragments are also displayed in other selected molecular orbitals shown in Figure 2.10. The HOMO−34, HOMO−35, HOMO−36, HOMO−40, HOMO−41 as well as HOMO−47, show both the σ- and π- bonding of the $AuPPh_3$ group with the center Ir atom indicating the interaction between these two atoms is very strong.

The transformation of **2.5** to **2.6** is intriguing because it represents the complete replacement of one of the ring Ru(CO) groups with an $Au(PPh_3)$ group by the formal elimination of $Ru(CO)_5$, see Scheme 2.2 where the CO ligands are shown simply as lines. Interestingly, compound **2.6** also exhibits a significant absorption in the visible region of the spectrum: two overlapping at 494 nm (ε = 14082 cm^{-1} M^{-1}), 520 nm (ε = 16858 cm^{-1} M^{-1}) and one broad absorption at 649 nm, (ε = 3198 cm^{-1} M^{-1}), see Figure 2.11. These absorptions were also accurately simulated by TDDFT calculations, see Figure 2.12.

TDDFT calculated singlet excited-states of $Ru_5Ir(CO)_{20}AuPPh_3$ with stronger oscillator strengths are summarized in Table 2.3. The HOMO and LUMO are orbitals 267 and 268. We can see the excited state 7 and 8 are the strongest transitions of $Ru_5Ir(CO)_{20}AuPPh_3$ with oscillator strengths of 0.3 and 0.2. Compare to the degenerate excited state 7 and 8 of $Ru_6Ir(CO)_{23}^-$, the 7^{th} and 8^{th} excited states of $Ru_5Ir(CO)_{20}AuPPh_3$ blue-shifted about 50 nm and have about 20 nm difference in wavelength. The first two excited states are primarily the transitions from HOMO to LUMO and LUMO+1. Although the oscillator strengths of these transitions are weak, they should be able to be observed in experiment.

As already demonstrated with **2.3**,[8] it may be possible to fix these 2D clusters on supports and study their catalytic properties. It should also be possible to synthesize complexes related to **2.5** and **2.6** having different metal–ligand combinations both in the center of the cluster and in the ring itself that may exhibit interesting absorption and emission properties.

Summary

Two dimensional metal cluster complexes are very intriguing for they are candidates to mimic the surface of heterogeneous catalysts. The new 2-D cluster complex, $Ru_6Ir(CO)_{23}^-$, **2.5**, which is a wheel-like cluster compound containing only transition metal and carbonyl ligands, can be obtained in very high yield from both the mono iridium anion**, [**$Ir(CO)_4]^-$, and the bimetallic anion $[IrRu_3(CO)_{13}]^-$. A metal substitution reaction occured when **2.5** was reacted with $[AuPPh_3]^+$, to yield the compound $Ru_5Ir(CO)_{20}AuPPh_3$, **2.6**. Compound **2.6** is also a 2-D wheel-like complex. Computational analyses were performed in order to obtain a deeper insight into the bonding in these unique 2-D cluster complexes. These 2-D complexes may serve as homogeneous or precursors of heterogeneous catalysts in the future.

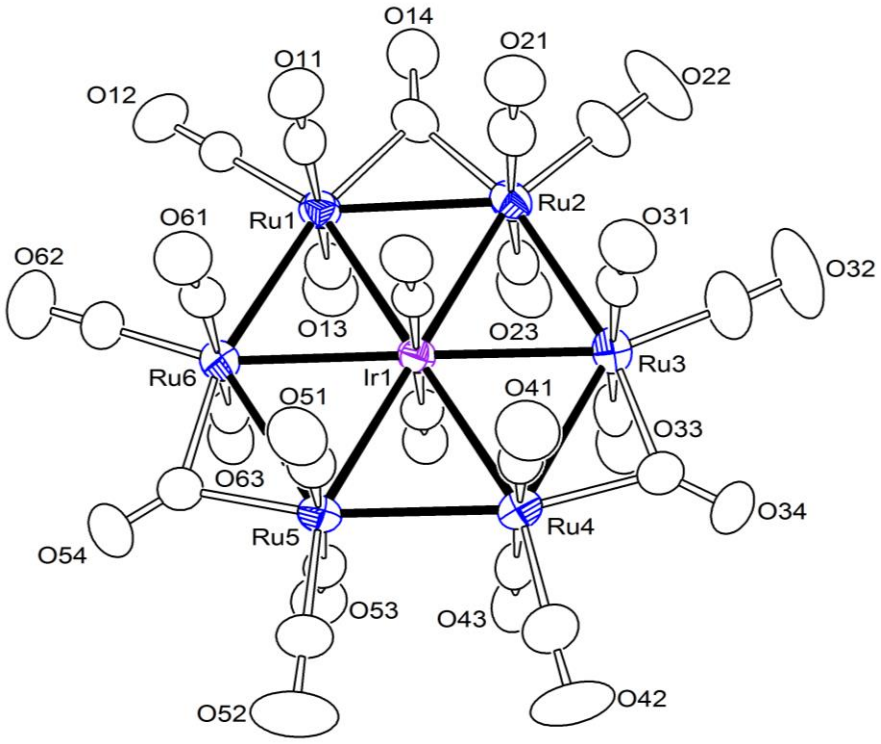

Figure 2.1. An ORTEP diagram of cluster anion $[Ru_6Ir(CO)_{23}]^-$, **2.5**, showing 40% thermal probability.

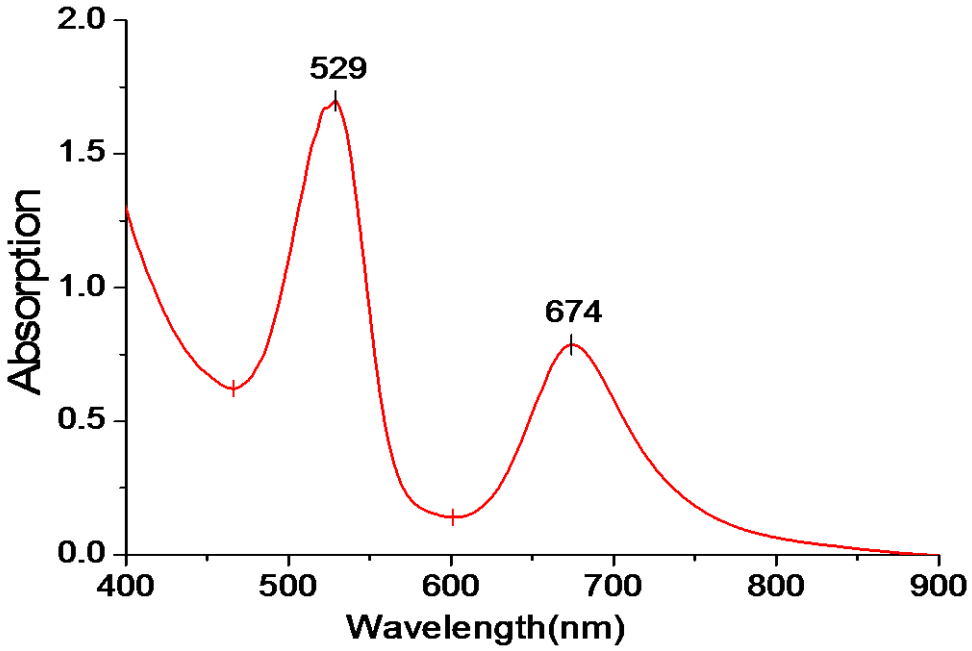

Figure 2.2. UV-vis absorption spectrum of **2.5** in CH_2Cl_2 solvent.

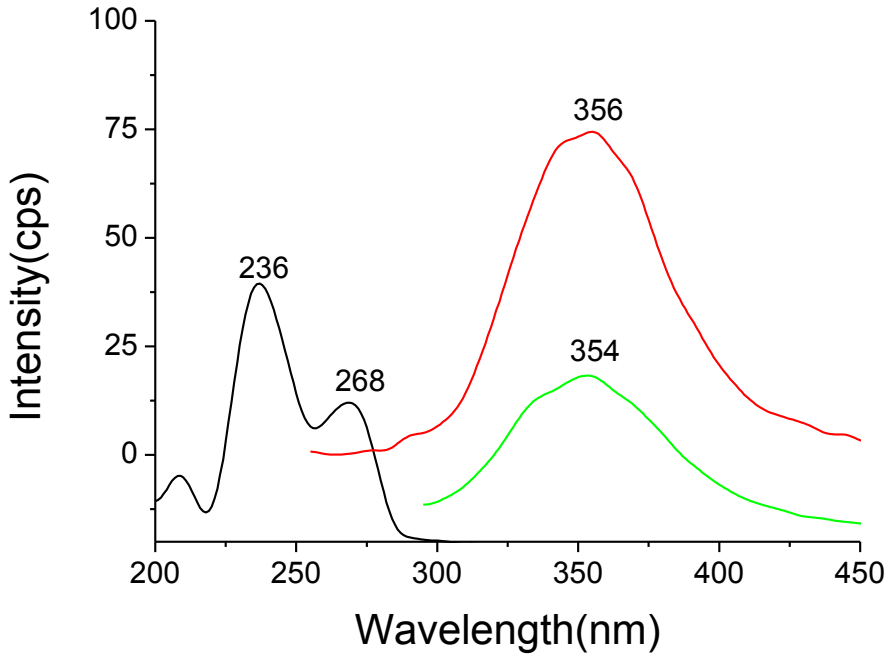

Figure 2.3. Excitation (black, left) and emission spectra for **2.5** (blue, 275nm excitation) and (red, 235 excitation) in CH_2Cl_2 solvent.

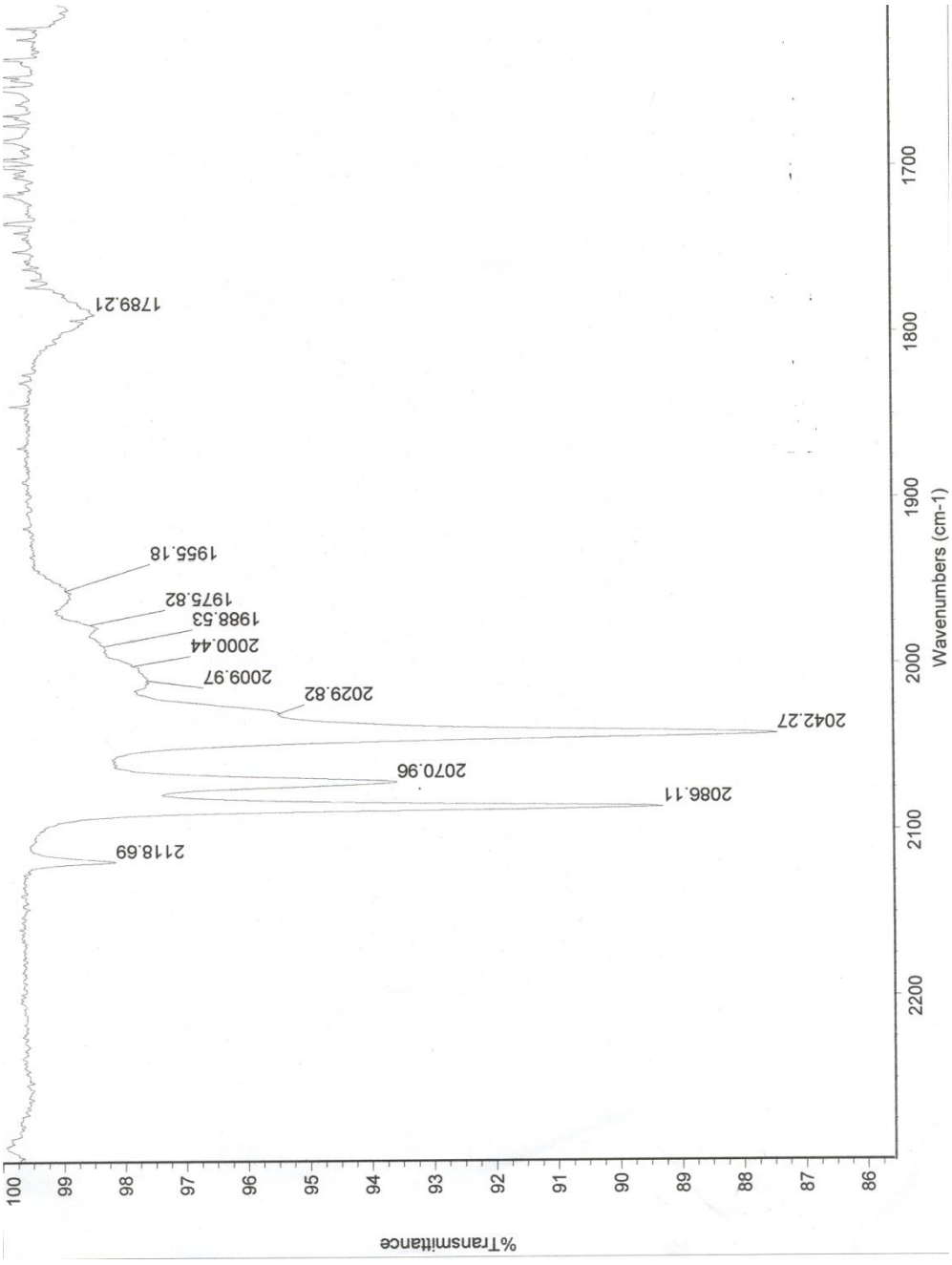

Figure 2.4. The infrared spectrum of the purple intermediate.

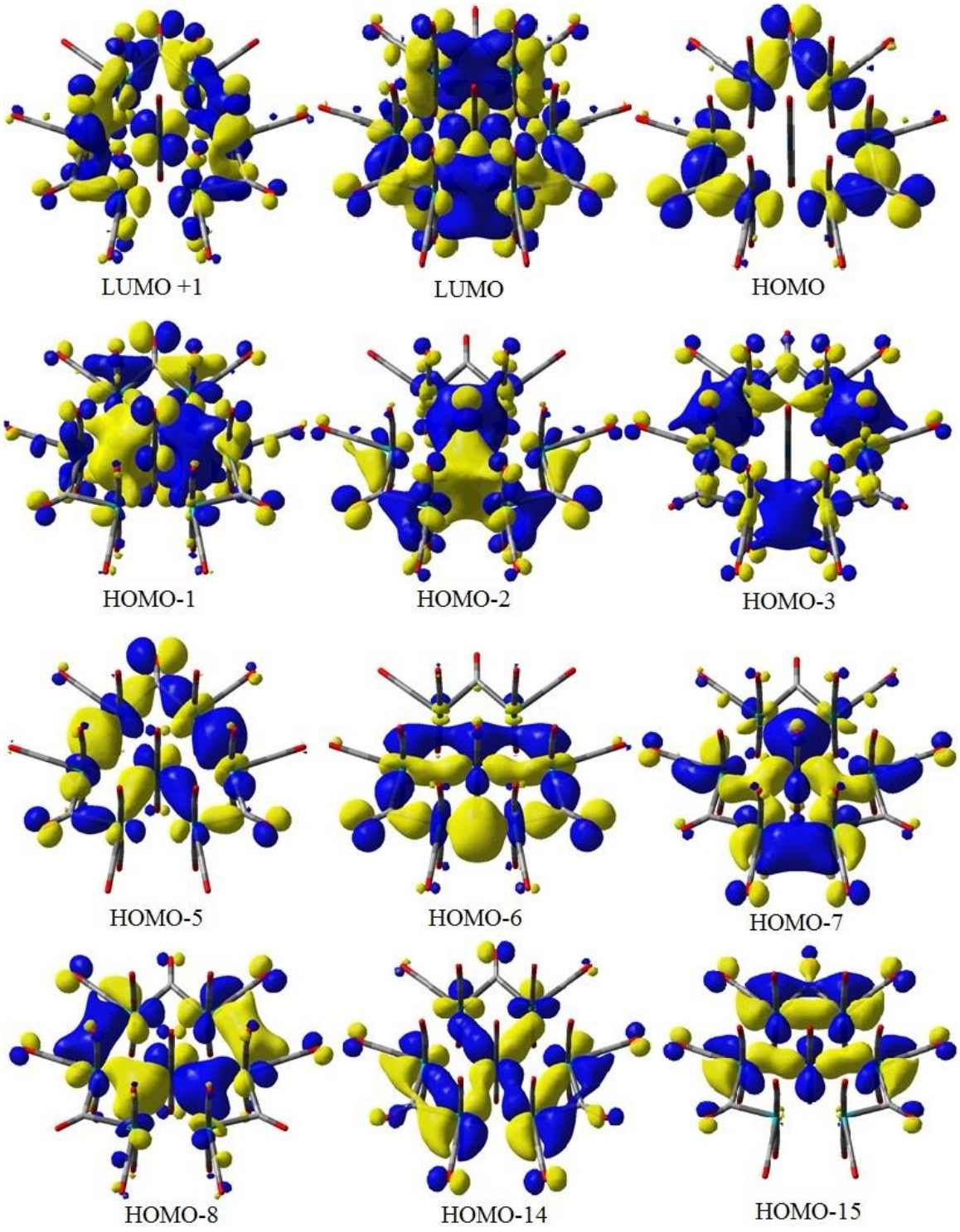

Figure 2.5. Selected molecular orbitals that show the two lowest unoccupied orbitals and some important metal–metal bonding orbitals for $Ru_6Ir(CO)_{23}^-$, **2.5**.

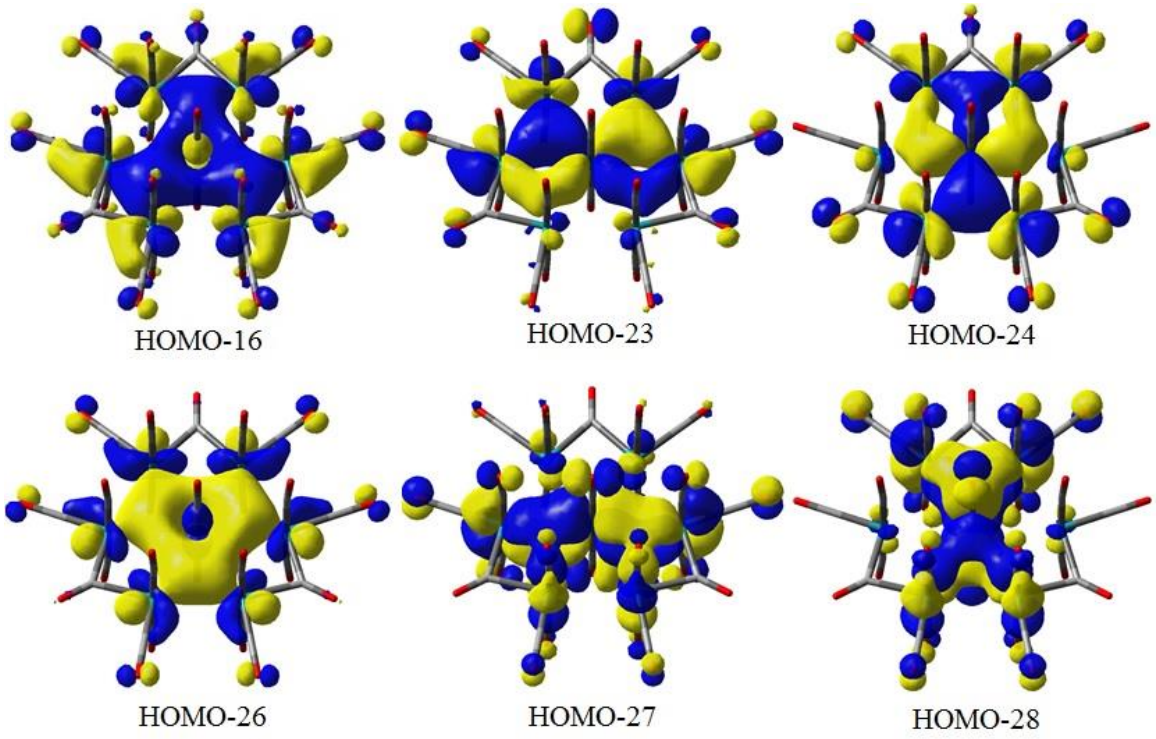

Figure 2.6. Selected molecular orbitals of the low energy metal–metal bonding orbitals for **$Ru_6Ir(CO)_{23}^-$**, **2.5**.

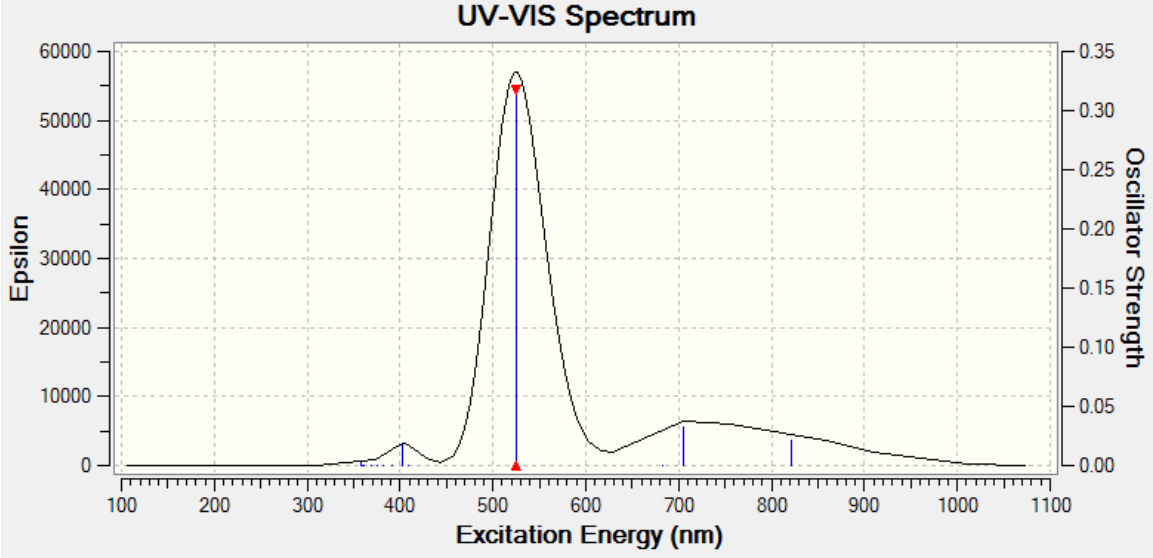

Figure 2.7. Simulated TDDFT UV-vis absorption spectrum for anion **2.5.**

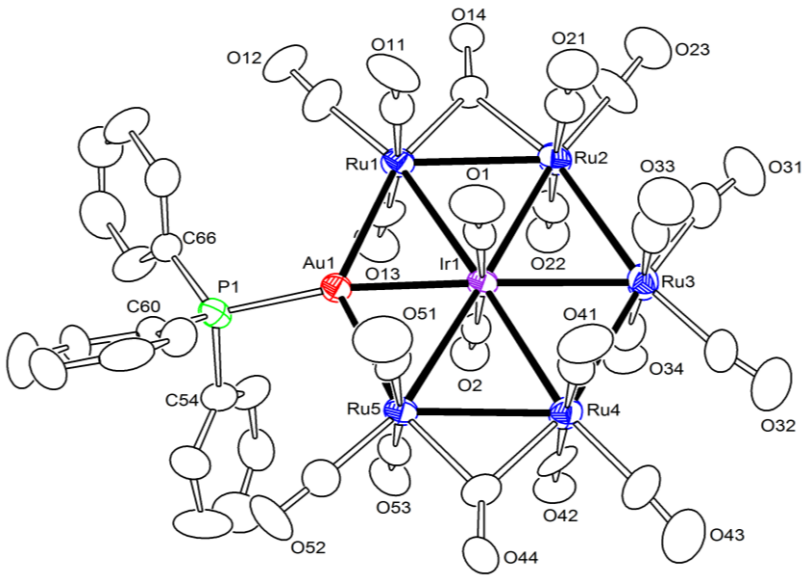

Figure 2.8. An ORTEP diagram of **2.6** showing 40% thermal probability. Hydrogen atoms have been omitted for clarity.

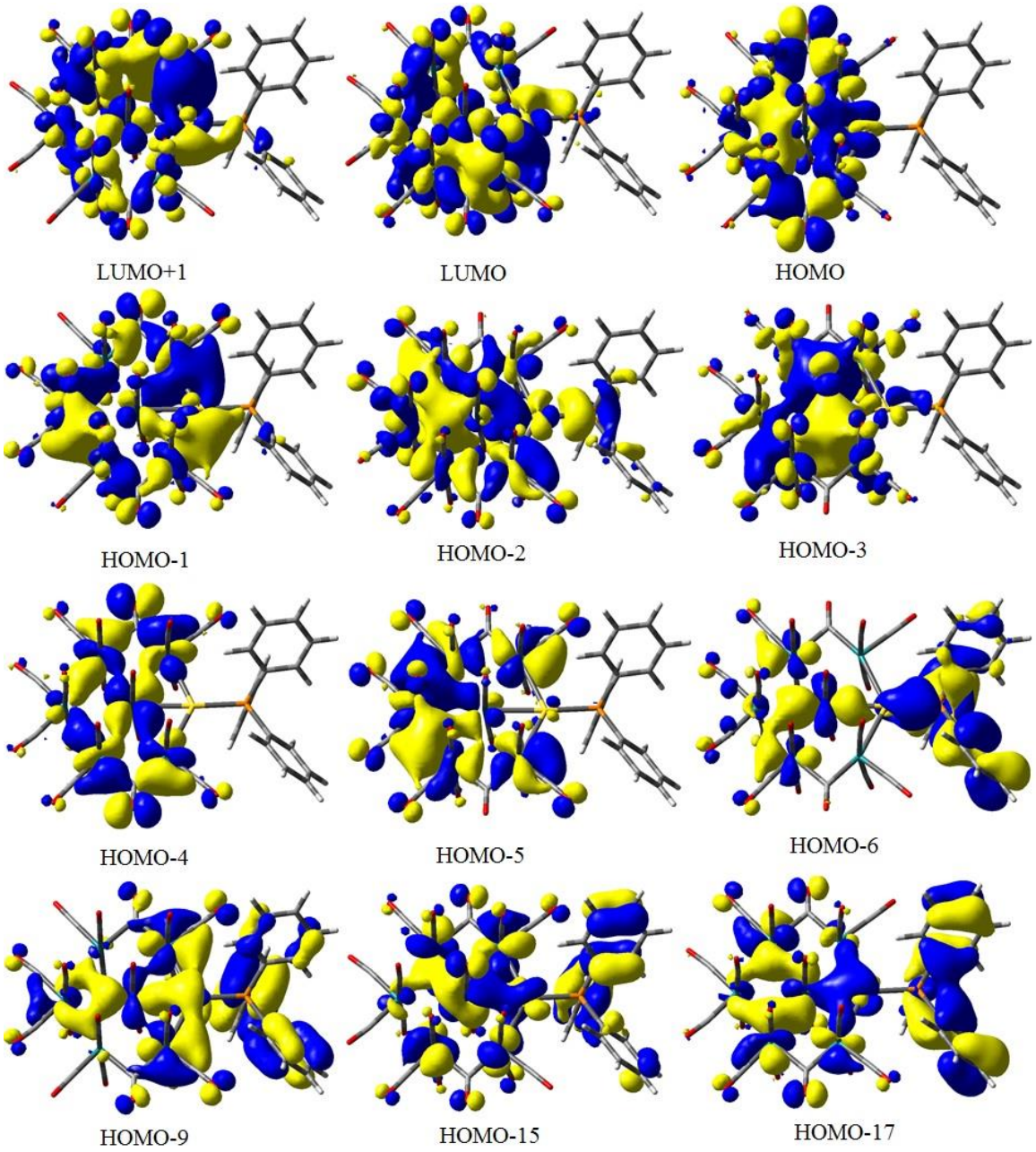

Figure 2.9. Selected Molecular Orbital Diagrams Show Metal-Metal Interactions In Compound $Ru_5Ir(CO)_{20}AuPPh_3$, **2.6**.

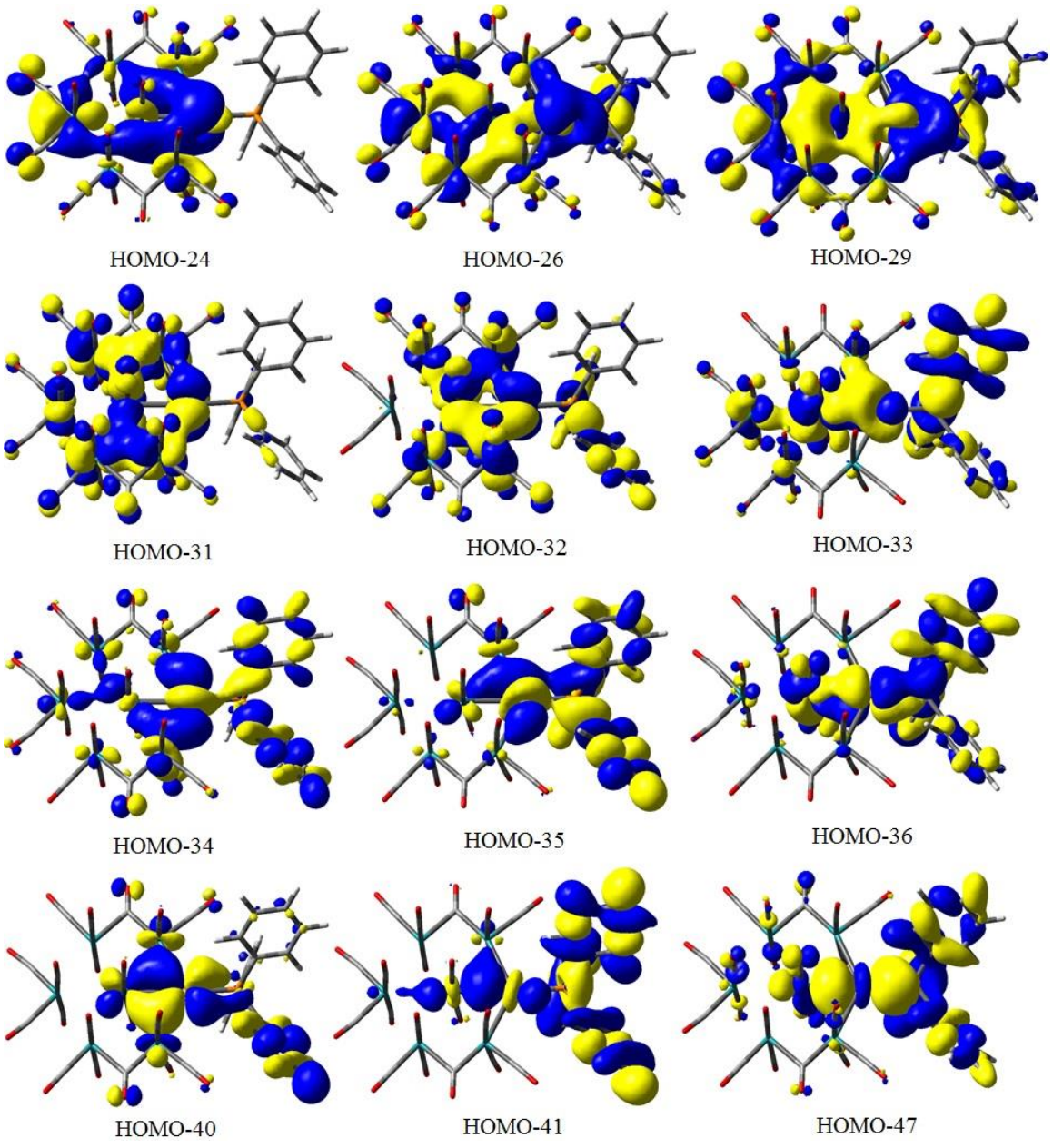

Figure 2.10. Selected Low energy Molecular Orbital Diagrams Show Gold-Iridium Interactions In $Ru_5Ir(CO)_{20}AuPPh_3$, **2.6**.

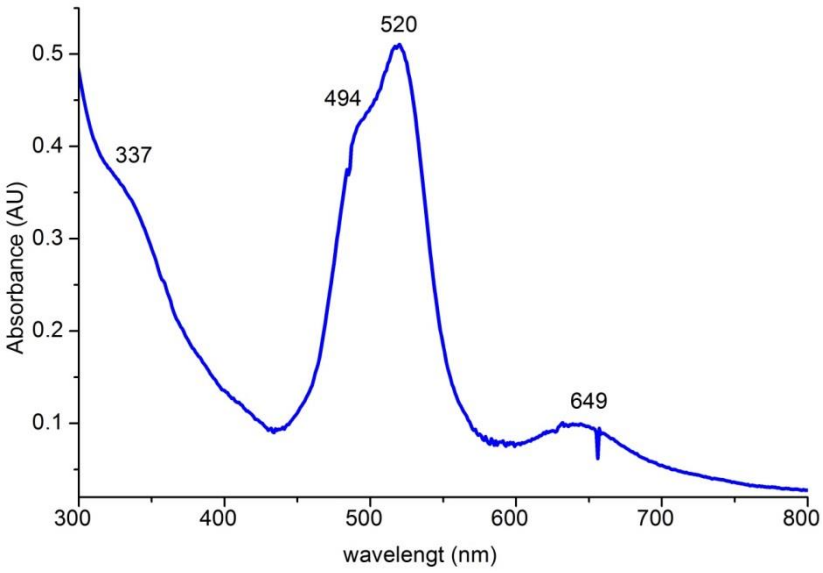

Figure 2.11. UV-vis absorption spectrum of **2.6** in CH_2Cl_2 solvent.

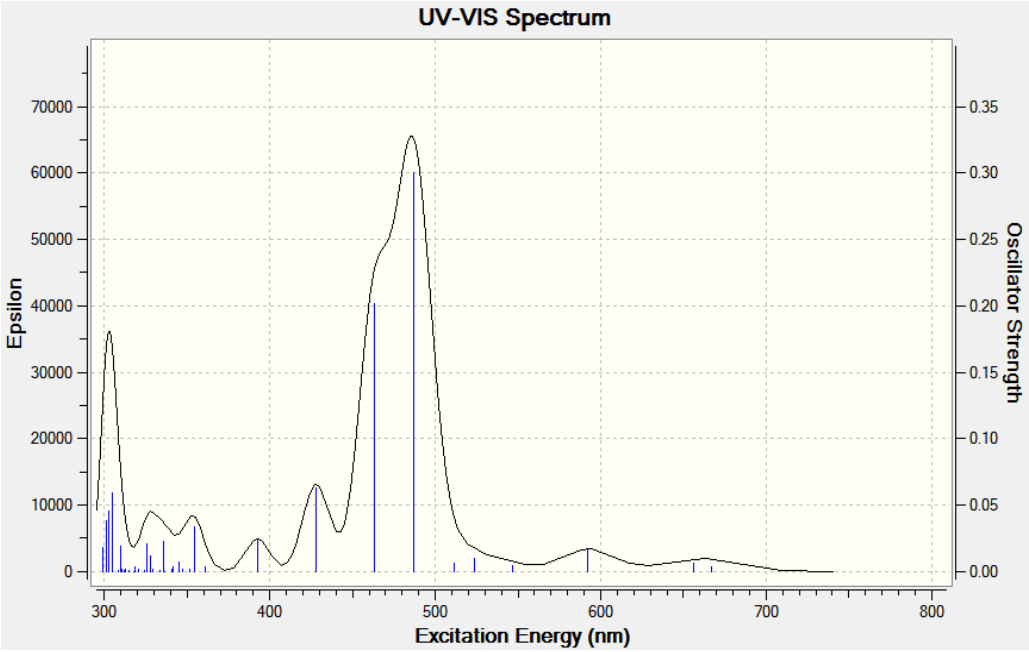

Figure 2.12. Simulated TDDFT UV-vis absorption spectrum for $Ru_5Ir(CO)_{20}AuPPh_3$, **2.6.**

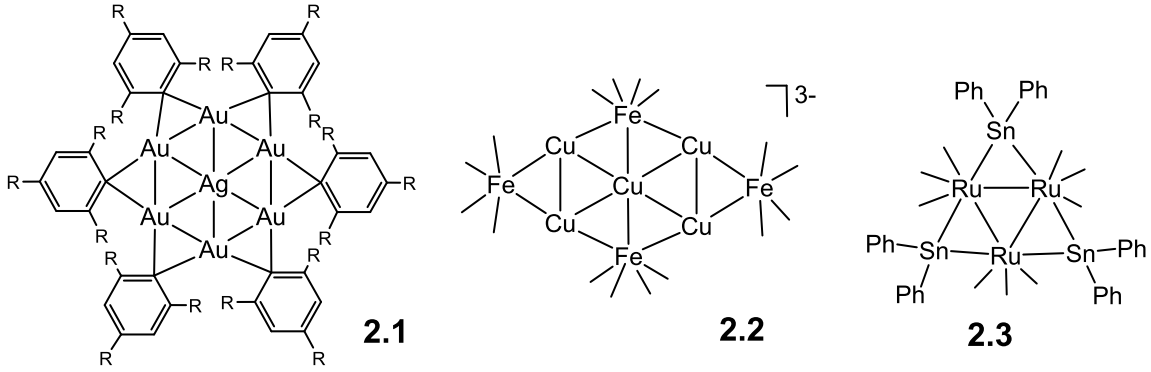

Scheme 2.1 Some reported 2-D cluster complexes.

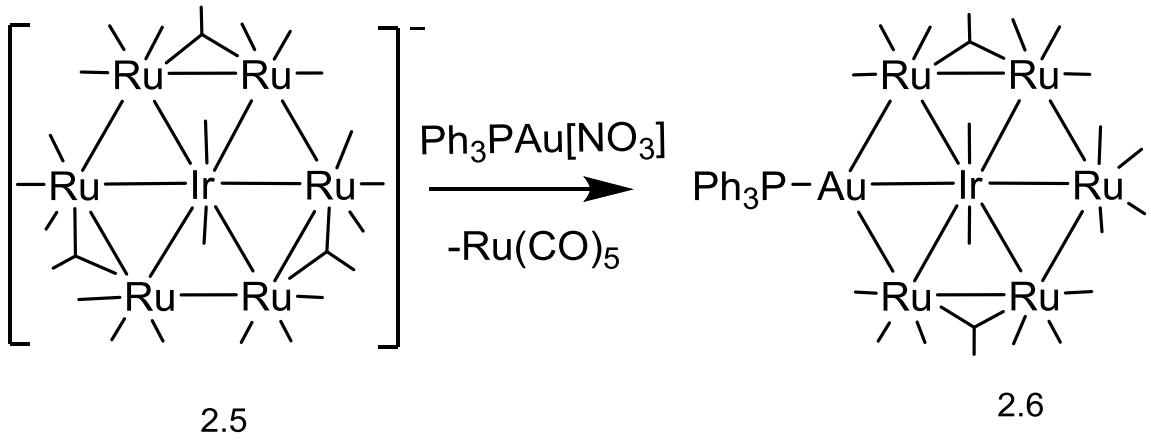

Scheme 2.2. Transformation of **2.5** to **2.6**.

Table 2.1. Crystallographic Data for Compounds **2.5** and **2.6**.

Compound	**2.5**	**2.6**
Empirical formula	$Ru_6IrP_2NO_{23}C_{65}H_{36}$	$Ru_5IrAuPO_{20}C_{41}H_{22}$
Formula weight	2059.51	1760.07
Crystal system	Triclinic	Triclinic
Lattice parameters		
a (Å)	10.1110(3)	10.624(2)
b (Å)	17.9859(6)	13.983(3)
c (Å)	21.6380(7)	17.735(4)
α (deg)	66.504(1)	68.360(4)
β (deg)	77.043(1)	88.205(4)
γ (deg)	85.474(1)	80.330(4)
V (Å^3)	3516.61(19)	2412.8(9)
Space group	$P\ \bar{1}$ (#2)	$P\ \bar{1}$ (#2)
Z value	2	2
ρ_{calc} (g / cm^3)	1.945	2.423
μ (Mo Kα) (mm^{-1})	3.259	7.406
Temperature (K)	293(2)	294(2)
$2\Theta_{max}$ (°)	50.06	48.80
No. Obs. (I > 2σ(I))	12409	7831
No. Parameters	811	608
Goodness of fit (GOF)	1.069	1.029
Max. shift in cycle	0.001	0.001
Residuals*: R1; wR2	0.0500;0.1248	0.0736;0.1689
Absorpn Corr., Max/min	1.000 / 0.875	1.000 / 0.618
Largest peak in Final Diff. Map (e$^-$ / Å^3)	1.635	3.376

* $R = \Sigma_{hkl}(||F_{obs}|-|F_{calc}||)/\Sigma_{hkl}|F_{obs}|$; $R_w = [\Sigma_{hkl}w(|F_{obs}|-|F_{calc}|)^2/\Sigma_{hkl}wF^2_{obs}]^{1/2}$; $w = 1/\sigma^2(F_{obs})$; $GOF = [\Sigma_{hkl}w(|F_{obs}|-|F_{calc}|)^2/(n_{data} - n_{vari})]^{1/2}$.

Table 2.2. Calculated TDDFT Electronic Transtions for $Ru_6Ir(CO)_{23}^-$, **2.5**.

Structure	Excited state	Primary Molecular Orbitals	Excited energy (eV)	Excited wavelength (nm)	Oscillator strength
$Ru_6Ir(CO)_{23}^-$	1	218 → 219	1.5104	820.86	0.0209
	2	218 → 220	1.5107	820.86	0.0209
	3	217 → 219	1.7580	705.25	0.0191
	4	216 → 220	1.7585	705.07	0.0130
	5	216 → 219 217 → 220	1.7591	704.83	0.0320
	7	215 → 219	2.3632	524.66	0.3173
	8	215 → 220	2.3633	524.63	0.3172
	10	210 → 219 211 → 220	3.0766	402.99	0.0177
	11	210 → 220 211 → 219	3.0773	402.90	0.0175

Table 2.3. Summary of TDDFT calculated singlet excited-states of $Ru_5Ir(CO)_{20}AuPPh_3$ **2.6**, with stronger oscillator strength.

Structure	Excited states	Primary Molecular Orbitals[a]	Excited energy (eV)	Excited wavelength (nm)	Oscillator strength
$Ru_5Ir(CO)_{20}AuPPh_3$	1	267 → 268	1.8586	667.08	0.0039
	2	267 → 269	1.8903	655.88	0.0063
	3	266 → 268	2.0929	592.42	0.0163
	7	265 → 268 266 → 269	2.5460	486.98	0.3007
	8	264 → 268 265 → 269	2.6747	463.55	0.2015
	9	263 → 268	2.8975	427.91	0.0631
	10	263 → 269	3.1596	392.41	0.0239
	12	267 → 272	3.5010	354.13	0.0340
	19	266 → 272	3.6942	335.61	0.0228

[a] HOMO and LUMO are orbitals 267 and 268.

Table 2.4. Selected intramolecular angles and bond distances for compound **2.5**.[a]

Distances			**Angles**			
Atom	Atom	Distance(Å)	Atom	Atom	Atom	Angle(deg)
Ir1	Ru1	2.8774(8)	Ru3	Ir1	Ru1	119.48(3)
Ir1	Ru2	2.8945(8)	Ru3	Ir1	Ru5	120.24(2)
Ir1	Ru3	2.8728(8)	Ru1	Ir1	Ru5	120.28(2)
Ir1	Ru4	2.9021(8)	Ru3	Ir1	Ru6	178.92(3)
Ir1	Ru5	2.8585(8)	Ru1	Ir1	Ru6	60.25(2)
Ir1	Ru6	2.904598)	Ru5	Ir1	Ru6	60.06(2)
Ru1	Ru2	2.8884(11)	Ru3	Ir1	Ru2	59.87(2)
Ru1	Ru6	2.9068(10)	Ru1	Ir1	Ru2	59.61(2)
Ru2	Ru3	2.8942(11)	Ru5	Ir1	Ru2	179.49(3)
Ru3	Ru4	2.8712(11)	Ru6	Ir1	Ru2	119.82(3)
Ru4	Ru5	2.8744(11)	Ru3	Ir1	Ru4	59.89(2)
Ru5	Ru6	2.8777(10)	Ru1	Ir1	Ru4	179.24(3)
			Ru5	Ir1	Ru4	60.35(2)
			Ru6	Ir1	Ru4	120.37(2)
			Ru2	Ir1	Ru4	119.75(2)

[a] Estimated standard deviations in the least significant figure are given in parentheses.

Table 2.5. Selected intramolecular angles and bond distances for compound **2.6**.[a]

Distances			**Angles**			
Atom	Atom	Distance(Å)	Atom	Atom	Atom	Angle(deg)
Au1	Ir1	2.6580(12)	Au1	Ir1	Ru2	119.12(5)
Au1	Ru1	2.7480(17)	Au1	Ir1	Ru4	118.77(4)
Au1	Ru5	2.7403(17)	Ru2	Ir1	Ru4	121.90(5)
Ir1	Ru1	2.9080(17)	Au1	Ir1	Ru1	58.97(4)
Ir1	Ru2	2.9052(17)	Ru2	Ir1	Ru1	60.27(5)
Ir1	Ru3	2.9120(18)	Ru4	Ir1	Ru1	177.47(6)
Ir1	Ru4	2.9057(18)	Au1	Ir1	Ru5	58.77(4)
Ir1	Ru5	2.9089(16)	Ru2	Ir1	Ru5	177.82(5)
Ru1	Ru2	2.918(2)	Ru4	Ir1	Ru5	60.16(5)
Ru2	Ru3	2.959(2)	Ru1	Ir1	Ru5	117.66(5)
Ru3	Ru4	2.942(2)	Au1	Ir1	Ru3	176.51(5)
Ru4	Ru5	2.914(2)	Ru2	Ir1	Ru3	61.15(5)
			Ru4	Ir1	Ru3	60.76(5)
			Ru1	Ir1	Ru3	121.42(5)
			Ru5	Ir1	Ru3	120.92(5)

[a] Estimated standard deviations in the least significant figure are given in parentheses.

REFERENCE

1. (a) Mingos, D. M. P.; May, A. S. in *The Chemistry of Metal Cluster Complexes*, Shriver, D. F.; Kaesz, H. D.; Adams, R. D., VCH Publishers, New York, NY, **1990**, Ch. 2. (b) Fajardo, Holden, H. D.; Johnson, B. F. G.; Lewis, J., Raithby, P. R. *J. Chem. Soc., Chem. Commun*. **1984**, 24 − 25. (c) Schollenberg, M.; Nuber, B.; Ziegler, M. L. *Angew. Chem. Int. Ed.* **1992**, *31*, 350 – 351. (d) Kong, G.; Harakas, G. N.; Whittlesey, B. R. *J. Am. Chem. Soc.* **1995**, *117*, 3502 − 3509. (e) Egold, H.; Schraa, M.; Florke, U.; Partyka, J. *Organometallics* **2002**, *21*, 1925 − 1932. (f) Brayshaw, S. K.; Green, J. C.; Edge, R.; McInnes, E. J. L.; Raithby, P. R.; Warren, J. E.; Weller, A. S. *Angew. Chem. Int. Ed.* **2007**, *46*, 7844 – 7848.

2. Cerrada, E.; Contel, M.; Valencia, A. D.; Laguna, M.; Gelbrich, T.; Hursthouse, M. B. *Angew. Chem. Int. Ed.* **2000**, *39*, 2353 − 2356.

3. Doyle, G.; Eriksen, K. A.; Van Engen, D. *J. Am. Chem. Soc.* **1986**, *108*, 445 − 451.

4. Adams, R. D.; Captain, B.; Trufan, E. *J. Am. Chem. Soc.* **2007**, *129*, 12328 − 12340.

5. Hungria, A.B.; Raja, R.; Adams, R. D.; Captain, B.; Thomas, J. M.; Midgley, P. A.; Golvenko, V.; Johnson, B. F. G. *Angew. Chem. Int. Ed.* **2006**, *45*, 4782 − 4785.

6. Adams, R. D.; Boswell, E. M.; Captain, B.; Hungria, A. B.; Midgley, P. A.; Raja, R.; Thomas, J. M. *Angew. Chem.. Int. Ed.* **2007**, *46*, 8182 − 8185.

7. Adams, R. D.; Blom, D. A.; Captain, B.; Raja, R.; Thomas, J. M.; Trufan, E. *Langmuir* **2008**, *24*, 9223 − 9226.

8. Yang, F.; Trufan, E.; Adams, R. D.; Goodman, D. W. *J. Phys. Chem. C* **2008**, *112*, 14233 − 14235.

9. (a) Waldmann, O. *Coord. Chem .Rev.* **2005**, *249*, 2550 – 2566. (b) Pizzagalli, L.; Stoeffler, D.; Gautier, F. *Phys. Rev. B* **1996**, *54*, 12216 – 12224.

10. Garlaschelli, L.; Chini, P.; Martinengo, S., *Gazz. Chim. Ital.*, **1982**, *112*, 285 − 288.

11. Malatesta L.; Naldini L.; Simonetta G. and Cariati F., Coordin. Chem. Rev., **1966**, *1*, 255 − 262.

12. SAINT+, version 6.2a, Bruker Analytical X-ray Systems, Inc., Madison, WI, **2001**.

13. Sheldrick, G. M. SHELXTL, version 6.1, Bruker Analytical X-ray Systems, Inc., Madison, WI, **1997**.

14. Gaussian 03, Revision E.01, suite of programs for *ab initio* calculation; Frisch, M. J.; Trucks, G. W.; Schlegel, H. B.; Scuseria, G. E.; Robb, M. A.; Cheeseman, J. R.; Montgomery, J. A., Jr.; Vreven, T.; Kudin, K. N.; Burant, J. C.; Millam, J. M.; Iyengar, S. S.; Tomasi, J.; Barone, V.; Mennucci, B.; Cossi, M.; Scalmani, G.; Rega, N.; Petersson, G. A.; Nakatsuji, H.; Hada, M.; Ehara, M.; Toyota, K.; Fukuda, R.; Hasegawa, J.; Ishida, M.; Nakajima, T.; Honda, Y.; Kitao, O.; Nakai, H.; Klene, M.; Li, X.; Knox, J. E.; Hratchian, H. P.; Cross, J. B.; Bakken, V.; Adamo, C.; Jaramillo, J.; Gomperts, R.; Stratmann, R. E.; Yazyev, O.; Austin, A. J.; Cammi, R.; Pomelli, C.; Ochterski, J. W.; Ayala, P. Y.; Morokuma, K.; Voth, G. A.; Salvador, P.; Dannenberg, J. J.; Zakrzewski, V. G.; Dapprich, S.; Daniels, A. D.; Strain, M. C.; Farkas, O.; Malick, D. K.; Rabuck, A. D.; Raghavachari, K.; Foresman, J. B.; Ortiz, J. V.; Cui, Q.; Baboul, A. G.; Clifford, S.; Cioslowski, J.; Stefanov, B. B.; Liu, G.; Liashenko, A.; Piskorz, P.; Komaromi, I.; Martin, R. L.; Fox, D. J.; Keith, T.; Al-Laham, M. A.; Peng, C. Y.; Nanayakkara, A.; Challacombe, M.; Gill, P. M. W.; Johnson, B.; Chen, W.; Wong, M. W.; Gonzalez, C.; Pople, J. A. *Gaussian, Inc.*: Wallingford CT, **2004.**

15. Boese, A. D.; Martin, J. M. L. *J. Chem. Phys.* **2004**, *121*, 3405 − 3416.

16. Peterson, K. A.; Figgen, D.; Dolg, M.; Stoll, H. *J. Chem. Phys.* **2007**, *126*, 124101.

17. Süss-Fink, G.; Haak, S.; Ferrand, V.; Stoeckli-Evans, H. *J. Chem. Soc, Dalton Trans.* **1997**, 3861 − 3865.

18. Mingos, D. M. P. *Acc. Chem. Res.* **1984**, *17*, 311 – 319.

19. Gaussian 03, Revision E.01, suite of programs for ab initio calculation; Frisch, M. J. et al. Gaussian, Inc.: Wallingford CT, **2004**.

20. (a) Wong, W.Y.; Ting, F. L.; Guo, Y.; Lin, Z. *J. Cluster Sci.* **2005**, *16*, 185 – 200. (b) Wong, W.Y.; Choi, K.H.; Lin, Z. *Eur. J. Inorg. Chem.* **2002**, 2112 – 2120. (c) Wong, W.Y.; Wong, W. T. *J. Chem. Soc., Dalton Trans.* **1996**, 1853 – 1856.

CHAPTER 3

Structures and Bonding of η^2-bridging CO Ligands and their Influence on the Structures and Rearrangements of Higher Nuclearity Metal Carbonyl Cluster Complexes

Introduction

The η^2-bridging carbonyl ligand has been shown to exist in a number of different coordination modes in polynuclear metal carbonyl complexes. In general, it serves as a 4 electron donor as represented by the structures **A**,[1] **C**,[2] **E**[3] and **F**,[4] but on rare occasions, it can even serve as a 6 electron donor, as found in the structures **B**[5] and **G**[6], see Scheme 3.1. There is evidence that quadruply bridging CO ligands, such as **E**, are precursors to carbido ligands via cleavage of the CO bond,[6] and the ability of the CO ligand to adopt various bridging coordinations can play a role in the growth and transformations of polynuclear metal complexes, particularly when the transformations are accompanied by the addition or elimination of other CO ligands.[7] Multi-center coordination to metal atoms has been shown to modify the reactivity of the CO ligand.[6d] This is also central to the transformations of CO on surfaces[8] and in heterogeneous catalysis.[9]

Studies have shown that certain bimetallic cluster complexes exhibit catalytic activity that is superior to that of their homonuclear components.[10-11] The $IrRu_3$ complex, $IrRu_3(CO)_{13}(\mu_3\text{-}H)$,[12] is a precursor to an effective homogeneous bimetallic catalyst for the selective hydrogenation of alkynes.[11] We have recently shown $IrRu_3(CO)_{13}(\mu_3\text{-}H)$ reacts with $HGePh_3$ in a cluster opening process to yield the complex $IrRu_3(CO)$

$_{11}(GePh_3)_3(\mu\text{-}H)_4$ which subsequently cleaves five phenyl groups from the three $GePh_3$ ligands to yield the bis-germylyne complex $IrRu_3(CO)_9(\mu\text{-}\eta^2\text{-}C_6H_5)(\mu_4\text{-}GePh)_2(\mu\text{-}GePh_2)$, when it is heated, Scheme 3.2.[13]

We have now investigated the reaction of $IrRu_3(CO)_{13}(\mu_3\text{-}H)$ with the sterically encumbered phosphine, P(t-Bu)$_3$. Four new compounds including the unsaturated $IrRu_2$ complex $IrRu_2(CO)_9[P(t\text{-}Bu)_3](\mu\text{-}H)$, **3.3** and $IrRu_3(CO)_{10}(\mu_3\text{-}\eta^2\text{-}CO)[P(t\text{-}Bu)_3]_2(\mu\text{-}H)$, **3.4** which contains one of the rare $\mu_3\text{-}\eta^2$-CO ligands **D** have been obtained. Compound **3.4** can be enlarged to the $IrRu_4$ complex $IrRu_4(CO)_{12}(\mu_4\text{-}CO)[P(t\text{-}Bu)_3]_2(\mu_3\text{-}H)$, **3.5** which contains a type **E** quadruply bridging CO ligand by reaction with $Ru(CO)_5$. Compound **3.5** reacts with CO to yield the new compound $IrRu_4(CO)_{14}(\mu_4\text{-}\eta^2\text{-}CO)P(t\text{-}Bu)_3(\mu\text{-}H)$, **3.6** which contains a type **F** quadruply bridging CO ligand. The results of these studies of these reactions are reported herein.

Experimental

General Data.

Reagent grade solvents were dried by the standard procedures and were freshly distilled prior to use. Infrared spectra were recorded on a Thermo Nicolet Avatar 360 FT-IR spectrophotometer. Room temperature ^{1}H NMR and ^{31}P{^{1}H} NMR were recorded on a Bruker Avance/DRX 400 NMR spectrometer operating at 400.3 and 162.0 MHz, respectively. Positive/negative ion mass spectra were recorded on a Micromass Q-TOF instrument by using electrospray (ES) ionization or electron impact (EI) ionization. $IrRu_3(CO)_{13}(\mu\text{-}H)$[11] and $Ru(CO)_5$[14] were prepared according to previously reported procedures. $Ru_3(CO)_{12}$ was purchased from STREM and tri-*t*-butylphosphine (PBu^t_3) was

purchased from Alfa Aesar and was used without further purification. Product separations were performed by TLC in air on Analtech 0.25 mm silica gel 60 Å F254 glass plates.

Reaction of $IrRu_3(CO)_{13}(\mu\text{-}H)$ with Tri-*tert*-butylphosphine.

30.0 mg (0.0349mmol) of $IrRu_3(CO)_{13}(\mu\text{-}H)$ was dissolved in 30 mL of methylene chloride solvent in a 100 mL three neck flask. 7.5 mg of $P(t\text{-}Bu)_3$ (0.0371mmol) was added and the reaction solution was heated to reflux. The heat was removed after 30 min, after cooling to room temperature, another equivalent of $P(t\text{-}Bu)_3$ was added and the reaction mixture was stirred overnight at room temperature. The solvent was removed *in vacuo* and the products were then isolated by TLC by eluting with a 6:1 hexane/methylene chloride solvent mixture. In order of elution, this yielded: 2.5 mg of $Ru_3(CO)_{12}$ (11%), 1.8 mg of $IrRu_3(CO)_{13}(\mu\text{-}H)$, (6.0%) starting material, 5.3 mg of $IrRu_3(CO)_{12}P(t\text{-}Bu)_3(\mu\text{-}H)$, **3.1**, (15%), 1.2 mg of $Ir_2Ru_3(CO)_{15}P(t\text{-}Bu)_3$, **3.2**, (2.6% based on Ruthenium), 8.6 mg of $IrRu_2(CO)_9[P(t\text{-}Bu)_3](\mu\text{-}H)$, **3.3**, (29%) and 8.1 mg of $IrRu_3(CO)_{10}[P(t\text{-}Bu)_3]_2(\mu_3\text{-}\eta^2\text{-}CO)(\mu\text{-}H)$, **3.4**, (19%).

Spectral data for **3.1**: IR νCO (cm^{-1} in CH_2Cl_2): 2085(m), 2045(vs), 2016(s), 1993(m), 1958(w), 1859(w). ^1H NMR (CD_2Cl_2, 25 ^oC, TMS) δ = 1.53 (s, 27H, PBu^t_3), -18.39 (d, 1H, $J_{P\text{-}H}$ = 6.80 Hz, hydride). $^{31}P\{^1H\}$ NMR (CD_2Cl_2, 25 ^oC, 85% ortho-H_3PO_4) δ = 78.56 (s,1P, P-Ir). Mass Spec. EI+, m/z, 1036 (M^+), 1008 (M^+-CO).

Spectral data for **3.2**: IR νCO (cm^{-1} in CH_2Cl_2): 2093(w), 2069(m), 2046(vs), 2021(m), 2013(sh), 1986(w), 1605(br). ^1H NMR (CD_2Cl_2, 25 ^oC, TMS) δ = 1.58 (d, $J_{P\text{-}H}$ = 12.60Hz, 27H, PBu^t_3),. $^{31}P\{^1H\}$ NMR (CD_2Cl_2, 25 ^oC, 85% ortho-H_3PO_4) δ = 93.25 (s,1P, P-Ir). Mass Spec. EI+, m/z, 1311 (M^+).

Spectral data for **3.3**: IR νCO (cm^{-1} in CH_2Cl_2): 2087(s), 2047(vs), 2014(s), 2000(sh), 1986(m), 1786(w). ^{1}H NMR (CD_2Cl_2, 25 ^{o}C, TMS) δ = 1.49 (d, J_{P-H}=12.84Hz, 27H, PBu^t_3), -9.54 (d, 1H, J_{H-P} =4.96 Hz, hydride). $^{31}P\{^1H\}$ NMR (CD_2Cl_2, 25 ^{o}C, 85% ortho-H_3PO_4) δ = 98.72 (s,1P, P-Ir).). Mass Spec. EI+, m/z 852 (M^+).

Spectral data for **3.4**: IR νCO (cm^{-1} in CH_2Cl_2): 2061(s), 2024(vs), 2011(s), 1999(s), 1984(m), 1976(m), 1954(w), 1547(w). ^{1}H NMR (CD_2Cl_2, 25 ^{o}C) δ = 1.54 (s, 27H, PBu^t_3), 1.51 (s, 27H, PBu^t_3), -17.34 (dd, 1H, hydride, $^2J_{H-P}$ = 2.26 Hz, $^3J_{H-P}$ = 3.86 Hz). $^{31}P\{^1H\}$ NMR (CD_2Cl_2, 25 ^{o}C, 85% ortho-H_3PO_4) δ = 91.22 (s, 1P, P-Ru), δ = 67.46 (s,1P, P-Ir). Mass Spec. ES+/MS m/z. 1210 (M^+), 1182 (M^+ -CO).

Reaction of 3.1 with Tri-*tert*-butylphosphine.

18.6 mg (0.0180mmol) of $IrRu_3(CO)_{13}(\mu\text{-}H)P(t\text{-}Bu)_3$ was dissolved in 30 mL of methylene chloride solvent in a 100 mL three neck flask. 5.5 mg of $P(t\text{-}Bu)_3$ (0.0272mmol) was added and the reaction solution was heated to reflux. The heating was stopped after 30 min, after the removal of solvent *in vacuo* the products were isolated by TLC by eluting with a 6:1 hexane/methylene chloride solvent mixture. In order of elution, this yielded: 0.8 mg of $Ru_3(CO)_{12}$ (7.00%), 4.1 mg of **3.1**, (22.0%) (starting material), 2.8 mg of **3.3**, (18.3%), 8.0 mg of **3.4**, (36.8%).

Reaction of 3.4 with $Ru(CO)_5$.

22.6 mg (0.0187mmol) of **3.4** was added to 20 mL hexane in a 100mL three neck flask. $Ru(CO)_5$ (generated by irradiation of $Ru_3(CO)_{12}$ (10.0 mg) in a hexane solution) was then added. After heating for 2 h at 68^{o}C, the solvent was removed in *vacuo*, and the

product was isolated by TLC by using a 3:1 hexane/methylene chloride solvent mixture. 16.9 mg (66 % yield) of $IrRu_4(CO)_{12}(\mu_4\text{-}CO)[P(t\text{-}Bu)_3]_2(\mu_3\text{-}H)$, **3.5** was obtained.

Spectral data for **3.5**: IR νCO (cm^{-1} in CH_2Cl_2): 2065(s), 2031(s), 2016(vs), 1994(m), 1965(m), 1934(w), 1828(sh), 1780(w), 1605(w). ^1H NMR (CD_2Cl_2, 25 ^oC, TMS) δ = 1.65 (s, 27H, PBu^t_3), 1.62 (s, 27H, PBu^t_3) and -19.59 (dd, 1H, hydride, $^2J_{P\text{-}H}$ = 2.4 Hz, $^3J_{P\text{-}H}$ = 1.6 Hz). $^{31}P\{^1H\}$ NMR (CD_2Cl_2, 25 ^oC, 85% ortho-H_3PO_4) δ = 95.79 (s,1P, P-Ru) and 84.63 (s,1P, P-Ir). Mass Spec. ES+, m/z. 1368 (M^++H), 1340 (M^++H-CO).

Reaction of 3.5 with CO.

10.0 mg (0.0073 mmol) of **3.5** was added to 10 mL hexane in a 50 mL three neck rb flask. CO was then purged continuously through the solution with heating to reflux for 30 min. After cooling, the solvent was removed in *vacuo*, and the product was then isolated by TLC by using a 4:1 hexane/methylene chloride solvent mixture. This yielded in order of elution: 0.5 mg of $Ru_3(CO)_{12}$, 1.6 mg (18%) of $IrRu_4(CO)_{14}P(t\text{-}Bu)_3(\mu_4\text{-}\eta^2\text{-}CO)(\mu\text{-}H)$, **3.6** and 1.1 mg (11%) of **3.5**.

Spectral data for **3.6**: IR νCO (cm^{-1} in CH_2Cl_2): 2093(w), 2069(s), 2056(vs), 2037(vs), 2013(s), 1981(w). ^1H NMR (CD_2Cl_2, 25 ^oC, TMS) δ= 1.58 (d, $J_{P\text{-}H}$ = 12.68Hz, 27H, PBu^t_3), and -17.22 (s, 1H, hydride). $^{31}P\{^1H\}$ NMR (CD_2Cl_2, 25 ^oC, 85% ortho-H_3PO_4) δ= 94.70 (s,1P, P-Ru). Mass Spec. EI+, m/z 1193 (M^+-CO).

Reaction of 3.6 with CO.

9.2 mg (0.0075 mmol) of **3.6** was added to 10 mL hexane in a Parr high pressure reactor. The reactor was then filled and released with CO five times and finally charged with CO (10 atm), the bomb was placed in an oil bath and heated to 70^{o}C for 1h. After cooling, the solvent was removed *in vacuo*, and the product was then isolated by TLC by using a 4:1 hexane/methylene chloride solvent mixture. This yielded in order of elution: 3.6 mg of $Ru_3(CO)_{12}$ (56% yield), 1.0 mg uncharacterized product that decomposed in air, and 2.3 mg of (36% yield) of $IrRu_2(CO)_9P(t\text{-}Bu)_3(\mu\text{-}H)$, **3.3**.

Crystallographic Analyses:

Black crystals of **3.1**, red crystals of **3.2**, green crystals of **3.3**, red crystals of **3.4**, black crystals of **3.5** and red crystals of**3. 6** suitable for x-ray diffraction analyses were all obtained by slow evaporation of a solvent from solutions in at -25 ℃. Each data crystal was glued onto the end of a thin glass fiber. X-ray intensity data were measured by using a Bruker SMART APEX CCD-based diffractometer using Mo Kα radiation (λ = 0.71073 Å). The raw data frames were integrated with the SAINT+ program by using a narrow-frame integration algorithm.[15] Correction for Lorentz and polarization effects were also applied using SAINT+. An empirical absorption correction based on the multiple measurement of equivalent reflections was applied using the program SADABS. All structures were solved by a combination of direct methods and difference Fourier syntheses, and were refined by full-matrix least-squares on F^2 by using the SHELXTL software package.[16] All non-hydrogen atoms were refined with anisotropic thermal parameters. Hydrogen atoms were placed in geometrically idealized positions and included as standard riding atoms during the least-squares refinements. The hydride

ligands were located and refined with isotropic thermal parameters, except as noted below. Crystal data, data collection parameters, and results of the analyses are listed in Table 3.1.

Compounds **3.1** crystallized in the monoclinic crystal system. The space group $P2_1/c$ was uniquely identified on the basis of the systematic absences observed in the data and by the subsequent successful solution and refinement for the structure. Compounds **3.2**, **3.3**, **3.4** and **3.6** crystallized in the triclinic crystal system. The space group $P\ \bar{1}$ was assumed in all four cases and was confirmed by the successful solution and refinement of the structures. Compound **3.5** crystallized in the monoclinic crystal system. The space group $P2_1/n$ was identified uniquely on the basis of the systematic absences observed in the data and by the subsequent successful solution and refinement of the structure. For compound **3.1**, there were two independent molecules in the asymmetric unit. For compound **3.4**, the positional parameters and thermal parameter for the hydride ligand were fixed. The hydride ligand was located along an M–M bond in compounds **3.1**, **3.3**, **3.5**, and **3.6**, and was refined without constraints in each of these structural analyses. The methyl groups on the *t*-butyl groups in compound **3.6** were disordered and were treated and satisfactorily refined accordingly.

Computational Details.

Density functional theory (DFT) calculations were performed with the Amsterdam Density Functional (ADF) suite of programs [17] by using the PBEsol functional[18] with scalar relativistic correction and valence quadruple-ζ + 4 polarization, relativistically optimized (QZ4P) basis sets for iridium and ruthenium and valence triple-

ζ + 2 polarization function (TZ2P) basis sets for the phosphorus, carbon, oxygen, and hydrogen atoms with no frozen cores. The molecular orbitals for **3.3**, **3.4**, **3.5** and **3.6** and their energies were determined by a geometry optimized calculations that were initiated with the structures as determined from the crystal structure analyses.

Results and Discussion

Four compounds were obtained from the reaction of $IrRu_3(CO)_{13}(\mu_3\text{-H})$ with P(t-Bu)$_3$ in a hexane solution at reflux for 30 min. These have been identified as $IrRu_3(CO)_{12}P(t\text{-}Bu)_3(\mu\text{-H})$, **3.1**, (15% yield), $Ir_2Ru_3(CO)_{12}P(t\text{-}Bu)_3(\mu\text{-H})$, **3.2**, (6.1% yield) $IrRu_2(CO)_9[P(t\text{-}Bu)_3](\mu\text{-H})$, **3.3**, (29% yield) and $IrRu_3(CO)_{10}(\mu_3\text{-}\eta^2\text{-CO})[P(t\text{-}Bu)_3]_2(\mu\text{-H})$, **3.4**, (19% yield). All four products were characterized by a combination of IR, ^{1}H NMR, mass spec and single-crystal X-ray diffraction analyses. An ORTEP diagram of the molecular structure of **3.1** is shown in Figure 3.1. Compound **3.1** is simply a P(t-Bu)$_3$ substitution derivative of its parent $IrRu_3(CO)_{13}(\mu_3\text{-H})$.[12] Compound **3.1** contains a closed tetrahedral cluster of four metal atoms, one of Ir and three of Ru. There is one hydrido ligand in **3.1** that bridges the Ir(1) – Ru(1) bond. The Ir(1) – Ru(1) bond distance, 2.9115(5) Å, is significantly longer than the two other Ir - Ru bonds, Ir(1) – Ru(2) = 2.7750(5) Å and Ir(1) – Ru(3) = 2.8257(5) Å. It is well known that bridging hydrido ligands increase the length of the metal – metal bonds that they bridge.[19] The hydrido ligand in **3.3** exhibits the expected high-field resonance shift in the ^{1}H NMR spectrum, -18.39 ppm with small coupling, $^2J_{H\text{-}P}$ = 6.80 Hz, to the phosphorus atom of the proximate P(t-Bu)$_3$ ligand. The phosphine ligand is coordinated to the iridium atom, Ir(1) – P(1) =

2.4825(15) Å. The cluster contains a total of 60 valence electrons and is thus, electronically saturated, i.e. all metal atoms formally have 18 electron configurations.

Compound **3.2** was also characterized by a single crystal X-ray diffraction analysis, and an ORTEP diagram of the molecular structure of **3.2** is shown in Figure 3.2. Compound **3.2** contains five metal atoms, two of Ir and three of Ru. The metal atoms are arranged in the form of a spiked-tetrahedron. The tetrahedral group contains the two iridium atoms and two of the ruthenium atoms, Ir(1) – Ir(2) = 2.7055(5) Å, Ir(1) – Ru(2) = 2.7616(7) Å, Ir(1) – Ru(3) = 2.7723(7) Å, Ir(2) – Ru(3) = 2.7561(7) Å, Ir(2) – Ru(2) = 2.7568(7) Å, Ru(2) – Ru(3) = 2.7827(9) Å. The fourth Ru atom, Ru(1), is the "spike" that is bonded only to the iridium atom Ir(1), Ir(1) – Ru(1) = 2.8040(7) Å. There is one P(t-Bu)$_3$ ligand in **3.2**, and it is coordinated to Ru(1), Ru(1) – P(1) = 2.522(2) Å. Most interestingly, there is an η^2-quadruply bridging carbonyl ligand, C(1) – O(1), of the general type **F** (Scheme 3.1) and it is coordinated to three metal atoms Ir(1), Ru(2) and Ru(3) by its carbon atom, Ir(1) – C(1) = 2.021(8) Å, Ru(2) – C(1) = 2.129(8) Å and Ru(3) – C(1) = 2.101(8) Å. The oxygen atom is coordinated only to Ru(1), Ru(1) – O(1) = 2.165(5) Å. The CO bond distance is long, C(1) – O(1) = 1.269(7) Å. Assuming that the quadruply bridging CO ligand serves as a four electron donor, compound **3.2** contains a total of 76 valence electrons which is precisely the number expected for a spiked-tetrahedral cluster of five metal atoms, i.e. all of the metal atoms formally have 18 electron configurations.

An ORTEP diagram of the molecular structure of **3.3** is shown in Figure 3.3. Compound **3.3** contains only three metal atoms, one of Ir and two Ru. They are arranged in a triangle. The Ir – Ru bonds are short, but are not exceptionally short, Ir(1) – Ru(1) =

2.7570(3) Å, Ir(1) – Ru(2) = 2.7659(3) Å, Ru(1) – Ru(2) = 2.8243(4) Å. There is one hydrido ligand that bridges the Ir(1) – Ru(1) bond, Ir(1) – H(1) = 1.83(4) Å and Ru(1) – H(1) = 1.77(4) Å. The hydride ligand exhibits a high field resonance shift, -9.54 ppm with coupling to the neighboring phosphorus atom, $^{2}J_{P\text{-}H}$ = 4.96 Hz, but the shift is not nearly as high as that found in **3.1** or the other complexes **3.4** – **3.6**. This may be related to the electronic unsaturation found in **3.3**, see below.[20] The phosphine ligand is coordinated to the iridium atom, Ir(1) – P(1) = 2.3863(9) Å. There are eight terminally coordinated carbonyl ligands and there is one CO, C(1) – O(1), ligand that bridges the Ir(1) – Ru(1) bond. Overall, compound **3.3** contains a total of 46 valence electrons and it is thus electron deficient by the amount of two electrons. The deficiency appears to be located primarily at the iridium atom which formally contains only 16 valence electrons. Indeed, there appears to be a vacant coordination site on Ir(1) that lies approximately trans to the bond to the bridging CO ligand. This site is protected in part by one of the methyl groups, C26, on one of t-butyl groups of the bulky $P(t\text{-}Bu)_3$ ligand and the distance to C(26) and one of the hydrogen atoms, H(26a) on that methyl group is notably short, Ir(1)···C(26) = 3.310(4) Å, Ir(1)···H(26a) = 2.71 Å. This could be interpreted as a weak agostic C-H interaction to the Ir atom. A similar arrangement was found in the unsaturated vacant site complex, $Re_2(CO)_6[P(t\text{-}Bu)_3][\mu\text{-}P(t\text{-}Bu_2)](\mu\text{-}H)$.[20] Indeed, the location of this methyl group prevents the addition of CO to the Ir atom at this site in **3.3**.

In order to examine electronic structure of **3.3** further, DFT molecular orbital calculations were performed by using the PBEsol functional in the ADF program library. A diagram of the LUMO of **3.3** is shown in Figure 3.4 and in accordance with the conventional electron counting procedures the LUMO shows a large a component which

lies at approximately that same location as the vacant coordination site on the iridium atom. Süss-Fink reported two related $IrRu_2$ cluster complexes, $HRu_2Ir(CO)_5(dppm)_3$ and $HRu_2Ir(CO)_6(PCy_3)_3$.[21] The former complex contains 48 valence electrons, but the latter which contains three bulky PCy_3, Cy = cyclohexyl, ligands contains only 44 valence electrons. The geometry optimized coordinates for **3.3** are listed in table 3.8.

An ORTEP diagram of the molecular structure of **3.4** is shown in Figure 3.5. Compound **3.4** contains four metal atoms, one of Ir and three of Ru. They are arranged in the form of a butterfly tetrahedron. There are two $P(t\text{-}Bu)_3$ ligands, one on Ir(1) and the other on Ru(1) and these two metal atoms occupy the less crowded "wing-tip" positions of the butterfly tetrahedron. The metal – metal bond distances are fairly normal, Ir(1) – Ru(2) = 2.8722(8) Å, Ir(1) – Ru(3) = 2.8783(9) Å, Ir(1) – P(1) = 2.470(2), Ir(1) – C(2) = 1.917(9), Ru(1) – Ru(2) = 2.8563(9) Å, Ru(2) – Ru(3) = 2.7311(11) except for Ru(1) – Ru(3) which is unusually long at 3.0574(10) Å. The long length of Ru(1) – Ru(3) can be attributed to the presence of a hydrido ligand that bridges that bond.[19] The hydrido ligand exhibits a high field resonance shift, -17.34 ppm, with coupling to the two phosphorus atoms, $^2J_{H\text{-}P}$ = 2.26 Hz and $^3J_{H\text{-}P}$ = 3.86 Hz. The most interesting ligand in **3.4** is a η^2-triply-bridging CO ligand, C(2) – O(2) of the type **D**. The carbon atom is bonded to three of the metal atoms. The Ru(1) – C(2) bond distance, 2.476(10) Å, is significantly longer than the other two bonds to C(2), Ir(1) – C(2) = 1.917(9) Å and Ru(2) – C(2) = 2.150(10) Å, but seems to contain important bonding interactions, see below. The oxygen atom is bonded to Ru(1), Ru(1) – O(2) = 2.168(8) Å, and as a result, the CO bond distance is long, C(2) – O(2)= 1.250(11) Å, compared that of the terminally coordinated CO ligands, ave 1.14(2) Å.

In order to understand the nature of the coordination of the triply-bridging CO ligand better, a geometry-optimized DFT molecular orbital analysis of compound **3.4** was performed. Selected MOs that show bonding of the bridging CO ligand to the metal atoms are shown in Figure 3.6. The HOMO and HOMO-2 show π-backbonding between the three metal atoms and one of the π* molecular orbitals of the CO ligand. The HOMO-53 and HOMO-93 show donation of electrons via the filled π-bonding orbitals on the CO ligand with the same metal atoms. In addition, the HOMO-103 shows bonding interactions of the CO π-bonding orbital, frequently referred to as the "lone" pair of electrons on the carbon atom to the metal atoms Ru(2) and Ir(1). The geometry optimized coordinates for **3.4** are listed in table 3.9.

Assuming the bridging CO ligand serves as a four electron donor, the metal cluster in **3.4** contains a total of 62 valence electrons which is exactly the number expected for an electron-precise cluster of four metal atoms having five metal – metal bonds, i.e. each of the metal atoms formally achieves an 18 electron configuration.

Compound **3.4** was found to react with $Ru(CO)_5$ to give the higher nuclearity cluster complex, $IrRu_4(CO)_{12}(\mu_4\text{-}CO)[P(t\text{-}Bu)_3]_2(\mu_3\text{-}H)$, **3.5** in 66 % yield. An ORTEP diagram of the molecular structure of **3.5** is shown in Figure 3.7. Compound **3.5** contains five metal atoms, one of Ir and four of Ru. The metal atoms are arranged in the form of an iridium-capped butterfly tetrahedron of four ruthenium atoms. There are two $P(t\text{-}Bu)_3$ ligands, one on the iridium atom Ir(1) and the other on Ru(2). The Ir – Ru bond distances are normal, Ir(1) – Ru(1) = 2.8440(4) Å, Ir(1) – Ru(3) = 2.8061(4) Å and Ir(1) – Ru(4) = 2.8353(4) Å. The Ru – Ru distances are also typical Ru(1) – Ru(2) = 2.9081(5) Å, Ru(1) – Ru(3) = 2.9128(5) Å, Ru(1) – Ru(4) = 2.7816(5) Å, Ru(2) – Ru(3) = 2.8958(5) Å and

Ru(3) – Ru(4) = 2.8204(5), Å. The hydrido ligand, located and refined in the structural analysis, was found to be a triply-bridging ligand across the Ir(1) - Ru(1) - Ru(3) triangle, Ir(1) – H(1) = 1.78(4) Å, Ru(1) – H(1) = 1.99(4) Å, Ru(3) – H(1) = 1.96(4) Å. It exhibits a very high-field resonance shift in the ^{1}H NMR spectrum, -19.47 ppm, with coupling to the two phosphorus atoms, $^{2}J_{P\text{-}H}$ = 2.4 Hz and $^{3}J_{P\text{-}H}$ = 1.6 Hz. Compound **3.5** contains a η^2-quadruply-bridging CO ligand, C(1) – O(1), of the type **E**. The carbon atom is bonded to all four ruthenium atoms, Ru(1) – C(1) = 2.164(4) Å, Ru(2) – C(1) = 2.242(4) Å, Ru(3) – C(1) = 2.156(4) Å and Ru(4) – C(1) = 2.083(5) Å. The oxygen atom is bonded only to Ru(2), Ru(2) – O(1) = 2.139(3) Å. As found in **3.4**, the CO bond distance is also long, C(1) – O(1) = 1.256(15) Å.

DFT molecular orbital calculations have revealed the nature of the coordination of the quaduply-bridging CO ligand to the four ruthenium atoms. Selected MOs that show the bonding of the η^2-quadruply-bridging CO ligand to the four metal atoms in **3.5** are shown in Figure 3.8. The HOMO-1 and HOMO-13 show η^2-π-backbonding from the metal atoms into one of the π^*-orbitals of the CO ligand at both the carbon and oxygen atoms. The HOMO-60 and HOMO-61 show π-donation from the filled π-orbitals on the CO ligand to the metal atoms. The HOMO-110 and HOMO-111 show σ-donation from the CO ligand π-bond to the metal atoms, principally to Ru(2). The HOMO-112 shows π-donation from the filled π-orbitals on the CO ligand to the metal atoms and the HOMO-132 shows a strong σ-donation from the CO carbon atom to the Ru3 triangle, Ru(1), Ru(3) and Ru(4). In this way the quadruply-bridging CO ligand is able to serve formally as a four electron donor and the cluster thus contains a total of 74 valence electrons which is exactly the number expected for an electron-precise edge-bridged tetrahedron or a

capped butterfly tetrahedron, that is, all of the metal atoms achieve 18 electron configurations.[22] The geometry optimized coordinates for **3.5** are listed in table 3.10.

When compound **3.5** was treated with CO (1 atm) in a hexane solution at reflux for 30 min the new compound $IrRu_4(CO)_{14}P(t\text{-}Bu)_3(\mu_4\text{-}\eta^2\text{-}CO)(\mu\text{-}H)$, **3.6** was obtained in 18 % yield. Compound **3.6** was characterized crystallographically and an ORTEP diagram of its molecular structure is shown in Figure 3.9. Like **3.5**, compound **3.6** also contains five metal atoms, one of Ir and four of Ru. The cluster is very similar to that of **3.2** having the metal atoms are arranged in the form of a spiked-tetrahedron. The iridium atom is contained in the tetrahedral portion of the cluster, Ir(1) – Ru(2) = 2.7831(5) Å, Ir(1) – Ru(3) = 2.7295(6) Å, Ir(1) – Ru(4) = 2.7814(5) Å. Ru(1) is the "spike" that is bonded only to the iridium atom, Ir(1) – Ru(1) = 2.8215(5) Å. There is only one $P(t\text{-}Bu)_3$ ligand in **3.6**, and it is coordinated to the ruthenium atom labeled Ru(1), Ru(1) – P(1) = 2.5205(16) Å. There is one hydrido ligand H(1) that bridges the Ru(2) – Ru(3) bond, Ru(2) – H(1) = 1.79(6) Å, Ru(3) – H(1) = 1.74(5) Å, and as a result that metal – metal bond is significantly longer, Ru(2) – Ru(3) = 2.9569(7) Å, than the other two, Ru(2) – Ru(4) = 2.7921(7) Å and Ru(3) – Ru(4) = 2.7940(7) Å.[19] The hydrido ligand exhibits a high-field resonance shift in the ^1H NMR spectrum, -17.22 ppm. No coupling was observed to the remotely positioned phosphorus atom of the $P(t\text{-}Bu)_3$ ligand. An η^2-quadruply bridging carbonyl ligand, C(1) – O(1), of the general form **F** and is coordinated to three metal atoms Ir(1), Ru(2) and Ru(4) by its carbon atom. Two of the M - C bonds are quite short, Ir(1) – C(1) = 2.009(6) Å, Ru(4) – C(1) = 2.036(6) Å, the third bond Ru(2) – C(1) which lies trans to the bridging hydrido ligand (see below) is much longer at 2.287(6) Å. The oxygen atom is coordinated only to Ru(1), Ru(1) – O(1) =

2.159(4) Å, which is very similar to that found in **3.2**. The Ru(1) - C(1) distance at 2.619(6) Å is believed to be largely nonbonding. As found in **3.2**, **3.3** and **3.4**, the CO bond distance is also long, C(1) – O(1) = 1.269(7) Å. Like **3.2**, compound **3.6** contains a total of 76 valence electrons which is precisely the number expected for a spiked-tetrahedral cluster of five metal atoms. Compound **3.6** was formed by the loss of one of the $P(t\text{-}Bu)_3$ ligands from **3.5** and the addition of two CO ligands. Thus, in converting from **3.5** to **3.6**, the number of ligands was increased by one and accordingly the number of metal – metal bonds was decreased by one. Assuming that the $P(t\text{-}Bu)_3$ ligand is bonded to the same Ru atom in **3.6** that it was in **3.5**, then that Ru grouping must make a shift from the Ru atoms to the Ir atom. This can be achieved by a series of ligand additions and eliminations as shown schematically in Scheme 3.3 where ligand additions lead to cleavage of metal – metal bonds and ligand eliminations lead to formation of metal – metal bonds.

In order to obtain a better understanding of the bonding of the η^2-quaduply-bridging CO ligand to the four metal atoms in **3.6**, DFT molecular orbital calculations were performed. Selected MOs that show the bonding of the bridging CO ligand to the four metal atoms in **3.6** are shown in Figure 3.10. The HOMO and HOMO-15 show η^2-π-backbonding from Ru(1) and Ir(1) both to the carbon and to oxygen atom of the CO ligand via one of the CO π^*-orbitals. The HOMO-3 shows η^1-π-backbonding to the other CO π^* orbital via the carbon atom alone. Recalling that the η^2-quaduply-bridging CO ligand serves formally as a 4-electron donor, a search of the low lying orbitals revealed evidence for electron donating interactions to support this model. In particular, the HOMO-44 and HOMO-85 show η^2-π-donations to the metal atoms from each of the

filled CO π-bonding orbitals and HOMO-92 shows donation from the CO σ-orbital that is frequently referred to as lone pair or electrons on the carbon atom. The CO portion of HOMO-92 is distorted from its classical linear form because its bonding to the metal atoms. The geometry optimized coordinates for **3.6** are listed in table 3.11. When compound **3.6** was treated with CO at 70^{o}C/10 atm for 1h, it was converted to **3.3** in 36% yield by removal of two of the Ru groups. $Ru_3(CO)_{12}$ was isolated as a coproduct in 56% yield.

Summary

A summary of the results of this study are shown in Scheme 3.4. The principal products formed by the reaction of $IrRu_3(CO)_{13}(\mu_3\text{-}H)$ with $P(t\text{-}Bu)_3$ are the closed and open $IrRu_3$ cluster complexes **3.1** and **3.4**. Complex **3.3** is a lower nuclearity cluster complex formed by the loss of one Ru grouping. Compound **3.2** is higher nuclearity minor product formed by an aggregation process that has not yet been elucidated. Complex **3.3** is particularly interesting because it is electronically unsaturated and exhibits a high reactivity for the addition of H_2 to yield **3.7**. Compound **3.5** is a higher nuclearity species obtained from **3.4** by the addition of an Ru grouping from $Ru(CO)_5$. Compound **3.6** was obtained from **3.5** by treatment with CO accompanied by a rearrangement of the metal atoms. Compounds **3.2**, **3.4**, **3.5** and **3.6** all contain a η^2-bridging CO ligand which stabilizes the open structures of the clusters.

Conclusions

In previous studies we showed that the introduction of the bulky $P(t\text{-}Bu)_3$ ligand into polynuclear transition metal carbonyl complexes can induce electronic unsaturation around the metal atoms via ligand deficiencies.[20, 23] This is also evident by the electronically unsaturated compound **3.3** described in this work. Compounds **3.4** - **3.6** are formally electron precise, but all of them have a bridging CO ligand that serves as a 4 electron donor. If the bridging CO ligand was a terminally coordinated 2 electron donor, then all of these complexes would also be electronically unsaturated. In other words, we feel that these higher nuclearity metal complexes have adopted the observed structures with 4 electron bridging CO ligands in order to eliminate the electronic unsaturation problem. One might ask why doesn't the molecule simply add another CO ligand and then have two terminally coordinated 2 electron donating CO ligands instead of one 4 electron η^2-bridging CO ligand. The answer might simply be steric effects. Two terminally coordinated CO ligands will almost certainly occupy more space than one η^2-bridging CO ligand. Although two atoms are coordinated to the metal atoms in both cases, for the η^2-bridging CO, the two atoms, C and O, are bonded to each other at a short distance, approx. 1.25 Å, and thus would occupy must less space in the coordination sphere of the metal atoms than two nonbonded carbon atoms from two terminally coordinated CO ligands.

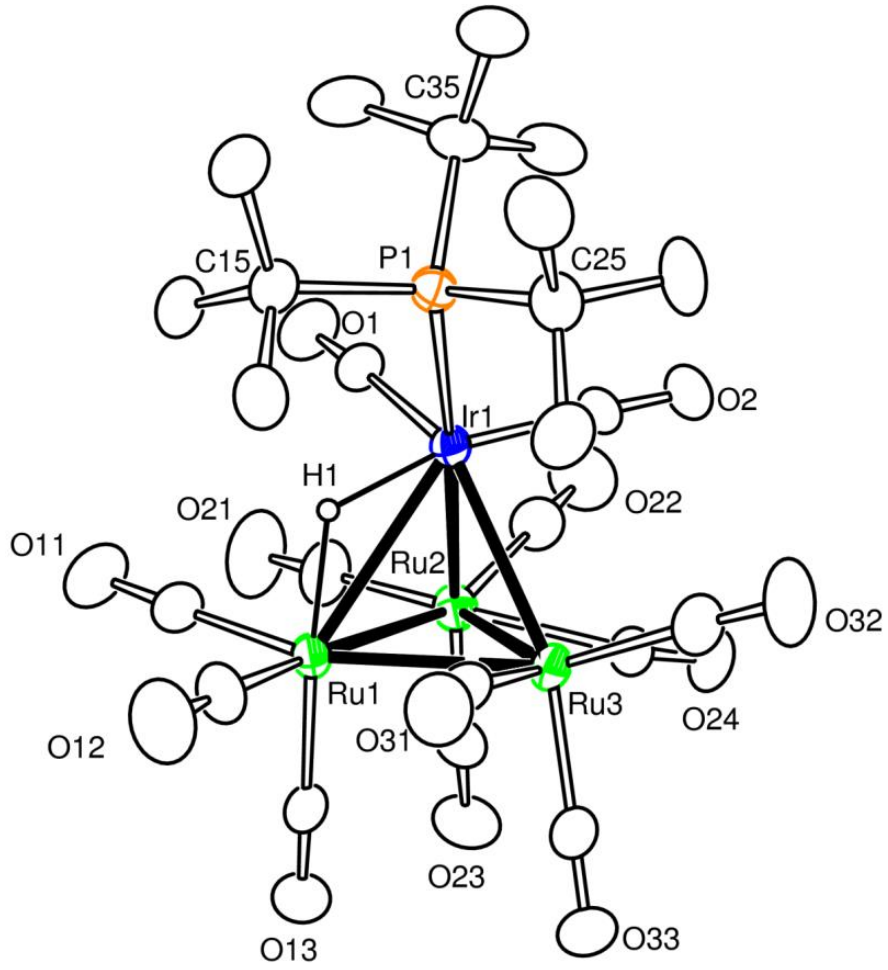

Figure 3.1. An ORTEP diagram of the molecular structure of $IrRu_3(CO)_{12}P(t\text{-}Bu)_3(\mu\text{-}H)$, **3.1** showing 30% thermal ellipsoid probability.

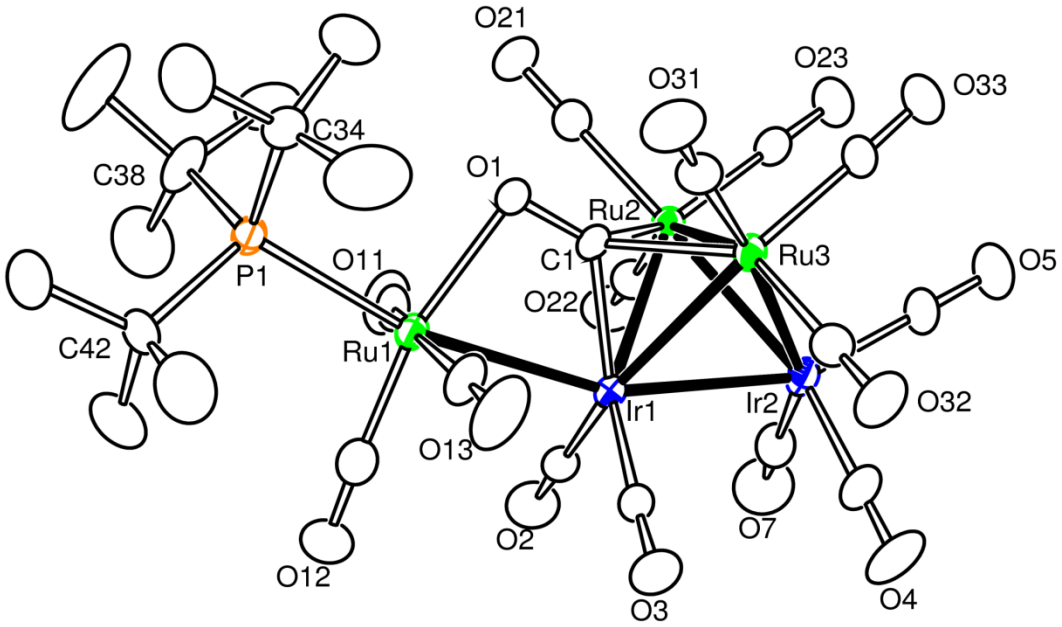

Figure 3.2. An ORTEP diagram of the molecular structure of $Ir_2Ru_3(CO)_{15}P(t\text{-}Bu)_3(\mu\text{-}H)$, **3.2** showing 30% thermal ellipsoid probability.

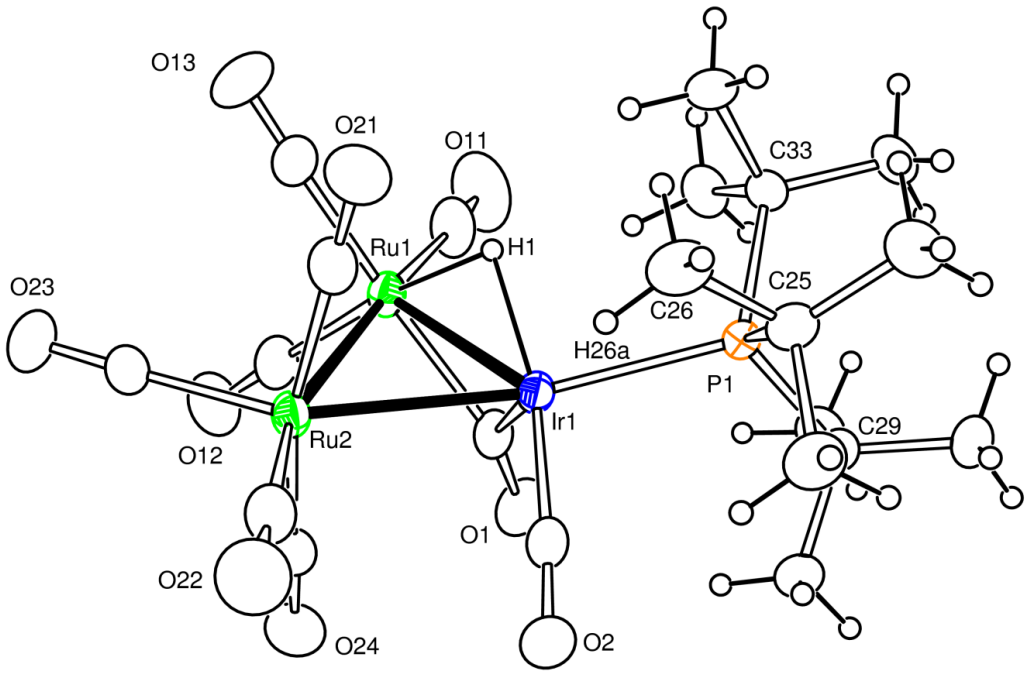

Figure 3.3. An ORTEP diagram of molecular structure of $IrRu_2(CO)_9P(t\text{-}Bu)_3(\mu\text{-}H)$, **3.3** showing 30% thermal ellipsoid probability.

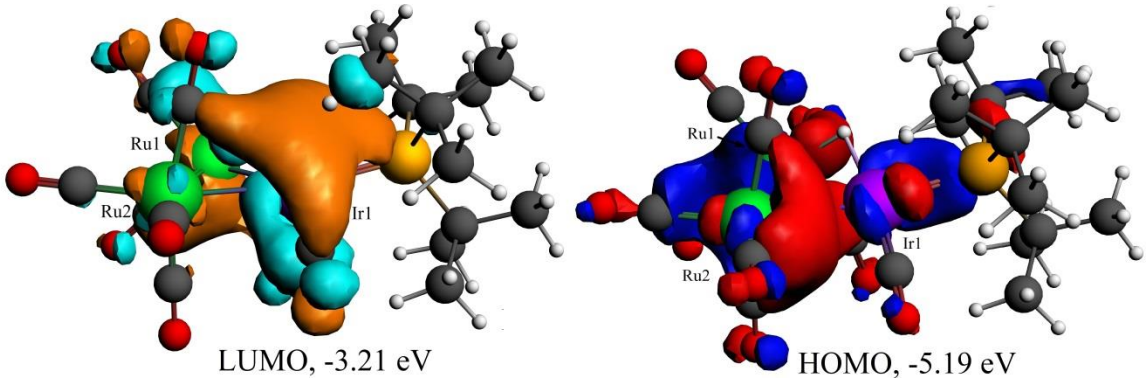

Figure 3.4. ADF MO diagrams of the LUMO, (left) and HOMO, (right) for compound **3.3**. A large component of the LUMO in golden color lies in the proximity of the vacant coordination site on the iridium atom, violet = Ir, green = Ru; Isovalue = 0.03.

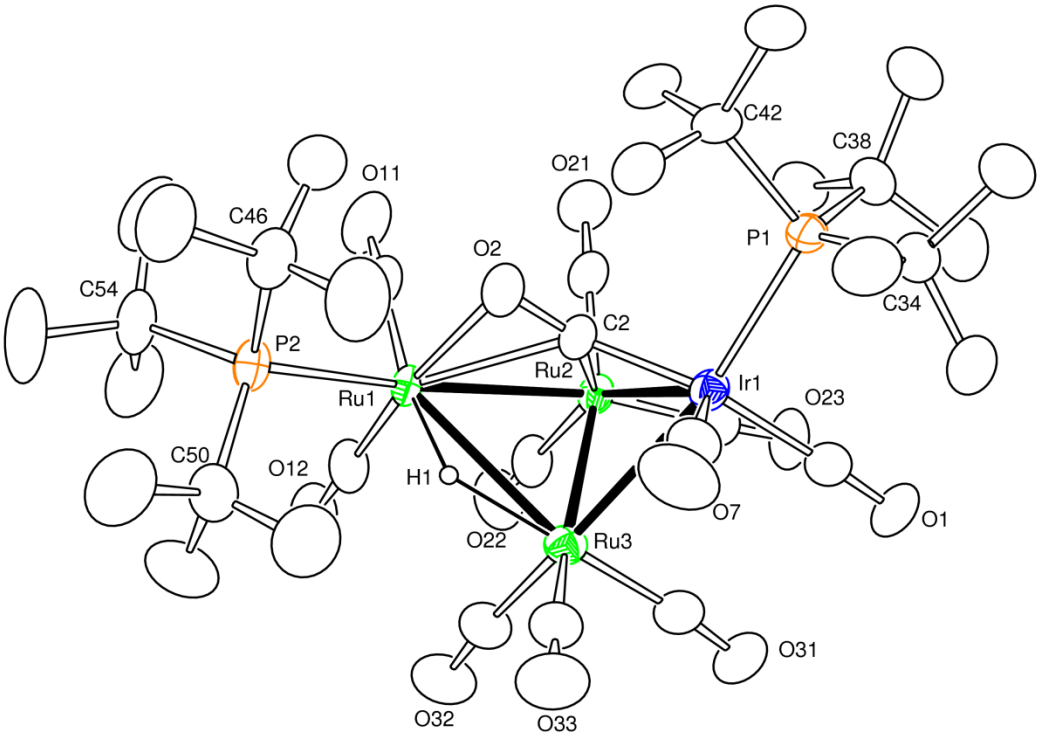

Figure 3.5. An ORTEP diagram of molecular structure of $IrRu_3(CO)_{10}(\mu_3\text{-}CO)[P(t\text{-}Bu)_3]_2(\mu\text{-}H)$, **3.4**, showing 30% thermal ellipsoid probability.

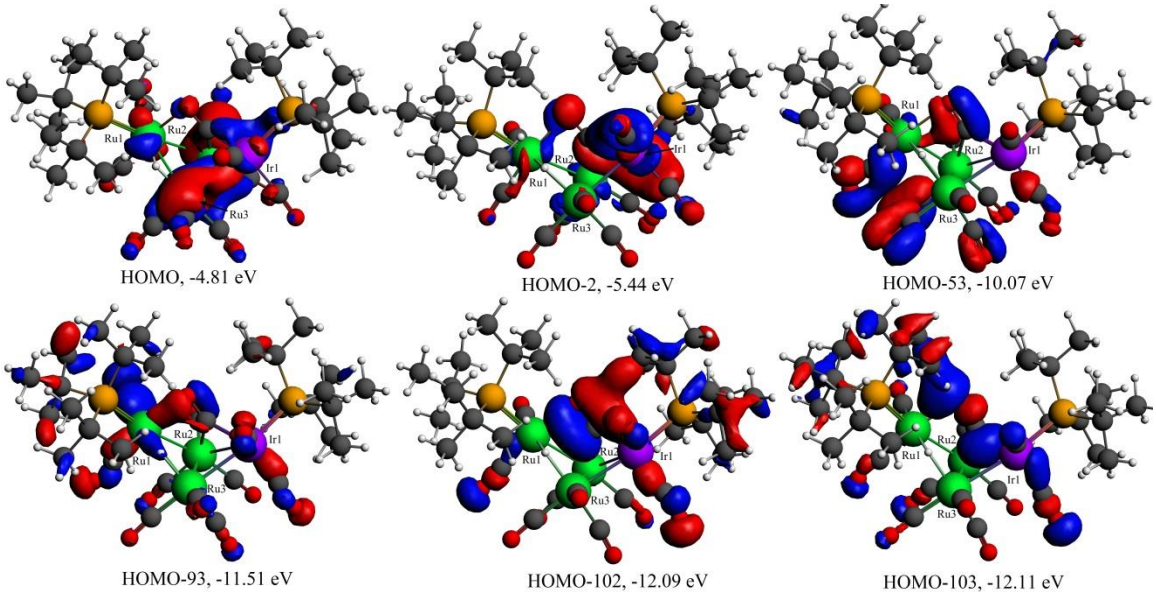

Figure 3.6. Selected ADF MO diagrams for compound **3.4** showing the bonding of the bridging CO ligand to the metal atoms, violet = Ir, green = Ru; Isovalue = 0.03.

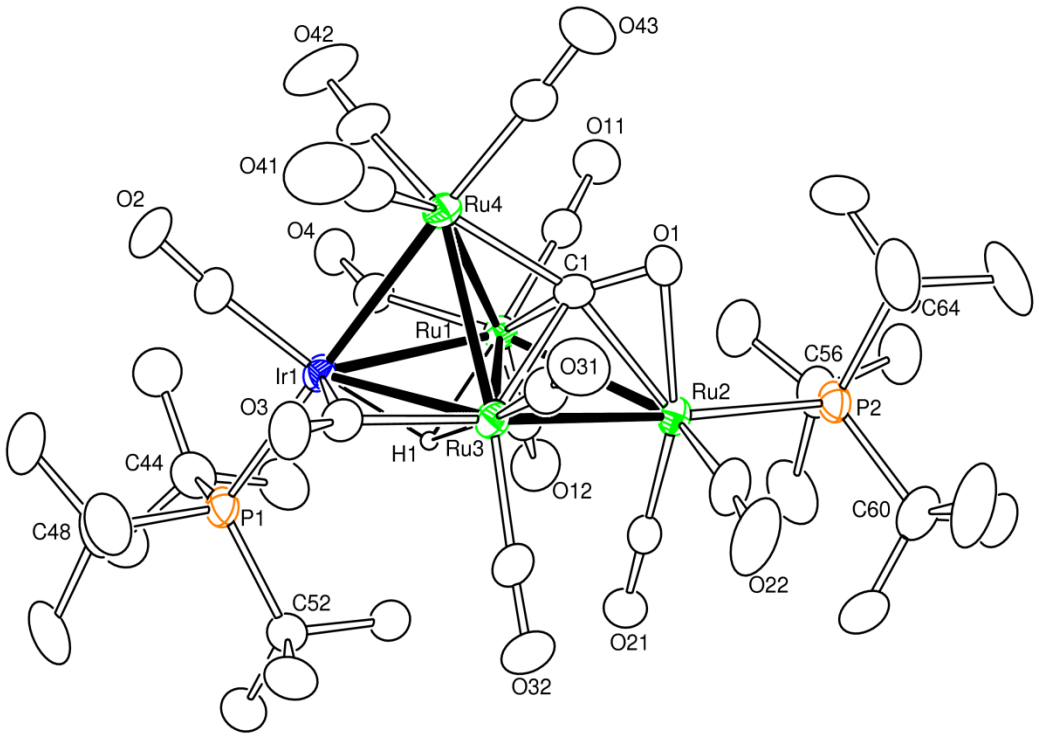

Figure 3.7. An ORTEP diagram of molecular structure of $IrRu_4(CO)_{12}[P(t\text{-}Bu)_3]_2(\mu_4\text{-}\eta^2\text{-}CO)(\mu_3\text{-}H)$, **3.5**, showing 30% thermal ellipsoid probability.

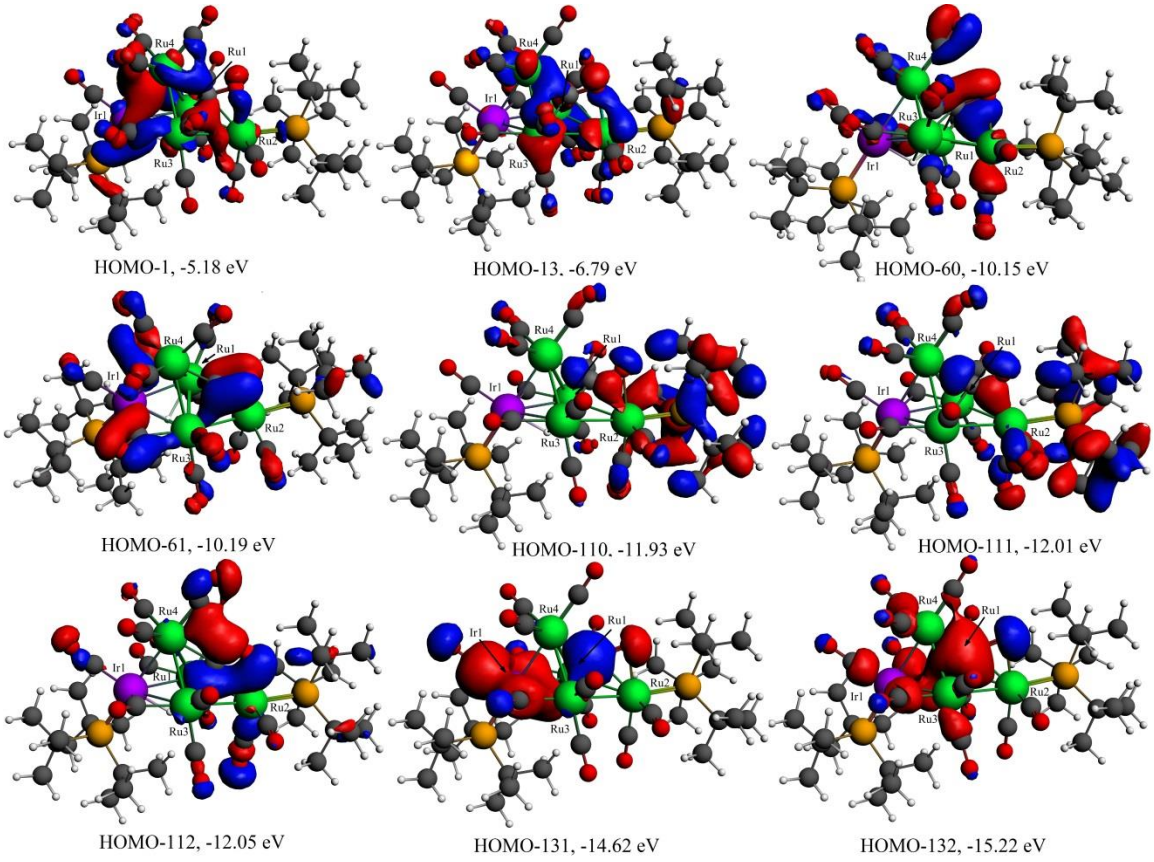

Figure 3.8. Selected ADF MO diagrams with energies for compound **3.5** showing the bonding of the quadruply bridging CO ligand to the metal atoms of the cluster, violet = Ir, green = Ru; Isovalue = 0.03.

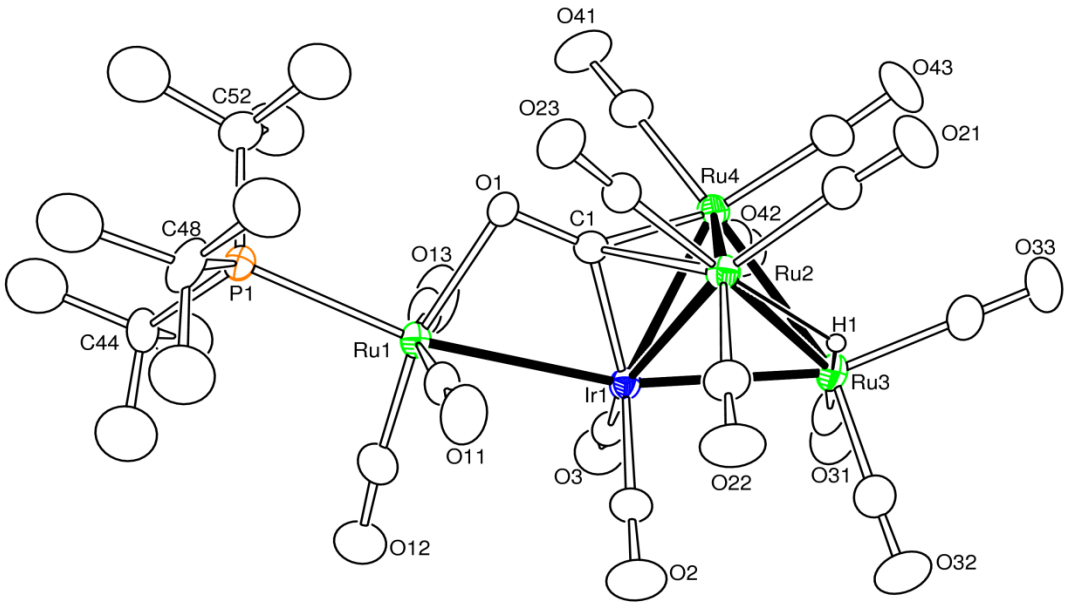

Figure 3.9. An ORTEP diagram of molecular structure of $IrRu_4(CO)_{14}P(t\text{-}Bu)_3(\mu_4\text{-}\eta^2\text{-}CO)(\mu\text{-}H)$, **3.6**, showing 30% thermal ellipsoid probability.

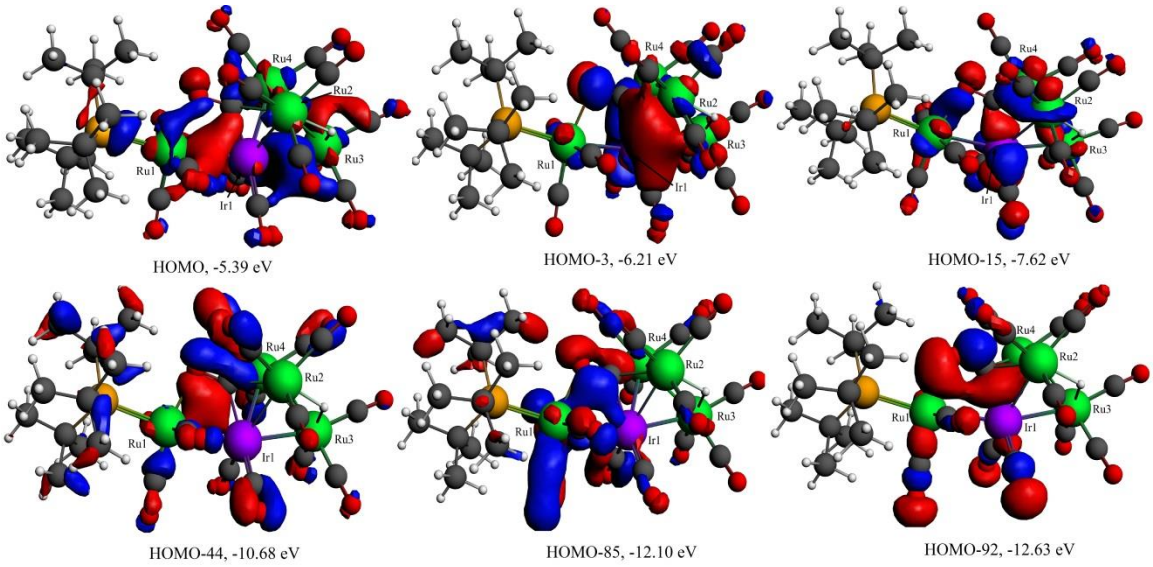

Figure 10. ADF MO diagrams with energies for compound **3.6** showing the bonding of the quadruply bridging CO ligand to the metal atoms of the cluster, violet = Ir, green = Ru; Isovalue = 0.03.

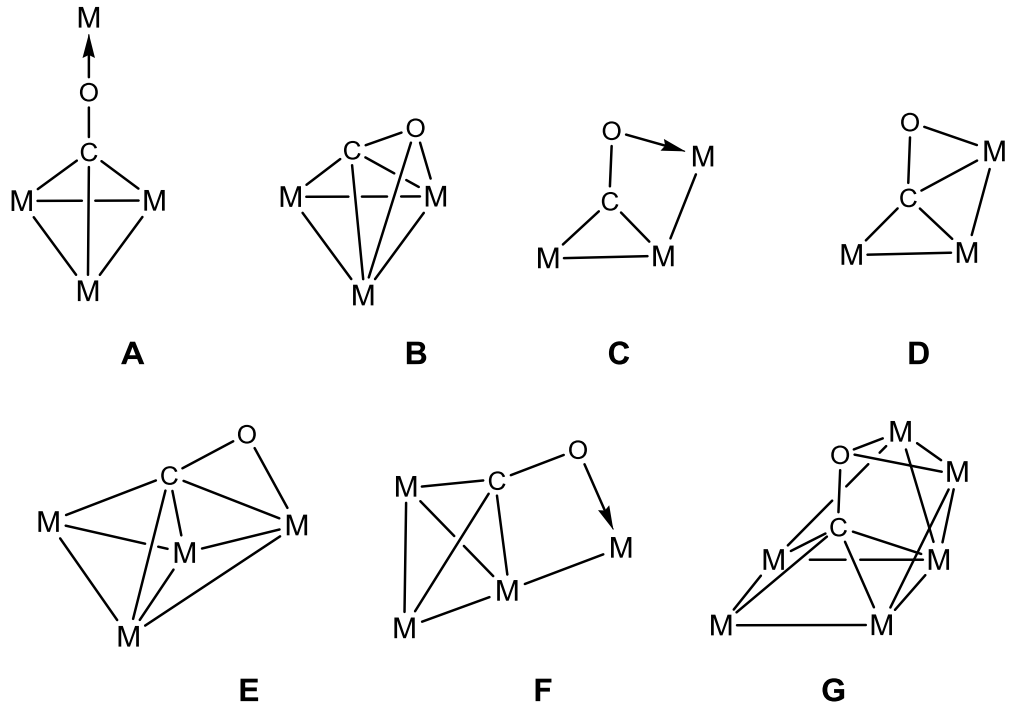

Scheme 3.1 Bonding modes of η^2-carbonyl ligand in different metal clusters.

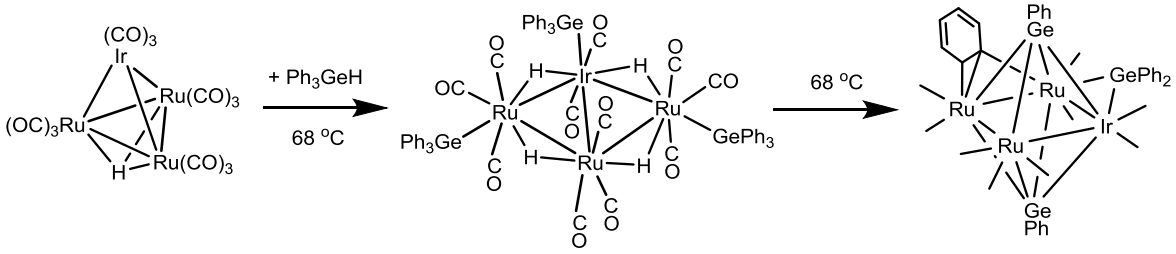

Scheme 3.2 The formation of μ-η^2-phenyl ligand in Ir-Ru cluster complex.

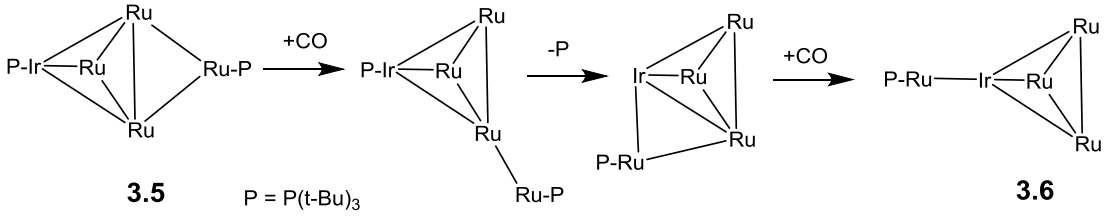

3.5 P = $P(t\text{-}Bu)_3$ **3.6**

Scheme 3.3 The transformation of compound **3.5** to **3.6** under CO atmosphere.

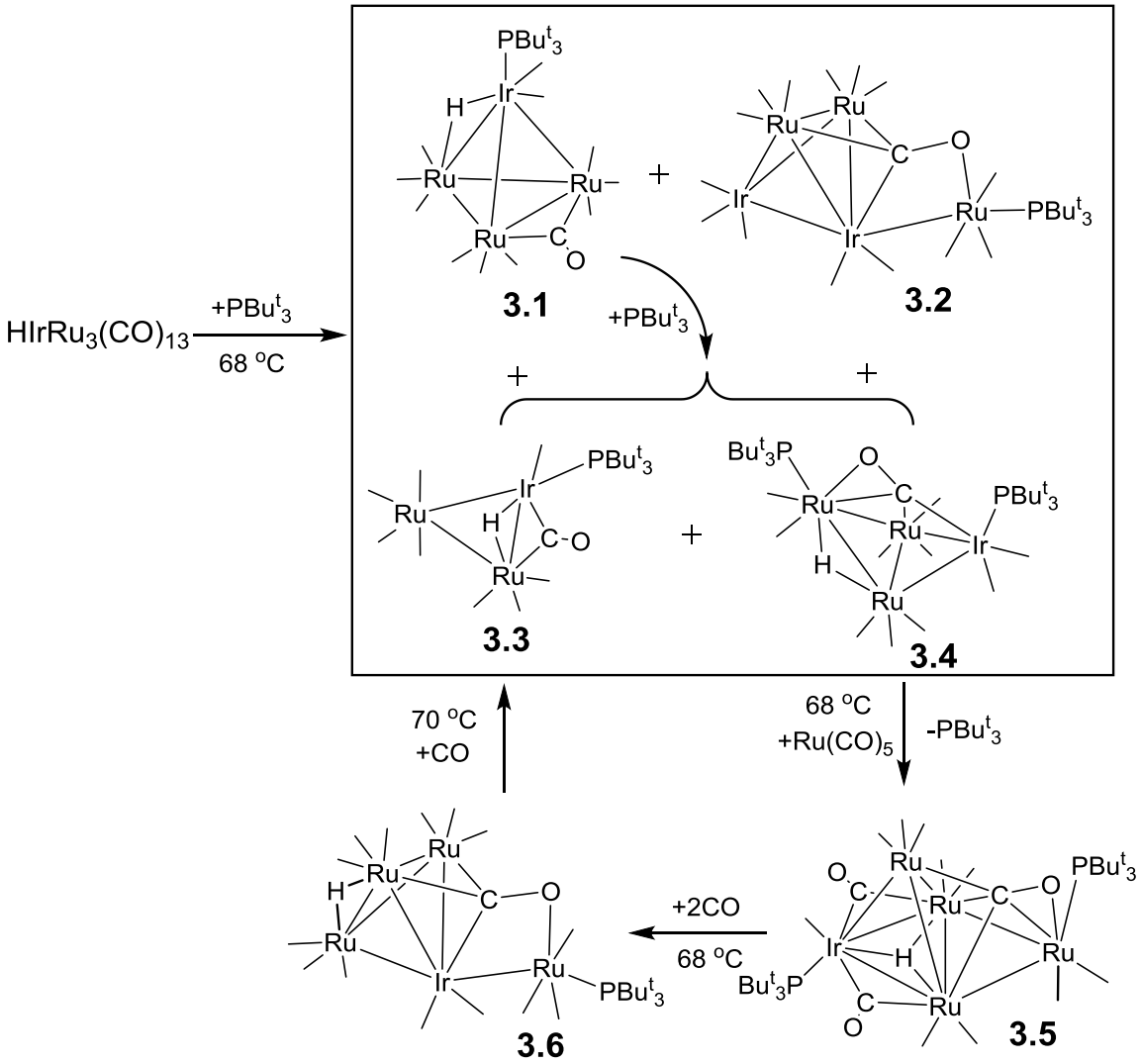

Scheme 3.4 The reaction of $HIrRu_3(CO)_{13}$ with PBu^t_3 and the transformation of carbonyl ligand through Ir-Ru cluster complexes.

Table 3.1. Crystallographic Data for Compounds **3.1** – **3.6**.

Compound	**3.1**	**3.2**	**3.3**
Empirical formula	$C_{24}H_{28}O_{12}PIrRu_3$	$C_{27}H_{27}O_{15}PIr_2Ru_3$	$C_{21}H_{28}O_9PIrRu_2$
Formula weight	1034.84	1310.07	849.47
Crystal system	Monoclinic	Triclinic	Triclinic
Lattice parameters			
a (Å)	23.3890(5)	9.2176(5)	8.7946(2)
b (Å)	15.3868(3)	13.8635(7)	11.6347(3)
c (Å)	18.0450(4)	15.3533(8)	14.5421(4)
α (deg)	90	69.963(1)	88.916(1)
β (deg)	93.661(1)	83.723(1)	87.306(1)
γ (deg)	90	75.776(1)	69.431(1)
V (Å3)	6480.8(2)	1786.03(16)	1391.58(6)
Space group	$P2_1/c$	*P*-1	*P*-1
Z value	8	2	2
ρcalc (g / cm^3)	2.121	2.436	2.028
μ(Mo Kα) (mm-1)	5.569	8.773	5.942
Temperature (K)	293(2)	293(2)	293(2)
2Θ max (°)	50.06	50.06	50.06
No.Obs.(I >2σ(I))	11446	5454	4919
No. Parameters	765	442	419
Goodness of fit (GOF)	1.034	1.088	1.026
Max. shift in cycle	0.001	0.001	0.001
Residuals[a]: R_1; wR_2	0.0340;0.0622	0.0382;0.0940	0.0176;0.0416
Absorp.Corr. Max/min	1.000/0.627	1.000/ 0.716	1.000/ 0.786
Largest peak in Final Diff. Map (e^- / $Å^3$)	0.735	1.34	0.545

[a]$R_1 = \Sigma_{hkl}(\,|\,|F_{obs}|-|F_{calc}|\,|)/\Sigma_{hkl}|F_{obs}|$; $wR_2 = [\Sigma_{hkl}w(|F_{obs}|-|F_{calc}|)^2/\Sigma_{hkl}wF^2_{obs}]^{1/2}$; $w = 1/\sigma^2(F_{obs})$; GOF = $[\Sigma_{hkl}w(|F_{obs}|-|F_{calc}|)^2/(n_{data}-n_{vari})]^{1/2}$.

Table 3.1. Crystallographic Data for Compounds **3.1** – **3.6**. (continued)

Compound	**3.4**	**3.5**	**3.6**
Empirical formula	$C_{35}H_{55}O_{11}P_2IrRu_3$	$C_{37}H_{55}O_{13}P_2IrRu_4$	$C_{27}H_{28}O_{15}PIrRu_4$
Formula weight	1209.14	1366.23	1219.94
Crystal system	Triclinic	Monoclinic	Triclinic
Lattice parameters			
a (Å)	10.9111(10)	9.0240(3)	9.2160(5)
b (Å)	14.2152(13)	19.1783(6)	13.6780(7)
c (Å)	16.7887(16)	27.1206(8)	15.3477(8)
α (deg)	67.474(2)	90	71.504(1)
β (deg)	72.862(2)	94.873(1)	85.536(1)
γ (deg)	73.707(2)	90	76.886(1)
V (Å3)	2256.7(4)	4676.7(3)	1786.86(16)
Space group	*P*-1	$P2_1/n$	*P*-1
Z value	2	4	2
ρcalc (g / cm^3)	1.779	1.940	2.267
μ(Mo Kα) (mm^{-1})	4.044	4.222	5.472
Temperature (K)	293(2)	293(2)	293(2)
2Θ max (°)	50.06	50.06	50.06
No.Obs. (I>2σ(I))	7944	8270	6303
No. Parameters	486	536	477
Goodness of fit (GOF)	1.072	1.041	1.064
Max. shift in cycle	0.001	0.001	0.001
Residuals[a]:R_1; wR_2	0.0531;0.1528	0.0282;0.0612	0.0334;0.0735
Absorp. Corr. Max/min	1.000/0.748	1.000/0.859	1.000/0.720
Largest peak in Final Diff. Map (e^- / $Å^3$)	3.522	0.759	1.145

[a] $R_1 = \Sigma_{hkl}(||F_{obs}|-|F_{calc}||)/\Sigma_{hkl}|F_{obs}|$; $wR_2 = [\Sigma_{hkl}w(|F_{obs}|-|F_{calc}|)^2/\Sigma_{hkl}wF^2_{obs}]^{1/2}$; $w = 1/\sigma^2(F_{obs})$; GOF = $[\Sigma_{hkl}w(|F_{obs}|-|F_{calc}|)^2/(n_{data} - n_{vari})]^{1/2}$.

Table 3.2. Selected intramolecular angles and bond distances for compound **3.1**.[a]

Distances			**Angles**			
Atom	Atom	Distance(Å)	Atom	Atom	Atom	Angle(deg)
Ir1	Ru1	2.9115(5)	Ru2	Ir1	Ru3	59.600(15)
Ir1	Ru2	2.7750(5)	Ru2	Ir1	Ru1	58.477(15)
Ir1	Ru3	2.8257(5)	Ru3	Ir1	Ru1	57.796(13)
Ru1	Ru2	2.7801(7)	Ru3	Ru1	Ru2	60.164(17)
Ru1	Ru3	2.7735(6)	Ru3	Ru1	Ir1	59.549(13)
Ir1	H1	1.70(5)	Ru2	Ru1	Ir1	58.306(14)
Ru1	H1	1.76(5)	Ir1	Ru2	Ru1	63.216(15)
Ru2	Ru3	2.8937(7)	Ir1	Ru2	Ru3	61.104(15)
Ir1	P1	2.4825(15)	Ru1	Ru2	Ru3	59.800(17)

[a] Estimated standard deviations in the least significant figure are given in parentheses.

Table 3.3. Selected intramolecular angles and bond distances for compound **3.2**.[a]

Distances			**Angles**			
Atom	Atom	Distance(Å)	Atom	Atom	Atom	Angle(deg)
Ir1	Ir2	2.7055(5)	Ir2	Ir1	Ru2	60.552(17)
Ir1	Ru2	2.7616(7)	Ir2	Ir1	Ru3	60.402(17)
Ir1	Ru3	2.7723(7)	Ru2	Ir1	Ru3	60.38(2)
Ir1	Ru1	2.8040(7)	Ir2	Ir1	Ru1	159.74(2)
Ir2	Ru3	2.7511(7)	Ru2	Ir1	Ru1	101.17(2)
Ir2	Ru2	2.7568(7)	Ru3	Ir1	Ru1	104.11(2)
Ru2	Ru3	2.7827(9)	Ir1	Ir2	Ru3	60.998(16)
Ir1	C1	2.021(8)	Ir1	Ir2	Ru2	60.731(17)
Ru2	C1	2.129(8)	Ru3	Ir2	Ru2	60.63(2)
Ru3	C1	2.101(8)	Ir2	Ru2	Ir1	58.717(16)
Ru1	O1	2.165(5)	Ir2	Ru2	Ru3	59.67(2)
Ru1	P1	2.522(2)	Ir1	Ru2	Ru3	60.00(2)
C1	O1	1.276(9)	Ir2	Ru3	Ir1	58.599(16)

[a] Estimated standard deviations in the least significant figure are given in parentheses.

Table 3.4. Selected intramolecular angles and bond distances for compound **3.3**.[a]

Distances			**Angles**			
Atom	Atom	Distance(Å)	Atom	Atom	Atom	Angle(deg)
Ir1	Ru1	2.7570(3)	Ru1	Ir1	Ru2	61.511(8)
Ir1	Ru2	2.7659(3)	Ir1	Ru1	Ru2	59.401(8)
Ru1	Ru2	2.8243(4)	Ir1	Ru2	Ru1	59.088(8)
Ir1	P1	2.3863(9)	Ru1	Ir1	H1	39.3(13)
Ir1	C1	2.013(4)	Ru2	Ir1	H1	82.9(13)
Ru1	C1	2.089(4)	Ir1	Ru1	H1	40.7(13)
Ir1	H1	1.83(4)	Ru2	Ru1	H1	82.0(14)
Ru1	H1	1.77(4)	Ir1	C1	Ru1	84.53(13)
Ir1	C26	3.310(4)	O1	C1	Ir1	131.7(3)
Ir1	H26a	2.71	O1	C1	Ru1	143.6(3)

[a] Estimated standard deviations in the least significant figure are given in parentheses.

Table 3.5. Selected intramolecular angles and bond distances for compound **3.4**.[a]

Distances			**Angles**			
Atom	Atom	Distance(Å)	Atom	Atom	Atom	Angle(deg)
Ir1	Ru2	2.8722(8)	Ru2	Ru1	Ru3	54.87(2)
Ir1	Ru3	2.8783(9)	Ru3	Ru2	Ru1	66.33(2)
Ir1	P1	2/470(2)	Ru3	Ru2	Ir1	61.77(2)
Ir1	C2	1.917(9)	Ru1	Ru2	Ir1	93.54(2)
Ru1	Ru2	2.8563(9)	Ru2	Ru3	Ir1	61.51(2)
Ru1	Ru3	3.0574(10)	Ru2	Ru3	Ru1	58.80(2)
Ru2	P2	2.496(2)	Ir1	Ru3	Ru1	89.28(2)
Ru1	C2	2.476(10)	Ru2	Ir1	Ru3	56.72(2)
Ru1	O2	2.168(8)	O2	Ru1	C2	30.5(2)
Ru1	H1	1.627	O2	Ru1	Ru2	74.59(17)
Ru2	Ru3	2.7311(11)	C2	Ru1	Ru2	46.90(19)
Ru2	C2	2.150(10)	O2	Ru1	Ru3	84.28(18)
Ru3	H1	1.829	C2	Ru1	Ru3	59.5(2)
C2	O2	1.250(11)	C2	Ru2	Ru3	68.6(2)

[a] Estimated standard deviations in the least significant figure are given in parentheses.

Table 3.6. Selected intramolecular angles and bond distances for compound **3.5**.[a]

Distances			**Angles**			
Atom	Atom	Distance(Å)	Atom	Atom	Atom	Angle(deg)
Ir1	Ru1	2.8440(4)	Ru3	Ir1	Ru4	59.991(11)
Ir1	Ru3	2.8061(4)	Ru3	Ir1	Ru1	62.063(11)
Ir1	Ru4	2.8353(4)	Ru4	Ir1	Ru1	58.652(10)
Ir1	P1	2.4582(12)	Ru3	Ir1	H1	43.9(12)
Ir1	H1	1.78(4)	Ru4	Ir1	H1	86.1(12)
Ru1	Ru2	2.9081(5)	Ru1	Ir1	H1	43.8(12)
Ru1	Ru3	2.9128(5)	Ru4	Ru1	Ir1	60.518(11)
Ru1	Ru4	2.7816(5)	Ru4	Ru1	Ru2	96.874(14)
Ru1	C1	2.164(4)	Ir1	Ru1	Ru2	116.836(14)
Ru1	H1	1.99(4)	Ru4	Ru1	Ru3	59.325(12)
Ru2	Ru3	2.8958(5)	Ir1	Ru1	Ru3	58.330(10)
Ru2	P2	2.4932(12)	Ru2	Ru1	Ru3	59.668(12)
Ru2	C1	2.242(4)	Ru4	Ru1	H1	83.9(11)
Ru2	O1	2.139(3)	Ir1	Ru1	H1	38.2(12)
Ru3	Ru4	2.8204(5)	Ru2	Ru1	H1	85.7(11)
Ru3	H1	1.96(4)	Ru3	Ru1	H1	42.1(11)
Ru3	C1	2.156(4)	Ru3	Ru2	Ru1	60.248(12)
Ru4	C1	2.083(5)	Ir1	Ru3	Ru4	60.519(11)
C1	O1	1.256(5)	Ir1	Ru3	Ru2	118.491(14)

[a] Estimated standard deviations in the least significant figure are given in parentheses.

Table 3.7. Selected intramolecular angles and bond distances for compound **3.6**.[a]

Distances			**Angles**			
Atom	Atom	Distance(Å)	Atom	Atom	Atom	Angle(deg)
Ir1	Ru1	2.8215(5)	Ru3	Ir1	Ru4	60.919(16)
Ir1	Ru2	2.7831(5)	Ru3	Ir1	Ru2	64.866(15)
Ir1	Ru3	2.7295(6)	Ru4	Ir1	Ru2	60.233(15)
Ir1	Ru4	2.7814(5)	Ru3	Ir1	Ru1	163.360(18)
Ir1	C1	2.009(6)	Ru4	Ir1	Ru1	104.440(16)
Ru1	P1	2.5206(16)	Ru2	Ir1	Ru1	101.741(16)
Ru1	O1	2.159(4)	Ir1	Ru2	Ru4	59.852(15)
Ru1	C1	2.619(6)	Ir1	Ru2	Ru3	56.690(14)
Ru2	Ru3	2.9569(7)	Ru4	Ru2	Ru3	58.072(17)
Ru2	Ru4	2.7921(7)	Ir1	Ru3	Ru4	60.457(15)
Ru2	C1	2.287(6)	Ir1	Ru3	Ru2	58.444(14)
Ru2	H1	1.79(6)	Ru4	Ru3	Ru2	58.008(17)
Ru3	Ru4	2.7940(7)	Ir1	Ru4	Ru2	59.914(15)
Ru3	H1	1.74(5)	Ir1	Ru4	Ru3	58.623(16)
Ru4	C1	2.036(6)	Ru2	Ru4	Ru3	63.920(18)
C1	O1	1.269(7)	O1	C1	Ir1	128.8(4)

[a] Estimated standard deviations in the least significant figure are given in parentheses.

Table 3.8. Geometry optimized coodinates of **3.3**, hydrogens are not included.

Atom	Coordinate			Atom	Coordinate		
	x	y	z		x	y	z
Ir1	10.77272	8.88172	10.64105	C14	9.986225	12.11528	12.11552
Ru1	12.44527	6.959934	11.68158	C15	8.577026	11.53319	11.98767
Ru2	10.49311	6.274956	9.711074	C16	9.915196	13.62444	11.86503
P1	11.18322	11.19752	10.93268	C17	10.40469	11.87458	13.56886
C1	10.83609	8.096686	12.45656	C18	12.97357	11.60902	11.49166
C2	8.97408	9.032685	10.27541	C19	13.23172	13.0823	11.82254
C3	13.68105	7.488398	13.00429	C20	13.30839	10.77555	12.72993
C4	11.9912	5.38519	12.61583	C21	13.96006	11.17193	10.4035
C5	13.73144	6.072143	10.56916	O1	10.17269	8.231325	13.42709
C6	11.80048	7.003074	8.510794	O2	7.830576	9.048544	10.0692
C7	9.077912	6.39914	8.461086	O3	14.46116	7.684858	13.83405
C8	10.96556	4.449233	9.459271	O4	11.72167	4.433237	13.20659
C9	9.305848	5.958785	11.20722	O5	14.52905	5.534324	9.935537
C10	10.95333	11.89192	9.157116	O6	12.5619	7.436691	7.758199
C11	11.54231	10.84328	8.20562	O7	8.227425	6.422689	7.681512
C12	9.466747	12.00321	8.806977	O8	11.2425	3.344623	9.278185
C13	11.59916	13.2494	8.877859	O9	8.575911	5.757477	12.07352

Table 3.9. Geometry optimized coodinates of **3.4**, hydrogens are not included.

Atom	Coordinate			Atom	Coordinate		
	x	y	z		x	y	z
Ru1	15.44499	12.85114	10.85752	C21	11.07604	15.82689	11.79596
Ru2	16.3028	15.49878	10.23818	C22	11.678	16.41509	9.484958
Ru3	16.64469	14.7506	12.85637	C23	9.984268	17.76154	10.69423
Ir1	14.62621	16.68857	12.22478	C24	12.42838	11.0585	11.65088
P1	12.77928	18.07275	11.47274	C25	11.94219	11.73561	10.36071
P2	14.33289	10.788	11.58769	C26	12.13378	12.0047	12.81995
C1	11.30969	17.00784	10.84801	C27	11.58091	9.796285	11.83327
C2	15.74023	18.15763	12.79279	C28	14.90482	10.19822	13.33768
C3	14.45729	15.04769	11.17008	C29	15.04161	11.37888	14.30331
C4	13.76579	16.03802	13.73075	C30	13.97841	9.180288	14.01319
C5	15.19265	12.53935	9.036954	C31	16.31033	9.597273	13.22983
C6	17.10196	12.06465	10.77543	C32	14.63262	9.292641	10.39961
C7	15.58659	15.53654	8.493759	C33	14.30182	7.921903	10.9997
C8	17.96253	14.69056	9.839442	C34	16.09134	9.267628	9.937345
C9	17.08253	17.21936	10.18597	C35	13.78813	9.435714	9.130097
C10	17.84333	16.19723	12.90087	O1	16.4591	18.98087	13.17175
C11	18.11732	13.61569	13.01558	O2	13.68932	14.08112	11.03169
C12	16.23387	14.64397	14.69371	O3	13.24563	15.56127	14.65403
C13	12.11075	19.15236	12.93107	O4	15.0754	12.3865	7.893802
C14	11.24893	18.31859	13.88332	O5	18.15033	11.57321	10.69235
C15	13.27119	19.68621	13.77573	O6	15.20256	15.5601	7.401496
C16	11.26378	20.3477	12.48302	O7	18.99714	14.26717	9.547897
C17	13.27503	19.28259	10.05847	O8	17.61989	18.23816	10.06711
C18	12.1147	19.95998	9.324809	O9	18.66523	17.0067	12.96154
C19	14.09386	18.52915	9.011668	O10	19.06689	12.98643	13.21693
C20	14.20073	20.36047	10.63064	O11	16.08004	14.58524	15.83881

Table 3.10. Geometry optimized coodinates of **3.5**, hydrogens are not included.

Atom	Coordinate			Atom	Coordinate		
	x	y	z		x	y	z
Ir1	1.903937	3.365123	3.858029	C22	2.756438	0.082199	2.61294
Ru1	1.089291	4.622482	1.458173	C23	2.463512	-1.41047	2.417807
Ru2	3.163618	5.431153	-0.4312	C24	4.250066	0.266069	2.896323
Ru3	3.860499	4.543189	2.229851	C25	2.484221	0.746456	1.261416
Ru4	2.0098	6.197693	3.593622	C26	1.049185	6.17024	-3.27321
P1	1.764794	0.940274	4.028803	C27	0.040042	6.177149	-2.12904
P2	2.7923	6.567785	-2.55483	C28	1.042182	4.742642	-3.82955
H1	2.382694	3.3394	2.071146	C29	0.534591	7.134655	-4.34554
C1	2.593142	6.167813	1.61239	C30	4.071289	6.111508	-3.92758
C2	1.396853	3.581129	5.609398	C31	3.604577	6.476836	-5.34108
C3	3.948735	3.741009	4.130549	C32	4.36038	4.607904	-3.89289
C4	-0.01283	3.909477	3.008994	C33	5.415033	6.815299	-3.70862
C5	-0.24084	5.837788	1.030277	C34	2.915387	8.463408	-2.27199
C6	0.506662	3.395447	0.162563	C35	2.987853	9.298414	-3.55464
C7	3.119151	3.722257	-1.13512	C36	4.159024	8.779426	-1.43024
C8	4.973022	5.541755	-0.65714	C37	1.697107	8.931227	-1.4679
C9	5.34671	5.622824	2.514073	O1	2.84762	7.116236	0.808754
C10	4.953227	3.289522	1.372411	O2	1.077202	3.7936	6.705222
C11	3.161796	6.374905	5.091904	O3	4.738449	3.661035	5.002373
C12	0.380832	6.283577	4.583324	O4	-1.12863	3.886178	3.388893
C13	1.969935	8.058824	3.292427	O5	-1.09471	6.591771	0.828991
C14	-0.05497	0.320048	3.940691	O6	0.068239	2.67649	-0.63601
C15	-0.56795	0.537356	2.514486	O7	3.118144	2.642821	-1.56437
C16	-0.94373	1.134585	4.888099	O8	6.135019	5.510666	-0.69762
C17	-0.25748	-1.1574	4.295435	O9	6.265074	6.286567	2.739453
C18	2.483897	0.257676	5.69631	O10	5.679205	2.561913	0.837033
C19	1.493905	0.444227	6.852417	O11	3.855271	6.544266	5.99694
C20	2.842375	-1.23247	5.668311	O12	-0.59617	6.413325	5.180938
C21	3.738316	1.04122	6.084111	O13	1.924591	9.201271	3.140788

Table 3.11. Geometry optimized coodinates of **3.6**, hydrogens are not included.

Atom	Coordinate			Atom	Coordinate		
	x	y	z		x	y	z
Ir1	7.703271	-0.90728	2.877697	C19	7.796089	6.904128	3.090428
Ru1	7.197981	1.885971	2.916494	C20	4.89695	4.671135	2.527355
Ru2	5.452541	-1.95766	4.122951	C21	4.854213	4.190588	1.067322
Ru3	7.866752	-3.54904	3.570224	C22	4.504015	6.152155	2.500991
Ru4	7.817147	-1.58847	5.571359	C23	3.83161	3.90953	3.323127
P1	6.599876	4.256589	3.329081	C24	6.499279	4.680899	5.211408
C1	6.795585	-0.16404	4.524187	C25	7.915473	4.759369	5.788256
C2	7.122738	-1.24919	1.13027	C26	5.762261	5.981757	5.540842
C3	9.533754	-0.6769	2.547091	C27	5.801473	3.556093	5.983146
C4	5.600515	1.280698	2.020228	O1	6.411862	1.017055	4.726753
C5	8.012891	2.149549	1.282266	O2	6.736038	-1.44351	0.056828
C6	8.902878	2.018774	3.807768	O3	10.66428	-0.52152	2.354779
C7	4.618642	-3.16146	5.333443	O4	4.666269	0.873858	1.482653
C8	4.563975	-2.33752	2.493526	O5	8.543465	2.246263	0.256164
C9	4.203816	-0.62203	4.554136	O6	9.92532	2.028517	4.335556
C10	9.75526	-3.57372	3.429595	O7	4.085208	-3.94196	5.990407
C11	7.574412	-4.33413	1.892121	O8	4.010006	-2.61313	1.522325
C12	7.797901	-5.19583	4.468677	O9	3.399532	0.168127	4.798933
C13	7.736865	-0.37666	7.021138	O10	10.89746	-3.66271	3.300975
C14	9.704166	-1.616	5.646369	O11	7.387442	-4.83954	0.871211
C15	7.441677	-3.13335	6.617266	O12	7.774162	-6.22726	4.986179
C16	7.881046	5.470034	2.555987	O13	7.729934	0.346646	7.920913
C17	9.308992	4.965943	2.786819	O14	10.85579	-1.57507	5.71817
C18	7.677226	5.542054	1.039934	O15	7.191808	-3.99821	7.341287

REFERENCE

1. (a) Niibayashi, S.; Mitsui, K.; Matsubara, K.; Nagashima, H. *Organometallics* **2003**, *22*, 4885 – 4892. (b) Stutte, B.; Batzel, V.; Boese, R.; Schmid, G. *Chem. Ber.* **1978**, *111*, 1603 – 1618. (c) Schmid, G.; Stutte, B.; Boese, R. *Chem. Ber.* **1978**, *111*, 1239 – 1245. (d) Gambarotta, S.; Stella, S.; Floriani, C.; Chiesi-Villa, A.; Guastini, C. *Angew. Chem., int. Ed.* **1986**, *25*, 254 – 255. (e) Fachinetti, G.; Fochi, G.; Funaioli, T.; Zanazzi, P. F. *Angew. Chem., int. Ed.* **1987**, *26*, 680 – 681.

2. (a) Field, J. S.; Haines, R. J.; Jay, J. A. *J. Organomet. Chem.* **1989**, *377*, C35 – C39. (b) Adams, R. D.; Li, Z.; Lii, J.-C.; Wu, W. *Organometallics* **1992**, *11*,4001 – 4009.

3. (a) Adams, R. D.; Babin, J. E.; Tasi, M. *Inorg. Chem.* **1988**, *27*, 2618 – 2625. (b) Cabeza, J. A.; del Rio, I.; Miguel, D.; Pérez-Carreno, E.; Sánchez-Vega, M. G. *Dalton Trans.* **2008**, 1937 – 1942. (c) Yun, C.; Su, C. J.; Tseng, W. C.; Peng, S. M.; Lee, G. H. *J. Cluster Sci.* **1997**, *8*, 507 – 519. (d) Yun, C.; Su, C. J.; Peng, S. M.; Lee, G. H. *J. Am. Chem. Soc.* **1997**, *119*, 11114 – 11115. (e) Su, P. C.; Chi, Y.; Su, C. J.; Peng, S. M.; Lee, G. H. *Organometallics* **1997**, *16*, 1870 – 1874. (f) Adams, R. D.; Alexander, M. S.; Arafa, I.; Wu, W. *Inorg. Chem.* **1991**, *30*, 4717 – 4723. (g) Gibson, C. P.; Dahl, L. F. *Organometallics* **1988**, *7*, 535 – 543. (h) Chi, Y.; Chuang, S. H.; Liu, L. K.; Wen, Y. S. *Organometallics* **1991**, *10*, 2485 – 2492. (i) Notaras, E. G. A.; Lucas, N. T.; Humphrey, M. G. *J. Organomet. Chem.* **2001**, *631*, 139 – 142. (j) Nahar, S.; Davies, J. E.; Shields, G. P.; Raithby, P. R. *J. Cluster Sci.* **2010**, *21*, 379 – 396. (k) Femoni, C.; Iapalucci, M.C.; Longoni, G.; Zacchini, S. *Dalton Trans.* **2011**, *40*, 8685 – 8694. (l) Horwitz, C. P., Holt, E. M.; Brock, C. P.; Shriver, D. F. *J. Am. Chem. Soc.* **1985**, *107*, 8136 – 8146. (m) Bailey, P. J.; Duer, M. J.; Johnson, B. F. G.; Lewis, J.; Conole, G.; McPartlin, M.; Powell, H. R.; Anson, C. E. *J. Organomet. Chem.***1990**, *383*, 441 – 461.

4. (a) Brun, P.; Dawkins, G. M.; Green, M.; Miles, A. D.; Orpen, A. G.; Stone, F. G. A. *Chem. Commun.***1982**, 926 – 927. (b) Johnson, B. F. G.; Lewis, J.; McPartlin, M.; Pearsall, M. -A.; Sironi, A. *Chem. Commun.* **1984**, 1089 – 1090. (c) Leung, K. S. -Y. *Inorg. Chem. Commun.* **1999**, *2*, 498 – 502. (d) Leung, K. S. -Y.; Wong, W. T. *J. Chem. Soc., Dalton Trans.* **1997**, 4357 – 4360. (e) Chisholm, M. H.; Folting, K.; Hampden-Smith, M. J.; Hammond, C. E. *J. Am. Chem. Soc.* **1989**, *111*, 7283 – 7285.

5. (a) Herrmann, W. A.; Ziegler, M. L.; Windenhammer, K.; Biersack, H. *Angew. Chem., int. Ed. Engl.*, **1979**, *18*, 960 – 962. (b) Herrmann, W. A.; Biersack, H.; Ziegler, M. L.; Windenhammer, K.; Siegel, R.; Rehder, D. *J. Am. Chem. Soc.* **1981**, *103*, 1692 – 1699.

6. (a) Bailey, P. J.; Johnson, B. F. G.; Lewis, J. *Inorg. Chim. Acta* **1994**, *227*, 197 – 200. (b) Martin, C. M.; Dyson, P. J.; Ingham, S. L.; Johnson; B. F. G.; Blake, A. J. *J. Chem. Soc., Dalton Trans.* **1995**, 2741 – 2748. (c) Anson, C. E.; Bailey, P. J.; Conole, G.; Johnson, B. F. G.; Lewis, J.; McPartlin, M.; Powell, H. R. *J. Chem. Soc., Chem.*

Commun., **1989**, 442 – 444. (d) Shriver, D. F.; Sailor, M. J. *Acc. Chem. Res.* **1988**, *21*, 374 – 379.

7. (a) Corrigan, J. F.; Doherty, S.; Taylor, N. J.; Carty, A. J. *Organometallics* **1993**, *12*, 993 – 995. (b) Chi, Y.; Su, C. J.; Farrugia, L. J.; Peng, S. M.; Lee, G. H. *Organometallics* **1994**, *13*, 4167 – 4169.

8. Van Santen, R. A.; Neurock, M. in *Molecular Heterogeneous Catalysis. A Conceptual and Computational Approach*, Wiley-VCH, Weinheim, **2006**, 121 – 125.

9. (a) Muetterties, E. L.; Stein, J., *Chem. Rev.* **1979**, *79*, 479 – 490. (b) Herrmann, W.A. *Angew. Chem. lnt. Eng. Ed.*, **1982**, *21*, 117 – 130.

10. (a) Adams, R. D. *J. Organomet. Chem.* **2000**, *600*, 1 – 6. (b) Adams, R. D.; Li, Z.; Swepston, P.; Wu, W.; Yamamoto, J. *J. Am. Chem. Soc*., **1992**, *114*, 10657 – 10658. (c) Adams, R. D.; Barnard, T. S.; Li, Z.; Wu, W.; Yamamoto, J. *J. Am. Chem. Soc.*, **1994**, *116*, 9103 – 9113. (d) Adams, R. D.; Barnard, T. S. *Organometallics*, **1998**, *17*, 2567 – 2573. (e) Pignolet, L. H.; Aubart, M. A.; Craighead, K. L.; Gould, R. A. T.; Krogstad, D. A.; Wiley, J. S. *Coord. Chem. Rev.* **1995**, *143*, 219 – 263.

11. Ferrand, V.; Süss-Fink, G.; Neels, A.; Stoeckli-Evans, H. *J. Chem. Soc., Dalton Trans.* **1998**, 3825 – 3831.

12. Süss-Fink, G.; Haak, S.; Neels, A. Ferrand, V.; Stoeckli-Evans, H. *J. Chem. Soc.*, *Dalton Trans.*, **1997**, 3861 – 3865.

13. Adams, R. D.; Kan, Y.; Zhang, Q. *Organometallics* **2011**, *30*, 328 – 333.

14. Huq, R.; Poe, A. J.; Chawla, S. *Inorg. Chim. Acta* **1980**, *38*, 121 – 125.

15. SAINT+, version 6.2a, Bruker Analytical X-ray Systems, Inc., Madison, WI, **2001**.

16. Sheldrick, G. M., SHELXTL, version 6.1, Bruker Analytical X-ray Systems, Inc., Madison, WI, **1997**.

17 ADF2013; SCM Theoretical Chemistry, Vrije Universiteit, Amsterdam, The Netherlands, http://www.scm.com.

18. Perdew, J. P.; Ruzsinszky, A.; Csonka, G. I.; Vydrov, O. A.; Scuseria, G. E. *Phys. Rev. Lett.* **2008**, *100*, 136406.

19. (a) Bau, R.; Drabnis, M. H. *Inorg. Chim. Acta* **1997**, *259*, 27 - 50. (b) Teller, R. G.; Bau, R. *Struc. Bonding* **1981**, *41*, 1 – 82.

20. Adams, R. D.; Captain, B. *Organometallics* **2007**, *26*, 6564 – 6575

21. Haak, S.; Süss-Fink, G.; Neels, A.; Stoeckli-Evans, H. *Polyhedron* **1999**, *18*, 1675 – 1683.

22. Mingos D. M. P. *Acc. Chem. Res.***1984**, *17*, 311 – 319.

23. Adams, R. D.; Captain, B. *Acc. Chem. Res.***2009**, *42*, 409 – 418.

CHAPTER 4

Iridium-Ruthenium-Gold Cluster Complexes: Structures and Skeletal Rearrangements

Introduction

Applications for iridium in catalysis continue to grow.[1] Although most catalytic applications are of a homogeneous type,[1, 2] it has been shown that iridium complexes can also serve as precursors to catalysts that exhibit good activity for the hydrogenation of aromatics and olefins when placed on supports.[3] Heterogeneous iridium-iron catalysts derived from bimetallic cluster complexes have been shown to exhibit good catalytic activity for the formation of methanol from synthesis gas.[4] Iridium-ruthenium complexes have been shown to serve as precursors to catalysts for the carbonylation methanol.[5] Supported bimetallic iridium-ruthenium catalysts have been shown to produce C_2 oxygenates from syngas[6] and also to exhibit unusually high catalytic activity for the oxygen evolution reaction in the electrolysis of water.[7] Recently, gold nanoparticles have been shown to exhibit significant catalytic activity for the oxidation of CO and certain olefins.[8] Combining transition metals with gold has led to interesting new bimetallic oxidation nanocatalysts.[9]

There have been very few structural characterizations of iridium-ruthenium-gold carbonyl cluster complexes.[10] In the course of the studies of the chemistry of $[IrRu_3(CO)_{13}]^-$,[11] its reactions with $[AuPPh_3]NO_3$ and $[(AuPPh_3)_3O][BF_4]$ was investigated. Three new iridium-ruthenium-gold carbonyl cluster complexes have been

obtained, their molecular structures have been established and their properties in solution have been investigated. These results are discussed in this chapter.

Experimental

General Data.

Reagent grade solvents were dried by the standard procedures and were freshly distilled prior to use. Infrared spectra were recorded on a Thermo Nicolet Avatar 360 FT-IR spectrophotometer. Room temperature ^{1}H NMR and $^{31}P\{^{1}H\}$ NMR were recorded on a Bruker Avance/DRX 400 NMR spectrometer operating at 400.3 and 162.0 MHz, respectively. Different temperature $^{31}P\ \{^{1}H\}$ NMR for compound **4.3** were recorded on a Varian Mercury 400 spectrometer operating at 161.9 MHz. $^{31}P\ \{^{1}H\}$ NMR spectra were externally referenced against 85% *o*-H_3PO_4. Positive/negative ion mass spectra were recorded on a Micromass Q-TOF instrument by using electrospray (ES) ionization. $Ru_3(CO)_{12}$ and $Ir_4(CO)_{12}$ were obtained from STREM and were used without further purification. $HIrRu_3(CO)_{13}$, [12] $[PPN][IrRu_3(CO)_{13}]$,[12] $[AuPPh_3][NO_3]$ [13] and $[(AuPPh_3)_3O][BF_4]$[14] were prepared according to the previously reported procedures. Product separations were performed by TLC in air on Analtech 0.25 silica gel 60 Å F254 glass plates. Dynamic NMR simulations for compound **4.3** were performed by using the SpinWorks program**.** [15] The exchange rates were determined at seven different temperatures in the temperature range -60 to +20 ℃. The activation parameters were determined from a least-squares Eyring plot by using the program Microsoft Excel 2007: $\Delta H^{\ddagger} = 48.8(5)\ kJ{\cdot}mol^{-1}$, $\Delta S^{\ddagger} = 17.3(5)\ J{\cdot}mol^{-1}\ K^{-1}$.

Reaction of $HIrRu_3(CO)_{13}$ with $[(AuPPh_3)_3O][BF_4]$.

A mixture of 18.70 mg (0.01263 mmol) of $[(AuPPh_3)_3O][BF_4]$ and 21.35 mg (0.02481 mmol) of $HIrRu_3(CO)_{13}$ was stirred in 30 mL of THF for 2 h. The solvent was removed in vacuo, and the product was then isolated by TLC by using a 4:1 hexane/methylene chloride solvent mixture to yield in order of elution the following: 5.8 mg (36.8%) of $Ru_3(CO)_{12}$, 1.2 mg (6.3%) of $H_2Ru_4(CO)_{13}$, 2.3 mg (7% yield) of $IrRu_3(CO)_{13}AuPPh_3$, **4.1**, 3.2 mg (7.3% yield) of $HIrRu_3(CO)_{12}(AuPPh_3)_2$, **4.2** and 1.6 mg (2.9% yield) of $IrRu_3(CO)_{12}(AuPPh_3)_3$, **4.3,** and some uncharacterized compounds.

Spectral data for **4.1**: IR ν_{CO} (cm^{-1} in CH_2Cl_2): 2084(m), 2041(s), 2007(m), 1990(m), 1844(w). ^1H NMR (CD_2Cl_2, 25 ^oC, TMS) δ = 7.29-7.55 (m, 15H, Ph). $^{31}P\{^1H\}$ NMR (CD_2Cl_2, 25 ^oC), δ = 73.85 (s,1P, P-Au). Mass Spec: ES-/MS m/z = 1365 ($M + CO_2H^-$).

Spectral data for **4.2**: IR ν_{CO} (cm^{-1} in CH_2Cl_2): 2070(s), 2046(s), 2009(vs), 1961(m), 1809(w). ^1H NMR (CD_2Cl_2, 25 ^oC, TMS) δ = 7.08-7.52 (m, 30H, Ph), δ = -17.43 (s, 1H, hydride). $^{31}P\{^1H\}$ NMR (CD_2Cl_2, 25 ^oC) δ = 70.20 (s, 2P); at -80 ^oC in CD_2Cl_2: δ = 70.23 (s, 1P), 67.67 (s, 1P). Mass Spec: ES+/MS, m/z = 1752 M^+.

Spectral data for **4.3**: IR ν_{CO} (cm^{-1} in CH_2Cl_2): 2051(vs), 2010(vs), 1986(s), 1955(m), 1914(w), 1784(br). ^1H NMR (CD_2Cl_2, 25 ^oC, TMS) δ = 7.12-7.33 (m, 45H, Ph). $^{31}P\{^1H\}$ NMR (CD_2Cl_2, 25 ^oC) δ = 65.59 (s, 3P, P-Au); at -80 ^oC δ = 68.47 (2P) and 58.00 (1P). Mass Spec: ES+/MS, m/z = 2210.

Improved Synthesis of $IrRu_3(CO)_{13}AuPPh_3$, 4.1.

11.2 mg (0.0215 mmol) of $[AuPPh_3][NO_3]$ was added to a 100 mL three neck flask with a solution of 30.0 mg (0.0215 mmol) $[PPN][IrRu_3(CO)_{13}]$ in 30 mL THF. The solvent was removed in vacuo after 15 min at room temperature, and the product was then isolated by TLC using a 4:1 hexane/methylene chloride solvent mixture: 23.3 mg of **1** (82% yield) was obtained.

Improved Synthesis of 4.3.

To a 100 mL three neck flask, 25.8 mg (0.0174 mmol) of $[(AuPPh_3)_3O][BF_4]$ was added to 24.37 mg (0.0174 mmol) of $[PPN][IrRu_3(CO)_{13}]$ dissolved in 30 mL of THF. After 2h at 25 ^oC, the solvent was removed *in vacuo*, and the product was then isolated by TLC using a 2:1 hexane/methylene chloride solvent mixture. 32.24 mg of **4.3** (84% yield) was obtained.

Crystallographic Analyses:

Red single crystals of **4.1**, orange single crystals of **4.2** and black single crystals of **4.3** suitable for x-ray diffraction analyses were all obtained by slow evaporation of solvent from solutions of the pure compounds in hexane/methylene chloride solvent mixture at -25 ℃. Each data crystal was glued onto the end of a thin glass fiber. X-ray intensity data were measured by using a Bruker SMART APEX CCD-based diffractometer by using Mo Kα radiation (λ = 0.71073 Å). The raw data frames were integrated with the SAINT+ program by using a narrow-frame integration algorithm.[16] Correction for Lorentz and polarization effects were also applied using SAINT+. An empirical absorption correction based on the multiple measurement of equivalent

reflections was applied using the program SADABS. All structures were solved by a combination of direct methods and difference Fourier syntheses, and were refined by full-matrix least-squares on F^2 by using the SHELXTL software package.[17] All non-hydrogen atoms were refined with anisotropic thermal parameters. Hydrogen atoms were placed in geometrically idealized positions and included as standard riding atoms during the least-squares refinements. Crystal data, data collection parameters, and results of the analyses are listed in Table 4.1.

Compound **4.1** crystallized in the monoclinic crystal system. The space group $P2_1/n$ was indicated by the unique pattern of systematic absences observed in the data and was confirmed by the successful solution and refinement of the structure.

Compounds **4.2** and **4.3** both crystallized in the triclinic crystal system. The space group $P\ \bar{1}$ was assumed in both cases and was confirmed by the successful solutions and refinements of the structures. For the structure of **4.2**, there were two independent molecules of the complex and two hexane molecules from the crystallization solvent present in the asymmetric unit. The hydride ligand was located along one of the Ru–Ru bonds in each molecule. The hydride ligand in both molecules was refined with fixed Ru-H bond distances (1.75Å). The iridium atom Ir(1) and the ruthenium atom Ru(3) in compound **4.3** were disordered in the solid state. The occupancies of these two atoms were refined by using EXYZ and EADP constraints. The occupancies in the final cycle of refinement were 0.78/0.22.

Results and Discussion

Three new IrRuAu compounds: $IrRu_3(CO)_{13}AuPPh_3$, **4.1** (7% yield), $HIrRu_3(CO)_{12}(AuPPh_3)_2$, **4.2** (7.3% yield) and $IrRu_3(CO)_{12}(AuPPh_3)_3$, **4.3** (2.9% yield) were obtained from the reaction of $HIrRu_3(CO)_{13}$ with $[(AuPPh_3)_3O][BF_4]$. Compounds **4.1** and **4.3** were subsequently obtained in much better yields (82%) and (84%) from the reactions of $[AuPPh_3][NO_3]$ and $[(AuPPh_3)_3O][BF_4]$ with $[PPN][IrRu_3(CO)_{13}]$, respectively, see Scheme 4.1. Each of the new complexes was characterized by a combination of IR, ^1H NMR, mass spectral and single crystal X-ray diffraction analyses.

An ORTEP diagram of the molecular structure of compound **4.1** is shown in Figure 4.1. The basic framework of the $IrRu_3Au$ metal cluster in **4.1** is best described as an Au-capped $IrRu_3$ tetrahedron. The Au atom caps the Ru_3 triangle. The Ru – Au distances in **4.1** span a considerable range, Au(1) – Ru(1) = 3.0056(4) Å, Au(1) – Ru(2) = 2.8063(4) Å, Au(1) – Ru(3) = 2.7486(4) Å, and this may be related to the unsymmetric distribution of the CO ligands on the Ru atoms, see below. Compound **4.1** is similar to the $CoRu_3Au$ compound $CoRu_3(CO)_{13}AuPPh_3$, **4.4**, but in **4.4** the Au atom caps one of the $CoRu_2$ triangles of the $CoRu_3$ tetrahedron.[18] For comparison, the Au – Ru distances in **4.4** are 2.776(1) Å and 2.774(1) Å. Two of the three Ru – Ru bonds in **4.1** contain bridging CO ligands and the associated Ru - Ru bond distances, Ru(1) – Ru(2) = 2.8266(5) Å, Ru(1) – Ru(3) = 2.7918(5) Å, are significantly shorter than the third Ru –Ru bond distance, Ru(2) – Ru(3) = 3.0064(5) Å, which has no bridging CO ligand. The Ir – Ru bond distances, Ir(1) – Ru(1) = 2.7586(4) Å, Ir(1) – Ru(2) = 2.7336(4) Å, and Ir(1) – Ru(3) = 2.7643(4) Å, are similar to the Ir – Ru bond distances, 2.680(4) Å – 2.771(5) Å in the compound $[PPh_3][Ir_6Ru_3(CO)_{21}(AuPPh_3)]$[10a] which contains $Ru(CO)_3$ capping groups on three triangular faces of an Ir_6 octahedron. If the $AuPPh_3$ group is considered

as a one electron donor to the $IrRu_3$ tetrahedron, then the $IrRu_3$ cluster contains a total of 60 valence electrons which means that the Ir atom and each of the Ru atoms formally have 18 electron configurations.

An ORTEP diagram of the molecular structure of compound **4.2** is shown in Figure 4.2. The metal cluster in **4.2** can be described as an $Au(PPh_3)$ capped trigonal bipyramidal $AuIrRu_3$ cluster, but this $AuIrRu_3$ cluster is not the same as that in **4.1**. The Au atom in $AuIrRu_3$ cluster in **4.2** caps an $IrRu_2$ triangle not the Ru_3 triangle as in **4.1** and the $Au(PPh_3)$ cap on that bridges one of the AuIrRu triangles. The Au – Au bond distance, Au(1) – Au(2) = 2.8563(10) Å, is slightly longer than the Au – Au bond distance in the Au_2CoRu_3 compound $HCoRu_3(CO)_{13}(AuPPh_3)_2$, **4.5**, 2.787 (1) Å, which contains an $Au(PPh_3)$ capping group on a trigonal-bipyramidal $AuCoRu_3$ cluster that has a similar structure to **4.2**.[10a] Compound **4.2** contains one hydride ligand, δ = -17.43 in the H NMR spectrum, which was found bridge the Ru(1) – Ru(2) bond. As a result, the associated Ru(1) – Ru(2) bond distance is elongated, 2.992(2) Å, due to the presence of this ligand.[19] Otherwise, the Ir - Ru and Ru – Ru distances in **4.2** are similar to those observed in **4.1**. Compound **4. 2** exhibits only one phosphorus resonance at δ = 70.20 in its ^{31}P NMR spectrum at room temperature, (Figure 4.4), but it shows two resonances as expected at δ = 70.23 and 67.67 at -80 ^{o}C. This temperature dependence can be explained by a dynamical exchange process that leads to an averaging of the two inequivalent $Au(PPh_3)$ groups in **4.2** on the NMR timescale at room temperature. A number of examples of similarly structured metal cluster complexes containing $Au(PPh_3)$ groups have been reported to exhibit similar molecular dynamics (Scheme 4.2).[20] As in **4.1**, if each of the $AuPPh_3$ group is considered as a one electron donor to the $IrRu_3$ tetrahedron,

then the $IrRu_3$ cluster contains a total of 60 valence electrons and the Ir atom and each of the Ru atoms formally have 18 electron configurations.

An ORTEP diagram of the molecular structure of compound **4.3** is shown in Figure 4.3. Compound **4.3** contains three $Au(PPh_3)$ groups combined with the $IrRu_3$ cluster of the original reagents $HIrRu_3(CO)_{13}$ or anion $[IrRu_3(CO)_{13}]^-$. The metal cluster in **4.3** can be described in different ways. It could be described as an $IrRu_3$ tetrahedron with three bridging three $Au(PPh_3)$ groups. Alternatively, the cluster could be described as a seven atom pentagonal bipyramidal Au_3IrRu_3 cluster with an additional bond between the apical atoms Ir(1) and Ru(3), Ir(1) - Ru(3), 2.8770(5) Å. The other Ir – Ru bond distances are Ir(1) – Ru(1) = 2.8406(6) Å and Ir(1) – Ru(2) = 2.9387(6) Å. There are two bridging CO ligands that bridge the Ir(1) – Ru(1) and Ru(2) – Ru(3) bonds. The $Au(PPh_3)$ groups are mutually bonded, but the Au – Au bond distances, Au(1) – Au(2) = 2.9781(4) Å, Au(1) – Au(3) = 2.9726(4) Å, are significantly longer than that in **4.2**, but are still within normal bonding range. For comparison, the Au – Au bond distances in the octahedral hexagold complex$[Au_6\{P\text{-}p\text{-}tolyl_3\}][BPh_4]_2$ range from 2.932(2) Å – 3.091(2) Å.[21] If one considers compound **4.3** as a $IrRu_3$ tetrahedron with three one electron $Au(PPh_3)$ donors, then the cluster contains a total of 60 electrons and the Ir and each Ru atom would formally have 18 electron configurations. Two related $M_4(AuPPh_3)_3$ complexes have been reported. These are $H_2Ru_4(CO)_{12}(AuPPh_3)_3$, **4.4** [22, 23] and $CoRu_3(CO)_{12}(AuPPh_3)_3$, **4.5**.[18] The structures of the clusters of these two compounds both contain $(AuPPh_3)_3$ groups in which the central Au atom forms a μ_3-bridge across a triangle of the M_4 cluster, **A**, but in **4.3** the central Au atom bridges the Ir - Ru edge of the transition metal M_4 cluster, **B**, see Scheme 4.3. The stoichiometry of the reaction of

$[(AuPPh_3)_3O][BF_4]$ with $[PPN][IrRu_3(CO)_{13}]$ is a little unusual. A similar result was observed similarly in the synthesis of compound **4.5** from the reaction of $[(AuPPh_3)_3O][BF_4]$ with $[PPN][CoRu_3(CO)_{13}]$. This was explained by assuming that the oxonium oxygen atom of the cation $[(AuPPh_3)_3O]$ combines with CO to form CO_2 which in turn releases two electrons for use in cluster bonding.[18]

As with **4.2**, the ^{31}P NMR spectrum of **4.3** exhibits only one phosphorus resonance at room temperature, at $\delta = 65.59$ but shows two in a 2/1 ratio resonances as expected $\delta = 68.47$ (2P) and 58.00 (1P) at -80 ^oC. As the temperature is raised the two resonances broaden and coalesce in a process indicative of a dynamical averaging. These spectra are shown in Figure 4.5. The broadened spectra were simulated in order to obtain exchange rates and activation parameters for the exchange process. The simulated spectra are shown in Figure 4.6. From these data the activation parameters were determined $\Delta H^{\ddagger} = 48.8(5)$ $kJ \cdot mol^{-1}$, $\Delta S^{\ddagger} = 17.3(5)$ $J \cdot mol^{-1}K^{-1}$. Dynamical activity in polynuclear metal complexes containing $Au(PPh_3)$ groups has been observed previously.[22,24,25] Note: the addition of free PPh_3 to our NMR samples of **4.3** did not affect the exchange broadened spectra, so a mechanism that involves dissociation of PPh_3 from the gold atoms is ruled out. Therefore, a dynamical exchange process that leads to an interchange of the two types $Au(PPh_3)$ groups on the NMR timescale at room temperature seems to be the most likely. A variety of mechanisms can be envisioned, but all must involve the cleavage of at least one of the Au - Au bonds. One mechanism that we find attractive is shown in Scheme 4.4. Assuming the Au2 – Au3 bond is cleaved as in structure **B** on the left and the two bonded Au atoms Au1 and Au2, then pivot around the Ir atom to the position shown in intermediate **C**, the exchange can then be accomplished by shifting atom Au3 to

the neighboring $IrRu_2$ triangle with the formation of an Au – Au bond between Au1 and Au3 in the equivalent structure **B'**. In the process Au1 becomes the central Au atom of the Au_3 group and Au2 becomes one of the outer Au atoms. Alternatively, a cleavage of the Au1 – Au2 bond in **B** followed by formation of a similar C type intermediate (a mirror image of the one shown in Scheme 4.4) would ultimately lead to the placement of atom Au3 into the center of the of the Au_3 grouping.

Somewhat similar rocking shifts of $Au_2(PPh_3)_2$ groups have been proposed to explain the averaging of two of the inequivalent phosphorus resonances in the compound $Ru_6(CO)_{16}(AuPPh_3)_3(\mu_6\text{-B})$. [26] It has recently been shown that $Pd(P\text{-}t\text{-}Bu_3)$ groups complexes can migrate from face to face in some polynuclear ruthenium carbonyl cluster complexes.[25]

Conclusions

The family of mixed transition metal – gold polynuclear metal complexes has been expanded to include the series $IrRu_3Au(PPh_3)_n$, n = 1 – 3. The $Au(PPh_3)$ groups are mutually bonded to each other and undergo dynamical averaging on the NMR time scale at ambient temperatures when two or more $Au(PPh_3)$ groups are present in the complex. These complexes may serve as precursors to new multi-metallic catalysts in the future.[27]

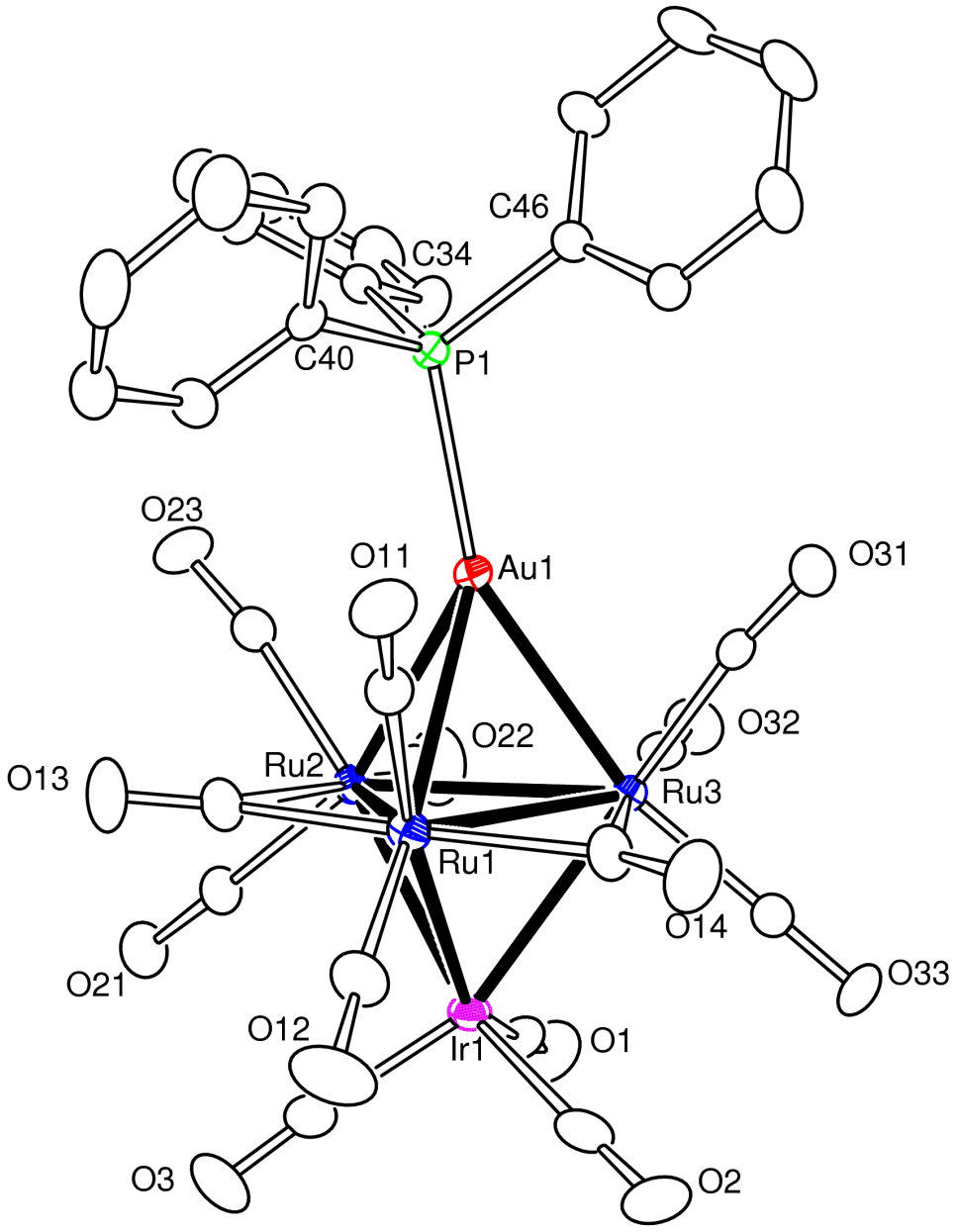

Figure 4.1. An ORTEP diagram of the molecular structure of $IrRu_3(CO)_{13}AuPPh_3$, **4.1** showing 20% thermal ellipsoid probability.

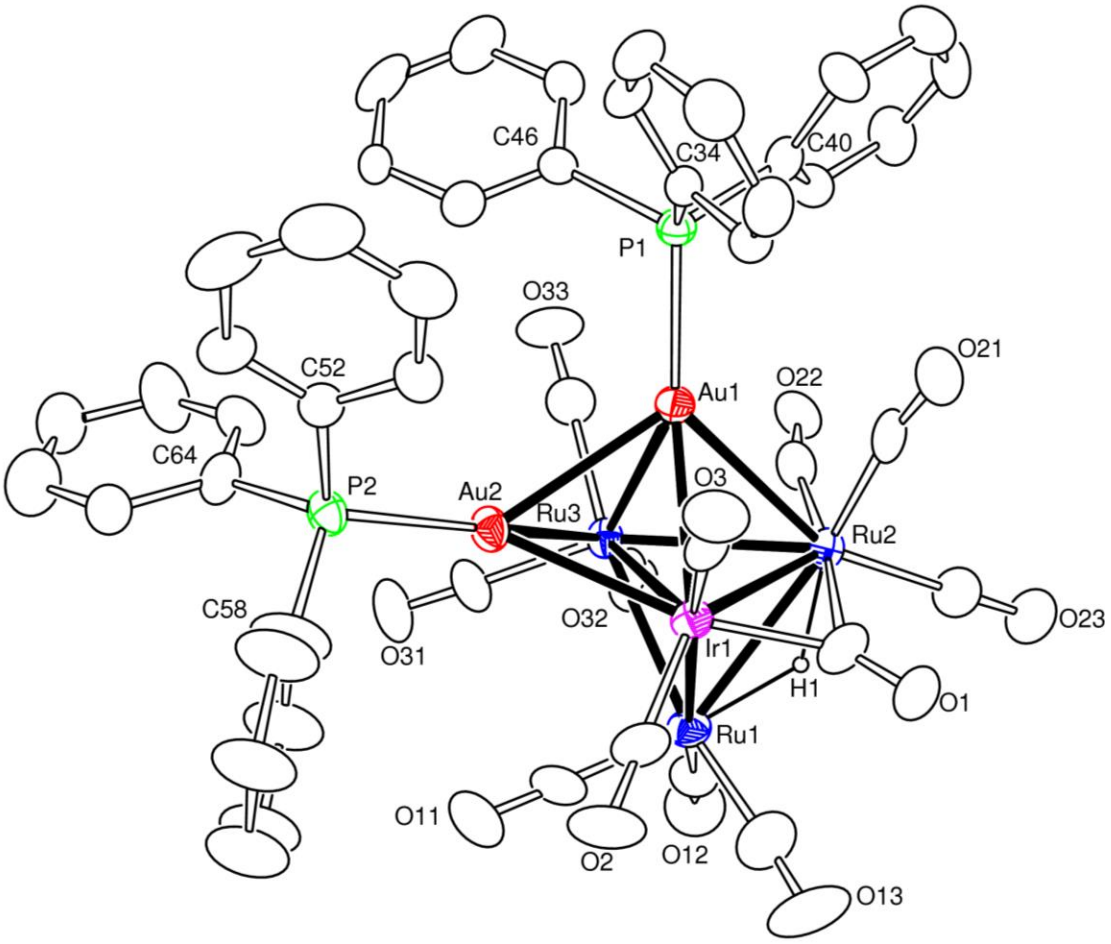

Figure 4.2. An ORTEP diagram of the molecular structure of $HIrRu_3(CO)_{12}(AuPPh_3)_2$, **4.2** showing 20% thermal ellipsoid probability.

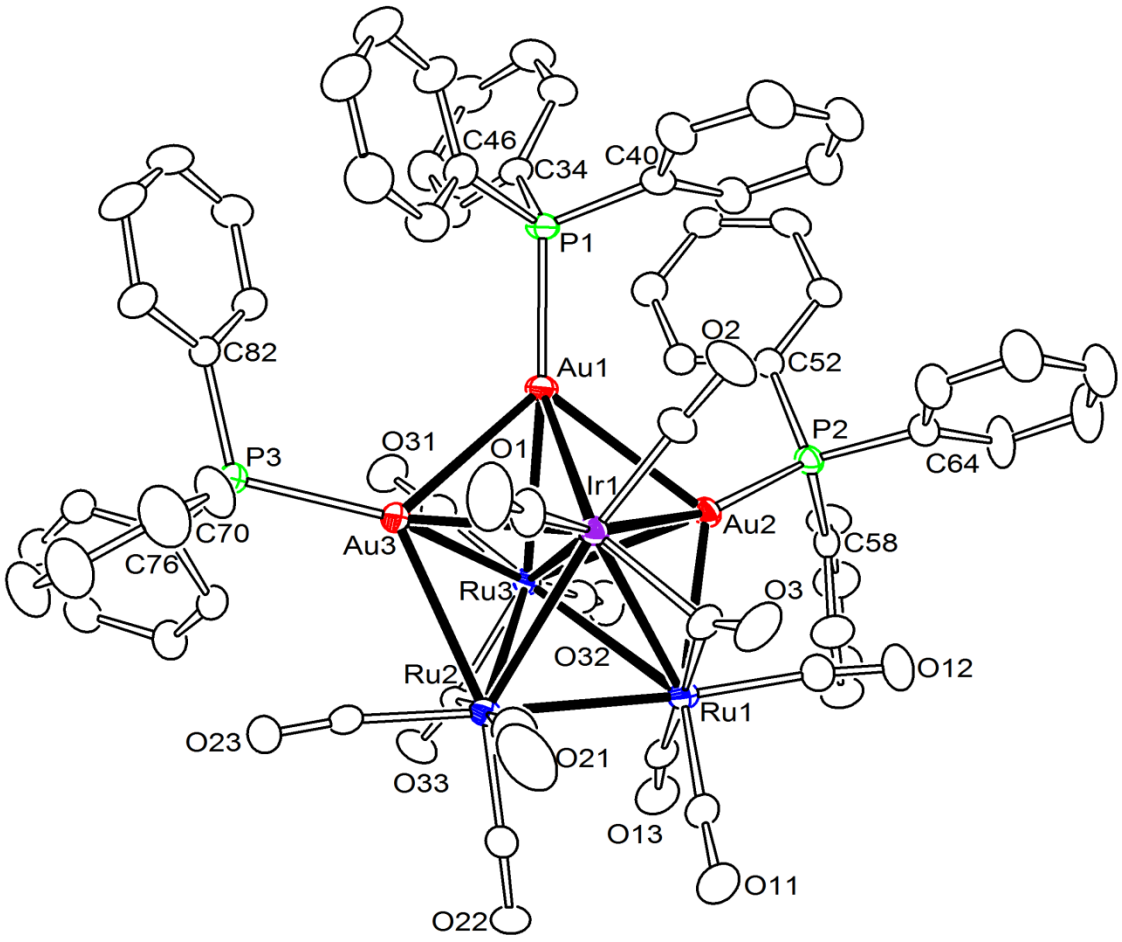

Figure 4.3. An ORTEP diagram of the molecular structure of $IrRu_3(CO)_{12}(AuPPh_3)_3$, **4.3** showing 20% thermal ellipsoid probability.

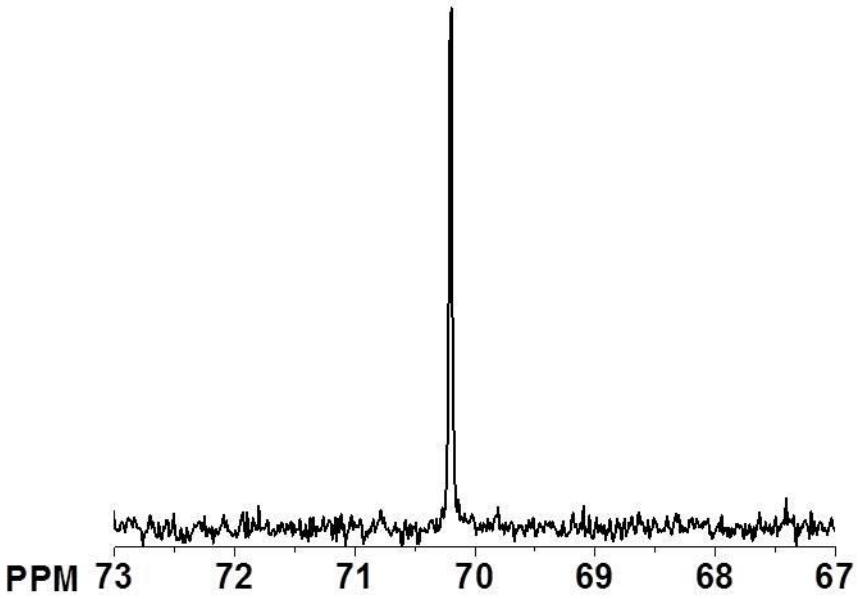

Figure 4.4. ^{31}P {H} NMR spectra for compound **4.2** in CD_2Cl_2 solvent at room temperature.

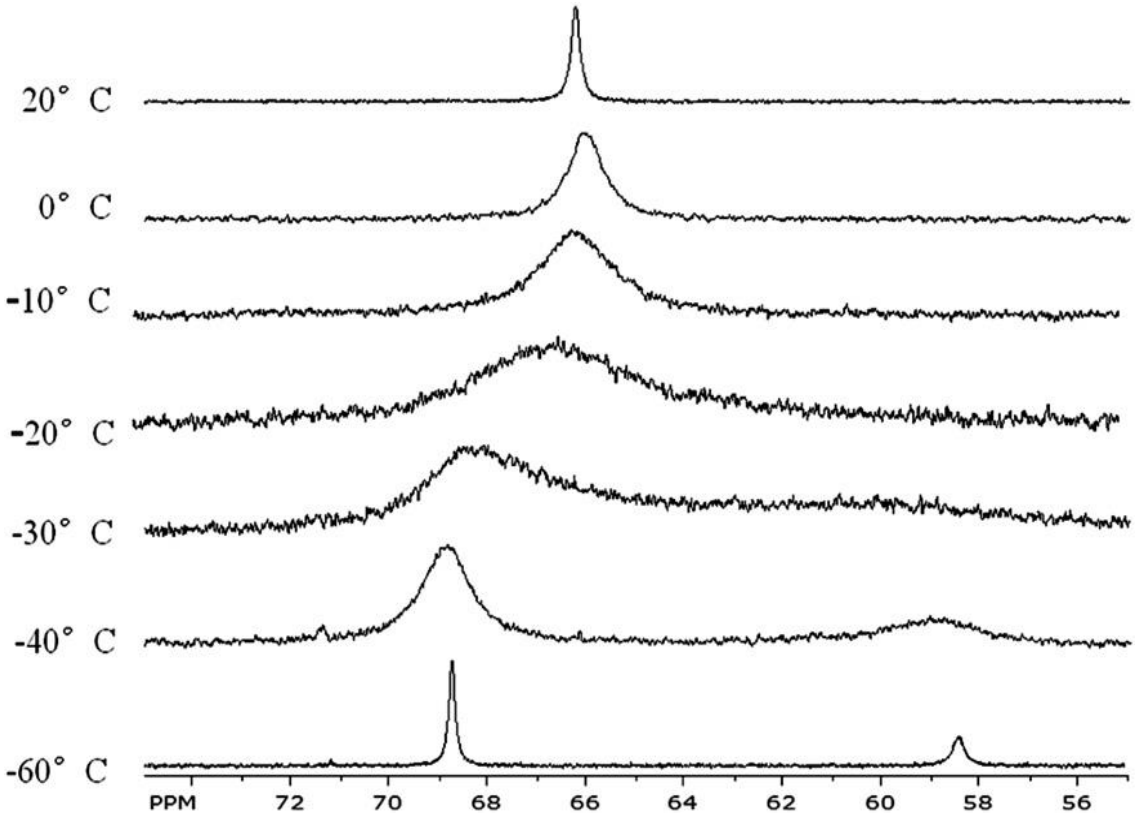

Figure 4.5. ^{31}P {H} NMR spectra for compound **4.3** in CD_2Cl_2 solvent at various temperatures.

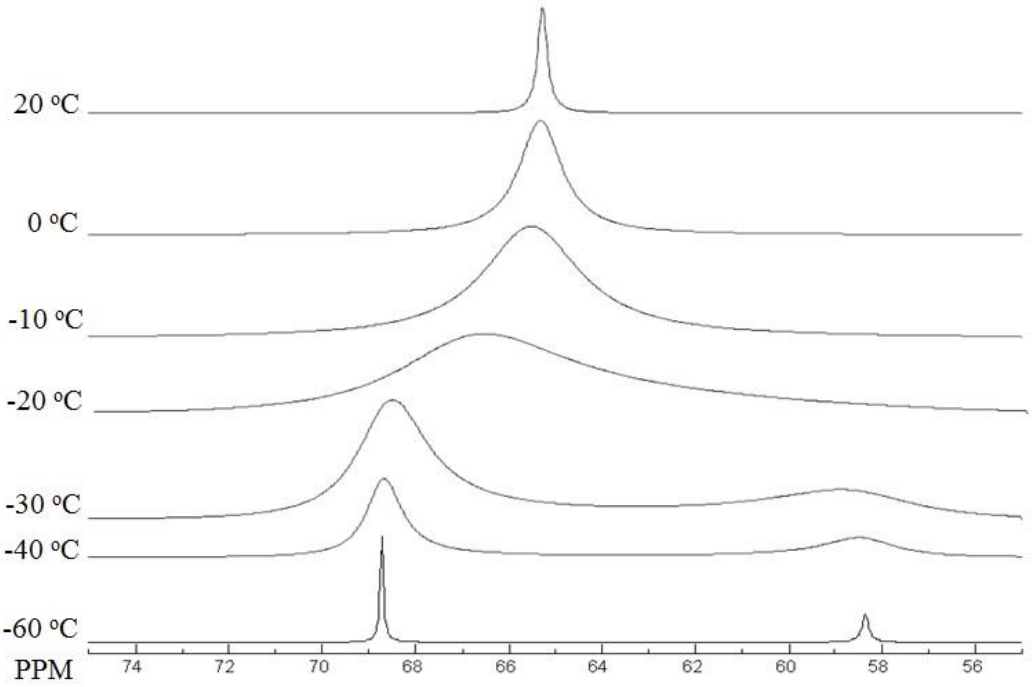

Figure 4.6. Simulated NMR ^{31}P {H} NMR spectra for compound **4.3** at various temperatures**.**

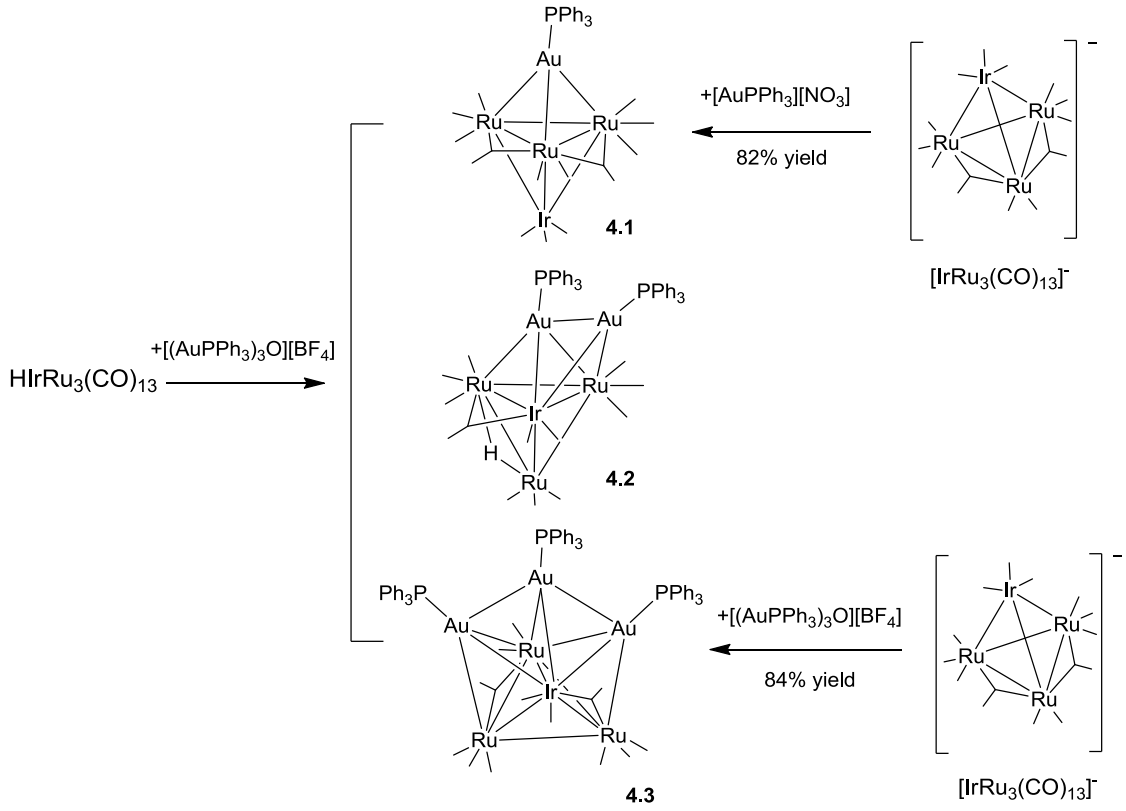

Scheme 4.1 $IrRu_3(AuPPh_3)_n$ complexes obtained from reaction of $IrRu_3$ complexes with Au cations.

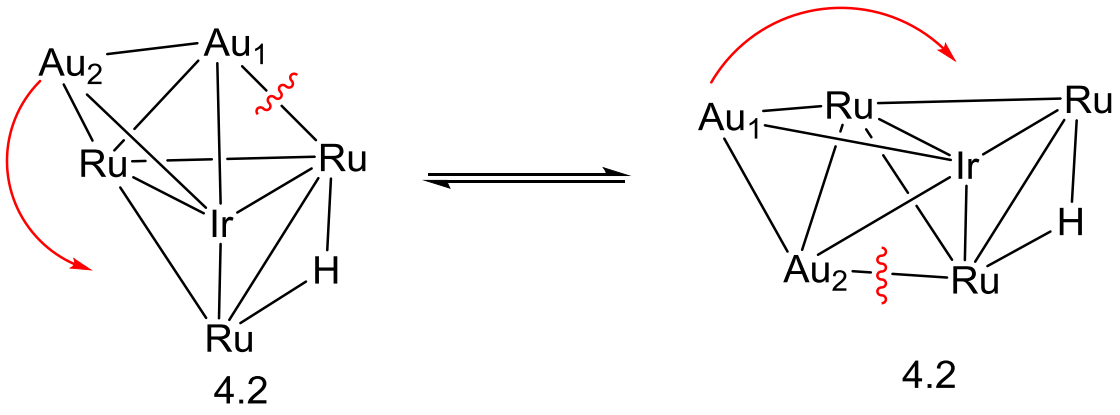

Scheme 4.2. Proposed mechanism for the dynamic averaging of ($AuPPh_3$) groups in **4.2**.

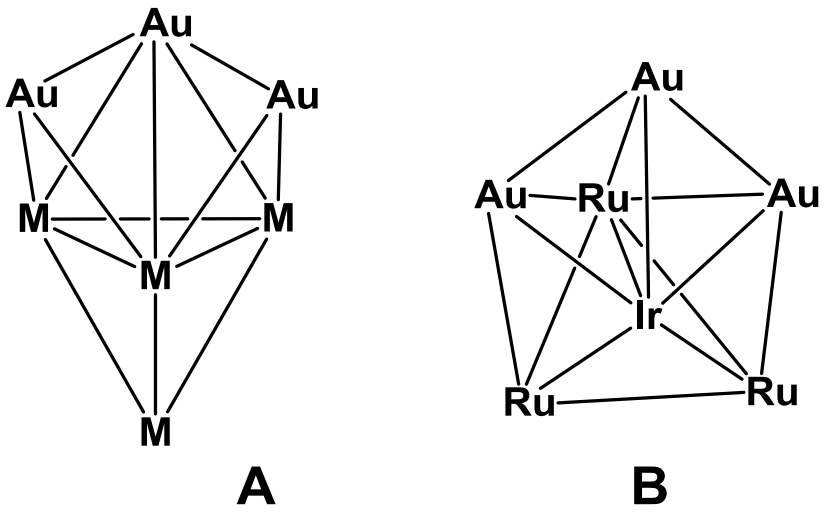

Scheme 4.3. The $IrRu_3Au_3$ structure compared with the normal M_4Au_3.

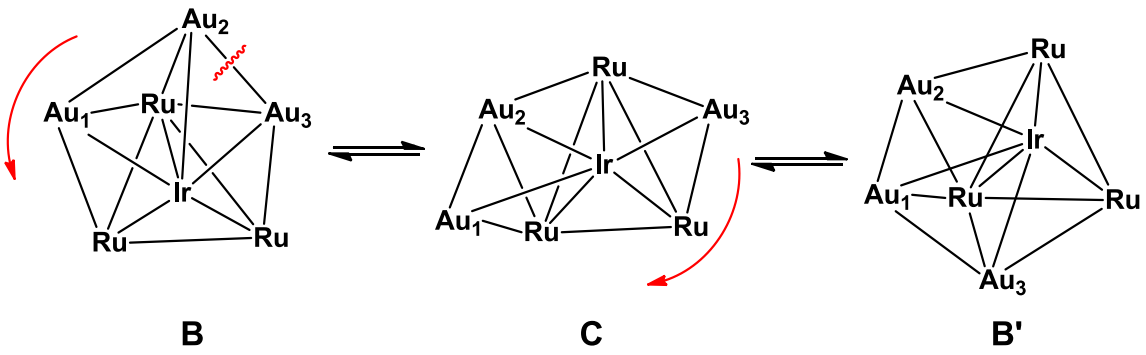

Scheme 4.4. Proposed mechanism for the dynamic averaging of ($AuPPh_3$) groups in **4.3.**

Table 4.1. Crystallographic Data for Compounds **4.1** – **4.3**.

Compound	**4.1**	**4.2**	**4.3**
Empirical formula	$C_{31}H_{15}O_{13}PAuIrRu_3$	$C_{48}H_{31}O_{12}P_2Au_2IrRu_3 \cdot C_6H_{14}$	$C_{66}H_{45}O_{12}P_3Au_3IrRu_3$
Formula weight	1318.78	1837.18	2209.24
Crystal system	Monoclinic	Triclinic	Triclinic
Lattice parameters			
a (Å)	16.6814(6)	13.7813(6)	13.4662(3)
b (Å)	9.7331(4)	20.8227(9)	14.7194(3)
c (Å)	22.0846(8)	20.8318(9)	19.1092(4)
α (deg)	90	90.055(1)	107.322(1)
β (deg)	99.996(1)	100.701(1)	99.010(1)
γ (deg)	90	96.540(1)	109.378(1)
V ($Å^3$)	3531.3(2)	5834.3(4)	3271.04(12)
Space group	$P2_1/n$	P -1	P -1
Z value	4	4	2
ρcalc (g / cm^3)	2.481	2.092	2.243
μ (Mo Kα) (mm^{-1})	9.257	8.150	9.534
Temperature (K)	294(2)	294(2)	293(2)
2Θ max (°)	50.04	48.22	50.04
No. Obs. ($I > 2\sigma(I)$)	6239	18532	11556
No. Parameters	451	1161	794
Goodness of fit	1.096	1.026	1.094
Max. shift in cycle	0.001	0.002	0.001
Residuals*: R1; wR2	0.0220; 0.0545	0.0686; 0.1413	0.0321; 0.0734
Absor.Corr, Max/min	1.000/0.423	1.000/0.689	1.000/0.628
Largest peak in Final Diff. Map ($e^- / Å^3$)	2.146	1.738	4.287

[a] $R = \Sigma_{hkl}(||F_{obs}| - |F_{calc}||)/\Sigma_{hkl}|F_{obs}|$; $R_w = [\Sigma_{hkl} w(|F_{obs}| - |F_{calc}|)^2/\Sigma_{hkl} wF^2_{obs}]^{1/2}$; $w = 1/\sigma^2(F_{obs})$; GOF = $[\Sigma_{hkl} w(|F_{obs}| - |F_{calc}|)^2/(n_{data} - n_{vari})]^{1/2}$.

Table 4.2. Selected intramolecular angles and bond distances for compound **4.1**.[a]

Distances			**Angles**			
Atom	Atom	Distance(Å)	Atom	Atom	Atom	Angle(deg)
Au1	Ru1	3.0056(4)	Au1	Ru1	Ir1	102.433(12)
Au1	Ru2	2.8063(4)	Au1	Ru2	Ir1	108.489(13)
Au1	Ru3	2.7486(4)	Au1	Ru2	Ir1	109.278(13)
Ir1	Ru1	2.7586(4)				
Ir1	Ru2	2.7336(4)				
Ir1	Ru3	2.7643(4)				
Ru1	Ru2	2.8266(5)				
Ru1	Ru3	2.7918(5)				
Ru2	Ru3	3.0064(5)				

[a] Estimated standard deviations in the least significant figure are given in parentheses.

Table 4.3. Selected intramolecular angles and bond distances for compound **4.2**.[a]

Distances			**Angles**			
Atom	Atom	Distance(Å)	Atom	Atom	Atom	Angle(deg)
Au1	Au2	2.8563(10)	Au1	Ir1	Ru1	111.91(4)
Au1	Ir1	2.7769(10)	Au1	Ru2	Ru1	98.25(5)
Au1	Ru2	3.0746(16)	Au1	Ru3	Ru1	111.38(6)
Au1	Ru3	2.8049(15)	Au1	Au2	Ru3	58.82(3)
Au2	Ir1	2.7908(10)	Au1	Au2	Ir1	58.90(3)
Au2	Ru3	2.8555(16)	Au2	Au1	Ru2	105.67(4)
Ir1	Ru1	2.7597(17)	Au2	Ir1	Ru1	101.18(4)
Ir1	Ru2	2.7915(16)	Au2	Ir1	Ru2	115.77(4)
Ir1	Ru3	2.9606(16)	Au2	Ru3	Ru1	99.84(6)
Ru1	Ru2	2.992(2)	Au2	Ru3	Ru2	108.72(5)
Ru1	Ru3	2.749(2)				
Ru2	Ru3	2.9621(19)				

[a] Estimated standard deviations in the least significant figure are given in parentheses.

Table 4.4. Selected intramolecular angles and bond distances for compound **4.3**.[a]

Distances			**Angles**			
Atom	Atom	Distance(Å)	Atom	Atom	Atom	Angle(deg)
Au1	Au2	2.9781(4)	Au1	Ir1	Ru1	116.201(16)
Au1	Au3	2.9726(4)	Au1	Ir1	Ru2	112.975(16)
Au1	Ir1	2.8243(4)	Au1	Au2	Ru1	110.138(14)
Au1	Ru3	2.8692(5)	Au1	Au3	Ru2	107.993(14)
Au2	Ir1	2.8829(4)	Au2	Au1	Au3	103.828(10)
Au2	Ru1	2.8878(6)	Ir1	Au1	Ru3	60.698(11)
Au2	Ru3	2.7596(5)	Au2	Ir1	Au3	110.692(13)
Au3	Ir1	2.8107(4)	Au2	Ru3	Au3	114.137(16)
Au3	Ru2	2.9674(6)	Au2	Ru1	Ru2	107.14(2)
Au3	Ru3	2.8206(5)	Au3	Ru2	Ru1	108.75(2)
Ir1	Ru1	2.8406(6)				
Ir1	Ru2	2.9387(6)				
Ir1	Ru3	2.8770(5)				
Ru1	Ru2	2.8334(8)				
Ru1	Ru3	3.0959(7)				
Ru2	Ru3	2.8895(7)				

[a] Estimated standard deviations in the least significant figure are given in parentheses.

REFERENCE

1. (a) Crabtree, R. H. *Topics Organomet. Chem.* **2011**, *34*, 1 – 10. (b) J. H. Jones, *Platinum Metals Rev.* **2000**, *44*, 94 – 105.

2. (a) C. M. Jensen, *Chem. Commun.* **1999**, 2443 – 2449. (b) V. César, S. Bellemin-Laponnaz, L. H. Gade, *Chem. Soc. Rev.* **2004**, *33*, 619 – 636. (c) S.-M. Lu, X.-W. Han, Y.-G. Zhou, *Adv. Synth. Catal.* **2004**, *346*, 909 – 912. (d) W. Matthias, M. W. Haenel, S. Oevers, K. Angermund, W. C. Kaska, H.-J. Fan, M.B. Hall, *Angew. Chem. int. Ed.* **2001**, *40*, 3596 – 3600.

3. (a) J. Lu, P. Pedro Serna, C. Aydin, N. D. Browning, B. C. Gates, *J. Am. Chem. Soc.* **2011**, *133*, 16186 – 16195. (b) B. C. Gates, *Chem. Rev.* **1995**, *95*, 511 – 522. (c) E. Bayram, M. Zahmakiran, S. Ozkar, R. G. Finke, *Langmuir*, **2011**, *26*, 12455 – 12464. (d) A. Uzun, D. A. Dison, B. C. Gates, *ChemCatChem* **2011**, *3*, 95 – 107. (e) B. C. Gates, in *Catalysis by Di- and Polynuclear Metal Complexes*, R. D. Adams, F. A. Cotton, Eds., Wiley-VCH Publishers, New York, **1998**, Ch. 14.

4. R. Psaro, C. Dossi, R. Della Pergola, L. Garlaschelli, S. Calmotti, S. Marngo, M. Bellatreccia, R. Zanoni, *Appl. Catal. A: Gen.* **1995**, *121*, L19 – L23.

5. G. Süss-Fink, S. Haak, V. Ferrand, H. Stoeckli-Evans, *J. Molec. Catal.* **1999**, *143*, 163 – 170.

6. H. Hamada, Y. Kuwahara, Y. Kintaichi, T. Ito, K. Wakabayashi, H. IIjima, K.-I. Sano, *Chem. Lett.* **1984**, 1611 – 1612.

7. R. E. Fuentes, J. Farell, J. W. Weidner, *Electrochem. Solid-State Lett.* **2011**, *14*, E5 – E7.

8. (a) M. Haruta, *Catal. Today* **1997**, *36*, 153 – 166. (b) M. Haruta, M. Date, *Appl. Catal. A: Gen.* **2001**, *222*, 427 – 437. (c) A. S. K. Hashmi, G. J. Hutchings, *Angew. Chem. int. Ed.* **2006**, *45*, 7896 – 7936.

9. (a) G. J. Hutchings, *Angew. Chem. int. Ed.* **2008**. 1148 – 1164. (b) L. B., Ortiz-Soto, O. S. Alexeev, M. D. Amiridis *Langmuir* **2006**, *22*, 3112 – 3117.

10. (a) T. Chihara, M. Sato, H. Konomoto, S. Kamiguchi, H. Ogawa, Y. Wakatsuki, *J. Chem. Soc., Dalton Trans.* **2000**, 2295 – 2299. (b) J. R. Galsworthy, A. D. Hattersley, C. E. Housecroft, A. L. Rheingold, A. Waller, *J. Chem. Soc., Dalton Trans.* **1995**, 549 – 557.

11. R. D. Adams, Q. Zhang, Z. Yang, *J. Am. Chem. Soc.*, **2011**, *133*, 15950 – 15953.

12. G. Süss-Fink, S. Haak, V. Ferrand, H. Stoeckli-Evans, *J. Chem. Soc., Dalton Trans.* **1997**, 3861 – 3865.

13. L. Malatesta, L. Naldini, G Simonetta, F. Cariati, *Coord. Chem. Rev.* **1966**, *1*, 255 – 262.

14. A. N. Nesmeyanov, E. G. Perevalova, Y. T. Struchkov, M. Y. Antipin, K. I. Grandberg, V. P. Dyadchenko, *J. Organomet. Chem.* **1980**, *201*, 343 – 349.

15. (a) SpinWorks 3.1.7, Copyright ©, Kirk Marat, University of Manitoba, **2010**. (b) A. R. Quirt, J. S. Martin, *J. Magn. Reson.* **1971**, *5*, 318 – 327.

16. SAINT+, version 6.2a, Bruker Analytical X-ray Systems, Inc., Madison, WI, **2001**.

17. G. M. Sheldrick, SHELXTL, version 6.1, Bruker Analytical X-ray Systems, Inc., Madison, WI, **1997**.

18. M. I. Bruce, B. K. Nicholson *Organometallics* **1984**, *3*, 101 – 108.

19. (a) R. Bau, M. H. Drabnis, *Inorg. Chim. Acta* **1997**, *259*, 27-50. (b) R. G. Teller, R. Bau, *Struct. Bonding*, **1981**, *44*, 1 – 82.

20. (a) M. J. Freeman, A. G. Orpen, I. D. Salter, *J. Chem. Soc., Dalton Trans.* **1987**, *379* – 390. (b) A. G. Orpen, I. D. Salter, *Organometallics* **1991**, *10*, 111 – 117.

21. P. Bellon, M. Manassero, M. Sansoni, *J. Chem. Soc., Dalton Trans.* **1973**, 2423 – 2427.

22. J. A. K. Howard, I. D. Salter, F. G. A. Stone, *Polyhedron* **1984**, *3*, 567 – 573.

23. M. I. Bruce, B. K. Nicholson *J. Organomet. Chem.* **1983**, *252*, 243 – 255.

24. (a) I. D. Salter, in *Comprehensive Organometallic Chemistry*, E. W. Abel, F. G. A. Stone, G. Wilkinson, Elsevier, London, **1995**, Vol. 10, Ch. 5. (b) Salter, I. D. in *Metal Clusters in Chemistry*, P. Braunstein, L. A. Oro, P. R. Raithby, Wiley-VCH, Weinheim, **1999**, Vol. 1, Ch. 1.*27*, 509 – 534.

25. R. D. Adams, B. Captain, W. Fu, P. J. Pellechia, M. D. Smith, *Inorg. Chem.* **2003**, *42*, 2094 – 2101.

26. C. E. Housecroft, D. M. Mathews, A. Waller, A. J. Edwards, A. L. Rhenigold, *J. Chem. Soc., Dalton Trans.* **1993**, 3059 – 3070.

27. J. Evans, J. Gao, *J. Chem. Soc., Chem. Commun.* **1985**, 39 – 40. (b) Y. Li, W.-X. Pan, W.-T. Wong, *J. Cluster Sci*. **2002**, *13*, 223 – 233.

CHAPTER 5

Structures and Transformations of Bridging Aryl Ligands in Triosmium Carbonyl Cluster Complexes

Introduction

Years ago Johnson and Lewis showed that the triosmium carbonyl complex $Os_3(CO)_{10}(NCMe)_2$, **5.1** reacts with arenes to yield the complexes $Os_3(CO)_{10}(\mu_3\text{-}C_6H_2R^1R^2)(\mu\text{-}H)_2$, R^1, R^2 = H, H; H, Me; H, Pr^n; H, CHCHPh; H, Cl; Me, Me which contain a triply bridging aryne ligand.[1] A variety of triosmium-aryne complexes have also been obtained from the reactions of $Os_3(CO)_{12}$ with aryl-substituted phosphines,[2,3] arsines,3 stibines,[4] and thioethers,[5] etc. at elevated temperatures. Over the years very little has been established with regard to the mechanism(s) of the formation of the aryne ligands in these reactions. Presumably, they begin with the loss of a ligand(s) from the osmium cluster which is followed by a series of two CH cleavages from the arene or a cleavage of an aryl group from an aryl-substituted Group V or VI donor and a cleavage of one CH bond from the aryl ligand. Hartwig et al. have investigated the transformation of a σ–phenyl ligand into an η^2-benzyne ligand in a mononuclear ruthenium complex.[6] Johnson et al. showed that the triply-bridging η^6-C_6H_6 ligand in the complex $Os_3(CO)_9(\mu_3\text{-}C_6H_6)$ is converted into the benzyne ligand in the complex $Os_3(CO)_9(\mu_3\text{-}C_6H_4)(\mu\text{-}H)_2$ under irradiation.[7]

We have now discovered the first example of the formation of triply bridging arynes directly from bridging aryl ligands in stable unsaturated triosmium complexes

generated from reactions of $Os_3(CO)_{10}(NCMe)_2$ with the gold complexes ArylAu(PPh_3), Aryl = Phenyl, Naphthyl or Pyrenyl.

Experimental Details

General Data.

Reagent grade solvents were dried by the standard procedures and were freshly distilled prior to use. Infrared spectra were recorded on a Thermo Nicolet Avatar 360 FT-IR spectrophotometer. Room temperature ^1H NMR and $^{31}P\{^1H\}$ NMR were recorded on a Bruker Avance/DRX 400 NMR spectrometer operating at 400.3 and 162.0 MHz, respectively. Positive/negative ion mass spectra were recorded on a Micromass Q-TOF instrument by using electrospray (ES) ionization. UV-vis absorption spectra were recorded on a JASCO Corp., UV-530, Rev. 1.00 Spectrometer/Data System. $Os_3(CO)_{10}(NCMe)_2$,[8] $PhAuPPh_3$,[9] 2-$NapAuPPh_3$[10] and 1-Pyryl$AuPPh_3$[11] were prepared according to previously reported procedures. Product separations were performed by TLC in air on Analtech 0.25mm silica gel 60 Å F254 glass plates and Alltech 0.25mm aluminum oxide UV_{254} glass plates.

Synthesis of $Os_3(CO)_{10}(\mu\text{-}C_6H_5)(\mu\text{-}AuPPh_3)$, 5.2.

20.56 mg (0.022 mmol) of $Os_3(CO)_{10}(NCMe)_2$ was added to a 100 mL three neck flask with a solution of 15.50 mg (0.029mmol) $PhAuPPh_3$ in 30 mL methylene chloride. After heating to reflux for 6 h, the solvent was removed *in vacuo*, and the product was then isolated by TLC using a 3:1 hexane/methylene chloride solvent mixture to yield on order of elution: 3.8 mg of $Os_3(CO)_{10}(\mu\text{-}Cl)(\mu\text{-}AuPPh_3)$, (13% yield) and

14.34 mg of $Os_3(CO)_{10}(\mu\text{-}C_6H_5)(\mu\text{-}AuPPh_3)$, **5.2**, (47%). The $Os_3(CO)_{10}(\mu\text{-}Cl)(\mu\text{-}AuPPh_3)$ was evidently formed by reaction of adventitious chloride present in the methylene chloride reaction solvent.

Spectral data for **5.2**: IR νCO (cm^{-1} in hexane): 2084(m), 2038(vs), 2029(m), 2000(m), 1995(s), 1980(w), 1969(w), 1960(m). ^1H NMR (CD_2Cl_2, 25 ^oC, TMS) δ = 9.62 (d, 1H, Ph), δ =8.78 (d, 1H, Ph), δ =8.26 (t, 1H, Ph), δ =6.97 (t, 1H, Ph), δ =6.88 (t, 1H, Ph), δ =7.57-7.47 (m, 15H, PPh_3). $^{31}P\{^1H\}$ NMR (CD_2Cl_2, 25 ^oC, 85% ortho-H_3PO_4) δ = 80.57 (s,1P, P-Au). Mass Spec. EI+/MS m/z. 1388 (M^+), 1360 (M^+-CO), 1332 (M^+-2CO).

Synthesis of $Os_3(CO)_9(\mu_3\text{-}C_6H_4)(\mu\text{-}AuPPh_3)(\mu\text{-}H)$, 5.3.

To a 50 mL three neck flask was added 11.83 mg (0.0085 mmol) of 5.2 and 15 mL of octane. After heating to reflux for 15 min (125 ^oC), the solvent was removed in *vacuo*, and the product was then isolated by TLC using a 3:1 hexane/methylene chloride solvent mixture. This yielded in order of elution: 10.78 mg of $Os_3(CO)_9(\mu_3\text{-}C_6H_4)(\mu\text{-}AuPPh_3)(\mu\text{-}H)$, **5.3** (94% yield).

Spectral data for **5.3**: IR ν_{CO} (cm^{-1} in CH_2Cl_2): 2076(w), 2055(vs), 2031(vs), 1998(m), 1982 (s), 1948(sh). ^1H NMR (CD_2Cl_2, 25 ^oC, TMS) δ = 7.89 (q, 2H, C_6H_4), δ =7.59-7.48 (m, 15H, PPh_3), δ =6.73 (q, 2H, C_6H_4), δ =-20.79 (d, 1H, Hydride). $^{31}P\{^1H\}$ NMR (CD_2Cl_2, 25 ^oC, ref. 85% ortho-H_3PO_4) δ = 73.05 (s, 1P, P-Au). Mass Spec. EI+/MS m/z. 1360(M^+), 1332(M^+-CO), 1304(M^+-2CO), 1276(M^+-3CO).

Synthesis of $Os_3(CO)_{10}(2\text{-}C_{10}H_7)(\mu\text{-}AuPPh_3)$, 5.4.

A mixture of 20.77 mg (0.022 mmol) of $Os_3(CO)_{10}(NCMe)_2$ and 12.82 mg (0.022 mmol) of 2-NapAuPPh$_3$ was stirred under reflux in 30 mL of Methylene Chloride for 6h. The solvent was removed *in vacuo*, and the product was then isolated by TLC using a 3:1 hexane/methylene chloride solvent mixture to yield in order of elution the following: 6.3 mg of $Os_3(CO)_{10}(\mu\text{-Cl})(\mu\text{-AuPPh}_3)$ (21% yield) and 18.2 mg of $Os_3(CO)_{10}(2\text{-}C_{10}H_7)(\mu\text{-AuPPh}_3)$, **5.4** (58% yield). The $Os_3(CO)_{10}(\mu\text{-Cl})(\mu\text{-AuPPh}_3)$ was evidently formed by reaction of adventitious chloride present in the methylene chloride reaction solvent.

Spectral data for **5.4**: IR ν_{CO} (cm^{-1} in CH_2Cl_2): 2083(m), 2035(vs), 2024(m), 2002(sh), 1992(s), 1967(w), 1942(sh). ^{1}H NMR (Toluene, 25 ^{o}C, TMS) δ = 8.65 (dd, 1H, Nap), δ =8.50 (d, 1H, Nap), δ =7.85 (d, 1H, Nap), δ =7.52 (dd, 2H, Nap), δ =7.25 (d, 1H, Nap), δ =7.10-6.98 (m, 15H, PPh_3), δ =6.58 (d, 1H, Nap). ^{31}P{^{1}H} NMR (Toluene, 25 ^{o}C, 85% ortho-H_3PO_4) δ = 82.84 (s, 1P, P-Au). Mass Spec. EI+/MS m/z. 1438(M^+), 1410 (M^+-CO), 1382 (M^+-2CO),1354 (M^+-3CO).

Synthesis of $Os_3(CO)_{10}(\mu_3\text{-}1,2\text{-}\eta^2\text{-}C_{10}H_6)(\mu\text{-AuPPh}_3)(\mu\text{-H})$, 5.5.

To a 50 mL three neck flask was added 7.06 mg (0.0049 mmol) of **5.4** and 10 mL of octane. The solution was heated to reflux for 30 min at 125 ^{o}C and the solvent was removed in *vacuo*. The product was then isolated by TLC by using a pure hexane solvent to yield: 0.8 mg of unreacted **5.4** and 4.33 mg of yellow $Os_3(CO)_{10}(\mu_3\text{-}1,2\text{-}\eta^2\text{-}C_{10}H_6)(\mu\text{-AuPPh}_3)(\mu\text{-H})$, **5.5** (63% yield).

Spectral data for **5.5**: IR ν_{CO} (cm^{-1} in CH_2Cl_2): 2075(w), 2053(vs), 2033(vs), 1998(m), 1981 (s), 1952(sh). ^{1}H NMR (CD_2Cl_2, 25 ^{o}C, TMS) δ = 7.90 (dd, 1H, $C_{10}H_6$), δ

= 7.64 (s, 1H, $C_{10}H_6$), δ =7.61-7.49 (m, ,3H, $C_{10}H_6$, 15H, PPh_3), δ =6.81 (d, 1H, $C_{10}H_6$), δ =-20.05 (d, 1H, Hydride). $^{31}P\{^1H\}$ NMR (CD_2Cl_2, 25 ^oC, ref. 85% ortho-H_3PO_4) δ = 75.35 (s, 1P, P-Au). Mass Spec. EI+/MS m/z. 1410(M+), 1382(M+ -CO), 1354(M+ -2CO), 1326(M+ -3CO), 1298(M+ -4CO).

Reaction of $Os_3(CO)_{10}(NCMe)_2$ with 1-PyrylAuPPh$_3$.

30.0 mg (0.0276mmol) of $Os_3(CO)_{10}(NCMe)_2$ was added to a 100 mL three neck flask with a solution of 20.0 mg (0.0303mmol) 1-PyrylAuPPh$_3$ in 30 mL Methylene chloride. The solvent was removed in vacuo after refluxing for 6 hours, and the product was then isolated by TLC by using a 4:1 hexane/methylene chloride solvent mixture: 1.8 mg of $ClOs_3(CO)_{10}AuPPh_3$, (5% yield) and 25.6 mg of $Os_3(CO)_{10}(AuPPh_3)$ (2-Pyryl), **5.6**, (61%), 3.2 mg of $Os_3(CO)_{10}(AuPPh_3)$(4-Pyryl), **5.7**, (8%) and some uncharacterized products were obtained.

Spectral data for **5.6**: IR νCO (cm^{-1} in CH_2Cl_2): 2082(m), 2036(vs), 2028(m), 2001(m), 1992(s), 1962(w). ^1H NMR (CD_2Cl_2, 25 ^oC, TMS) δ = 10.16 (s, 1H, Pyryl), δ =9.53 (s, 1H, Pyryl), δ =8.23-7.97 (m, 7H, Pyryl), δ =7.63-7.50 (m, 15H, PPh_3) . $^{31}P\{^1H\}$ NMR (CD_2Cl_2, 25 ^oC, 85% ortho-H_3PO_4) δ = 80.67 (s,1P, P-Au). Mass Spec. EI+/MS m/z. 1512 (M^+).

Spectral data for **5.7**: IR νCO (cm^{-1} in CH_2Cl_2): 2082(m), 2036(vs), 2023(m), 2001(m), 1991(s), 1964(w). ^1H NMR ($CDCl_3$, 25 ^oC, TMS) δ = 9.19 (d, 1H, Pyryl), δ =9.09 (s, 1H, Pyryl), δ =8.34 (d, 1H, Pyryl), δ =8.22 (d, 1H, Pyryl), δ =7.99 (s, 2H, Pyryl), δ =7.94-7.86 (m, 3H, Pyryl), δ =7.50-7.44 (m, 15H, PPh_3). $^{31}P\{^1H\}$ NMR ($CDCl_3$, 25 ^oC, 85% ortho-H_3PO_4) δ = 80.48 (s,1P, P-Au). Mass Spec. ES+/MS m/z. 1512 (M^+).

Synthesis of $Os_3(CO)_{10}(AuPPh_3)$(μ-Pyryne)(μ-H), 5.8/5.9.

To a 50 mL three neck flask, 20.0 mg (0.0132 mmol) of $Os_3(CO)_{10}(AuPPh_3)$(2-Pyryl), **5.6**, was added into 20 mL of octane. After heating for 30 min at 125 ^oC, the solvent was removed in *vacuo*, and the product was then isolated by TLC by using a 6:1 hexane/methylene chloride solvent mixture. 17.12 mg (87% yield) of a mixture of $Os_3(CO)_{10}(AuPPh_3)$(μ-Pyryne)(μ-H), **5.8**/**5.9**, was obtained. Compounds **5.8** and **5.9** could not be completely separated chromatographically. Pure crystalline forms of **5.8** and **5.9** were obtained by cutting the top (**5.8**) and bottom (**5.9**) edges of the broad band on a 0.25 mm aluminum TLC plate, and then recrystallizing from hexane solutions. The ratio of compound **5.8** and **5.9** in the initial mixture was 43/57 based on the integration of the corresponding hydride peaks in the ^1H NMR spectraum.

Spectral data for **5.8**: IR ν_{CO} (cm^{-1} in CH_2Cl_2): 2074(w), 2053(s), 2038(vs), 2001(m), 1988(m), 1978 (m), 1956(sh). ^1H NMR (CD_2Cl_2, 25 ^oC, TMS) δ = 8.40 (s, 1H, $C_{16}H_8$), δ =8.24 (d, 1H, $C_{16}H_8$), δ = 8.18 (d, 1H, $C_{16}H_8$), δ =8.09 (t, 1H, $C_{16}H_8$), δ =7.87 (dd, 2H, $C_{16}H_8$), δ =7.67 (d, 1H, $C_{16}H_8$), 7.63-7.51 (m, 1H, $C_{16}H_8$, 15H, PPh_3), δ =-19.75 (d, 1H, Hydride). $^{31}P\{^1H\}$ NMR (CD_2Cl_2, 25 ^oC, ref. 85% ortho-H_3PO_4) δ = 74.26 (s, 1P, P-Au). Mass Spec. EI+/MS m/z. 1484(M^+), 1456(M^+-CO), 1428(M^+-2CO), 1400(M^+-3CO), 1372(M^+-4CO), 1344(M^+-5CO).

Spectral data for **5.9**: IR ν_{CO} (cm^{-1} in CH_2Cl_2): 2073(w), 2052(s), 2038(vs), 2001(m), 1989 (w), 1979(m), 1957(w). ^1H NMR (CD_2Cl_2, 25 ^oC, TMS) δ = 8.00 (dd, 2H, $C_{16}H_8$), δ =7.97 (dd, 2H, $C_{16}H_8$), δ =7.90 (s, 2H, $C_{16}H_8$), δ =7.81 (t, 2H, $C_{16}H_8$) 7.56-7.42 (m, 15H, PPh_3), δ =-18.90 (d, 1H, Hydride). $^{31}P\{^1H\}$ NMR (CD_2Cl_2, 25 ^oC, ref. 85%

ortho-H_3PO_4) δ = 78.03 (s, 1P, P-Au). Mass Spec. EI+/MS m/z. 1484(M^+), 1456(M^+-CO), 1428(M^+-2CO), 1400(M^+-3CO), 1372(M^+-4CO), 1344(M^+-5CO).

Crystallographic Analyses:

Green crystals of **5.2**, orange crystals of **5.3**, green crystals of **5.4a**, yellow crystals of **5.5** and green crystals of **5.6** suitable for x-ray diffraction analyses were all obtained by slow evaporation of solvent from a pure hexane solvent at 25 ℃. Red crystals of **5.4b** black crystals of **5.7**, red crystals of **5.8** and orange crystals of **5.9** were obtained by cooling a solution in hexane solvent to -25 ℃. Each data crystal was glued onto the end of a thin glass fiber. X-ray intensity data were measured by using a Bruker SMART APEX CCD-based diffractometer using Mo Kα radiation (λ = 0.71073 Å). The raw data frames were integrated with the SAINT+ program by using a narrow-frame integration algorithm.[12] Corrections for Lorentz and polarization effects were also applied by using SAINT+. Empirical absorption corrections based on the multiple measurement of equivalent reflections was applied by using the program SADABS for each structural analysis. All of the structures were solved by a combination of direct methods and difference Fourier syntheses and were refined by full-matrix least-squares on F^2 by using the SHELXTL software package.[13] All non-hydrogen atoms were refined with anisotropic displacement parameters. The hydrogen atoms were placed in geometrically idealized positions and included as standard riding atoms during the least-squares refinements. Crystal data, data collection parameters, and results of the analyses are listed in Table 5.1.

Compounds **5.2**, **5.3**, **5.4a**, **5.5**, **5.6**, **5.7**, **5.8** and **5.9** all crystallized in the triclinic crystal system. The space group $P\ \bar{1}$ was assumed and confirmed by the successful

solution and refinement for all of the structures. Compounds **5.4b** and **5.5** crystallized in the monoclinic crystal system. The space group *C*2/c was assumed for **5.4b**. For **5.5** the space group $P2_1/c$ was identified by the systematic absences in the date and was confirmed by the successful solution and refinement of the structure. For compound **5.3**, there were two independent molecules of the complex. The bridging hydride ligand was located in each molecule and was satisfactorily refined without restraints. Compound **5.4a** contains a molecule of hexane from the crystallization solvent located on a center of symmetry site. The coordinates of the half hexane molecule which were included in the final cycles of refinement as fixed contributions. The hydride ligand in compound **5.6**, was located in a difference Fourier map as a bridge across the Os(1) – Os(3) bond, but it could not be refined. It was subsequently included in the final least refinements of the analysis as a fixed contribution. For compound **5.7**, there was one methylene chloride solvent molecule co-crystallized with one molecule of the compound in the asymmetric unit and the coordinates, s.o.f. and U or Uij for the solvent methylene chloride were fixed without refining. For compound **5.9**, there was a half of hexane solvent molecule co-crystallized with one molecule of the compound in the asymmetric unit and the coordinates, s.o.f. and U or Uij for the solvent hexane were fixed without refining. The hydride ligand was located along the Os–Os bond in both compound **5.8** and **5.9**, and was refined without restraints.

Computational Analyses:

Geometry optimized calculations were performed with ADF2012 program[14] by using the PBEsol functional[15] with scalar relativistic correction and valence quadruple-ζ

+ 4 polarization, relativistically optimized (QZ4P) basis sets for osmium and gold and valence double-ζ function (DZ) basis sets for the phosphorus, carbon, oxygen, and hydrogen atoms with no frozen cores. The molecular orbitals for **5.2** and **5.5** and their energies were determined by a geometry optimized calculations that were initiated with the structures as determined from the crystal structure analyses. The fragment analysis for compound **5.2** was also performed with the ADF programs by using the meta–Generalized Gradient Approximation (meta-GGA) level non-empirical Tao-Perdew-Staroverov-Scuseria (TPSS) functional[27] for the optimized structure of **5.2**, by using the same basis sets as described above.

Results and Discussion

The compound $C_6H_5Au(PPh_3)$[16] can be regarded as a close relative of C_6H_6 itself; the $Au(PPh_3)$ group is isolobal to H and also contains one odd electron for bonding to the carbon atom of the C_6H_5 group.[17] Compound **5.1** reacts with $C_6H_5Au(PPh_3)$ in CH_2Cl_2 at 40°C by elimination of both of its NCMe ligands and an oxidative-addition of the Au – C bond of the $C_6H_5Au(PPh_3)$ to the $Os_3(CO)_{10}$ group to yield the complex $Os_3(CO)_{10}(\mu\text{-}C_6H_5)(\mu\text{-}AuPPh_3)$, **5.2** in 47 % yield. The structure of **5.2** was established crystallographically and an ORTEP diagram of its molecular structure is shown in Figure 5.1. The molecule contains a triangular cluster of three osmium atoms with a η^1-bridging phenyl ligand and a bridging $AuPPh_3$ group across the Os1 - Os2 bond. The bond distances to the carbon atom C(1) of the bridging phenyl group, Os1 - C1 = 2.191(13) Å, Os2 - C1 = 2.236(11) Å, are shorter than those found in two previously reported triosmium cluster complexes containing bridging phenyl ligands: $Os_3(CO)_8(\mu_3\text{-}Se_2)(\mu\text{-}$

Ph)(μ-PhC=O),[18] 2.24(2) Å and 2.51(2) Å, and $Os_3(CO)_8(\mu\text{-}PPh_2)(\mu\text{-}Ph)(\mu\text{-}PPhC_6H_4)$,2[a] 2.19 Å and 2.39 Å. The doubly-bridged Os1 - Os2 bond in 5.2 is also significantly shorter, 2.7521(6) Å, than the two other Os – Os bonds, Os1 - Os3 = 2.8785(5) Å, Os2 - Os3 = 2.8746(5) Å. Assuming that the phenyl ligand and the $Au(PPh_3)$ group are both one electron donors, then compound **5.2** contains a total of only 46 electrons at the metal atoms and is formally unsaturated. Compound **5.2** is electronically similar to the 46 electron triosmium cluster complexes $Os_3(CO)_{10}(\mu\text{-}H)_2$,[19] $Os_3(CO)_8(\mu\text{-}AuPEt_3)_2$[20] and $Os_3(CO)_8(\mu\text{-}AuPPh_3)(\mu\text{-}H)$[21] for which their doubly-bridged Os - Os bond, 2.683(1) Å,[19 b] 2.684(1) Å[20] and 2.699(1) Å,[21] respectively, is also significantly shorter than the unbridged Os – Os bonds. The unsaturation in **5.2** results in delocalized bonding across the Os(1), Os(2) and C(1) atoms. The nature of this delocalized bonding can be seen in the DFT molecular orbitals, HOMO-3 and HOMO-5, of **5.2** that are shown in Figure 5.2. As a result of a small HOMO/LUMO gap of 1.63 eV, there is a strong absorption at λ = 632 nm, $\varepsilon = 560\ M^{-1}\cdot cm^{-1}$ in the visible spectrum which is responsible for the bright green color of the complex, see Figure 5.15.

In order to understand the nature of the coordination of the bridging phenyl ligand better, fragment analysis of compound **5.2** was performed. The fragment MOs were created for the phenyl ring (shown on the right hand side) and the $Os_3(CO)_{10}(\mu\text{-}AuPPh_3)$ group (shown on the left hand side) in the combined MO/energy level diagram shown Figure 5.3. The HOMO-14 of **5.2** is the most important orbital for the bonding of the phenyl ring to the metal cluster. The bonding is a combination of the singly-occupied MO (SOMO) of the phenyl ring fragment and the singly-occupied MO of the $Os_3(CO)_{10}(\mu\text{-}AuPPh_3)$ fragment. This orbital serves as the basis for what would commonly be referred

to as a Os – C – Os, three center two electron σ–bond. The HOMO-18 shows the existence of phenyl – Os_2 π-bonding interactions, Os – C – Os, three center two electron π–bond, represented which are derived from the HOMO-1 of the phenyl ring fragment and the HOMO-8 of the $Os_3(CO)_{10}(\mu\text{-}AuPPh_3)$ fragment. The electron donation from the filled π orbital of the phenyl to the cluster has reduced the unsaturation on the Os1 – Os2 bond, and leads to a longer bond distance compared to the di-gold bridged Os – Os bond in $Os_3(CO)_{10}(\mu\text{-}AuPEt_3)_2$.[20] There is also an antisymmetric combination of these two fragment orbitals that manifests itself in the HOMO-3. Even though there is a weak bonding interaction between the ring and the metal atoms in HOMO-3, both of these orbitals are filled, the phenyl – Os_2 bonding gained by formation of the HOMO-18 is reduced by the interactions in the HOMO-3. A similar competing relationship is found between the HOMO-6 and the HOMO-5 in **5.2**. The Os_2 – ring orbital interactions in these two MOs are created by symmetric and antisymmetric combinations of the HOMO-2 ring fragment orbital and the HOMO-7 of the $Os_3(CO)_{10}(\mu\text{-}AuPPh_3)$ fragment. Our calculations revealed no significant bonding interactions between the metal atoms and the unoccupied π–orbitals of the phenyl ring. One reason for this is because the ring π*–orbitals lie at too high energy, e.g. see the location of the ring lowest unoccupied molecular orbital (LUMO) shown in Figure 5.3.

When a solution of **5.2** was heated to reflux in octane solvent, it was decarbonylated and transformed into the benzyne compound $Os_3(CO)_9(\mu_3\text{-}C_6H_4)(\mu\text{-}AuPPh_3)(\mu\text{-}H)$, **5.3** in 94 % yield. Compound **5.3** was characterized crystallographically and an ORTEP diagram of its molecular structure is shown in Figure 5.4. The structure of **5.3** is similar to that of $Os_3(CO)_9(\mu_3\text{-}C_6H_4)(\mu\text{-}H)_2$ except for the presence of the bridging

$AuPPh_3$ in the place of one of the bridging hydride ligands.1 The benzyne C – C bond distance C1 - C2 = 1.429(14) Å is typical of those of other benzyne ligands.[2-5] Compound **5.3** was formed by the loss of a CO ligand from the $Os(CO)_4$ group and the activation of one of the ortho-positioned CH bonds in the bridging phenyl ligand in **5.2**. It is an electronically saturated 48 electron complex.

There have been no previous reports of naphthyne ligands so for comparison, we also investigated the reaction of **5.1** with 2-$NpAu(PPh_3)$,[22] 2-Np = 2-naphthyl. The reaction of 2-$NpAu(PPh_3)$ with **5.1** provided the product having the formula $Os_3(CO)_{10}$(2-Np)(μ-$AuPPh_3$), **5.4** in 58 % yield. Unlike **5.2**, the color of **5.4** is pink in solution.[23] Interestingly, however, crystals grown from hexane solutions at room temperature were green and similar in color to those of **5.2**, but crystals of **5.4** grown from hexane at -25 ^oC were pink in color. The molecular structures of **5.4** in both crystal modifications were established crystallographically. We will call the structure found in the green crystals **5.4a** and the isomeric structure found in the pink crystals will be called **5.4b**.

An ORTEP diagram of the molecular structure of **5.4a** is shown in Figure 5.5. The structure of **5.4a** is similar to that of **5.2** except that it contains an η^1-2-Np ligand that bridges the $AuPPh_3$-bridged Os – Os bond, Os1 - C1 = 2.313(11) Å and Os2 - C1 = 2.332(11) Å. The plane of C_{10}-ring is virtually perpendicular to the plane of the Os_3 triangle. If the 2-Np ligand and the $AuPPh_3$ group serve as 1 electron donors, then compound **5.4a** contains 46 electrons and is unsaturated just like **5.2**. Accordingly, the Os1 - Os2 bond is short, 2.7484(6) Å, compared to the other Os – Os bonds, Os1 - Os3 = 2.8745(6) Å, Os2 - Os3 = 2.8668(6) Å.

An ORTEP diagram of the molecular structure of **5.4b** is shown in Figure 5.6. This structure is an isomer of **5.4a** and it contains an η^2-2-Np ligand that bridges the $AuPPh_3$-bridged Os – Os bond. Naphthyl atom C(1) is bonded to both osmium atoms, Os1 - C1 = 2.313(11) Å and Os2 - C1 = 2.332(11) Å. Interestingly, naphthyl atom C(6) is also bonded to Os(2), Os2 - C6 = 2.544(10) although the distance is slightly longer.[23] As a result, the plane of the planar C_{10}-ring is not perpendicular to the Os_3 triangle but is 49.27 (0.27) ^{o} from the plane of the Os_3 triangle. The C1 - C6 distance is 1.380(14) Å. In this molecule the 2-Np ligand serves as a 3-electron donor. The $AuPPh_3$ group serves as 1-electron donor and the osmium atoms in the pink isomer **5.4b** contain 48 electrons. The triosmium cluster is electronically saturated, and as a result there is no unusually short Os – Os bond in **5.4b**. The doubly-bridged Os1 - Os2 bond, 2.8538(6) Å, is nearly as long as the other two Os - Os bonds, Os1 - Os3 = 2.8997(6) Å, Os2 - Os3 =2.8899(7) Å. Interestingly, the bridging carbon atom of the naphthyl ligand both in **5.4a** and **5.4b** lies at the 2-position. The HOMO/LUMO gap in **5.4b** is larger than that in **5.2** and the absorption in the visible spectrum lies at higher energy, λ = 518 nm, ε = 3009 $cm^{-1}\cdot M^{-1}$, which accounts for its pink color in solution, see Figure 5.16. Compound **5.4b** must obviously convert to **5.4a** when crystals are grown at room temperature. We have not yet obtained any spectroscopic evidence for the presence of a second isomer in solutions at room temperature. Further investigation of the **5.4a** - **5.4b** transformation is in progress.[24]

When a solution of **5.4** was heated to reflux in octane solvent, it was decarbonylated and transformed into the naphthyne compound $Os_3(CO)_9(\mu_3\text{-}C_{10}H_6)(\mu\text{-}AuPPh_3)(\mu\text{-}H)$, **5.5** in 63% yield. Compound **5.5** was also characterized crystallographically and an ORTEP diagram of its molecular structure is shown in Figure

5.7. The structure of **5.5** is similar to that of **5.3**. Compound **5.5** contains the first example of an unsubstituted triply bridging naphthyne ligand. The naphthyne C−C bond distance (C1−C6 = 1.435(16) Å) is similar in length to that found in the benzyne ligand in **5.3**. The Au- and H-bridged bonds (Os1−Os2 = 2.8950(6) Å, Os1−Os3 = 2.9882(7) Å) are longer than the remaining Os−Os bond (Os2−Os3 = 2.7494(6) Å). The naphthyne ligand in **5.5** is a 4-electron donor, and the metal atoms thus contain a total of 48 electrons and are electronically saturated.

In order to establish the mechanism of the naphthyne formation and the C−H activation step, DFT computational analyses were performed. The calculation was started from the decarbonylated form of **5.4b**, followed by geometry refinement. Intermediate and ground-state structures were located by using full geometry optimization. The approximate transition states were computed as maxima of total energy along the reaction coordinate with full geometry optimization of all other coordinates. The energy of the decarbonylated form of **5.4b** lies about +52 kcal/mol above the ground state **5.4b** as shown in the energy profile in Figure 5.8. This is due to the generation of a vacant site on Os3. As represented in Scheme 5.1, as the refinement starts, the naphthyl group moves toward Os3 which contains the vacant binding site. An intermediate iss formed. In this intermediate an agostic interaction is formed between the ortho-CH bond in the naphthyl and Os3. The geometry of this intermediate is shown in Figure 5.9 (left). The bond distances, Os3 – C3 = 2.37 Å, Os3 – H6 = 1.82 Å and C3 – H6 = 1.21 Å indicate the significant Os-C andOs-H interactions the weaken of the CH bond. The HOMO-13 of this intermediae has confirmed the CH-Os interaction. Since the vacant site has been filled by the two electrons from the CH bond, the energy dropped to +21.42 kcal/mol

above the ground state from +52 kcal/mol. As the process is continued, the intermediate goes to the final naphthyne complex via a small transition state, in which the CH bond is cleaved. The geometry of this transition state is shown in Figure 5.10 (left). The bond distance between carbon and hydrogen, C3 – H6 = 2.06 Å, clearly indicated that there is no C – H bonding interaction. The HOMO of the transition state shows the terminal hydrogen to metal bonding which is represented in Figure 5.10 (right). The ground state of the naphthyne complex is +3.9 kcal/mol higher than that of **5.4.b** This is mainly because **5.4b** has one more carbonyl ligand.

We also investigated the reaction of **5.1** with 1-PyrylAu(PPh_3),[25] 1-Pyryl = 1-pyrenyl. The reaction of 2-PyrylAu(PPh_3) with **5.1** provided product having the formula $Os_3(CO)_{10}$(2-Pyryl)(μ-$AuPPh_3$), **5.6** in 61 % yield. Like **5.2**, the color of **5.6** is green in solution.[23] Interestingly, however, there is another product $Os_3(CO)_{10}$(4-Pyryl)(μ-$AuPPh_3$), **5.7**, which is brown. The molecular structures of **5.6** and **5.7** were both established crystallographically.

An ORTEP diagram of the molecular structure of **5.6** is shown in Figure 5.11. The structure of **5.6** is similar to that of **5.2** and **5.4a** except that it contains an η^1-2-Pyryl ligand that bridges the $AuPPh_3$-bridged Os – Os bond, Os1 – C35 = 2.291(12) Å and Os2 – C35 = 2.345(13) Å. Similarly with **5.2** and **5.4a**, the plane of C_{16}-ring is virtually perpendicular to the plane of the Os_3 triangle. If the 2-Pyryl ligand and the $AuPPh_3$ group serve as 1 electron donors, then compound **5.6** contains a total of 46 valence electrons and is unsaturated just like **5.2** and **5.4a**. Accordingly, the Os1 - Os2 bond is short, 2.7485(7) Å, compared to the other Os – Os bonds, Os1 - Os3 = 2.8980(7) Å, Os2 - Os3 = 2.8863(7) Å. The HOMO/LUMO gap in **5.6** is similar to that in **5.2** and the absorption

in the visible spectrum lies at similar energy, λ = 644 nm, ε = 190956 $cm^{-1}{\cdot}M^{-1}$, which accounts for its green color in solution, see Figure 5.17.

An ORTEP diagram of the molecular structure of **5.7** is shown in Figure 5.12. This structure is an isomer of **5.6** and it contains an η^1-4-Pyryl ligand that bridges the $AuPPh_3$-bridged Os – Os bond, Os1 – C47 = 2.247(17) Å and Os2 – C47 = 2.364(18) Å. In **5.7**, the plane of the planar C_{16}-ring is not perpendicular to the Os_3 triangle but is 75.28 $(0.13)^o$ from the plane of the Os_3 triangle. But the 4-Pyryl ligand still serves as a 1-electron donor, the $AuPPh_3$ group serves as 1-electron donor so **5.7** contains 46 electrons indicating that it is also unsaturated like **5.6**. The doubly-bridged Os1 - Os2 bond, 2.7789(10) Å, is slightly longer than that found in **5.6**, Os1 - Os3 = 2.9313(12) Å, Os2 - Os3 =2.8897(11) Å. Interestingly, we found that compound **5.6** can be partially converted to compound **5.7** by heating to 40 ^oC for 48 h. We have not yet established the mechanism of the hydrogen shift between **5.6** and **5.7**. Further investigation of the **5.6** to **5.7** transformation is in progress.

When a solution of **5.6** was heated to reflux in octane solvent, it was decarbonylated and transformed into the pyryne compounds $Os_3(CO)_9(\mu_3\text{-}1,2\text{-}C_{16}H_9)(\mu\text{-}AuPPh_3)(\mu\text{-}H)$, **5.8** and $Os_3(CO)_9(\mu_3\text{-}4,5\text{-}C_{16}H_9)(\mu\text{-}AuPPh_3)(\mu\text{-}H)$, **5.9** in 87% yield. Compound **5.8** and **5.9** are isomers and were both characterized crystallographically and an ORTEP diagram of the molecular structure of **5.8** is shown in Figure 5.13. The structure of **5.8** is similar to that of **5.3** and **5.5**, where the pyryne ligand binds to the cluster on its 1 and 2 positions. Compound **5.8** contains an unsubstituted triply bridging "stand-up" pyryne ligand. The pyryne C−C bond distance (C35−C36 = 1.435(12) Å) is similar in length to that found for the benzyne ligand in **5.3** and **5.5**. The Au- and H-

bridged bonds (Os1−Os2 = 2.8799(5) Å, Os1−Os3 = 3.0044(5) Å) are longer than the remaining Os−Os bond (Os2−Os3 = 2.7525(5) Å). The pyryne ligand in **5.8** is a 4-electron donor, and the metal atoms thus contain a total of 48 electrons and are electronically saturated. An ORTEP diagram of the molecular structure of **5.9** is shown in Figure 5.14. The pyryne ligand in **5.9** binds to the cluster on its 4 and 5 positions, which is similar to that of the previously reported compound $Os_3(CO)_9(\mu_3\text{-}4,5\text{-}C_{16}H_9)(\mu\text{-}H)_2$ except for the presence of the bridging $AuPPh_3$ in the place of one of the bridging hydride ligands.[26] Compound **5.9** contains an unsubstituted triply bridging "lie-down" pyryne ligand. The pyryne C−C bond distance (C46−C47 = 1.419(9) Å) is similar in length to that found in the benzyne ligand in **5.3**, **5.5** and **5.8**. The Au- and H-bridged bonds (Os1−Os2 = 2.8777(4) Å, Os1−Os3 = 2.9702(4) Å) are longer than the remaining Os−Os bond (Os2−Os3 = 2.7634(4) Å). The pyryne ligand in **5.9** is also a 4-electron donor, and the metal atoms thus contain a total of 48 electrons and are electronically saturated.

Conclusions

By using the reagents $ArylAu(PPh_3)$, Aryl = phenyl, naphthyl or pyrenyl, the new unsaturated complexes **5.2**, **5.4a/b**, **5.6** and **5.7** have been prepared which contain η^1-bridging phenyl, η^1-bridging naphthyl and η^1-bridging pyrenyl ligands, respectively. The 2-naphthyl ligand in 5.4b also coordinates to the cluster in a η^2-bridging mode. Two isomers green **5.8** and brown **5.9** were obtained in the reaction of **5.1** with 1-$PyrenylAu(PPh_3)$. The bridging aryl ligands have been converted into triply-bridging aryne ligands under mild conditions (Scheme 5.2). Efforts to try to establish, by

computational methods, the mechanism of the transformation from **5.8** to **5.9** through hydrogen shift are in progress.

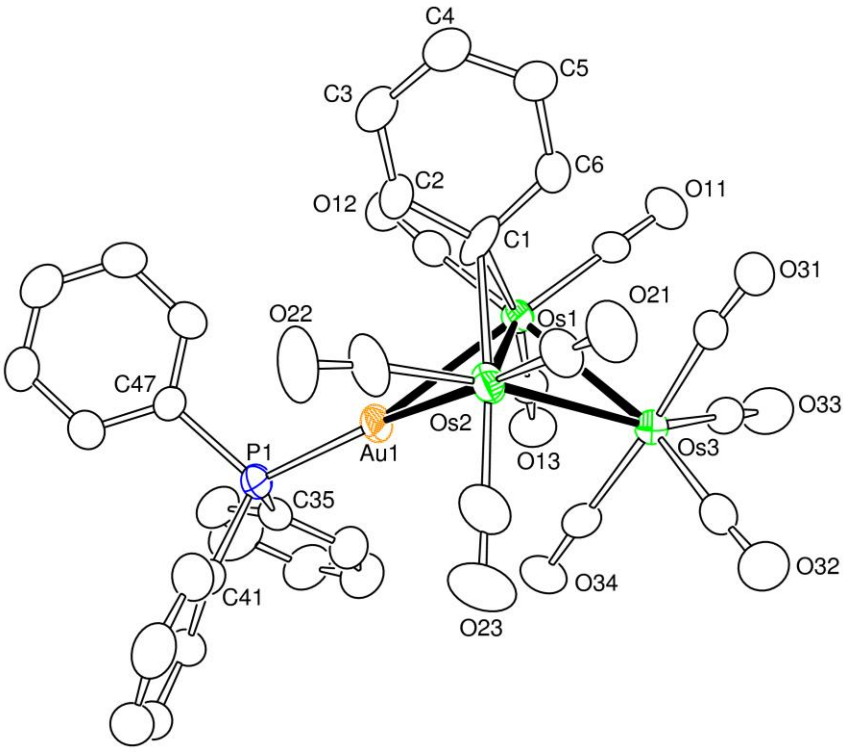

Figure 5.1. An ORTEP diagram of the molecular structure of $Os_3(CO)_{10}(\mu\text{-}C_6H_5)(\mu\text{-}AuPPh_3)$, **5.2** showing 30% thermal ellipsoid probability.

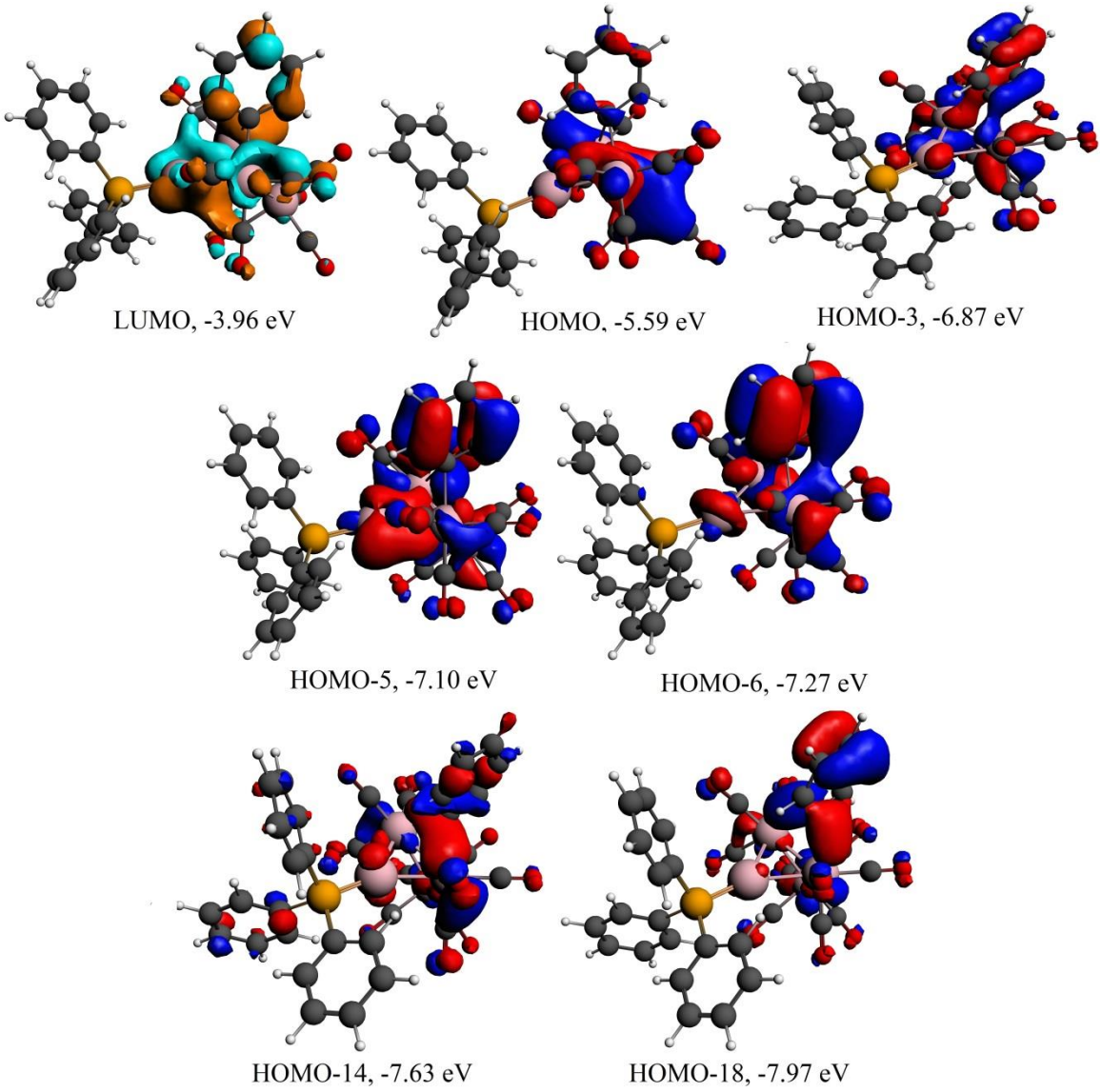

Figure 5.2. The LUMO, HOMO, HOMO-3, HOMO-5, HOMO-6, HOMO-14 and HOMO-18 with calculated energies show the bonding of the η^1-bridging phenyl ligand to the osmium atoms in **5.2**.

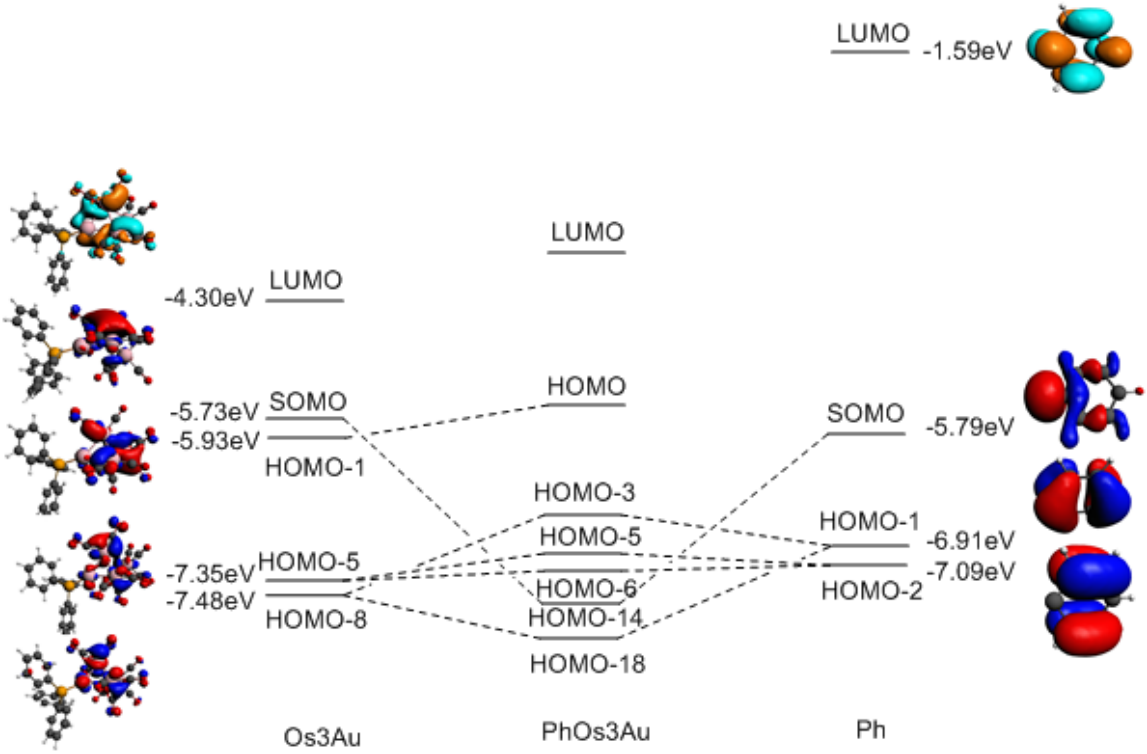

Figure 5.3. Energy level diagram of the molecular orbitals with calculated energies from fragment analysis shows the the origin of the MOs in Figure 5.2 for compound **5.2**.

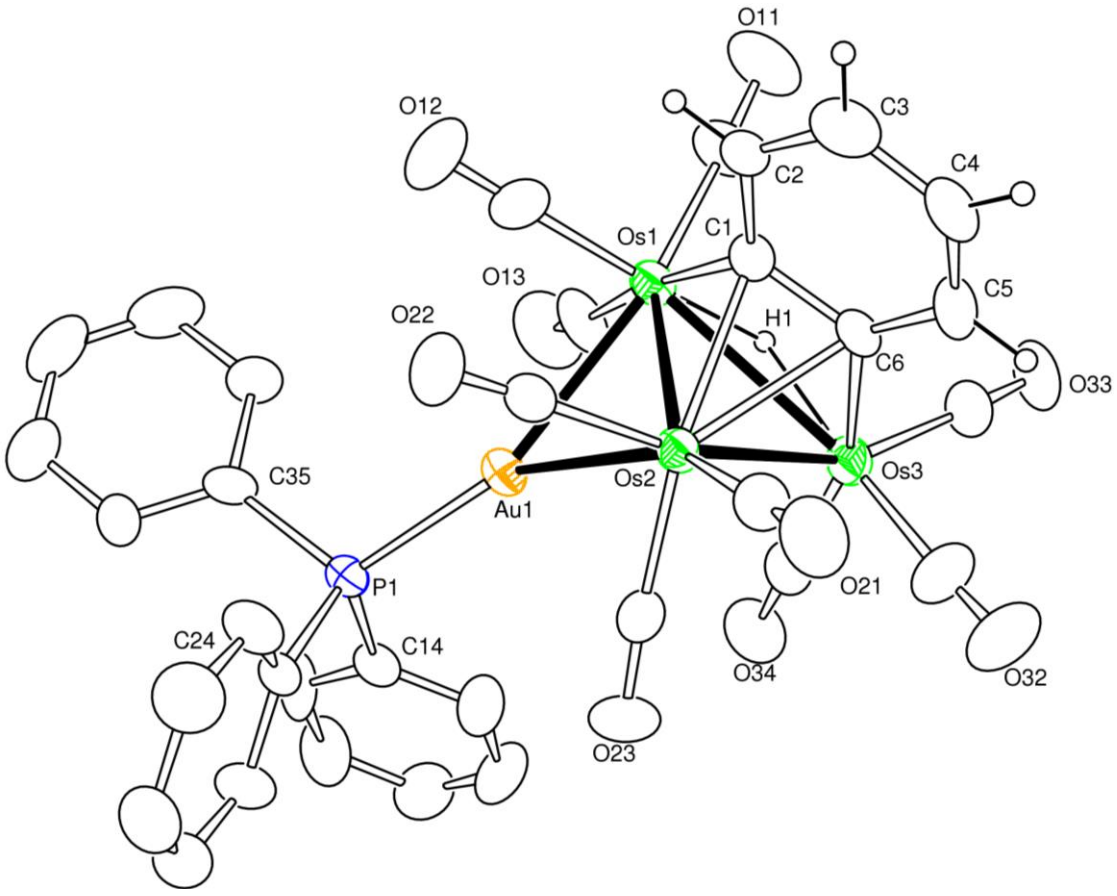

Figure 5.4. An ORTEP diagram of the molecular structure of $Os_3(CO)_9(\mu_3\text{-}C_6H_4)(\mu_3\text{-}AuPPh_3)(\mu\text{-}H)$, **5.3** showing 30% thermal ellipsoid probability.

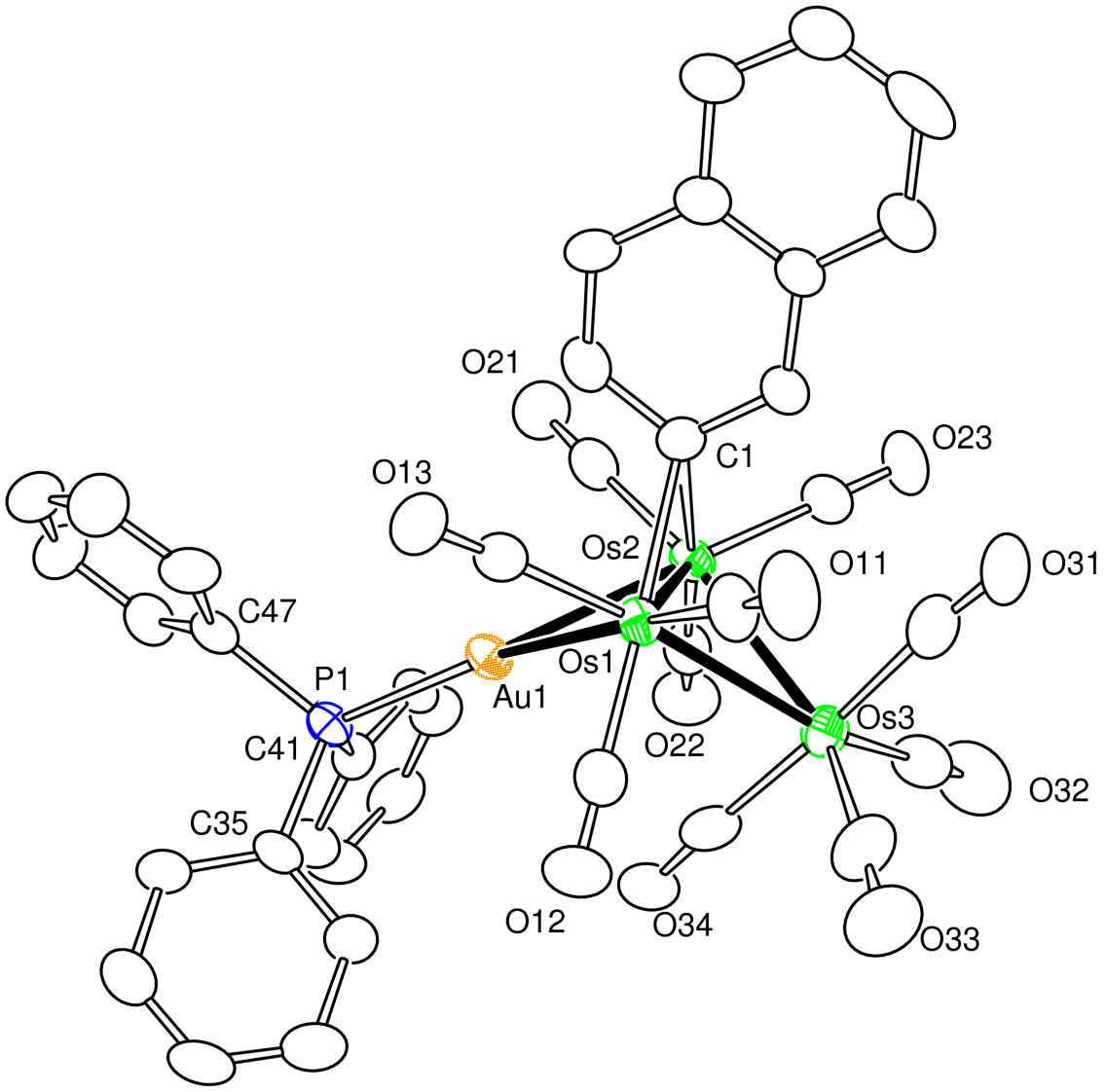

Figure 5.5. An ORTEP diagram of the molecular structure of $Os_3(CO)_{10}(\mu\text{-}2\text{-}Np)(\mu\text{-}AuPPh_3)$, **5.4a** obtained from the green crystals showing 30% thermal ellipsoid probability.

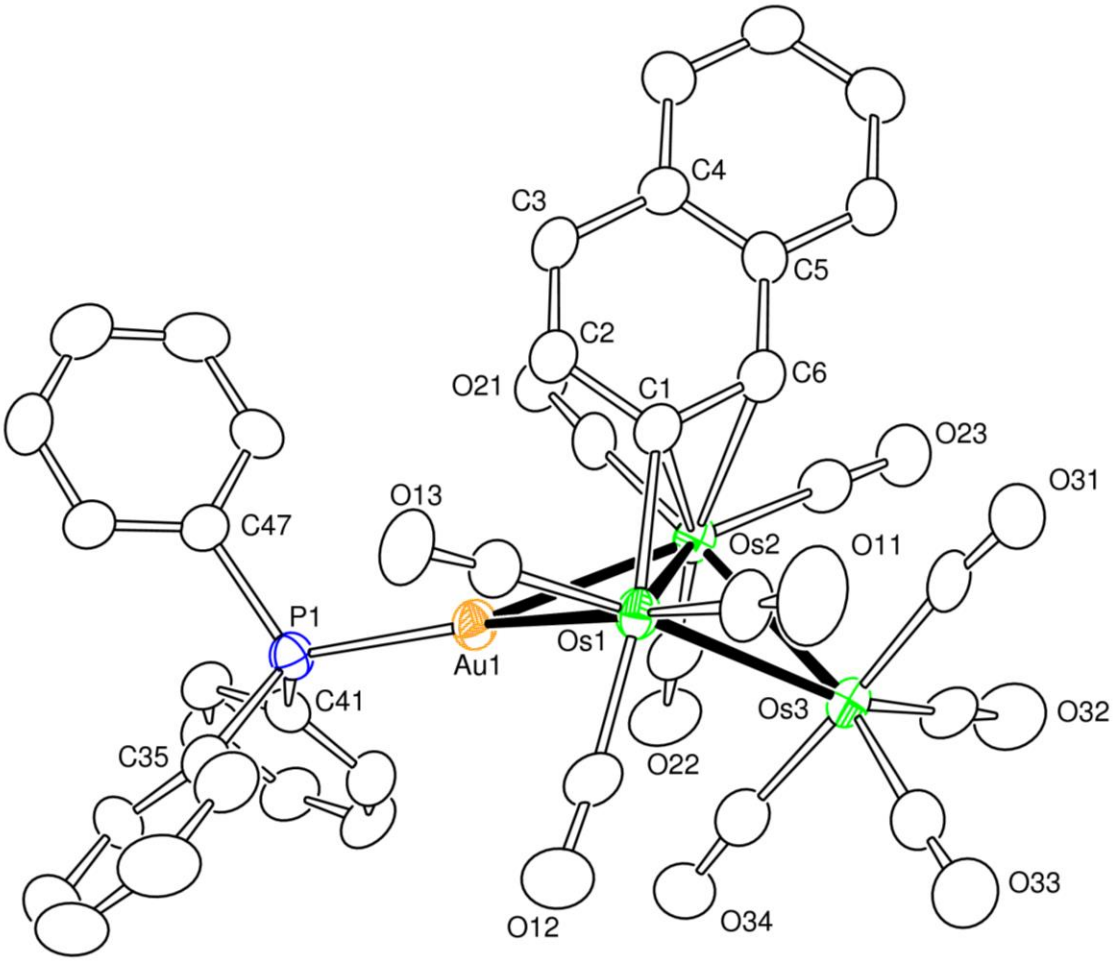

Figure 5.6. An ORTEP diagram of the molecular structure of $Os_3(CO)_{10}(\mu_3\text{-}\eta^2\text{-}2\text{-}Np)(\mu\text{-}AuPPh_3)$, **5.4b** showing 30% thermal ellipsoid probability.

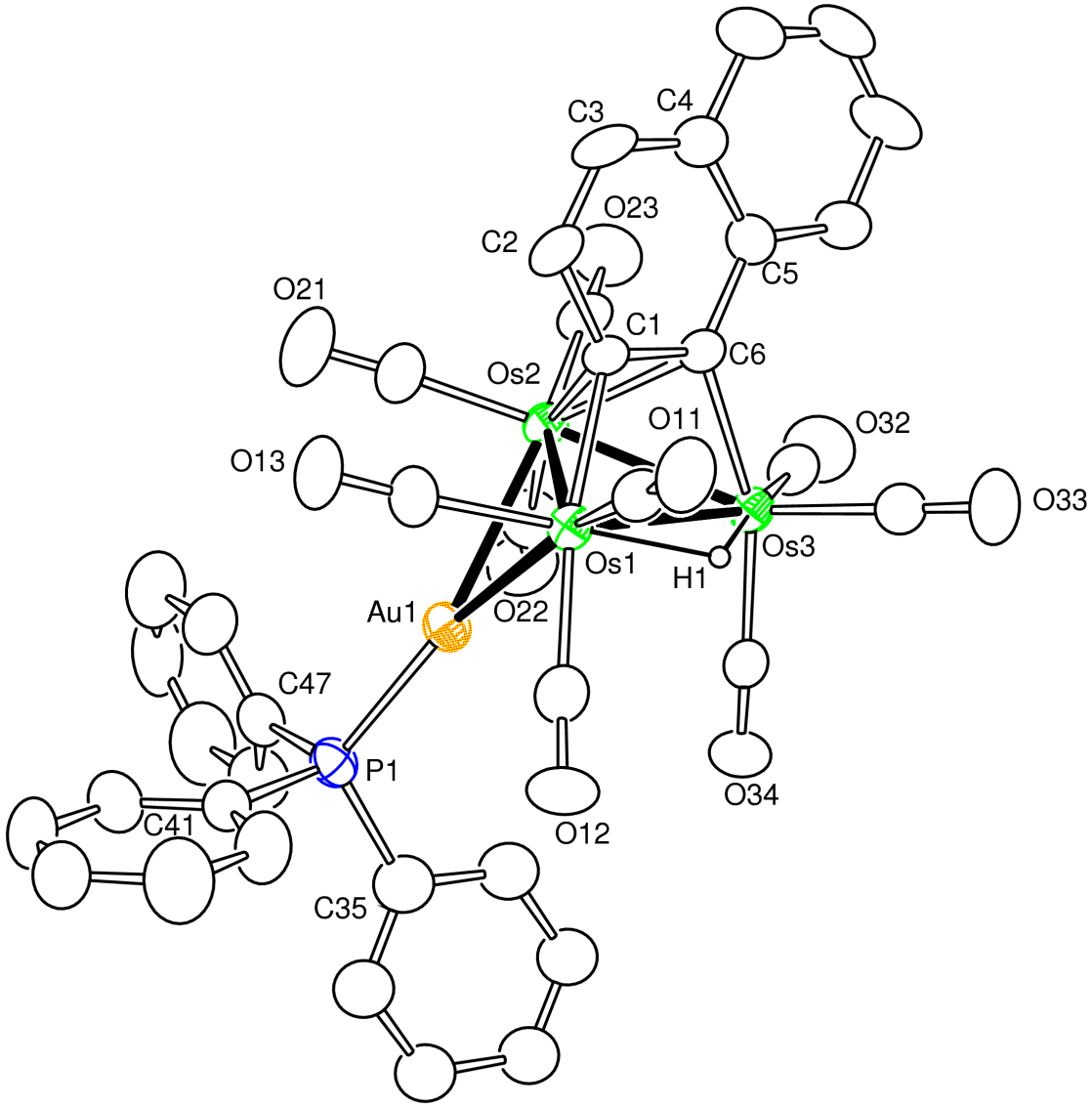

Figure 5.7. An ORTEP diagram of the molecular structure of $Os_3(CO)_9(\mu_3\text{-}C_{10}H_6)(\mu\text{-}AuPPh_3)(\mu\text{-}H)$, **5.5** showing 30% thermal ellipsoid probability.

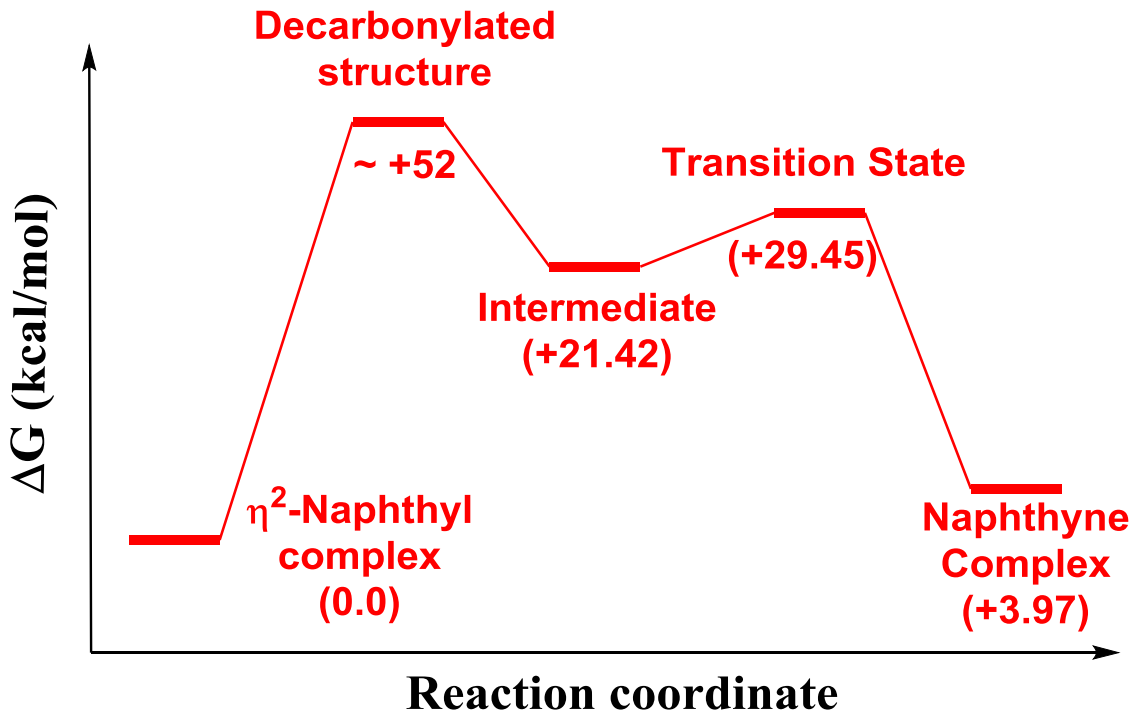

Figure 5.8. Calculated energy profile shows the decarbonylation and CH activation in the transformation from naphthyl to naphthyne.

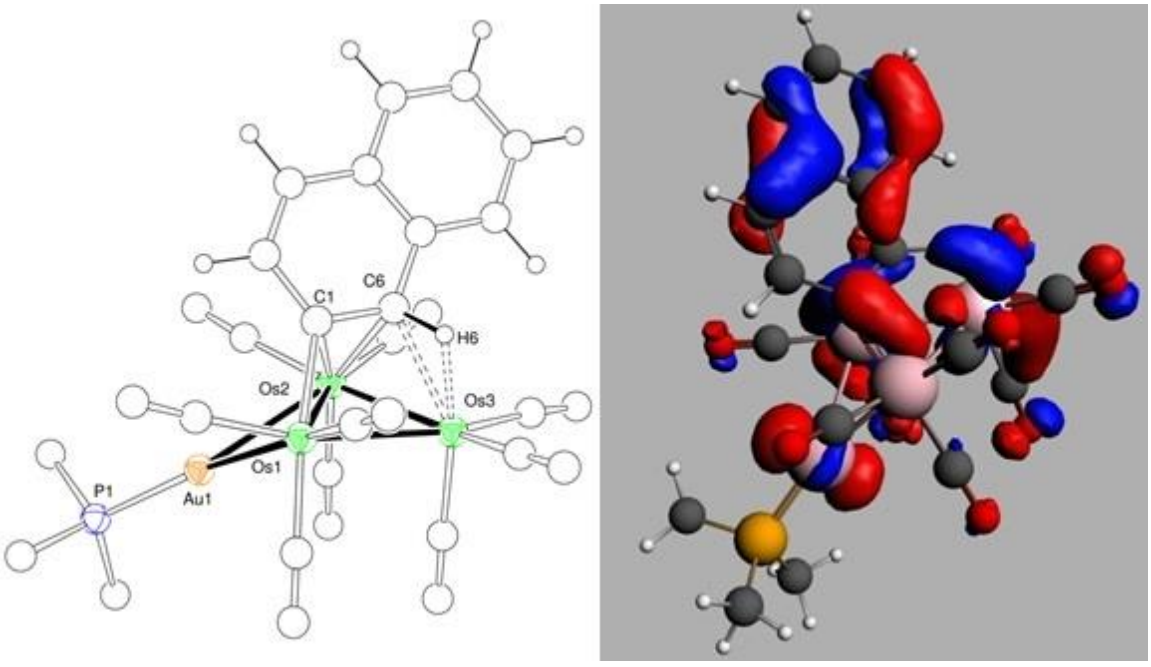

Figure 5.9. The computed intermediate of the naphthyne formation shows the agostic interaction between the ortho-CH bond in the Naphthyl group to the third osmium atom (left). The HOMO-13 of this intermediate shows the bonding of the hydrogen atom to the osmium (right).

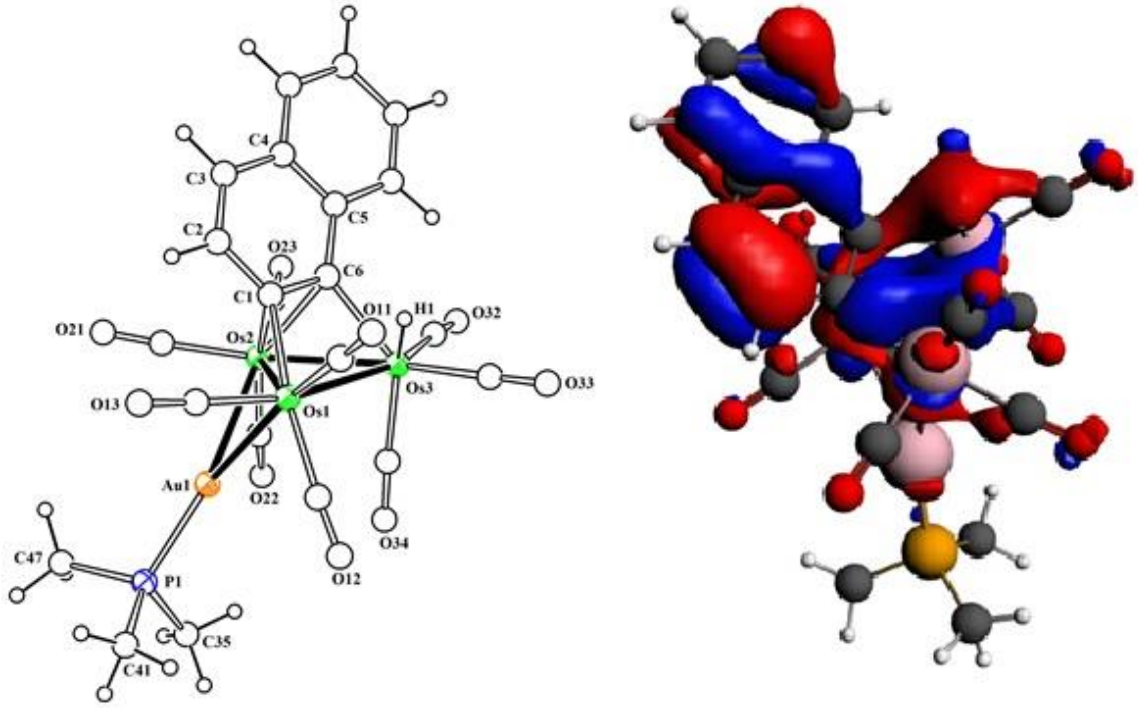

Figure 5.10. The computed transition state of the naphthyne formation shows the cleavage of the C-H bond (left). The HOMO of this transition state shows hydrogen-osmium bonding (right).

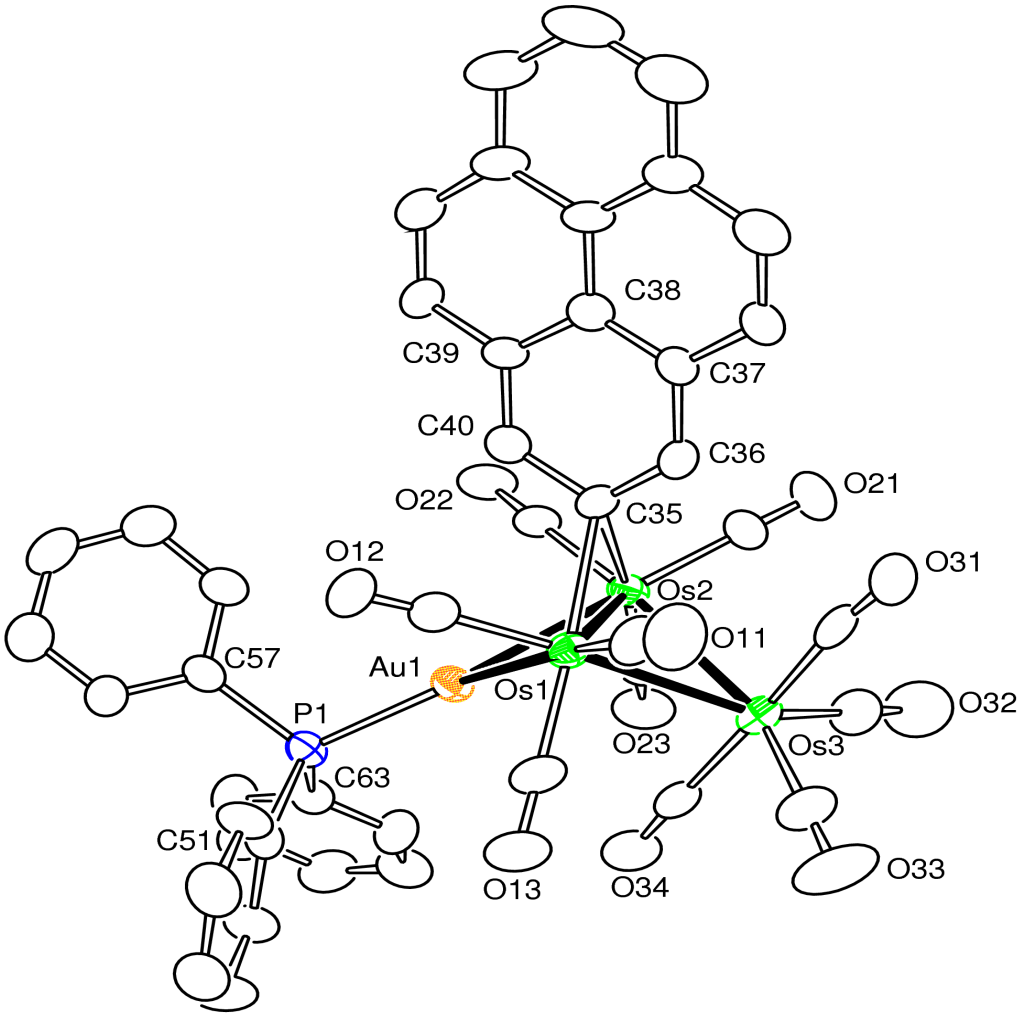

Figure 5.11. An ORTEP diagram of the molecular structure of $Os_3(CO)_{10}(AuPPh_3)$(2-Pyryl), **5.6** showing 30% thermal ellipsoid probability.

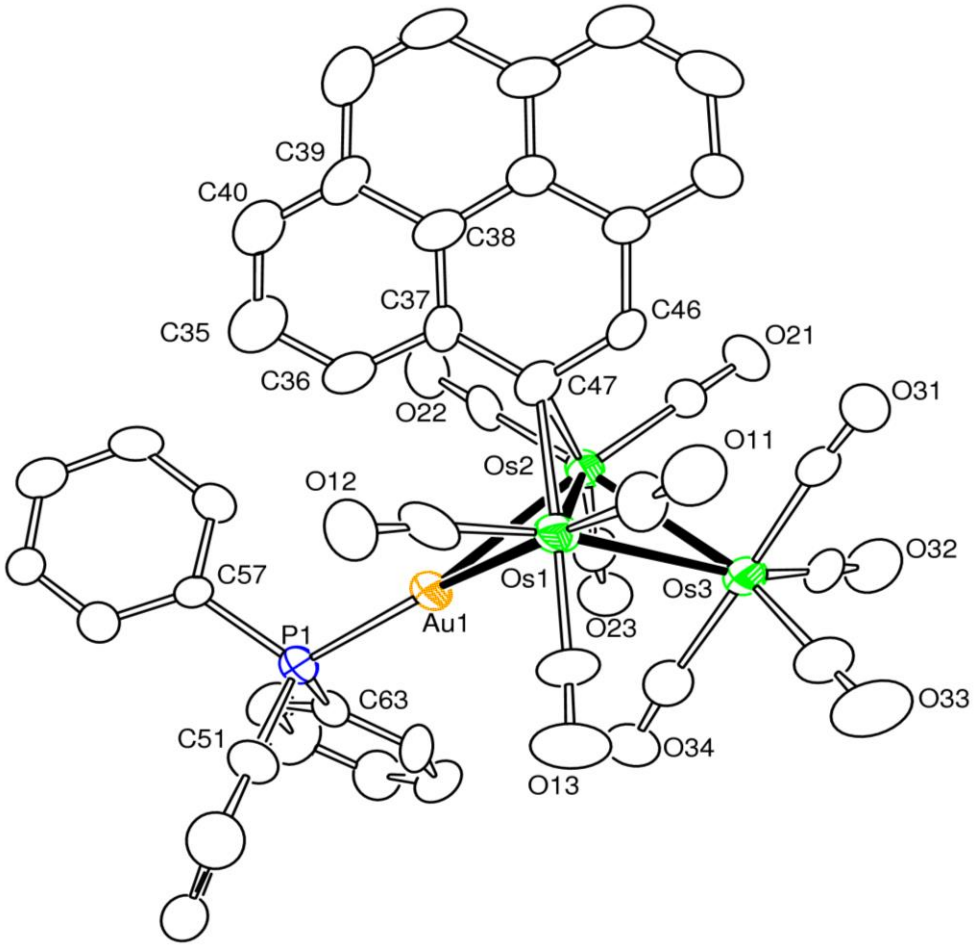

Figure 5.12. An ORTEP diagram of molecular structure of $Os_3(CO)_{10}(AuPPh_3)$(4-Pyryl), **5.7,** showing 30% thermal ellipsoid probability.

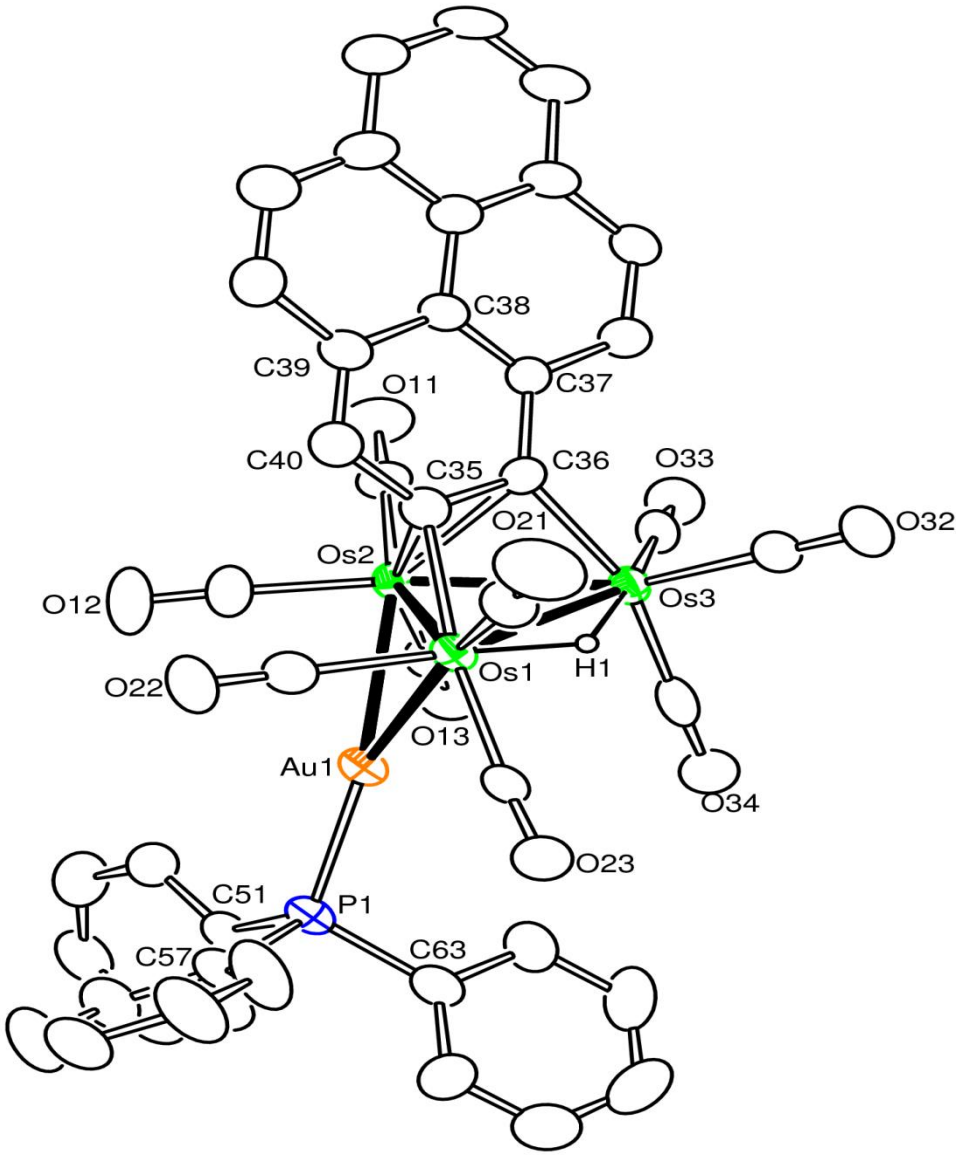

Figure 5.13. An ORTEP diagram of molecular structure of $Os_3(CO)_{10}(AuPPh_3)(\mu\text{-}1,2\text{-Pyryne})(\mu\text{-H})$, **5.8**, showing 30% thermal ellipsoid probability.

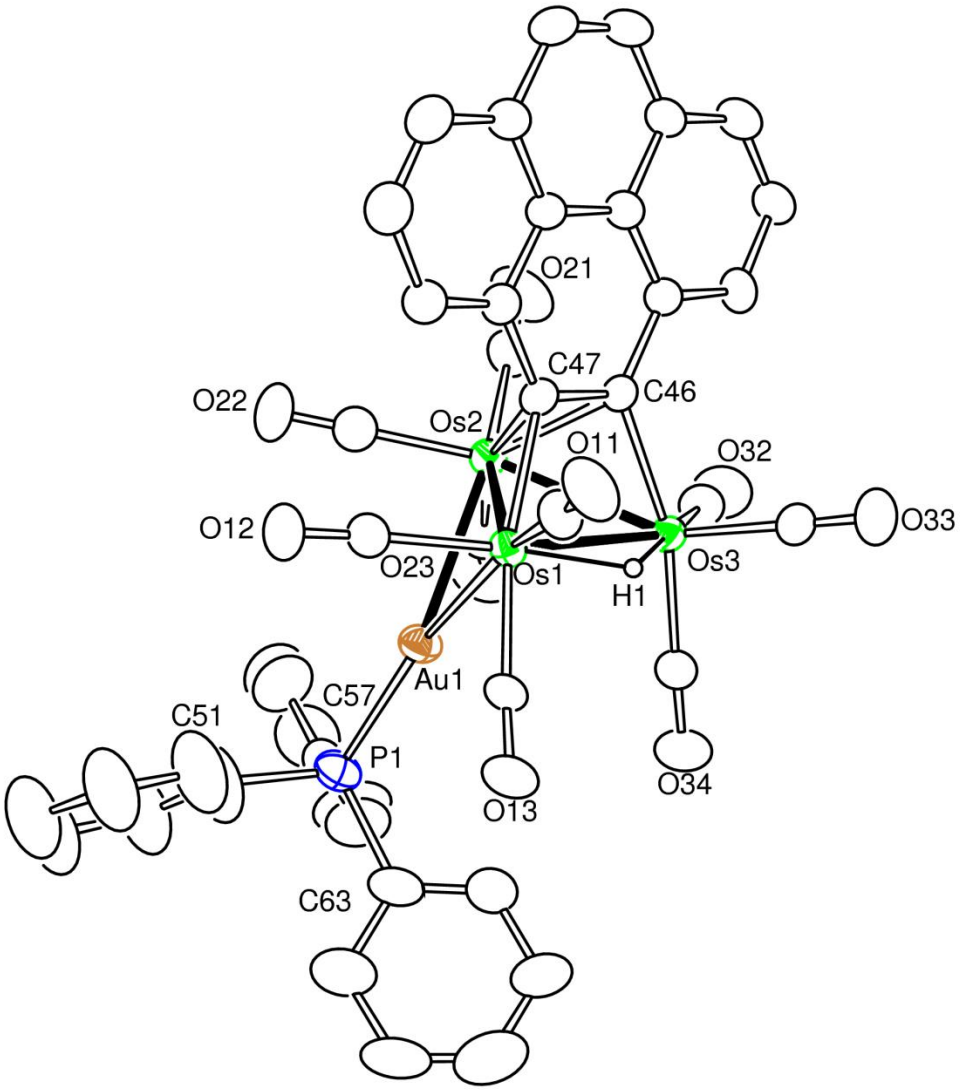

Figure 5.14. An ORTEP diagram of molecular structure of $Os_3(CO)_{10}(AuPPh_3)(\mu\text{-}4,5\text{-Pyryne})(\mu\text{-H})$, **5.9**, showing 30% thermal ellipsoid probability.

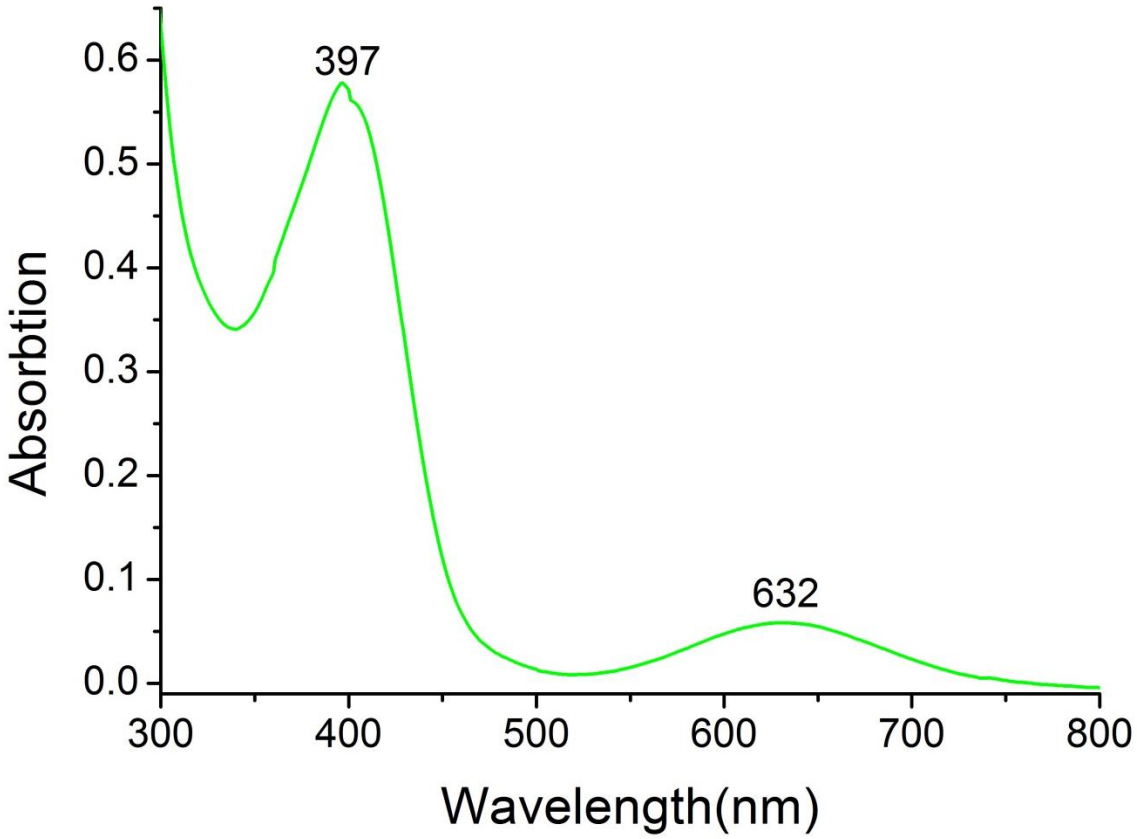

Figure 5.15. UV-Vis absorption spectra of compound **5.2,** 1.05×10^{-4} M in CH_2Cl_2, λ_{max} = 632nm, ε = $560M^{-1}\cdot cm^{-1}$.

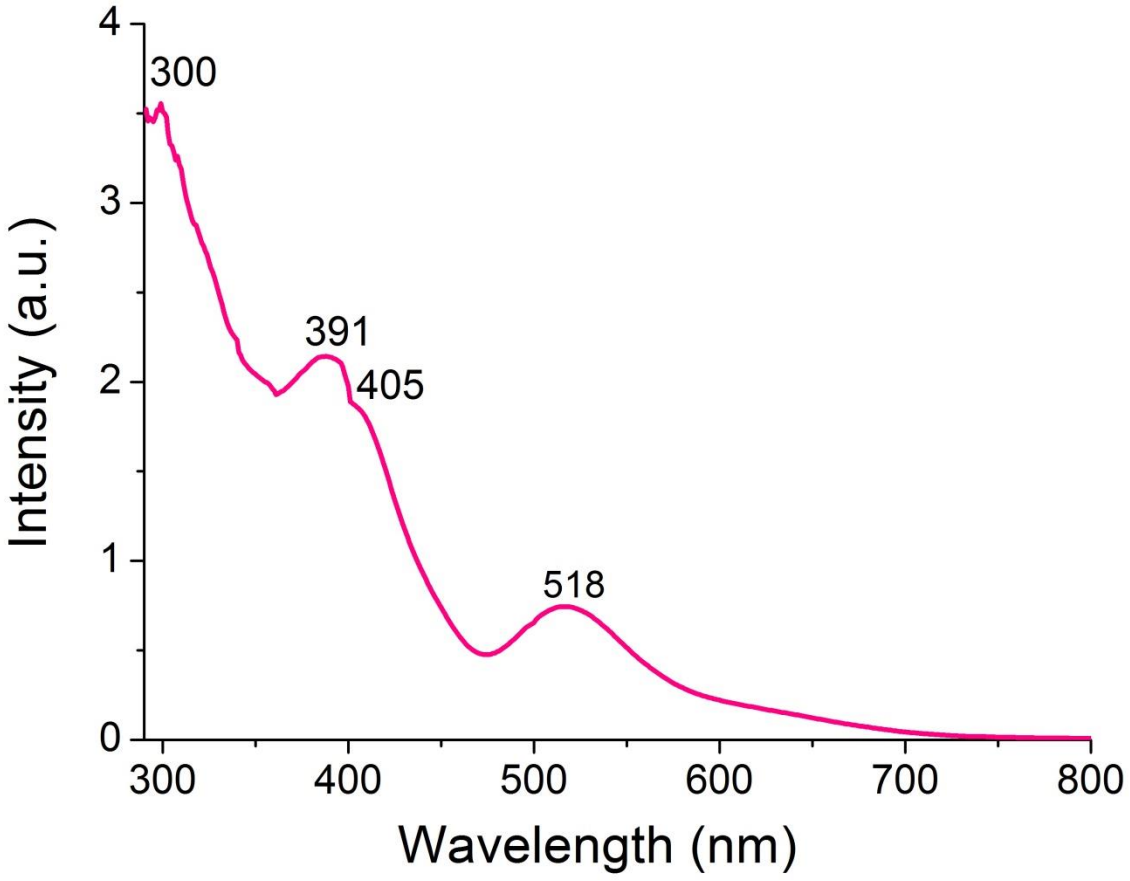

Figure 5.16. UV-vis absorption spectra for compounds **5.4b**, 2.47×10^{-4}M in CH_2Cl_2, λ_{max}=518 nm, $\varepsilon = 3009\ M^{-1}cm^{-1}$.

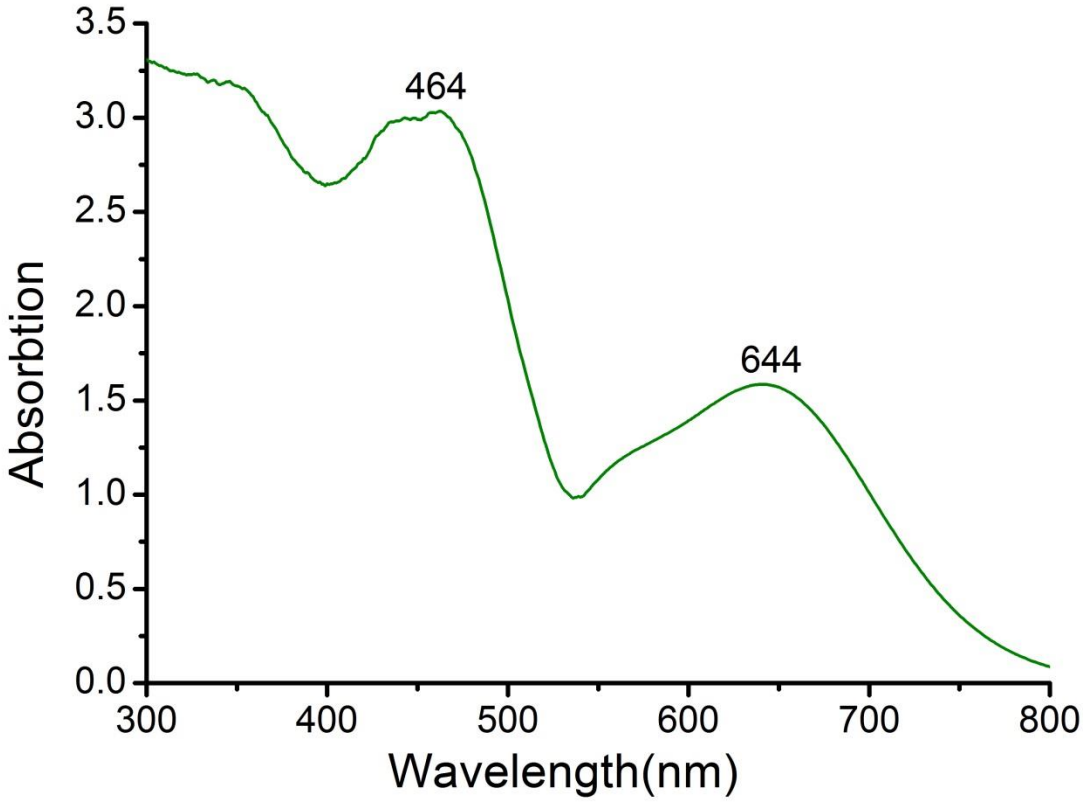

Figure 5.17. UV-vis absorption spectra for compounds **5.7**, 8.47×10^{-3}M in CH_2Cl_2, λ_{max}= 644 nm, ε =191 $M^{-1}cm^{-1}$.

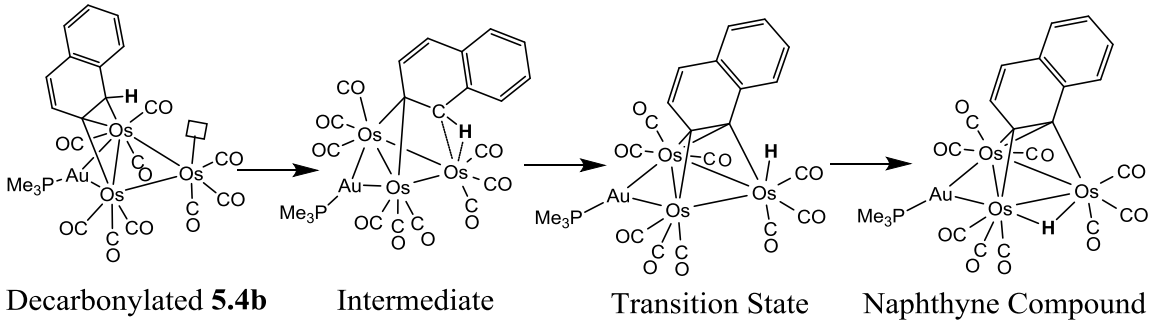

Scheme 5.1. The computed mechanism for the formation of Naphthyne compound **5.5** via ortho-C-H activation on the naphthyl ligand of **5.4b**.

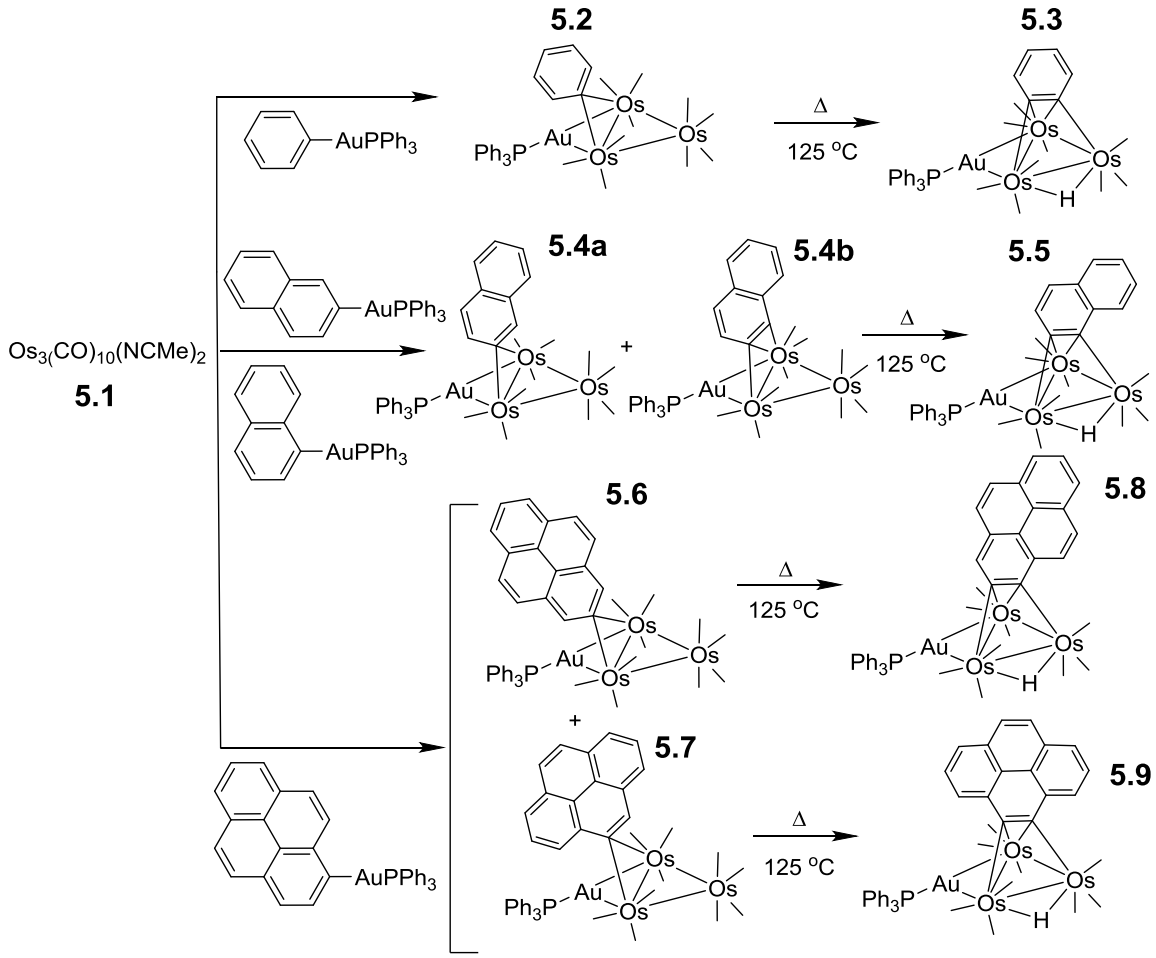

Scheme 5.2. The reaction of $Os_3(CO)_{10}(NCMe)_2$ with $ArylAuPPh_3$ and the transformations of $ArylOs_3(CO)_{10}AuPPh_3$ to $Aryne(\mu\text{-}H)Os_3(CO)_9AuPPh_3$.

Table 5.1. Crystallographic Data for Compounds **5.2** to **5.9**.

Compound	**5.2**	**5.3**	**5.4a**
Empirical formula	$C_{34}H_{21}O_{10}P\,Os_3Au$	$C_{33}H_{20}O_9P\,Os_3Au$	$C_{38}H_{22}O_{10}POs_3Au \cdot 1/2C_6H_{14}$
Formula weight	1388.04	1359.03	1480.18
Crystal system	Triclinic	Triclinic	Triclinic
Lattice parameters			
a (Å)	12.0376(4)	9.4965(2)	9.2085(6)
b (Å)	12.6331(4)	12.8917(3)	15.4986(11)
c (Å)	12.9189(4)	28.5192(6)	15.6967(11)
α (deg)	69.683(1) °	86.469(1)	69.710(1)
β (deg)	78.064(1) °	86.732(1)	87.315(1)
γ (deg)	84.682(1) °	88.964(1)	82.697(1)
V ($Å^3$)	1802.08(10)	3478.83(13)	2084.2(2)
Space group	*P*-1	*P* -1	*P* -1
Z value	2	4	2
ρcalc (g / cm^3)	2.558	2.595	2.359
μ (Mo Kα) (mm-1)	14.698	15.223	12.717
Temperature (K)	293(2)	294(2)	294(2)
2Θ max (°)	50.06	50.06	50.06
No. Obs. (I > 2σ(I))	6367	12303	7361
No. Parameters	442	855	479
Goodness of fit	1.033	1.031	1.025
Max. shift in cycle	0.001	0.002	0.001
Residuals[a]: R1; wR2	0.0380;0.1018	0.0368;0.0834	0.0404;0.1121
Absorp.Corr.	1.000/0.441	1.000/0.611	1.000/0.557
Largest peak in Final Diff. Map ($e^- / Å^3$)	3.537	0.773	1.528

[a] $R = \Sigma_{hkl}(\,|\,|F_{obs}|-|F_{calc}|\,|)/\Sigma_{hkl}|F_{obs}|$; $R_w = [\Sigma_{hkl}w(|F_{obs}|-|F_{calc}|)^2/\Sigma_{hkl}wF^2_{obs}]^{1/2}$; $w = 1/\sigma^2(F_{obs})$; $GOF = [\Sigma_{hkl}w(|F_{obs}|-|F_{calc}|)^2/(n_{data} - n_{vari})]^{1/2}$.

Table 5.1. continued….

Compound	**5.4b**	**5.5**	**5.6**
Empirical formula	$C_{38}H_{22}O_{10}P\ Os_3Au$	$C_{37}H_{22}O_9P\ Os_3Au$	$Os_3AuPC_{44}H_{24}O_{10}$
Formula weight	1437.09	1409.08	1511.17
Crystal system	Monoclinic	Monoclinic	Triclinic
Lattice parameters			
a (Å)	30.520(3)	9.1719(5)	12.5312(7)
b (Å)	10.1912(8)	16.0279(9)	12.7679(7)
c (Å)	27.194(3)	25.959(1)	14.9324(8)
α (deg)	90	90	83.943(2) °
β (deg)	115.246(4)	91.298(1)	66.9150(10) °
γ (deg)	90	90	72.7000(10) °
V ($Å^3$)	7650.2(12)	3815.2(4)	2098.2(2)
Space group	*C*2/c	$P2_1/c$	*P*-1
Z value	8	4	2
ρcalc (g / cm^3)	2.495	2.453	2.392
μ (Mo Kα) (mm-1)	13.854	13.886	12.635
Temperature (K)	294(2)	294(2)	294(2)
2Θ max (°)	50.06	50.06	50.06
No. Obs. (I > 2σ(I))	6749	6715	7406
No. Parameters	478	430	532
Goodness of fit (GOF)	1.073	1.053	1.003
Max. shift in cycle	0.001	0.001	0.001
Residuals[a]: R1; wR2	0.0444;0.0986	0.0435;0.1022	0.0473;0.0753
Absorp.Corr. Max/min	1.000/0.458	1.000/0.661	1.000/0.724
Largest peak in Final Diff. Map ($e^- / Å^3$)	1.579	1.137	1.219

[a] $R = \Sigma_{hkl}(\ |\ |F_{obs}|-|F_{calc}|\ |\ )/\Sigma_{hkl}|F_{obs}|$; $R_w = [\Sigma_{hkl}w(|F_{obs}|-|F_{calc}|)^2/\Sigma_{hkl}wF^2_{obs}]^{1/2}$; $w = 1/\sigma^2(F_{obs})$; GOF = $[\Sigma_{hkl}w(|F_{obs}|-|F_{calc}|)^2/(n_{data}-n_{vari})]^{1/2}$.

Table 5.1 Continued…

Compound	**5.7**	**5.8**	**5.9**
Empirical formula	$Os_3AuPC_{44}H_{24}O_{10}$ $\cdot CH_2Cl_2$	$Os_3AuPC_{43}H_{24}O_9$	$Os_3AuPC_{43}H_{24}O_9$ $\cdot 1/2C_6H_{14}$
Formula weight	1596.09	1483.16	1526.24
Crystal system	Triclinic	Triclinic	Triclinic
Lattice parameters			
a (Å)	12.716(3)	9.6219(3)	9.8364(3)
b (Å)	13.105(3)	11.2187(3)	12.6236(3)
c (Å)	15.765(4)	19.4363(6)	19.9043(5)
α (deg)	72.071(6)	97.673(1)	94.960(1)
β (deg)	73.087(6)	100.981(1)	103.500(1)
γ (deg)	68.724(5)	100.138(1)	111.308(1)
V ($Å^3$)	2281.3(10)	1996.96(10)	2198.57(10)
Space group	*P* -1	*P* -1	*P* -1
Z value	2	2	2
ρcalc (g / cm^3)	2.324	2.467	2.305
μ (Mo Kα) (mm-1)	11.741	13.271	12.058
Temperature (K)	294(2)	294(2)	294(2)
2Θ max (°)	50.06	50.06	50.04
No. Obs.(I> 2σ(I))	8072	7066	7763
No. Parameters	532	518	488
Goodness of fit	1.015	1.016	1.021
Max. shift in cycle	0.000	0.001	0.001
Residuals[a]:R1;wR2	0.0586;0.1362	0.0334;0.0786	0.0296;0.0829
Absorp. Corr.	1.000/ 0.532	1.000/0.597	1.000/0.495
Largest peak in Final Diff. Map ($e^- / Å^3$)	3.519	2.092	1.723

[a] $R = \Sigma_{hkl}(\,|\,|F_{obs}|-|F_{calc}|\,|)/\Sigma_{hkl}|F_{obs}|$; $R_w = [\Sigma_{hkl} w(|F_{obs}|-|F_{calc}|)^2/\Sigma_{hkl} w F^2_{obs}]^{1/2}$; $w = 1/\sigma^2(F_{obs})$; $GOF = [\Sigma_{hkl} w(|F_{obs}|-|F_{calc}|)^2/(n_{data} - n_{vari})]^{1/2}$.

Table 5.2. Selected intramolecular angles and bond distances for compound **5.2**.[a]

Distances			**Angles**			
Atom	Atom	Distance(Å)	Atom	Atom	Atom	Angle(deg)
Au1	Os1	2.7424(6)	Au1	Os1	Os2	60.767(15)
Au1	Os2	2.7772(6)	Au1	Os1	Os3	95.591(18)
Os1	Os2	2.7484(6)	Au1	Os2	Os1	59.508(14)
Os1	Os3	2.8745(6)	Au1	Os2	Os3	94.999(18)
Os2	Os3	2.8668(6)	Os1	Os2	Os3	61.539(15)
Os1	C1	2.313(11)	Os1	C1	Os2	72.5(3)
Os2	C1	2.332(11)	C6	C1	Os2	112.9(8)
C1	C2	1.423(15)				
C2	C3	1.348(14)				
C3	C4	1.444(15)				
C4	C5	1.408(16)				
C5	C6	1.398(14)				
C1	C6	1.373(14)				

[a] Estimated standard deviations in the least significant figure are given in parentheses.

Table 5.3. Selected intramolecular angles and bond distances for compound **5.3**.[a]

Distances			**Angles**			
Atom	Atom	Distance(Å)	Atom	Atom	Atom	Angle(deg)
Au1	Os1	2.7507(6)	Au1	Os1	Os3	85.921(18)
Au1	Os2	2.8131(6)	Au1	Os2	Os1	57.652(15)
Os1	Os3	3.0229(7)	Au1	Os2	Os3	90.043(18)
Os1	Os2	2.8902(6)	Os1	Au1	Os2	62.581(15)
Os1	H1	1.69(9)	Os1	Os2	Os3	64.688(16)
Os1	C1	2.085(10)	Os1	Os3	Os2	59.805(15)
Os2	Os3	2.756(6)	Os2	Os1	Os3	55.506(15)
Os3	H1	1.99(9)	Os1	C1	Os2	82.7(4)
Os3	C6	2.097(10)				

[a] Estimated standard deviations in the least significant figure are given in parentheses.

Table 5.4. Selected intramolecular angles and bond distances for compound **5.4a**.[a]

Distances			**Angles**			
Atom	Atom	Distance(Å)	Atom	Atom	Atom	Angle(deg)
Au1	Os1	2.7424(6)	Au1	Os1	Os2	60.768(15)
Au1	Os2	2.7772(6)	Au1	Os1	Os3	95.593(18)
Os1	Os2	2.7484(6)	Au1	Os2	Os1	59.508(14)
Os1	Os3	2.8745(6)	Au1	Os2	Os3	94.999(18)
Os1	C1	2.314(11)	Os1	Au1	Os2	59.724(14)
Os2	Os3	2.8669(6)	Os1	Os2	Os3	61.537(15)
Os2	C1	2.331(11)	Os1	Os3	Os2	57.201(14)
			Os1	C1	Os2	72.6(3)
			Os2	Os1	Os3	61.261(15)

[a] Estimated standard deviations in the least significant figure are given in parentheses.

Table 5.5. Selected intramolecular angles and bond distances for compound **5.4b**.[a]

Distances			**Angles**			
Atom	Atom	Distance(Å)	Atom	Atom	Atom	Angle(deg)
Au1	Os1	2.7573(6)	Au1	Os1	Os2	58.207(15)
Au1	Os2	2.8146(6)	Au1	Os1	Os3	101.940(19)
Os1	Os2	2.8538(6)	Os1	Au1	Os2	61.609(16)
Os1	Os3	2.8997(6)	Os1	Os2	Os3	60.639(15)
Os1	C1	2.174(11)	Os1	Os3	Os2	59.066(14)
Os2	Os3	2.8899(7)	Os1	C1	Os2	77.7(3)
Os2	C1	2.369(10)	Os2	C1	C6	80.8(6)
Os2	C6	2.544(10)	Os2	C6	C1	66.8(6)
			Os2	Os1	Os3	60.295(16)

[a] Estimated standard deviations in the least significant figure are given in parentheses.

Table 5.6. Selected intramolecular angles and bond distances for compound **5.5**.[a]

Distances			**Angles**			
Atom	Atom	Distance(Å)	Atom	Atom	Atom	Angle(deg)
Au1	Os1	2.7295(7)	Au1	Os1	Os3	86.394(19)
Au1	Os2	2.7923(7)	Au1	Os2	Os1	57.556(16)
Os1	Os2	2.8950(6)	Au1	Os2	Os3	90.180(19)
Os1	Os3	2.9882(7)	Os1	Au1	Os2	63.105(17)
Os1	C1	2.214(11)	Os1	Os2	Os3	63.870(16)
Os1	H1	1.8539	Os1	Os3	Os2	60.435(16)
Os2	Os3	2.7494(6)	Os1	C1	Os2	81.7(4)
Os2	C1	2.298(11)	Os2	C1	C6	74.8(7)
Os2	C6	2.370(12)	Os2	C6	C1	69.4(6)
Os3	H1	1.6700	Os2	C6	Os3	75.9(4)
			Os2	Os1	Os3	55.695(15)

[a] Estimated standard deviations in the least significant figure are given in parentheses.

Table 5.7. Selected intramolecular angles and bond distances for compound **5.6**.[a]

Distances			**Angles**			
Atom	Atom	Distance(Å)	Atom	Atom	Atom	Angle(deg)
Au1	Os1	2.7515(7)	Au1	Os1	Os2	60.043(17)
Au1	Os2	2.7518(7)	Au1	Os1	Os3	97.04(2)
Os1	Os2	2.7485(7)	Au1	Os2	Os1	60.032(17)
Os1	Os3	2.8980(7)	Au1	Os2	Os3	96.83(2)
Os2	Os3	2.8863(7)	Os1	Os2	Os3	61.369(18)
Os1	C35	2.291(12)	Os1	C1	Os2	72.7(4)
Os2	C35	2.345(13)	C40	C35	Os2	109.8(8)
C35	C36	1.370(15)				
C36	C37	1.422(16)				
C37	C38	1.407(15)				
C38	C39	1.431(15)				
C39	C40	1.374(15)				
C35	C40	1.464(15)				

[a] Estimated standard deviations in the least significant figure are given in parentheses.

Table 5.8. Selected intramolecular angles and bond distances for compound **5.7**.[a]

Distances			**Angles**			
Atom	Atom	Distance(Å)	Atom	Atom	Atom	Angle(deg)
Au1	Os1	2.7618(10)	Au1	Os1	Os2	60.58(3)
Au1	Os2	2.7945(10)	Au1	Os1	Os3	96.27(4)
Os1	Os3	2.9313(12)	Au1	Os2	Os1	59.41(2)
Os1	Os2	2.7789(10)	Au1	Os2	Os3	96.51(3)
Os1	C47	2.247(17)	Os1	Au1	Os2	60.01(3)
Os2	Os3	2.8897(11)	Os1	Os2	Os3	62.24(3)
Os2	C47	2.364(18)	Os1	Os3	Os2	57.02(2)
C46	C47	1.38(2)	Os2	Os1	Os3	60.73(3)
C37	C47	1.47(2)	Os1	C47	Os2	74.1(5)
C37	C38	1.40(2)				
C38	C44	1.43(2)				
C44	C45	1.43(2)				

[a] Estimated standard deviations in the least significant figure are given in parentheses.

Table 5.9. Selected intramolecular angles and bond distances for compound **5.8**.[a]

Distances			**Angles**			
Atom	Atom	Distance(Å)	Atom	Atom	Atom	Angle(deg)
Au1	Os1	2.7541(5)	Au1	Os1	Os2	59.356(13)
Au1	Os2	2.7917(5)	Au1	Os1	Os3	87.993(14)
Os1	Os2	2.8799(5)	Au1	Os2	Os1	58.079(13)
Os1	Os3	3.0044(5)	Au1	Os2	Os3	92.470(15)
Os1	C35	2.134(10)	Os1	Au1	Os2	62.564(13)
Os1	H1	1.54(7)	Os1	Os2	Os3	64.426(12)
Os2	Os3	2.7525(5)	Os1	Os3	Os2	59.843(12)
Os2	C35	2.300(9)	Os1	C35	Os2	80.9(3)
Os2	C36	2.441(9)	Os2	Os1	Os3	55.731(12)
Os3	C36	2.100(9)				
Os3	H1	1.91(7)				

[a] Estimated standard deviations in the least significant figure are given in parentheses.

Table 5.10. Selected intramolecular angles and bond distances for compound **5.9**.[a]

Distances			**Angles**			
Atom	Atom	Distance(Å)	Atom	Atom	Atom	Angle(deg)
Au1	Os1	2.7480(4)	Au1	Os1	Os2	59.441(10)
Au1	Os2	2.7909(4)	Au1	Os1	Os3	81.490(12)
Os1	Os2	2.8770(4)	Au1	Os2	Os1	57.980(10)
Os1	Os3	2.9702(4)	Au1	Os2	Os3	84.540(12)
Os1	H1	1.73(6)	Os1	Au1	Os2	62.579(11)
Os1	C47	2.144(7)	Os1	Os2	Os3	63.515(10)
Os2	Os3	2.7634(4)	Os1	Os3	Os2	60.105(10)
Os2	C46	2.303(7)	Os1	C47	Os2	80.9(2)
Os2	C47	2.287(7)	Os2	Os1	Os3	56.380(9)
Os3	C46	2.115(7)				
Os3	H1	1.78(6)				

[a] Estimated standard deviations in the least significant figure are given in parentheses.

REFERENCE

1. Goudsmit, R. J.; Johnson, B. F. G.; Lewis, J.; Raithby, P. R.; Rosales, M. J. *J. Chem. Soc. Dalton Trans.* **1983**, 2257 – 2261.

2. (a) Bradford, C. W.; Nyholm, R. S.; Gainsford, G. J.; Guss, J. M.; Ireland, P. R.; Mason, R. *J. Chem. Soc. Chem Commun.* **1972**, 87 – 89. (b) Gainsford, G. J.; Guss, J. M.; Ireland, P. R.; Mason, R.; Bradford, C. W.; Nyholm, R. S. *J. Organomet. Chem.* **1972**, *40*, C70 – C72. (c) Deeming, A. J.; Kimber, R. E.; Underhill, M. *J. Chem. Soc. Dalton Trans.* **1973**, 2589 – 2596.

3. Arce, A. J.; Deeming, A. J. *J. Chem. Soc. Dalton Trans.* **1982**, 1155 – 1157.

4. (a) Chan, K. H.; Leong, W. K.; Mak, K. H. G. *Organometallics* **2006**, *25*, 250 – 259. (b) Leong, W. K.; Chen, G. *Organometallics* **2001,** *20,* 2280 – 2287.

5. Adams. R. D.; Katahira, D. A.; Yang, L.-W. *Organometallics* **1982**, *1*, 235 – 239.

6. Hartwig, J. F.; Bergman, R. G.; Andersen, R. A. *J. Am. Chem. Soc.* **1991**, *113*, 3404 – 3418.

7. Johnson, B. F. G.; Nairn, J. G. M.; Brown, D. B.; Lewis, J.; Gallop, M.; Parker, D. G. *Chem. Eur. J.* **1995**, *1*, 252 – 260.

8. Braga, D.; Grepioni, F.; Parisini, E.; Johnson, B.F.G.; Martin, C.M.; Nairn, J.G.M.; Lewis, J.; Martinelli, M., *J. Chem. Soc. Dalton Trans.*, **1993**, 1891 – 1895.

9. PartyKa, D.V.; Zeller, M.; Hunter, A.D.; Gray, T.G., *Angew. Chem. Int. Ed.* **2006**, *45*, 8188 – 8191.

10. Osawa, M.; Hoshino, M.; Hashizume, D., *Dalton Trans.*, **2008**, 2248 – 2252.

11. Heng W.Y.; Hu J. and Yip J.H.K., *Organometallics* **2007**, *26*, 6760 – 6768.

12. SAINT+, version 6.2a, Bruker Analytical X-ray Systems, Inc., Madison, WI, **2001**.

13. Sheldrick, G. M. SHELXTL, version 6.1, Bruker Analytical X-ray Systems, Inc., Madison, WI, **1997**.

14. ADF2012, SCM, Theoretical Chemistry, Vrije Universiteit, Amsterdam, The Netherlands, http://www.scm.com

15. Perdew, J. P.; Ruzsinszky, A.; Csonka, G. I.; Vydrov, O. A.; Scuseria, G. E. *Phys. Rev. Lett.* **2008**, *100*, 136406.

16. Partyka, D.V.; Zeller, M.; Hunter, A.D.; Gray, T.G., *Angew. Chem. Int. Ed.* **2006**, *45*, 8188 – 8191.

17. (a) Raubenheimer, H. G.; Schmidbaur, H. *Organometallics* **2012**, *31*, 2507 – 2522. (b) Stone, F. G. A. *Angew. Chem. Int. Ed. Engl.* **1984**, *23*, 89 – 99.

18. Arce, A. J.; Arrojo, P.; Deeming, A. J.; De Sanctis, Y. *J. Chem. Soc., Chem. Commun.* **1991**, 1491 – 1492.

19. (a) Broach, R. W.; Williams, J. M. *Inorg. Chem.* **1979**, *18* , 314 – 319. (b) Churchill, M. R.; Hollander, F. J.; Hutchinson, J. P. *Inorg. Chem.* **1977**, *16*, 2697 – 2700; (c) Allen, V. F.; Mason, R.; Hitchcock, P. B. *J. Organomet. Chem.* **1977**, *140*, 297 – 307.

20. Burgess, K.; Johnson, B. F. G.; Kaner, D. A.; Lewis, J.; Raithby, P. R.; Syed,-Mustaffa, S. N. A. B. *J. Chem. Soc., Chem. Commun.* **1983**, 455 – 457.

21. Johnson, B. F. G.; Kaner, D. A.; Lewis, J.; Raithby, P. R. *J. Organomet. Chem.* **1981**, *215*, C33 – C37.

22. Osawa,M.; Hoshino, M.; Hashizume, D. *Dalton Trans.* **2008**, 2248 – 2252.

23. Although there are rare, 2-bridging phenyl ligands have been observed previously. Adams, R. D.; Kan, Y.; Zhang, Q. *Organometallics* **2011**, *30*, 328 – 333.

24. When the green crystals of **5.4a** are dissolved in hexane, the solutions are pink.

25. Osawa,M.; Hoshino, M.; Hashizume, D. *Dalton Trans.* **2008**, 2248 – 2252.

26. Arce, A. J.; Canavera, F.; De Sanctis, Y.; Ascanio, J.; Machado, R.; Gonzalez, T. *J. Organomet. Chem.* **2009**, *694*, 1834 – 1839.

CHAPTER 6

Rotational Behavior of Bridging Aryl Ligands in Unsaturated Metal Carbonyl Cluster Complexes

Introduction

Dynamical NMR spectroscopy has played a key role in developing our understanding of the molecular dynamics of ligands, metal complexes, reversible isomerizations and a variety of chemical transformations including the coordination and activation of hydrogen by metal complexes.[1,2] Hindered rotation of σ-bonded aryl rings is a topic of considerable interest and importance. The rotation behavior of aryl rings is dominated by steric effects and is influenced by the size of the substituents in ortho-positions of the rings.[3] Hindered rotations of aryl rings serve as a basis for the creation of molecular propellers[3] and they impart configurational stability to chiral phosphines so that they may be used as auxiliaries for asymmetric induction in homogeneous catalysis by metal complexes.[4]

We have now discovered a new example of hindered rotation of aryl groups which involves ligands having the η^1-bridging coordination mode across two metal atoms A, see Scheme 6.1. For these ligands, the ipso carbon atom is bonded to both metal atoms and plane of the aryl ring generally lies approximately perpendicular to the vector between the two metal atoms.

Experimental Section

Compound **6.1** is compound **5.2** and compound **6.2** is compound **5.6** in chapter 5. The experimental details will not be described here.

Computational details

All density functional theory (DFT) calculations were performed using the ADF suite of programs[5] with PBEsol exchange-correlation potential,[6] TZP basis set with small frozen core (1101 Slater-type basis functions), scalar relativistic correction (ZORA),[7] and integration accuracy of "6" as defined in the ADF program. We have found this model to perform well in our previous studies of Os-Au and Ru-Ge clusters, including relative energetic of isomers, and transition state energies.[8] Intermediate and ground state structures were located by using full geometry optimization. The approximate transition states were computed as maxima of total energy along the reaction coordinate, with full geometry optimization of all other coordinates.

Results and Discussion

η^1-bridging aryl ligands are commonly found in polynuclear aryl-copper compounds.[9] There are also a number of examples of polynuclear metal carbonyl complexes containing bridging aryl ligands.[10] We have recently reported the electronically unsaturated compound $Os_3(CO)_{10}(\mu\text{-}\eta^1\text{-}C_6H_5)(\mu\text{-}AuPPh_3)$, **6.1** (See Figure 5.1 in Chapter 5) that was obtained by the oxidative addition of $PhAu(PPh_3)$ to $Os_3(CO)_{10}(NCMe)_2$.[11] We have now found that the phenyl ligand **6.1** undergoes a facile dynamical rearrangement that is tantamount to a 180^o rotation of the plane of the ring about the bridging carbon atom, see Scheme 6.2.

Due to the low molecular symmetry of **6.1**, all of the hydrogen atoms on the phenyl ring are inequivalent. ^{1}H NMR spectra of the phenyl ring protons of **6.1** at several different temperatures are shown in Figure 6.1. As the temperature is raised, the two ortho-positioned protons H_1 and H_5 (Figure 6.1A) observed as doublets due to coupling to their neighboring hydrogen nuclei H_2 and H_4, respectively, broaden and collapse into the baseline of the spectrum. Likewise, the inequivalent meta protons H_2 and H_4 (Figure 6.1B), observed as triplets, also broaden as the temperature is raised, but since the chemical shift difference between them is much smaller than that for H_1 and H_5, these two resonances actually coalesce and re-form as a broad averaged resonance at 105 ℃, the highest temperature that could be recorded in the toluene-d_8 solvent that was used. As expected, the resonance of the para proton H_3 does not undergo any changes with temperature and thus is not shown in Figure 6.1.

Computer simulations of the exchange broadened spectra (Figure 6.1C) have provided exchange rates from which we have been able to calculate the activation parameters for the exchange process: $\Delta H^{\ddagger}$ = 73.33(42) KJ/mol, $\Delta S^{\ddagger}$= -2.66(1.25) J/K•mol. Assuming that the exchange process is not dissociative, two intramolecular mechanisms for the rearrangement are readily envisaged: 1) a simple 180^o rotation of the plane of the ring about the bridging carbon atom, as shown in Scheme 6.2. This rearrangement would encounter significant steric interactions between the ortho-protons H_1 and H_5 and two pairs of carbonyl ligands on the metal atoms Os_1 and Os_2,[11] and 2) a process in which the phenyl ring shifts to a terminal position on one of the metal atoms, generating an intermediate, such as B, shown in Scheme 6.3, followed by a rotation about the Os – C bond and return to the bridging position. Although the terminal phenyl ring in **B** would be

less crowded by the ligands on the metal atom Os(1), the shift of the ring to a terminal position would require breaking one of the Os – C bonds and that would formally generate an "vacant" coordination site the neighboring metal atom, Os(2). The generation of the vacant coordination site would clearly be energetically unfavorable.

In order to establish the mechanism of the rearrangement in greater detail, DFT computational analyses were performed. We have used the PBEsol functional with TZP basis set and small frozen core, as implemented in the ADF program.[12] Intermediate and ground-state structures were located by using full geometry optimization. The approximate transition states were computed as maxima of total energy along the reaction coordinate with full geometry optimization of all other coordinates. This analysis has revealed a mechanism that can be viewed as a combination of the two mechanisms described above. As represented in Scheme 6.4, as the phenyl ring begins to twist, one of the Os−C bonds, Os(1)−C(1), weakens. Simultaneously a weak bonding interaction forms to one of the ortho-positioned carbon atoms and its hydrogen atom H(1). This process proceeds to the formation of the intermediate C, in which the Os(1)−C(1) bond has been cleaved and an agostic interaction[13] between the orthopositioned carbon atom and H(1) has formed. Intermediate C lies +9.88 kcal/mol above the ground state 1. There is a transition state TS1 that lies +13.06 kcal/mol above **6.1** on going from **6.1** to C. The HOMO-27 of C, shown in Figure 6.2, reveals a significant orbital component representing this agostic CH(1)− Os(1) bond. HOMO-27 lies at −0.313 eV, in comparison with −0.194 eV for the HOMO and −0.107 eV for the LUMO of C.

By formation of the agostic interaction in C, the "vacant" site problem anticipated in B was avoided. As the twisting process is continued, a related second agostic C−H

bonded intermediate D is formed, which lies +11.58 kcal/mol above the ground state **6.1**. An approximate transition state TS2 that lies +21.77 kcal/mol above **6.1** is traversed in going from C to D. In search of this transition state, TS2, a reaction coordinate was defined as the bond angle Au−Os(1)−H(1) and scanned between its values in C and D, with all other coordinates optimized. A significant geometry rearrangement occurs past the TS value of the reaction coordinate of 78.8 ° and results in a flip of the tilted phenyl ring from one side of the Os−Os bond to the other. The actual computational transition state is likely to be a couple of kilocalories per mole lower than the approximate value calculated here. Exact transition states are difficult to locate for two reasons. First, analytic Hessians are not available for the PBEsol functional in the current version of ADF. Second, and more important, it is difficult to define and constrain a proper reaction coordinate. Intermediate D continues to **6.1′**, which is equivalent to **6.1**, via the lower energy transition state TS3 (15.27 kcal/mol above **6.1**) to complete the exchange. In contrast, a transition state for phenyl ring rotation with both Os−C bonds held equal, i.e. without any selective Os−C bond weakening, has a computed TS energy of +56 kcal above **6.1**. The geometry optimized coordinates for C, D and TS2 are listed in table 6.1, 6.2 and 6.3 respectively.

An energy profile of the rotational transformation via the various intermediates and transition states is shown in Figure 6.3. In order to investigate these rotational transformations further, we prepared and structurally characterized the related complex $Os_3(CO)_{10}(\mu\text{-}\eta^1\text{-Py})(\mu\text{-AuPPh}_3)$ (**6.2**; Py = 2-$C_{16}H_9$) (See Figure 5.11 in Chapter 5). The ortho protons of the coordinated pyrenyl ring of **6.2** are inequivalent, just as they are in **6.1**. Their resonances appear as separate singlets in the ^{1}H NMR spectrum at room

temperature. However, at elevated temperatures these resonances are broadened in a pattern similar to that of **6.1**, which is consistent with a similar rotational exchange process (see Scheme 6.5). The variable temperature ^{1}H NMR spectra of compound **6.2** are shown in Figure 6.4. Computer simulation was also performed to determine the exchange rates at different temperatures. The activation parameters for the process in **6.2** are very similar to those for **6.1**: $\Delta H^{\ddagger}$ = 70.93(61) kJ/mol and $\Delta S^{\ddagger}$ = −6.98(1.83) J/(K mol). We believe the mechanism for pyrenyl rotation should be similar to that of phenyl.

Summary

Herein, we have described the first examples of hindered rotation of bridging aryl ligands about a metal−metal bond in polynuclear metal carbonyl complexes. Computational analyses have revealed that the twisting rearrangement involves a cleavage of one of the metal−carbon bonds to the bridging carbon atom accompanied by the formation of intermediates containing agostic interactions to one of the ortho-positioned CH bonds of the aryl ring. The rearrangement appears to be facilitated by the intrinsic electronic unsaturation in the complexes themselves.

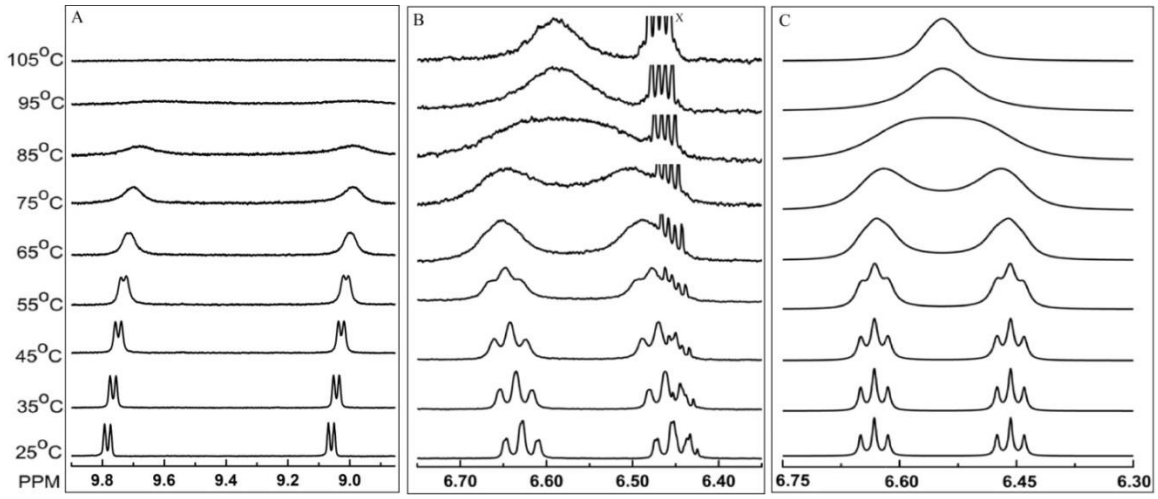

Figure 6.1. Variable temperature ^{1}H NMR spectra of **6.1** in the phenyl region of the spectrum recorded in d_8-toluene: spectra A (on left) show two doublets are room temperature corresponding to the inequivalent ortho-hydrogen atoms H_1 and H_5 of the bridging phenyl ligand; spectra B (center) show two triplets due to the inequivalent meta-hydrogen atoms H_2 and H_4, the resonances X are due to the compound $Os_3(CO)_9(\mu_3\text{-}C_6H_4)(\mu\text{-}AuPPh_3)(\mu\text{-}H)$, **6.3** (Figure 5.4 in Chapter 5) which is formed from **6.1** at elevated temperatures (See Chapter 5 for details); spectra C are simulations of the changing spectra of the triplets B at different exchange rates.

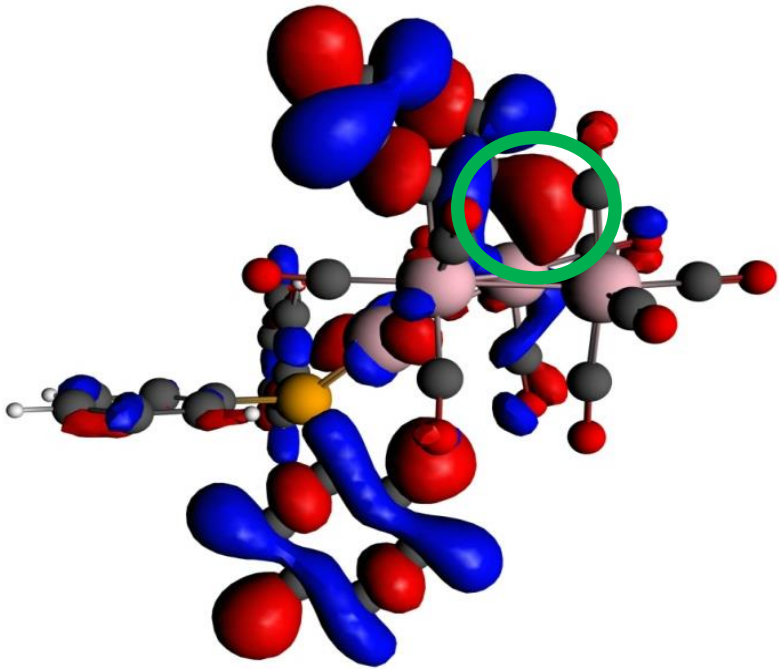

Figure 6.2. The HOMO-27 of the intermediate C.

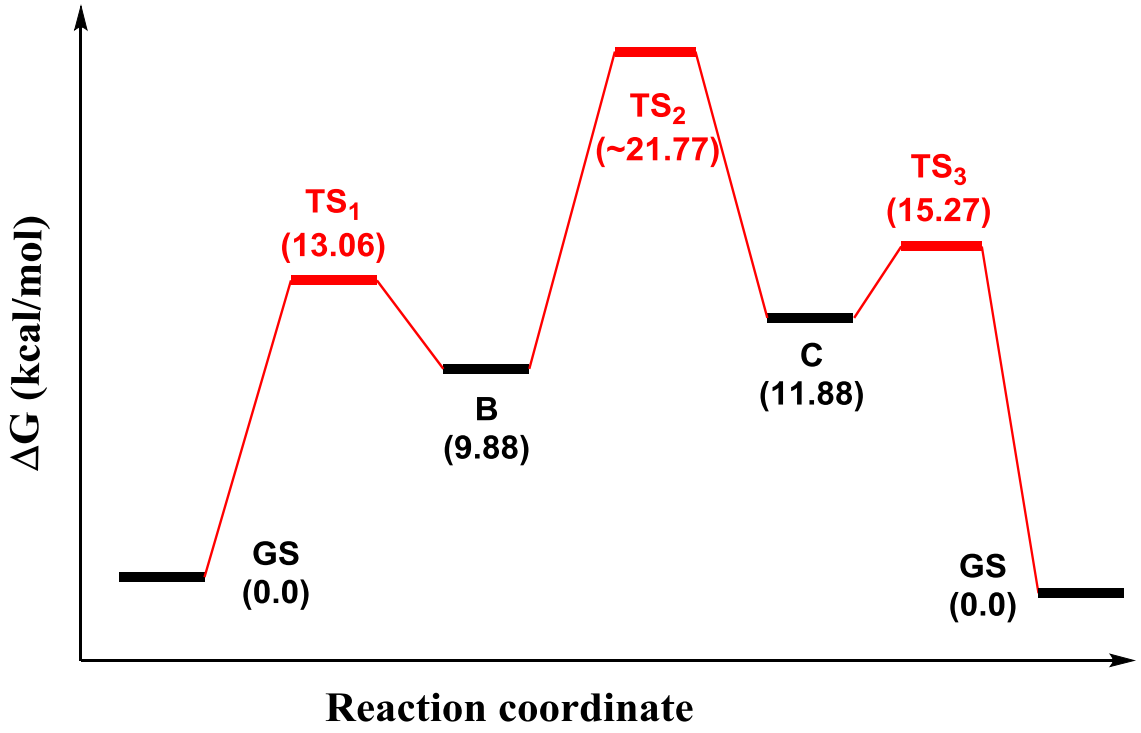

Figure 6.3. The energy profile shows energies for the two intermediates and three transition states in the pathway of phenyl rotation.

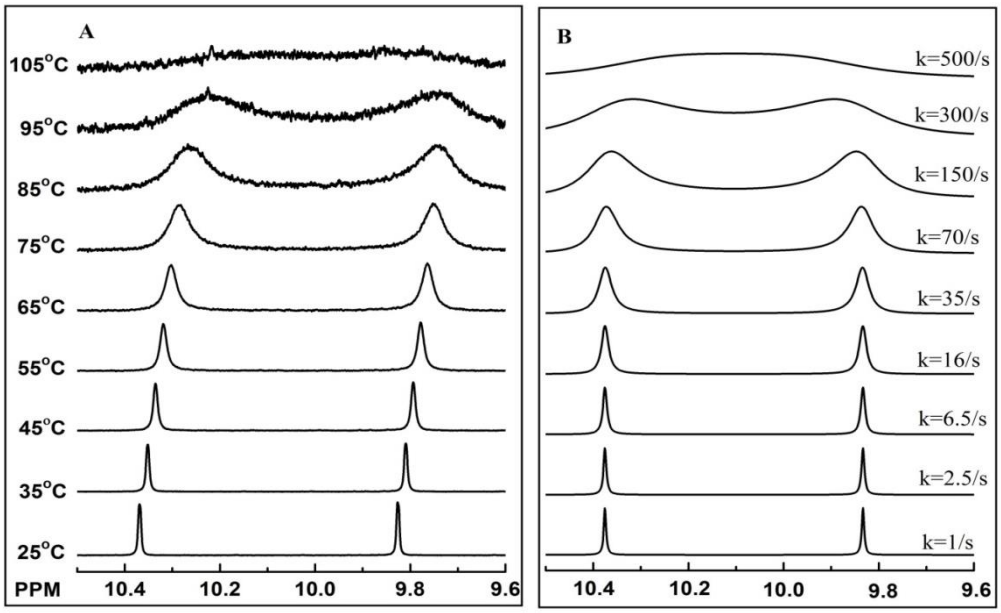

Figure 6.4. Variable temperature ^{1}H NMR spectra of **6.2** in the aromatic region of the spectrum recorded in d_8-toluene: spectra A (on left) show two singlets at room temperature corresponding to the inequivalent ortho-hydrogen atoms H_1 and H_5 of the bridging pyrenyl ligand; spectra B (on right) are simulations of the changing spectra of A at different exchange rates.

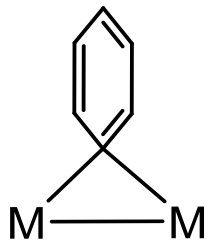

A

Scheme 6.1. η1-bridging phenyl ligand.

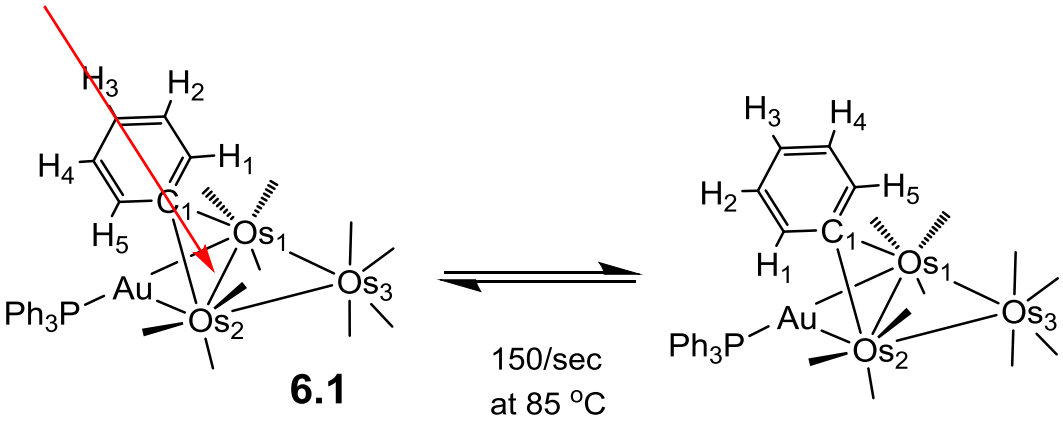

Scheme 6.2 The proposed mechanism for the phenyl rotation where the phenyl rotates along a C_2 axis.

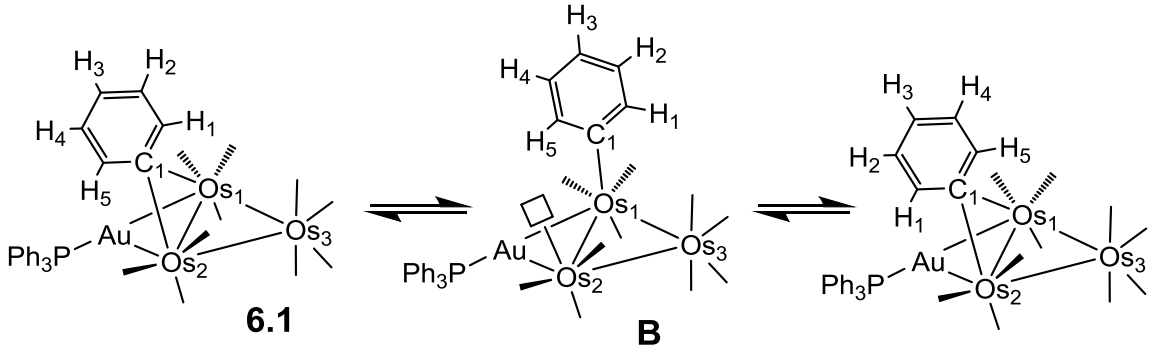

Scheme 6.3 The proposed mechanism for the phenyl rotation where the shifting of the phenyl from bridging position to terminal position is involved.

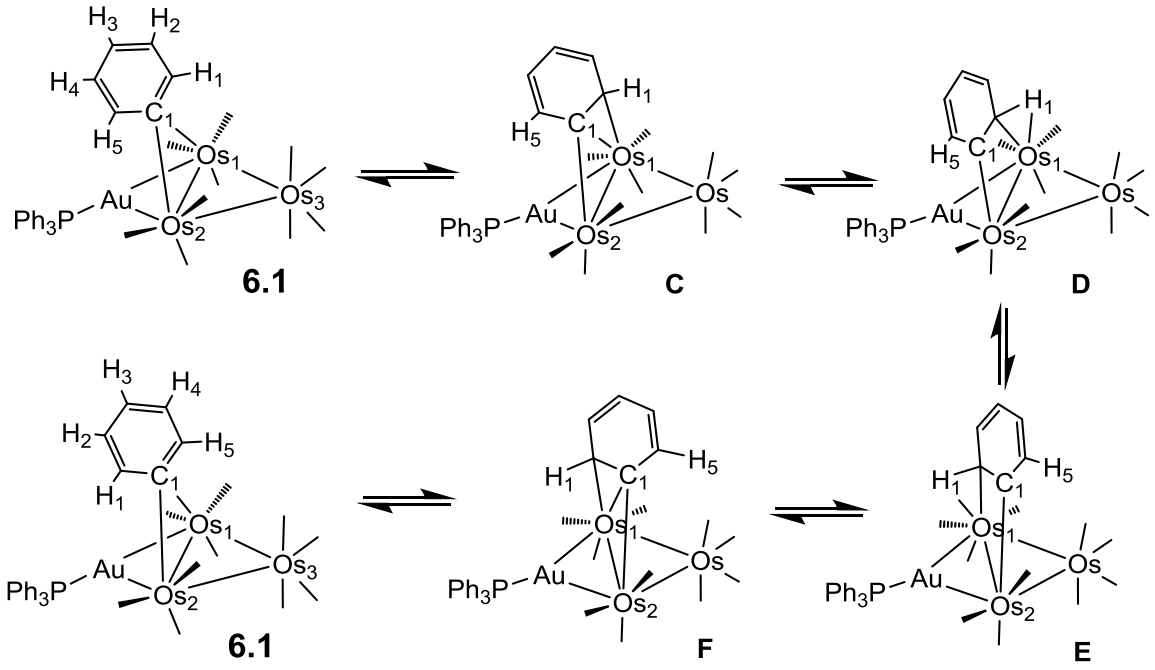

Scheme 6.4 The computed mechanism for the phenyl rotation.

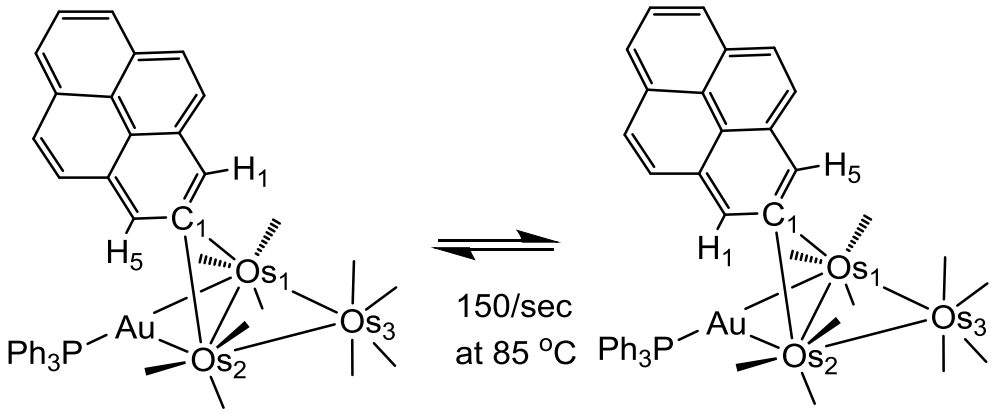

Scheme 6.5 The pyrenyl rotation in compound **6.2**.

Table 6.1 XYZ coordinates of C.

Atom	Coordinate			Atom	Coordinate		
	x	y	z		x	y	z
Au	-3.54438	-2.5466	-0.81742	O	-0.92992	-4.41617	0.706696
Os	-0.90028	-2.48989	-1.65849	O	-4.19436	0.728503	0.527635
Os	-2.59547	-0.12038	-1.94845	O	-5.06633	-0.95268	-3.49829
Os	-0.65405	-0.76312	-3.98588	O	-2.74317	2.630794	-3.26669
P	-5.34601	-3.74176	0.036829	O	1.763526	0.465132	-2.4779
C	-0.35001	-0.98656	-0.24132	O	-0.91299	1.624315	-5.88714
C	-0.75517	0.33395	-0.493	O	1.301925	-2.42169	-5.66037
H	-0.80502	0.653995	-1.58303	O	-3.04486	-2.25247	-5.27012
C	-0.63957	1.386695	0.430247	H	-6.02186	-2.84056	-2.63382
H	-0.97359	2.394676	0.161804	H	-4.80709	-1.65551	1.954038
C	-0.05094	1.130602	1.656166	C	-6.42017	-4.45915	-1.25304
C	0.390731	-0.1697	1.938182	C	-7.09243	-5.67052	-1.05262
C	0.231079	-1.20552	1.023003	C	-7.90481	-6.18846	-2.05893
H	0.568663	-2.20826	1.3073	C	-8.04699	-5.50492	-3.26623
C	-7.37665	-4.29897	-3.46849	C	-6.45944	-2.76546	1.103182
C	-6.56218	-3.77754	-2.46711	C	-7.84659	-2.94325	1.083401
H	-6.96516	-6.2168	-0.11147	C	-8.65723	-2.17748	1.919248
H	0.08424	1.933271	2.387166	C	-8.08873	-1.23605	2.775772
H	0.868218	-0.37658	2.902119	C	-6.70534	-1.05552	2.795768
H	-8.42151	-7.14023	-1.90127	C	-5.89177	-1.81263	1.958236
H	-8.67542	-5.92186	-4.05996	H	-8.29296	-3.67545	0.401678
H	-7.47412	-3.76495	-4.41856	H	-9.74284	-2.31348	1.892715
C	0.92051	-2.85531	-2.01267	H	-8.72917	-0.62946	3.424318
C	-1.62721	-3.80972	-2.88019	H	-6.25644	-0.30724	3.45573
C	-0.99994	-3.65396	-0.17063	C	-4.88072	-5.17913	1.063445
C	-3.60325	0.331617	-0.38799	C	-5.54405	-5.48198	2.256647
C	-4.09426	-0.70442	-2.90807	C	-5.16719	-6.60182	2.996496
C	-2.63948	1.589717	-2.765	C	-4.13147	-7.42009	2.54931
C	0.826263	0.013922	-2.9804	C	-3.46791	-7.11905	1.359112
C	-0.83438	0.723347	-5.16233	C	-3.83704	-6.00035	0.619493
C	0.573566	-1.79651	-5.01294	H	-6.3532	-4.83389	2.610857
C	-2.18004	-1.69833	-4.73888	H	-5.68527	-6.83076	3.932917
H	-3.30688	-5.75305	-0.30699	H	-3.83173	-8.29401	3.136734
O	2.040007	-3.11041	-2.18177	H	-2.64612	-7.75204	1.011183
O	-2.01859	-4.66807	-3.55371				

Table 6.2 XYZ coordinates of D.

Atom	Coordinate			Atom	Coordinate		
	x	y	z		x	y	z
Au	1.515526	-1.00778	-2.17089	O	-0.97193	-3.42592	-3.06389
Os	0.399366	-2.90761	-0.38706	O	1.282522	2.395298	-1.24901
Os	0.967145	-0.15671	0.405381	O	3.974258	-0.23619	0.79897
Os	1.143807	-2.34136	2.349515	O	0.445121	1.527261	2.910569
P	2.344371	-0.70844	-4.32849	O	-1.61807	-1.30466	3.311503
C	-1.42104	-1.92586	0.136036	O	2.406373	-0.90954	4.746048
C	-1.39885	-0.5197	0.09341	O	0.628135	-5.0276	3.715533
H	-0.70872	-0.05093	-0.67622	O	3.945727	-3.27397	1.423896
C	-2.46567	0.290903	0.514752	H	2.124662	2.027768	-3.41701
H	-2.388	1.381492	0.451007	H	-0.31418	-1.82962	-4.61263
C	-3.6299	-0.31713	0.955106	C	3.448286	0.732862	-4.54163
C	-3.70406	-1.71575	0.964872	C	4.656084	0.642033	-5.24038
C	-2.62457	-2.50455	0.57706	C	5.464716	1.769091	-5.38088
H	-2.72468	-3.59439	0.634057	C	5.072345	2.98672	-4.82853
C	3.866732	3.079508	-4.13166	C	1.054315	-0.46737	-5.59762
C	3.058663	1.956792	-3.98332	C	1.249334	0.390139	-6.68613
H	4.968343	-0.31656	-5.66868	C	0.244518	0.542555	-7.63939
H	-4.48584	0.285081	1.273644	C	-0.95446	-0.15744	-7.5113
H	-4.62881	-2.2003	1.29657	C	-1.15051	-1.01307	-6.42714
H	6.412706	1.689596	-5.92183	C	-0.15261	-1.16599	-5.46871
H	5.714161	3.86754	-4.93271	H	2.186842	0.949272	-6.77909
H	3.558386	4.030245	-3.68625	H	0.399053	1.220131	-8.48479
C	-0.26486	-4.49305	0.377931	H	-1.74549	-0.02868	-8.25726
C	2.107219	-3.6838	-0.89056	H	-2.09264	-1.55887	-6.31781
C	-0.39989	-3.17003	-2.08134	C	3.335754	-2.12077	-4.92157
C	1.114362	1.365001	-0.72768	C	3.310099	-2.53267	-6.25803
C	2.821725	-0.26032	0.667695	C	4.092073	-3.61118	-6.66665
C	0.63413	0.854852	1.986361	C	4.898988	-4.27986	-5.74688
C	-0.63372	-1.69184	2.850375	C	4.924958	-3.87139	-4.41334
C	1.911655	-1.42705	3.835293	C	4.142921	-2.79725	-3.99939
C	0.835055	-4.02311	3.176953	H	2.666157	-2.01413	-6.97678
C	2.883855	-2.91228	1.702619	H	4.062026	-3.93652	-7.71112
H	4.143925	-2.48946	-2.94793	H	5.502974	-5.13434	-6.069
O	-0.70574	-5.48425	0.795134	H	5.543476	-4.40309	-3.68423
O	3.070256	-4.22305	-1.24747				

Table 6.3 XYZ coordinates of TS2.

Atom	Coordinate			Atom	Coordinate		
	x	y	z		x	y	z
Au	-3.54438	-2.5466	-0.81742	O	-2.33788	-3.05165	2.30993
Os	-0.85881	-1.92518	-0.11377	O	-4.60838	-1.81343	-4.09046
Os	-1.84465	-1.58905	-2.79943	O	-1.11973	-4.39919	-3.63278
Os	0.78812	-0.63476	-2.13285	O	-0.97652	-0.21622	-5.39572
P	-5.34601	-3.74176	0.036829	O	-0.39949	2.0385	-1.09834
C	-2.16006	-0.23727	0.114017	O	1.92211	0.759224	-4.61376
C	-2.8873	0.191793	-1.00197	O	3.30746	-0.2779	-0.43455
H	-2.51612	0.037318	-2.06867	O	1.74992	-3.40832	-3.12666
C	-3.96504	1.07646	-0.97074	H	-6.02186	-2.84056	-2.63382
H	-4.4959	1.34729	-1.88946	H	-4.80709	-1.65551	1.95404
C	-4.31256	1.63538	0.257133	C	-6.42017	-4.45915	-1.25304
C	-3.58903	1.28201	1.39789	C	-7.09243	-5.67052	-1.05262
C	-2.55084	0.352895	1.32997	C	-7.90481	-6.18846	-2.05893
H	-2.03151	0.071797	2.25448	C	-8.04699	-5.50492	-3.26623
C	-7.37665	-4.29897	-3.46849	C	-6.45944	-2.76546	1.10318
C	-6.56218	-3.77754	-2.46711	C	-7.84659	-2.94325	1.0834
H	-6.96516	-6.2168	-0.11147	C	-8.65723	-2.17748	1.91925
H	-5.13416	2.35559	0.316421	C	-8.08873	-1.23605	2.77577
H	-3.84332	1.73553	2.36212	C	-6.70534	-1.05552	2.79577
H	-8.42151	-7.14023	-1.90127	C	-5.89177	-1.81263	1.95824
H	-8.67542	-5.92186	-4.05996	H	-8.29296	-3.67545	0.401678
H	-7.47412	-3.76495	-4.41856	H	-9.74284	-2.31348	1.89271
C	0.402654	-1.1842	1.0689	H	-8.72917	-0.62946	3.42432
C	0.027413	-3.61144	-0.45775	H	-6.25644	-0.30725	3.45573
C	-1.87163	-2.67058	1.31213	C	-4.88072	-5.17912	1.06344
C	-3.6114	-1.80402	-3.48496	C	-5.54405	-5.48198	2.25665
C	-1.36879	-3.31759	-3.29133	C	-5.16719	-6.60181	2.9965
C	-1.23408	-0.68973	-4.36764	C	-4.13147	-7.42009	2.54931
C	-0.01771	1.01092	-1.46012	C	-3.46791	-7.11905	1.35911
C	1.47348	0.220914	-3.69105	C	-3.83704	-6.00035	0.619493
C	2.34052	-0.41227	-1.05704	H	-6.3532	-4.83389	2.61086
C	1.35199	-2.39567	-2.73663	H	-5.68527	-6.83076	3.93292
H	-3.30688	-5.75305	-0.30699	H	-3.83173	-8.29401	3.13673
O	1.13323	-0.73072	1.85054	H	-2.64612	-7.75204	1.01118
O	0.509861	-4.65801	-0.58265				

REFERENCE

1. (a) Pregosin, P. S., *NMR in Organometallic Chemistry*, Wiley-VCH, Weinheim, **2012**, Ch. 8. (b) *Dynamic NMR Spectroscopy*, Jackman, L. M.; Cotton, F. A., Eds., Academic Press, New York, **1975**. (c) Pregosin, P. S.; Trabesinger, G. *Dalton Trans*., **1998**, 727 – 734.

2. Kubas, G. J. *Metal Dihydrogen and σ–Bond Complexes*, Kluwer Academic/Plenum Publisher, **2001**, Ch. 6.

3. (a) Brydges, S.; Harrington, L. E.; McGlinchey, M. J. *Coord. Chem. Rev.* **2002**, *233-234*, 75 – 105. (b) Mislow, K. *Accts. Chem. Res.* **1976**, *9*, 26 – 33.

4. Hayashi, T. *Acc. Chem. Res.* **2000**, *33*, 354 – 362.

5. (a) te Velde, G.; Bickelhaupt, F.M.; van Gisbergen, S.J.A.; Fonseca Guerra, C; Baerends, E.J.; Snijders J.G.; Ziegler, T. *J. of Comp. Chem*. **2001**, *22*, 931 – 967. (b) Fonseca Guerra, C.; Snijders, J.G.; te Velde, G.; Baerends, E.J. *Theo. Chem. Acc*. **1998**, *99*, 391 – 403. (c) ADF2012, SCM, Theoretical Chemistry, Vrije Universiteit, Amsterdam, The Netherlands, http://www.scm.com

6. Perdew, J.P.; Ruzsinszky, A.; Csonka, G.I.; Vydrov, O.A.; Scuseria, G.E. *Phys. Rev. Lett.* **2008**, *100*, 136406

7. van Lenthe, E.; Baerends, E.J.; Snijders, J.G. *J. Chem. Phys.* **1994**, *101*, 9783 – 9792.

8. Adams, R. D.; Rassolov, V.; Zhang, Q. *Organometallics* **2012**, *31*, 2961 − 2964.

9. (a) van Koten, G. *J. Organomet. Chem.* **1990**, *400*, 283 − 301 and references therein. (b) Eriksson, H.; Hakansson, M. *Organometallics* **1997**, *16*, 4243 – 4244. (c) He, X.; Ruhlandt-Senge, K.; Power, P.P. *J. Am. Chem. Soc.* **1994**, *116*, 6963 – 6964. (d) (b) Meyer, E. M.; Gambarotta, S.; Floriani, C.; Chiesi-Villa, A.; Guastini, C. *Organometallics*, **1989**, *8*, 1067 – 1079.

10. Bridging phenyls (a) Bradford, C. W.; Nyholm, R. S.; Gainsford, G. J.; Guss, J. M.; Ireland, P. R.; Mason, R. *J. Chem. Soc., Chem. Commun.* **1972**, 87 − 89. (b) Arce, A. J.; Arrojo, P.; Deeming, A. J.; De Sanctis, Y. *J. Chem. Soc., Chem. Commun.* **1991**, 1491 − 1492. (c) Adams, R. D.; Captain, B.; Zhu, L. *Inorg. Chem.* **2007**, *46*, 4605 − 4611. (d) Deng, M.; Leong, W. K. *Dalton Trans.* **2002**, 1020 − 1023. (e) Adams, R. D.; Pearl, W. C., Jr *J. Organomet. Chem.* **2011**, *696*, 1198 − 1210. (f) Garcia, M. E.; Ramos, A.; Ruiz, M. A.; Lanfranchi, M.; Marchio, L. *Organometallics* **2007**, *26*, 6197 − 6212. (g) Briard, P.; Cabeza, J. A.; Llamazares, A.; Ouahab, L.; Riera, V. *Organometallics* **1993**, *12*, 1006 − 1008. (h) Cabeza, J. A.; Franco, R. J.; Llamazares, A.; Riera, V. *Organometallics* **1994**, *13*, 55 − 59.

11. Adams, R. D.; Rassolov, V.; Zhang, Q. *Organometallics* **2012**, *31*, 2961 − 2964.

12. (a) te Velde, G.; Bickelhaupt, F. M.; van Gisbergen, S. J. A.; Fonseca Guerra, C.; Baerends, E. J.; Snijders, J. G.; Ziegler, T. *J. Comput. Chem.* **2001**, 22, 931 − 967. (b) Fonseca Guerra, C.; Snijders, J. G.; te Velde, G.; Baerends, E. J. *Theor. Chem. Acc.* **1998**, *99*, 391 − 403. (c) ADF2012; SCM, Theoretical Chemistry, Vrije Universiteit, Amsterdam, The Netherlands, 2012; http://www.scm.com. (d) Perdew, J. P.; Ruzsinszky, A.; Csonka, G. I.; Vydrov, O. A.; Scuseria, G. E. *Phys. Rev. Lett.* **2008**, *100*, 136406.

13. (a) Brookhart, M.; Green, M. H. L.; Wong, L.-L. *Prog. Inorg. Chem.* **1988**, *36*, 1. (b) Crabtree, R. H. *Angew. Chem. int. Ed.* **1993**, *32*, 789 − 805.

CUMULATIVE REFERENCS

F. A. Cotton, *Acc. Chem. Res.* **1969**, *2*, 240 − 247.

Dewar, J.; Jones, H. O. *Proc. Roy. Soc.* (London), **1905**, *A76*, 558 – 577.

Dewar, J.; Jones, H. O. *Proc. Roy. Soc.* (London), **1907**, *A79*, 66 − 80.

Wei, C. H.; Dahl, L. F. *J. Am. Chem. Soc.* **1966**, *88*, 1821 − 1822.

Wei, C. H.; Dahl, L. F. *J. Am. Chem. Soc.* **1969**, *91*, 1351 − 1361.

Corey, E. R.; Dahl, L. F. *J. Am. Chem. Soc.* **1961**, *83*, 2203 − 2204.

Chini, P.; Albano, V.; Martinengo, S. *J. Organomet. Chem.* **1969**, *16*, 471 − 477.

Cotton, F. A.; Wilkinson, G.; Murillo, C. A.; Bochmann, M. *Advanced Inorganic Chemistry*, six ed., Wiley, New York, **1999**.

Li, P.; Curtis, M. D. *J. Am. Chem. Soc.* **1989**, *111*, 8279 − 8280.

Adams, R. D.; Captain, B.; Pellechia, P. J.; Smith, J. L. Jr. *Inorg. Chem.* **2004**, *43*, 2695 − 2702.

Niibayashi, S.; Mitsui, K.; Matsubara, K.; Nagashima, H. *Organometallics* **2003**, *22*, 4885 − 4892.

Stutte, B.; Batzel, V.; Boese, R.; Schmid, G. *Chem. Ber.* **1978**, *111*, 1603 − 1618.

Schmid, G.; Stutte, B.; Boese, R. *Chem. Ber.* **1978**, *111*, 1239 − 1245.

Gambarotta, S.; Stella, S.; Floriani, C.; Chiesi-Villa, A.; Guastini, C. *Angew. Chem., int. Ed.* **1986**, *25*, 254 − 255.

Fachinetti, G.; Fochi, G.; Funaioli, T.; Zanazzi, P. F. *Angew. Chem., int. Ed.* **1987**, *26*, 680 − 681.

Field, J. S.; Haines, R. J.; Jay, J. A. *J. Organomet. Chem.* **1989**, *377*, C35 − C39.

Adams, R. D.; Li, Z.; Lii, J.-C.; Wu, W. *Organometallics* **1992**, *11*,4001 – 4009.

Adams, R. D.; Babin, J. E.; Tasi, M. *Inorg. Chem.* **1988**, *27*, 2618 − 2625.

Cabeza, J. A.; del Rio, I.; Miguel, D.; Pérez-Carreno, E.; Sánchez-Vega, M. G. *Dalton Trans.* **2008**, 1937 − 1942.

Yun, C.; Su, C. J.; Tseng, W. C.; Peng, S. M.; Lee, G. H. *J. Cluster Sci.* **1997**, *8*, 507 − 519.

Yun, C.; Su, C. J.; Peng, S. M.; Lee, G. H. *J. Am. Chem. Soc.* **1997**, *119*, 11114 − 11115.

Su, P. C.; Chi, Y.; Su, C. J.; Peng, S. M.; Lee, G. H. *Organometallics* **1997**, *16*, 1870 − 1874.

Adams, R. D.; Alexander, M. S.; Arafa, I.; Wu, W. *Inorg. Chem.* **1991**, *30*, 4717 − 4723.

Gibson, C. P.; Dahl, L. F. *Organometallics* **1988**, *7*, 535 − 543.

Chi, Y.; Chuang, S. H.; Liu, L. K.; Wen, Y. S. *Organometallics* **1991**, *10*, 2485 − 2492.

Notaras, E. G. A.; Lucas, N. T.; Humphrey, M. G. *J. Organomet. Chem.* **2001**, *631*, 139 − 142.

Nahar, S.; Davies, J. E.; Shields, G. P.; Raithby, P. R. *J. Cluster Sci.* **2010**, *21*, 379 − 396.

Femoni, C.; Iapalucci, M.C.; Longoni, G.; Zacchini, S. *Dalton Trans.* **2011**, *40*, 8685 − 8694.

Horwitz, C. P., Holt, E. M.; Brock, C. P.; Shriver, D. F. *J. Am. Chem. Soc.* **1985**, *107*, 8136 − 8146.

Bailey, P. J.; Duer, M. J.; Johnson, B. F. G.; Lewis, J.; Conole, G.; McPartlin, M.; Powell, H. R.; Anson, C. E. *J. Organomet. Chem.***1990**, *383*, 441 − 461.

Brun, P.; Dawkins, G. M.; Green, M.; Miles, A. D.; Orpen, A. G.; Stone, F. G. A. *Chem. Commun.***1982**, 926 − 927.

Johnson, B. F. G.; Lewis, J.; McPartlin, M.; Pearsall, M. -A.; Sironi, A. *Chem. Commun.* **1984**, 1089 − 1090.

Leung, K. S. -Y. *Inorg. Chem. Commun.* **1999**, *2*, 498 − 502.

Leung, K. S. -Y.; Wong, W. T. *J. Chem. Soc., Dalton Trans.* **1997**, 4357 − 4360.

Chisholm, M. H.; Folting, K.; Hampden-Smith, M. J.; Hammond, C. E. *J. Am. Chem. Soc.* **1989**, *111*, 7283 − 7285.

Herrmann, W. A.; Ziegler, M. L.; Windenhammer, K.; Biersack, H. *Angew. Chem., int. Ed. Engl.*, **1979**, *18*, 960 − 962.

Herrmann, W. A.; Biersack, H.; Ziegler, M. L.; Windenhammer, K.; Siegel, R.; Rehder, D. *J. Am. Chem. Soc.* **1981**, *103*, 1692 − 1699.

Bailey, P. J.; Johnson, B. F. G.; Lewis, J. *Inorg. Chim. Acta* **1994**, *227*, 197 − 200.

Martin, C. M.; Dyson, P. J.; Ingham, S. L.; Johnson; B. F. G.; Blake, A. J. *J. Chem. Soc., Dalton Trans.* **1995**, 2741 − 2748.

Anson, C. E.; Bailey, P. J.; Conole, G.; Johnson, B. F. G.; Lewis, J.; McPartlin, M.; Powell, H. R. *J. Chem. Soc., Chem. Commun*., **1989**, 442 − 444.

Shriver, D. F.; Sailor, M. J. *Acc. Chem. Res.* **1988**, *21*, 374 − 379.

Bernhardt, E.; Bley, B.; Wartchow, R.; Willner, H.; Bill, E.; Kuhn, P.; Sham, I. H. T.; Bodenbinder, M.; Bröchler, R.; Aubke, F. *J. Am. Chem. Soc.* **1999**, *121*, 7188 − 7200.

Johnson, B. F. G. *J. Organornet. Chem.* **1994**, *475*, 31 − 43.

Gallop, M. A.; Gomez-Sal, M. P.; Housecroft, C. E.; Johnson, B. F. G.; Lewis, J.; Owen, S. M.; Raithby, P. R.; Wright, A. H. *J. Am. Chem. Soc.*, **1992**, *114* , 2502 − 2509.

Johnson, B. F. J.; Lewis, J.; Martinelli, M.; Wright, A. H.; Braga, D.; Grepioni, F. *J. Chem. Soc., Chem. Commun.*, **1990**, 364 − 366.

Edwards, A. J.; Gallop, M. A.; Johnson, B. F. G.; Köhler, J. U.; Lewis, J.; Raithby, P. R. *Angew. Chem. Int. Ed. Eng.* **1994**, *33*, 1093 − 1094.

Edwards, A. J.; Leadbeater, N. E.; Lewis, J; Raithby, P. R. *J. Chem. Soc., Dalton Trans.***1995**, 3785 − 3787.

Inagaki, A.; Takaya, Y.; Takemori, T.; Suzaki, H. *J. Am. Chem. Soc.* **1997**, *119*, 625 − 626.

Taylor, N. J.; Chieh, P. C.; Carty, A. J. *J. Chem. Soc., Chem. Commun.*, **1975**, 448 − 449.

Cotton, F. A.; Millar, M. *J. Am. Chem. Soc.*, **1977**, *99*, 7886 − 7891.

Cotton, F. A.; Lewis, G. E.; Mott, G. N. *Inorg. Chem.*, **1983**, *22*, 560 − 561.

Adams, R. D.; Chen, M.; Elpitiya, G.; Yang, X.; Zhang, Q. *Organometallics*, **2013**, 2416 − 2426.

Arce, A. J.; Arrojo, P.; Deeming, A. J.; De Sanctis, Y. *J. Chem. Soc., Chem. Commun.*, **1991**,1491 − 1492.

Hoferkamp, L. A.; Rheinwald, G.; Stoeckli-Evans, H.; Süss-Fink, G. *Organometallics*, **1996**, *15*, 704 − 712.

Adams, R. D.; Kan, Y.; Zhang, Q. *Organometallics*, **2011**, *30*, 328 − 333.

Kabir, S. E.; Rosenberg, E.; Stetson, J.; Yin, M. *Organometallics*, **1996**, *15*, 4473 − 4479.

Al-Mandhary Muna, R. A.; Lewis, J.; Raithby, P. R. *J. Organomet. Chem.* **1997**, *530*, 247 − 250.

McLain, S. J.; Schrock, R. R.; Sharp, P. R.; Churchill, M. R.; Youngs, M. J. *J. Am. Chem. Soc.* **1979**, *101*,263 − 265.

Buchwald, S. L.; Watson, B. T.; Huffman, J. C.; *J. Am. Chem. Soc.*, **1986**, *108*, 7411 − 7413.

Arnold, J.; Wilkinson, G.; Hussain, B.; Hursthouse, M. B. *Organometallics*, **1989**, *8*, 415 − 420.

Bennett, M. A.; Drage, J. S.; Griffiths, K. D.; Roberts, N. K.; Robertson, G. B.; Wickramasinghe, W. A. *Angew. Chem. Int. Ed. Eng.*, **1988**, *27*, 941 − 942.

Tinga, M. A. G. M.; Akkerman, O. S.; Bickelhaupt, F.; Horn, E.; Spek, A. L. *J. Am. Chem. Soc.*, **1991**, *113*, 3604 − 3605.

Dam, M. A.; Nijbacker, T.; de Pater, B. C.; de Kanter, F. J. J.; Akkerman, O. S.; Bickelhaupt, F.;Smeets, W. J. J.; Spek, A. L. *Organometallics*, **1991**, *16*, 511 − 512.

McGhee, W. D.; Foo, T.; Hollander, F. G.; Bergman, R. G. *J. Am. Chem. Soc.*, **1988**, *110*, 8543 − 8545.

Adams, R. D.; Pearl, W. C. Jr. *Inorg. Chem.*, **2010**, *49*, 7170 − 7175.

Deeming, A. J.; Underhill, M. *J. Chem. Soc. Dalton Trans.*, **1974**, 1415 − 1419.

Gainsford, G. J.; Guss, J. M.; Ircland, P. R.; Mason, R.; Bradford, C. W.; Nyholm, R. S. *J. Organomet. Chem.* **1972**, *40*, C70 − C72.

Goudsmit, R. J.; Johnson, B. F. J.; Lewis, J.; Raithby, P. R.; Rosales, M. J. *J. Chem. Soc., Dalton Trans.*, **1983**, 2257 − 2261.

Gallop, M. A.; Johnson, B. F. G.; Lewis, J.; McCamley, A.; Perutz, R. N. *J. Chem. Soc., Chem. Commun.*, **1988**, 1071 − 1073.

Johnson, B. F. G.; Nairn, J. G. M.; Brown, D. B.; Lewis, J.; Gallop, M.; Parker, D. G. *Chem. Eur. J.*, **1995**, *1*, 252 − 260.

Bruce, M. I.; Humphrey, P. A.; Snow, M. R.; Tiekink, E. R. T.; Cullen, W. R. *Organometallics*, **1990**, *9*,2910 − 2919.

Zheng, T.; Cullen, W. R.; Rettig, S. J. *Organometallics*, **1994**, *13*, 3594 − 3604.

Knox, S. A. R.; Lloyd, B. R.; Orpen, A. G.; Vifias, I. M.; Weber, M. *J. Chem. Soc. Chem. Commum.***1987**, 1498 − 1500.

Knox, S. A. R.; Lloyd, B. R.; Morton, D. A. V.; Nicholls, S. M.; Orpen, A. G.; Viñas, J. M.; Weber, M.; Willaims, G. K. *J. Organomet. Chem.***1990**, *394*, 385 − 415.

Cullen, W. R.; Rettig, S. J.; Zheng, T. C. *Organometallics* **1995**, *14*, 1466 − 1470.

Deeming, A. J.; Speel, D. M. *Organometallics* **1997**, *16*, 289 − 291.

Cotton, F. A. *Inorg. Chem.***1966**, *5*, 1083 − 1085.

Adams, H.; Bailey, N. A.; Bentley, G. W.; Mann, B. E. *J. Chem. Soc., Dalton Trans.* **1989**, 1831 − 1844.

Johnson, B. F. G.; Bott, A. *J. Chem. Soc., Dalton Trans.* **1990**, 2437 − 2444.

Dorn, H. C.; Hanson, B. E.; Motell, E. *Inorg. Chim. Acta*, **1981**, *54*, L71 – L73;

Hanson, B. E.; Lisic, E. C.; Petty, J. T.; Iannaconne, G. A. *Inorg. Chem.* **1986**, *25*, 4062 − 4064;

Gleeson, G. W.; Vaughan, R. W. *J. Chem. Phys.***1983**, *78*, 5384 − 5392.

Lentz, D.;Marschall, R. *Organometallics* **1991**, *10*, 1487 − 1496.

Mann, B. E. *J. Chem. Soc., Dalton Trans*. **1997**, 1457 − 1471.

Aime, S.; Dastrù, W.; Gobetto, R.; Krause, J.; Milone, L. *Organometallics* **1996**, *14*, 4435 − 4438.

Forstebr, A.; Johnson, I. G.; Lewis, J.; Matheson, T. R.; Robinson, B. H.; Jackson, W. *J. Chem. Soc. Chem. Commun.*, **1974**, 1042 − 1044.

Hyder, M. I.; Begum, N.; Sikder, M. D. H.; Hossain, G. M. G.; Hogarth, G.; Kabir, S. E.; Richard, C. J. *J. Organomet. Chem.*, **2009**, *694*, 304 − 308.

Musaev, D. G.; Nowroozi-Isfahani, T.; Morokuna, K. *Organometallics*, **2006**, *25*, 203 − 213.

Adams, R. D.; Kan, Y.; Zhang, Q. *Organometallics* **2012**, *31*, 8639 − 8646.

Adams, R. D.; Chen, M.; Elpitiya, G.; Zhang, Q. *Organometallics* **2012**, *31*, 7264 − 7271.

Kneuper, H.-J.; Shapley, J. R. *Organometallics* **1987**, *6*, 2455 − 2456.

Adams, R. D.; Cotton, F. A. *J. Am. Chem. Soc.* **1970**, *92*, 5003 − 5004.

Adams, R. D.; Captain, B.; Fu, W.; Pellechia, P. J. *Inorg. Chem.* **2003**, *42*, 3111 − 3118.

Adams, R. D.; Captain, B.; Fu, W.; Pellechia, P. J. *Chem. Commun.*, **2000**, 937 − 938.

Adams, R. D.; Cotton, F. A.; Cullen, W. R.; Hunter, D. L. *Inorg. Chem.* **1975**, *14*, 1395 − 1399.

Adams, R. D.; Captain, B.; Fu, W.; Pellechia, P. J.; Smith, M. D. *Inorg. Chem.*, **2003**, *42*, 2094 − 2101.

Adams, R. D.; Captain, B.; Pellechia, P. J.; Smith, J. L. Jr. *Inorg. Chem.*, **2004**, *43*, 2695 − 2702.

Adams, R. D.; Captain, B.; Fu, W.; Pellechia, P. J.; Smith, M. D. *Angew. Chem. Int. Ed.* **2002**, *41*, 1951 − 1953.

Brown, S. D. S.; Salter, I. D. *J. Chem. Soc. Dalton Trans.* **1988**, 1795 − 1801.

Collins, C. A.; Salter, I. D., Šik, V.; Williams, S. A.; Adatia, T. *J. Chem. Soc., Dalton Trans.*, **1998**, 1107 − 1114.

Salter, I. D.; Šik, V.; Williams, S. A.; Adatia, T. *J. Chem. Soc., Dalton Trans.*, **1996**, 643 − 652.

Brown, S. D. S.; Salter, I. D. *J. Chem. Soc. Dalton Trans.* **1989**, 1227 − 1236.

Muetterties, E. L.; Rhodin, T. N.; Band, E.; Brucker, C. F.; Retzer, W. R. *Chem. Rev.* **1979**, *79*, 91 − 137.

Muetterties, E. L. *Bull. Soc. Chim. Belg.* **1976**, *85*, 451 − 470.

Muetterties, E. L. *Bull Soc. Chim. Belg.* **1975**, *84*, 959 − 968.

Brady, R. C. III; Pettit, R. *J. Am. Chem. Soc.* **1981**, *103*, 1287 − 1289.

Churchill, M. R.; Wasserman, H. J. *Inorg. Chem.* **1982**, *21*, 825 − 827.

Steinmetz, G. R.; Geoffroy, G. L. *J. Am. Chem. Soc.* **1981**, *103*, 1278 − 1279.

Adams, R. D.; Babin, J. E.; Kim, H.-S. *J. Am. Chem. Soc.* **1987**, *109*, 1414 − 1424.

Adams, R. D.; Babin, J. E. *Organometallics* **1987**, *6*, 2236 − 2241.

Adams, R. D.; Babin, J. E. *Organometallics* **1988**, *7*, 963 − 969.

Adams, R. D.; Babin, J. E. *Organometallics* **1988**, *7*, 2300 − 2306.

Adams, R. D.; Babin, J. E.; Kim, H.-S.; Tanner, J. T.; Wofe, T. A. *J. Am. Chem. Soc.* **1990**, *112*, 3426 − 3435.

Adams, R. D.; Chen, G.; Tanner, J. T.; Yin, J. *Organometallics* **1990**, *9*, 1523 − 1529.

Adams, R. D.; Chen, G.; Tanner, J. T. *Organometallics* **1990**, *9*, 1530 − 1538.

Adams, R. D.; Pompeo, M. P.; Tanner, J. T. *Organometallics* **1991**, *10*, 1068 − 1078.

Adams, R. D.; Chen, G. *Organometallics* **1991**, *10*, 3020 − 3027.

Adams, R. D.; Chen, G. *Organometallics* **1991**, *10*, 3028 − 3035.

Adams, R. D.; Chen, G. *Organometallics* **1992**, *11*, 837 − 845.

Adams, R. D.; Babin, J. E.; Kim, H.-S. *Inorg. Chem.* **1986**, *25*, 4319 − 4320.

Adams, R. D.; Babin, J. E. *J. Am. Chem. Soc.* **1987**, *109*, 6872 − 6873.

Adams, R. D.; Babin, J. E. *Organometallics* **1987**, *6*, 1364 − 1365.

Adams, R. D.; Tanner, J. T. *Organometallics* **1988**, *7*, 2241 − 2243.

Adams, R. D.; Chen, G.; Tanner, J. T.; Yin, J. *Organometallics* **1989**, *8*, 2493 − 2495.

Adams, R. D.; Chen, G. *Organometallics* **1990**, *9*, 2882 − 2883.

Amoroso, A. J.; Gade, L. H.; Johnson, B. F. G.; Lewis, J.; Raithby, P. R.; Wong, W. T. *Angew. Chem. Int. Ed. Engl.* **1985**, *24*, 697 − 698.

Fumagalli, A.; Martinengo, S.; Bernasconi, G.; Ciani, G.; Proserpio, D. M.; Sironi, A. *J. Am. Chem. Soc.* **1997**, *119*, 1450 − 1451.

Chini, P. *J. Organomet. Chem.* **1980**, *200*, 37 − 61;

Ceriotti, A.; Masciocchi, N.; Macchi, P.; Longoni, G. *Angew. Chem. Int. Ed.* **1999**, *38*, 3941 − 3944,

Roth, J . D.; Lewis, G. J.; Safford, L. K.; Jiang, X.; Dahl, L. F.; Weaver, M. J. *J. Am. Chem. Soc.* **1992**, *114*, 6159 − 6169.

Mednikov, E. G.; Ivanov, S. A.; Slovokhotova, I. V.; Dahl, L. F. *Angew. Chem. Int. Ed.* **2005**, *44*, 6848 − 6854.

Tran, N. T.; Powell, D. R.; Dahl, L. F. *Angew. Chem. Int. Ed.* **2000**, *39*, 4121 − 4125.

Braunstein, P.; Oro, L. A.; Raithby, P. R. *Metal Clusters in Chemistry*, Wiley, New York, **1999**.

Michelin-Lausarot, P.; Vaglio, G. A.; Valle, M. *J. Organomet. Chem.* **1984**, *275*, 233 − 237.

Adams, R. D.; Captain, B.; Zhu, L. *J. Am. Chem. Soc.* **2004**, *126*, 3042 − 3043.

Adams, R. D.; Barnard, T. S.; Li, Z.; Wu, W.; Yamamoto, J. H. *J. Am. Chem. Soc.* **1994**, *116*, 9103 − 9113.

Xiao, J.; Puddephatt, R. J. *Coord. Chem. Rev.* **1995**, *143*, 457 − 500.

Dees, M. J.; Ponec, V. *J. Catal.* **1989**, *115*, 347 − 355.

Rice, R. W.; Lu, K. *J. Catal.* **1982**, *77*, 104 − 117.

Rasser, J. C.; Beindorff, W. H.; Scholten, J. F. *J. Catal.* **1979**, *59*, 211 − 222.

Sinfelt, J. H. *Bimetallic Catalysts: Discoveries, Concepts, and Applications*; Wiley, New York, **1983**.

Sinfelt, J. H. *Adv. Chem. Eng.* **1964**, *5*, 37 − 74.

Sinfelt, J. H. *Sci. Am.* **1985**, 253, *3*, 90 − 98.

Sinfelt, J. H.; Via, G. H. *J. Catal.* **1979**, *56*, 1 − 11.

Johnson, B. F. G. *Coord. Chem. Rev.* **1999**, *192*, 1269 − 1285.

Hills, C. W.; Nashner, M. S.; Frenkel, A. I.; Shapely, J. R.; Nuzzo, R. G. *Langmuir*, **1999**, *15*, 690 − 700.

Thomas, J. M.; Johnson, B. F. G.; Raja, R.; Sankar, G. Midgley, P. *Acc. Chem. Res.* **2003**, *36*, 20 − 30.

Hungria, A. G.; Raja, R.; Adams, R. D.; Captain, B.; Thomas, J. M.; Midgley, P. A.; Golovko, V.; Johnson, B. F. G. *Angew. Chem. Int. Ed.* **2006**, *45*, 4782 − 4785.

Mingos, D. M. P.; May, A. S. in *The Chemistry of Metal Cluster Complexes*, Shriver, D. F.; Kaesz, H. D.; Adams, R. D., VCH Publishers, New York, NY, 1990, Ch. 2.

Fajardo, Holden, H. D.; Johnson, B. F. G.; Lewis, J., Raithby, P. R. *J. Chem. Soc., Chem. Commun*. **1984**, 24 − 25.

Schollenberg, M.; Nuber, B.; Ziegler, M. L. *Angew. Chem. Int. Ed.* **1992**, *31*, 350 – 351.

Kong, G.; Harakas, G. N.; Whittlesey, B. R. *J. Am. Chem. Soc.* **1995**, *117*, 3502 − 3509.

Egold, H.; Schraa, M.; Florke, U.; Partyka, J. *Organometallics* **2002**, *21*, 1925 − 1932.

Brayshaw, S. K.; Green, J. C.; Edge, R.; McInnes, E. J. L.; Raithby, P. R.; Warren, J. E.; Weller, A. S. *Angew. Chem. Int. Ed.* **2007**, *46*, 7844 – 7848.

Cerrada, E.; Contel, M.; Valencia, A. D.; Laguna, M.; Gelbrich, T.; Hursthouse, M. B. *Angew. Chem. Int. Ed.* **2000**, *39*, 2353 − 2356.

Doyle, G.; Eriksen, K. A.; Van Engen, D. *J. Am. Chem. Soc.* **1986**, *108*, 445 − 451.

Adams, R. D.; Captain, B.; Trufan, E. *J. Am. Chem. Soc.* **2007**, *129*, 12328 − 12340.

Hungria, A.B.; Raja, R.; Adams, R. D.; Captain, B.; Thomas, J. M.; Midgley, P. A.; Golvenko, V.; Johnson, B. F. G. *Angew. Chem. Int. Ed.* **2006**, *45*, 4782 − 4785.

Adams, R. D.; Boswell, E. M.; Captain, B.; Hungria, A. B.; Midgley, P. A.; Raja, R.; Thomas, J. M. *Angew. Chem.. Int. Ed.* **2007**, *46*, 8182 − 8185.

Adams, R. D.; Blom, D. A.; Captain, B.; Raja, R.; Thomas, J. M.; Trufan, E. *Langmuir* **2008**, *24*, 9223 − 9226.

Yang, F.; Trufan, E.; Adams, R. D.; Goodman, D. W. *J. Phys. Chem. C* **2008**, *112*, 14233 − 14235.

Waldmann, O. *Coord. Chem .Rev.* **2005**, *249*, 2550 – 2566.

Pizzagalli, L.; Stoeffler, D.; Gautier, F. *Phys. Rev. B* **1996**, *54*, 12216 – 12224.

Garlaschelli, L.; Chini, P.; Martinengo, S., *Gazz. Chim. Ital.*, ***1982***, *112*, 285 − 288.

Malatesta L.; Naldini L.; Simonetta G. and Cariati F., Coordin. Chem. Rev., **1966**, *1*, 255 − 262.

SAINT+, version 6.2a, Bruker Analytical X-ray Systems, Inc., Madison, WI, **2001**.

Sheldrick, G. M. SHELXTL, version 6.1, Bruker Analytical X-ray Systems, Inc., Madison, WI, **1997**.

Gaussian 03, Revision E.01, suite of programs for *ab initio* calculation; Frisch, M. J.; Trucks, G. W.; Schlegel, H. B.; Scuseria, G. E.; Robb, M. A.; Cheeseman, J. R.; Montgomery, J. A., Jr.; Vreven, T.; Kudin, K. N.; Burant, J. C.; Millam, J. M.; Iyengar, S. S.; Tomasi, J.; Barone, V.; Mennucci, B.; Cossi, M.; Scalmani, G.; Rega, N.; Petersson, G. A.; Nakatsuji, H.; Hada, M.; Ehara, M.; Toyota, K.; Fukuda, R.; Hasegawa, J.; Ishida, M.; Nakajima, T.; Honda, Y.; Kitao, O.; Nakai, H.; Klene, M.; Li, X.; Knox, J. E.; Hratchian, H. P.; Cross, J. B.; Bakken, V.; Adamo, C.; Jaramillo, J.; Gomperts, R.; Stratmann, R. E.; Yazyev, O.; Austin, A. J.; Cammi, R.; Pomelli, C.; Ochterski, J. W.; Ayala, P. Y.; Morokuma, K.; Voth, G. A.; Salvador, P.; Dannenberg, J. J.; Zakrzewski, V. G.; Dapprich, S.; Daniels, A. D.; Strain, M. C.; Farkas, O.; Malick, D. K.; Rabuck, A. D.; Raghavachari, K.; Foresman, J. B.; Ortiz, J. V.; Cui, Q.; Baboul, A. G.; Clifford, S.; Cioslowski, J.; Stefanov, B. B.; Liu, G.; Liashenko, A.; Piskorz, P.; Komaromi, I.; Martin, R. L.; Fox, D. J.; Keith, T.; Al-Laham, M. A.; Peng, C. Y.; Nanayakkara, A.; Challacombe, M.; Gill, P. M. W.; Johnson, B.; Chen, W.; Wong, M. W.; Gonzalez, C.; Pople, J. A. *Gaussian, Inc.*: Wallingford CT, **2004.**

Boese, A. D.; Martin, J. M. L. *J. Chem*. *Phys.* **2004**, *121*, 3405 − 3416.

Peterson, K. A.; Figgen, D.; Dolg, M.; Stoll, H. *J. Chem. Phys.* **2007**, *126*, 124101.

Süss-Fink, G.; Haak, S.; Ferrand, V.; Stoeckli-Evans, H. *J. Chem. Soc, Dalton Trans.* **1997**, 3861 − 3865.

Mingos, D. M. P. *Acc. Chem. Res.* **1984**, *17*, 311 – 319.

Gaussian 03, Revision E.01, suite of programs for ab initio calculation; Frisch, M. J. et al. Gaussian, Inc.: Wallingford CT, **2004**.

Wong, W.Y.; Ting, F. L.; Guo, Y.; Lin, Z. *J. Cluster Sci.* **2005**, *16*, 185 – 200.

Wong, W.Y.; Choi, K.H.; Lin, Z. *Eur. J. Inorg. Chem.* **2002**, 2112 – 2120.

Wong, W.Y.; Wong, W. T. *J. Chem. Soc., Dalton Trans.* **1996**, 1853 – 1856.

Corrigan, J. F.; Doherty, S.; Taylor, N. J.; Carty, A. J. *Organometallics* **1993**, *12*, 993 – 995.

Chi, Y.; Su, C. J.; Farrugia, L. J.; Peng, S. M.; Lee, G. H. *Organometallics* **1994**, *13*, 4167 − 4169.

Van Santen, R. A.; Neurock, M. in *Molecular Heterogeneous Catalysis. A Conceptual and Computational Approach*, Wiley-VCH, Weinheim, **2006**, 121 − 125.

Muetterties, E. L.; Stein, J., *Chem. Rev.* **1979**, *79*, 479 – 490.

Herrmann, W.A. *Angew. Chem. lnt. Eng. Ed.*, **1982**, *21*, 117 − 130.

Adams, R. D. *J. Organomet. Chem.* **2000**, *600*, 1 − 6.

Adams, R. D.; Li, Z.; Swepston, P.; Wu, W.; Yamamoto, J. *J. Am. Chem. Soc*., **1992**, *114*, 10657 − 10658.

Adams, R. D.; Barnard, T. S.; Li, Z.; Wu, W.; Yamamoto, J. *J. Am. Chem. Soc.,* **1994**, *116*, 9103 − 9113.

Adams, R. D.; Barnard, T. S. *Organometallics*, **1998**, *17*, 2567 − 2573.

Pignolet, L. H.; Aubart, M. A.; Craighead, K. L.; Gould, R. A. T.; Krogstad, D. A.; Wiley, J. S. *Coord. Chem. Rev.* **1995**, *143*, 219 – 263.

Ferrand, V.; Süss-Fink, G.; Neels, A.; Stoeckli-Evans, H. *J. Chem. Soc., Dalton Trans.* **1998**, 3825 − 3831.

Süss-Fink, G.; Haak, S.; Neels, A. Ferrand, V.; Stoeckli-Evans, H. *J. Chem. Soc., Dalton Trans.*, **1997**, 3861 − 3865.

Huq, R.; Poe, A. J.; Chawla, S. *Inorg. Chim. Acta* **1980**, *38*, 121 − 125.

ADF2013; SCM Theoretical Chemistry, Vrije Universiteit, Amsterdam, The Netherlands, http://www.scm.com.

Perdew, J. P.; Ruzsinszky, A.; Csonka, G. I.; Vydrov, O. A.; Scuseria, G. E. *Phys. Rev. Lett.* **2008**, *100*, 136406.

Bau, R.; Drabnis, M. H. *Inorg. Chim. Acta* **1997**, *259*, 27 - 50. (b) Teller, R. G.; Bau, R. *Struc. Bonding* **1981**, *41*, 1 − 82.

Adams, R. D.; Captain, B. *Organometallics* **2007**, *26*, 6564 – 6575

Haak, S.; Süss-Fink, G.; Neels, A.; Stoeckli-Evans, H. *Polyhedron* **1999**, *18*, 1675 – 1683.

Mingos D. M. P. *Acc. Chem. Res.***1984**, *17*, 311 – 319.

Adams, R. D.; Captain, B. *Acc. Chem. Res.***2009**, *42*, 409 – 418.

Crabtree, R. H. *Topics Organomet. Chem.* **2011**, *34*, 1 − 10.

Jones, J. H. *Platinum Metals Rev.* **2000**, *44*, 94 – 105.

Jensen, C. M., *Chem. Commun.* **1999**, 2443 – 2449.

César, V.; Bellemin-Laponnaz, S.; Gade, L. H., *Chem. Soc. Rev.* **2004**, *33*, 619 – 636.

Lu, S.-M.; Han, X.-W.; Zhou, Y.-G., *Adv. Synth. Catal.* **2004**, *346*, 909 – 912.

Matthias, W.; Haenel, M. W.; Oevers, S.; Angermund, K.; Kaska, W. C.; Fan, H.-J.; Hall, M.B., *Angew. Chem. int. Ed.* **2001**, *40*, 3596 – 3600.

Lu, J.; Pedro Serna, P.; Aydin, C.; Browning, N. D.; Gates, B. C., *J. Am. Chem. Soc.* **2011**, *133*, 16186 – 16195.

Gates, B. C., *Chem. Rev.* **1995**, *95*, 511 – 522.

Bayram, E.; Zahmakiran, M.; Ozkar, S.; Finke, R. G., *Langmuir*, **2011**, *26*, 12455 – 12464.

Uzun, A.; Dison, D. A.; Gates, B. C., *ChemCatChem* **2011**, *3*, 95 – 107.

Gates, B. C. in *Catalysis by Di- and Polynuclear Metal Complexes*, Adams, R. D.; Cotton, F. A., Eds., Wiley-VCH Publishers, New York, **1998**, Ch. 14.

Psaro, R.; Dossi, C.; Della Pergola, R.; Garlaschelli, L.; Calmotti, S.; Marngo, S.; Bellatreccia, M.; Zanoni, R., *Appl. Catal. A: Gen.* **1995**, *121*, L19 – L23.

Süss-Fink, G.; Haak, S.; Ferrand, V.; Stoeckli-Evans, H., *J. Molec. Catal.* **1999**, *143*, 163 –170.

Hamada, H.; Kuwahara, Y.; Kintaichi, Y.; Ito, T.; Wakabayashi, K.; IIjima, H.; Sano, K.-I. *Chem. Lett.* **1984**, 1611 – 1612.

R. E. Fuentes, J. Farell, J. W. Weidner, *Electrochem. Solid-State Lett.* **2011**, *14*, E5 – E7.

Haruta, M. *Catal. Today* **1997**, *36*, 153 – 166.

Haruta, M.; Date, M. *Appl. Catal. A: Gen.* **2001**, *222*, 427 – 437.

Hashmi, A. S. K.; Hutchings, G. J. *Angew. Chem. int. Ed.* **2006**, *45*, 7896 – 7936.

Hutchings, G. J. *Angew. Chem. int. Ed.* **2008**. 1148 – 1164.

Ortiz-Soto, L. B.; Alexeev, O. S.; Amiridis, M. D. *Langmuir* **2006**, *22*, 3112 – 3117.

Chihara, T.; Sato, M.; Konomoto, H.; Kamiguchi, S.; Ogawa, H.; Wakatsuki, Y. *J. Chem. Soc., Dalton Trans.* **2000**, 2295 – 2299.

Galsworthy, J. R.; Hattersley, A. D.; Housecroft, C. E.; Rheingold, A. L.; Waller, A. *J. Chem. Soc., Dalton Trans.* **1995**, 549 – 557.

Adams, R. D.; Zhang, Q.; Yang, X. *J. Am. Chem. Soc.*, **2011**, *133*, 15950 – 15953.

Süss-Fink, G.; Haak, S.; Ferrand, V.; Stoeckli-Evans, H. *J. Chem. Soc., Dalton Trans.* **1997**, 3861 – 3865.

Malatesta, L.; Naldini, L.; Simonetta, G.; Cariati, F. *Coord. Chem. Rev.* **1966**, *1*, 255 – 262.

Nesmeyanov, A. N.; Perevalova, E. G.; Struchkov, Y. T.; Antipin, M. Y.; Grandberg, K. I.; Dyadchenko, V. P. *J. Organomet. Chem.* **1980**, *201*, 343 – 349.

SpinWorks 3.1.7, Copyright ©, Kirk Marat, University of Manitoba, **2010**.

Quirt, A. R.; Martin, J. S. *J. Magn. Reson.* **1971**, *5*, 318 – 327.

Bruce, M. I.; Nicholson, B. K. *Organometallics* **1984**, *3*, 101 – 108.

Bau, R.; Drabnis, M. H. *Inorg. Chim. Acta* **1997**, *259*, 27 – 50.

Teller, R. G.; Bau, R. *Struct. Bonding*, **1981**, *44*, 1 – 82.

Freeman, M. J.; Orpen, A. G.; Salter, I. D. *J. Chem. Soc., Dalton Trans.* **1987**, *379* – 390.

Orpen, A. G.; Salter, I. D. *Organometallics* **1991**, *10*, 111 – 117.

Bellon, P.; Manassero, M.; Sansoni, M. *J. Chem. Soc., Dalton Trans.* **1973**, 2423 – 2427.

Howard, J. A. K.; Salter, I. D.; Stone, F. G. A. *Polyhedron* **1984**, *3*, 567 – 573.

Bruce, M. I.; Nicholson, B. K. *J. Organomet. Chem.* **1983**, *252*, 243 – 255.

Salter, I. D. in *Comprehensive Organometallic Chemistry*, E. W. Abel, F. G. A. Stone, G. Wilkinson, Elsevier, London, **1995**, Vol. 10, Ch. 5.

Salter, I. D. in *Metal Clusters in Chemistry*, P. Braunstein, L. A. Oro, P. R. Raithby, Wiley-VCH, Weinheim, **1999**, Vol. 1, Ch. 1.27, 509 – 534.

Adams, R. D.; Captain, B.; Fu, W.; Pellechia, P. J.; Smith, M. D. *Inorg. Chem.* **2003**, *42*, 2094 – 2101.

Housecroft, C. E.; Mathews, D. M.; Waller, A.; Edwards, A. J.; Rhenigold, A. L. *J. Chem. Soc., Dalton Trans.* **1993**, 3059 – 3070.

Evans, J.; Gao, J. *J. Chem. Soc., Chem. Commun.* **1985**, 39 – 40.

Li, Y.; Pan, W.-X.; Wong, W.-T. *J. Cluster Sci*. **2002**, *13*, 223 – 233.

Goudsmit, R. J.; Johnson, B. F. G.; Lewis, J.; Raithby, P. R.; Rosales, M. J. *J. Chem. Soc. Dalton Trans.* **1983**, 2257 – 2261.

Bradford, C. W.; Nyholm, R. S.; Gainsford, G. J.; Guss, J. M.; Ireland, P. R.; Mason, R. *J. Chem. Soc. Chem Commun.* **1972**, 87 – 89.

Gainsford, G. J.; Guss, J. M.; Ireland, P. R.; Mason, R.; Bradford, C. W.; Nyholm, R. S. *J. Organomet. Chem.* **1972**, *40*, C70 – C72.

Deeming, A. J.; Kimber, R. E.; Underhill, M. *J. Chem. Soc. Dalton Trans.* **1973**, 2589 – 2596.

Arce, A. J.; Deeming, A. J. *J. Chem. Soc. Dalton Trans.* **1982**, 1155 – 1157.

Chan, K. H.; Leong, W. K.; Mak, K. H. G. *Organometallics* **2006**, *25*, 250 – 259.

Leong, W. K.; Chen, G. *Organometallics* **2001,** *20*, 2280 – 2287.

Adams. R. D.; Katahira, D. A.; Yang, L.-W. *Organometallics* **1982**, *1*, 235 - 239.

Hartwig, J. F.; Bergman, R. G.; Andersen, R. A. *J. Am. Chem. Soc.* **1991**, *113*, 3404 – 3418.

Johnson, B. F. G.; Nairn, J. G. M.; Brown, D. B.; Lewis, J.; Gallop, M.; Parker, D. G. *Chem. Eur. J.* **1995**, *1*, 252 – 260.

Braga, D.; Grepioni, F.; Parisini, E.; Johnson, B.F.G.; Martin, C.M.; Nairn, J.G.M.; Lewis, J.; Martinelli, M., *J. Chem. Soc. Dalton Trans.*, **1993**, 1891 – 1895.

PartyKa, D.V.; Zeller, M.; Hunter, A.D.; Gray, T.G., *Angew. Chem. Int. Ed.* **2006**, *45*, 8188 – 8191.

Osawa, M.; Hoshino, M.; Hashizume, D., *Dalton Trans.*, **2008**, 2248 – 2252.

Heng W.Y.; Hu J. and Yip J.H.K., *Organometallics* **2007**, *26*, 6760–6768.

Partyka, D.V.; Zeller, M.; Hunter, A.D.; Gray, T.G., *Angew. Chem. Int. Ed.* **2006**, *45*, 8188 – 8191.

Raubenheimer, H. G.; Schmidbaur, H. *Organometallics* **2012**, *31*, 2507 – 2522.

Stone, F. G. A. *Angew. Chem. Int. Ed. Engl.* **1984**, *23*, 89 – 99.

Arce, A. J.; Arrojo, P.; Deeming, A. J.; De Sanctis, Y. *J. Chem. Soc., Chem. Commun.* **1991**, 1491 – 1492.

Broach, R. W.; Williams, J. M. *Inorg. Chem.* **1979**, *18* , 314 – 319.

Churchill, M. R.; Hollander, F. J.; Hutchinson, J. P. *Inorg. Chem.* **1977**, *16*, 2697 - 2700;

Allen, V. F.; Mason, R.; Hitchcock, P. B. *J. Organomet. Chem.* **1977**, *140*, 297 – 307.

Burgess, K.; Johnson, B. F. G.; Kaner, D. A.; Lewis, J.; Raithby, P. R.; Syed,-Mustaffa, S. N. A. B. *J. Chem. Soc., Chem. Commun.* **1983**, 455 – 457.

Johnson, B. F. G.; Kaner, D. A.; Lewis, J.; Raithby, P. R. *J. Organomet. Chem.* **1981**, *215*, C33 – C37.

Osawa,M.; Hoshino, M.; Hashizume, D. *Dalton Trans.* **2008**, 2248 – 2252.

Osawa, M.; Hoshino, M.; Hashizume, D. *Dalton Trans.* **2008**, 2248 – 2252.

Arce, A. J.; Canavera, F.; De Sanctis, Y.; Ascanio, J.; Machado, R.; Gonzalez, T. J. Organomet. Chem. **2009**, *694*, 1834 – 1839.

Pregosin, P. S., *NMR in Organometallic Chemistry*, Wiley-VCH, Weinheim, **2012**, Ch. 8.

Dynamic NMR Spectroscopy, Jackman, L. M.; Cotton, F. A., Eds., Academic Press, New York, **1975**.

Pregosin, P. S.; Trabesinger, G. *Dalton Trans*., **1998**, 727 – 734.

Kubas, G. J. *Metal Dihydrogen and σ–Bond Complexes*, Kluwer Academic/Plenum Publisher, **2001**, Ch. 6.

Brydges, S.; Harrington, L. E.; McGlinchey, M. J. *Coord. Chem. Rev.* **2002**, *233-234*, 75 – 105.

Mislow, K. *Accts. Chem. Res.* **1976**, *9*, 26 – 33.

Hayashi, T. *Acc. Chem. Res.* **2000**, *33*, 354 – 362.

te Velde, G.; Bickelhaupt, F.M.; van Gisbergen, S.J.A.; Fonseca Guerra, C; Baerends, E.J.; Snijders J.G.; Ziegler, T. *J. of Comp. Chem.* **2001**, *22*, 931 – 967.

Fonseca Guerra, C.; Snijders, J.G.; te Velde, G.; Baerends, E.J. *Theo. Chem. Acc.* **1998**, *99*, 391 − 403.

E. van Lenthe, E.J. Baerends and J.G. Snijders, *J. Chem. Phys.* **1994**, *101*, 9783 − 9792.

Adams, R. D.; Rassolov, V.; Zhang, Q. *Organometallics* **2012**, *31*, 2961 − 2964.

van Koten, G. *J. Organomet. Chem.* **1990**, *400*, 283-301 and references therein.

Eriksson, H.; Hakansson, M. *Organometallics* **1997**, *16*, 4243 – 4244.

He, X.; Ruhlandt-Senge, K.; Power, P.P. *J. Am. Chem. Soc.* **1994**, *116*, 6963 – 6964.

Meyer, E. M.; Gambarotta, S.; Floriani, C.; Chiesi-Villa, A.; Guastini, C. *Organometallics*, **1989**, *8*, 1067 – 1079.

Bradford, C. W.; Nyholm, R. S.; Gainsford, G. J.; Guss, J. M.; Ireland, P. R.; Mason, R. *J. Chem. Soc., Chem. Commun.* **1972**, 87 − 89.

Arce, A. J.; Arrojo, P.; Deeming, A. J.; De Sanctis, Y. *J. Chem. Soc., Chem. Commun.* **1991**, 1491 − 1492.

Adams, R. D.; Captain, B.; Zhu, L. *Inorg. Chem.* **2007**, *46*, 4605 − 4611.

Deng, M.; Leong, W. K. *Dalton Trans.* **2002**, 1020 − 1023.

Adams, R. D.; Pearl, W. C., Jr *J. Organomet. Chem.* **2011**, *696*, 1198 − 1210.

Garcia, M. E.; Ramos, A.; Ruiz, M. A.; Lanfranchi, M.; Marchio, L. *Organometallics* **2007**, *26*, 6197 − 6212.

Briard, P.; Cabeza, J. A.; Llamazares, A.; Ouahab, L.; Riera, V. *Organometallics* **1993**, *12*, 1006 − 1008.

Cabeza, J. A.; Franco, R. J.; Llamazares, A.; Riera, V. *Organometallics* **1994**, *13*, 55 − 59.

Brookhart, M.; Green, M. H. L.; Wong, L.-L. *Prog. Inorg. Chem.* **1988**, *36*, 1.

Crabtree, R. H. *Angew. Chem. int. Ed.* **1993**, *32*, 789 − 805.